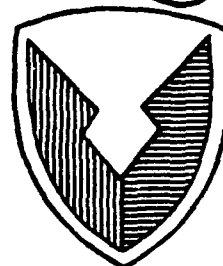


AD-A254 930



(2)



US ARMY
MATERIEL COMMAND

AD No. _____

DPG No. DPG-CR-92-902

METEOROLOGICAL INFLUENCES ON SMOKE/OBSCURANT
EFFECTIVENESS PHASE II

Volume II

by

Steven R. Hanna, David G. Strimaitis
Joseph C. Chang and Sharon M. McCarthy

Sigma Research Corporation
234 Littleton Road, Suite 2E
Westford, Massachusetts 01886

Contract DAAD09-89-C-0039

DTIC
ELECTED
AUG 05 1992
SAID

November 1991

Prepared for

METEOROLOGY DIVISION
MATERIEL TEST DIRECTORATE
U.S. ARMY DUGWAY PROVING GROUND
DUGWAY, UTAH 84022-5000

92-21104



425447

Approved for Public Release; Distribution Unlimited

92 8 03 105

Disposition Instructions

Destroy this report when no longer needed. Do not return to the originator.

Disclaimer Statement

The views, opinions, and/or findings in this report are those of the authors and should not be construed as an official Department of the Army position, unless so designed by other official documentation.

Trade Names Statement

The use of trade names in this report does not constitute an official endorsement or approval of the use of such commercial hardware or software. This report may not be cited for purpose of advertisement.

DTIC QUALITY CONTROLLED 5

Accession For	
NTIS CRA&I	<input checked="" type="checkbox"/>
DTIC TAB	<input type="checkbox"/>
Unannounced	<input type="checkbox"/>
Justification	
By	
Distribution /	
Availability Codes	
Dist	Avail and/or Special
A-1	

TABLE OF CONTENTS

- Appendix A: Representativeness of Wind Measurements on a Mesoscale Grid with Station Separations of 312 m to 10000 m
- Appendix B1: Uncertainty Associated with Emission Rate Estimation
- Appendix B2: Analysis of Fog-Oil Smoke Emissions
- Appendix C: Uncertainties in Source Emission Rate Estimates using Dispersion Models
- Appendix D: Display of Relations among Data using Box Plots
- Appendix E: User's Guide for the Sigplot Plotting Package
- Appendix F1: Listings of the Dugway Data Archives - Historical Datasets
- Appendix F2: Listings of the Dugway Data Archives - Smoke/Obscurant Datasets

APPENDIX A

REPRESENTATIVENESS OF WIND MEASUREMENTS ON A
MESOSCALE GRID WITH STATION SEPARATIONS OF 312m TO 10000m

To Appear in Boundary Layer Meteorology

Appendix A

Table of Contents

Abstract	A-1
1. Objective	A-2
2. Previous Studies of Mesoscale Wind Variability	A-2
Empirical Studies of St. Louis Data	A-3
Theoretical Analysis of Spatial Structure	A-4
3. Proposed Formula	A-6
4. Field Experiment at Hereford, Colorado	A-8
5. Analysis of Hereford Data	A-11
5.1 Single Station Variances as a Function of Averaging Time	A-11
5.2 Statistics of Pairs of Observing Stations	A-14
6. Recommended Empirical Formula for Variances	A-19
7. Test of General Equation with Independent Data	A-20
 Acknowledgement	 A-23
References	A-23

Appendix A

List of Tables

Table	Page
A-1 Steady-State Periods from the Herford Dataset Selected for Analysis.	A-12
A-2 Ratios ov Variances $\sigma^2(T_a)/\sigma^2(1 \text{ min})$ for Averaging Times, T_a , of 10 and 60 min., for Wind Speed and Wind Dirction at the Herford Site. Results are Given for Each Runs. The Median of the Ratios for the Thirteen Stations is Given. The Scatter of the Ratios for the Thirteen Stations about any Median has a Standard Deviation of about 0.05 to 0.10. Medians over all Dates are Given at the Bottom.	A-15
A-3 Observations and Model Predictions for Dugway Proving Ground Wind Data, with Tower Separation of 500m, for All Levels Combined, and Wind Speed and Direction Combined. Medians are Listed for the Observed Values. Model Parameters are given in the Footnotes.	A-22

Appendix A

Table of Figures

Figure	Page
A-1 Schematic diagram of wind station locations at the Hereford site. Terrain sloped slightly downward from west to east with an average slope of 1%. North is towards the tip of the figure and there is 10 km spacing between stations 1 and 7 or stations 7 and 13.	A-10
A-2 Time series of five-minute averaged wind speed (u) and wind direction (θ) for Station 3 for 31 March 1990 at the Hereford site. Thick lines indicate steady-state periods selected for analysis.	A-13
A-3 Spatial correlation coefficient, R , as a function of station separation for E-W and N-S legs of Hereford monitoring network. Wind speed (u) correlations are on the left, and wind direction (θ) correlations are on the right. Medians over all eleven runs are shown for averaging times of 1 min. (Long Dashes), 10 min. (Short Dashes), and 60 min. (Solid Line). The standard deviation of the scatter of the 11 points about each line is about 0.2.	A-17
A-4 Spatial correlation coefficients, R , for various spatial separations, Δx , and averaging times, T_a (1 min; * 10 min; + 60 min) from Hereford site. Plotted are the medians over eleven runs, E-W and N-S legs, and wind speed and wind direction observations. Typical scatter of all the data about each line is about 0.2 at a correlation of 0.5. Empirical curves from Equation (A-17) are drawn (dotted, $T_a = 1$ min.; dashed, $T_a = 10$ min.; solid, $T_a = 60$ min.).	A-18

Appendix A

Representativeness of Wind Measurements on a Mesoscale Grid with Station Separations of 312m to 10000m

by

Steven R. Hanna and Joseph C. Chang
Sigma Research Corp., 234 Littleton Road, Suite 2E, Westford, MA 01886

Abstract

A field experiment was carried out in which wind speed and direction were measured over flat terrain at a height of 10 m using 13 identical instruments spaced logarithmically along two perpendicular 10 km lines. Station separations ranged from 312 m to 1000 m. One-minute data from 11 sampling periods of duration 6 to 10 hours were studied.

The statistics showed little dependence on whether the line of instruments was oriented along the wind or across the wind, or whether wind speeds or wind directions were being analyzed. The integral time scale derived from the variation of the single station variances with averaging time was found to equal several minutes. The correlation coefficients between two stations separated by distance Δx were found to vary exponentially with Δx , with an integral distance scale on the order of 1 km. At a station separation of 10 km, the correlation coefficient equals 0.24, 0.37, and 0.47 for averaging times of 1, 10, and 60 minutes respectively. These correlation coefficients correspond to root-mean-square differences in wind speed at the two stations of about 1.2, 1.1, and 1.0 m/s respectively.

Empirical equations based on dimensional analysis are suggested for fitting these observations. It is found that the observations are best fit if two independent integral time scales are used - a boundary-layer time scale about 300s that best applies to small averaging times or small separations and a mesoscale time scale of about 1800s that applies to larger averaging times or large separations.

1. Objectives

In order to solve most atmospheric transport and dispersion problems, it is necessary to assume that the wind measurements at one site represent the wind flow at a nearby site. The separation between these two sites can range from 10 m to 100 km. This assumption is sometimes quite good, but situations often occur where wind direction observations differ by 180° between two towers in the same mesoscale network. There are a few limited studies of wind variability over mesoscale distances (e.g. Perry et al. (1978), Lockhart and Irwin (1980), Hanna (1982), and Panofsky and Dutton (1984)), but there is much more theoretical and observational work needed.

This study is part of a comprehensive research program in which the contributions of meteorological uncertainties to errors in air quality modeling and source emission estimation are being investigated. A cooperative two week field experiment was conducted in which 13 wind instruments were set up along an "L-shaped" pattern with maximum station separation of 10 km. Variances and spatial correlations of wind speeds and directions are calculated, with the objective being the development of simplified empirical/theoretical formulas. The accuracy of these simplified formulas is calculated and suggestions made for using these formulas in more generalized mesoscale settings. Finally, the formulas were tested with independent data from a wind study at Dugway Proving Ground.

2. Previous Studies of Mesoscale Wind Variability

The literature contains two types of studies of mesoscale wind variability. Both employ near-surface wind observations made by two or more wind monitors with separations of 10 m to 100 km. In the first type of study, the variances for a variety of wind monitor separations are calculated and presented, and a very simple empirical formula is suggested (e.g., Lockhart and Irwin (1980) and Hanna (1982)). In the second type of study, theoretical formulas based on spectral analyses are applied to the problem (e.g., Pielke and Panofsky (1970), Perry et al. (1978) and Panofsky and Dutton (1984)). Reviews of these two types of studies are given below.

Empirical Studies of St. Louis Data. During the St. Louis Regional Air Pollution Study (RAPS), hourly-averaged wind observations were recorded for one year from a network of twenty-five wind monitors. The separation of the wind monitors ranged from 3 km to 80 km. Lockhart and Irwin (1980) and Hanna (1982) report calculations of the standard deviation, σ , of the difference in wind speed, u , and wind direction, θ , for concurrent measurements between each pair of stations. For example, the following procedure is used to calculate $\sigma_{(u_a - u_b)}$ for any pair of stations, a and b , over the entire sampling period:

$$\sigma_{(u_a - u_b)}^2 = \frac{\sum_{i=1}^N (u'_a - u'_b)^2}{N} \quad (A-1)$$

where the primes indicate deviations from the average speed at each station and N is the total number of time periods being analyzed. As the separation distance between the stations decreases, this standard deviation should asymptotically approach the standard deviation due to instrument errors for two co-located wind monitors. Lockhart and Irwin (1980) suggested the regression formulas:

$$\sigma_{(\theta_a - \theta_b)} = 15 + 5.7 \ln x \quad (A-2)$$

$$\sigma_{(u_a - u_b)} = 0.47 + 0.24 \ln x \quad (A-3)$$

where x is in km, θ is in degrees, and u is in m/s. The median value of $\sigma_{(\theta_a - \theta_b)}$ is about 33° and $\sigma_{(u_a - u_b)}$ is about 1.2 m/s, at a median separation distance of about 20 km. The standard deviations of the points scattered about equations (A-2) and (A-3) are 0.16 m/s and 4° , respectively.

Hanna (1982) reported an analysis by Nappo of the same set of RAPS wind data, emphasizing the dependence of the standard deviations of the wind differences upon wind speed. Nappo defined the spatial standard deviations, $\sigma_{\Delta u}$ and $\sigma_{\Delta \theta}$ using the set of concurrent measurements at the 25 monitoring stations. For example, the following procedure is used to calculate $\sigma_{\Delta u}^2$ for any given hour:

$$\sigma_{\Delta u}^2 = \frac{\sum_{i=1}^{24} \sum_{n=i+1}^{25} (u'_i - u'_n)^2}{24!} \quad (A-4)$$

where the prime indicates a deviation from the overall average speed for the 25 stations. The magnitude of the spatial standard deviation, $\sigma_{\Delta u}$, is expected to be somewhat larger than that calculated from equation (A-2), since the differences in the means among the stations are included in equation (A-4). It was found that the differences in wind speed and direction among the stations increase by a factor of three or four as wind speed decreases from 5.0 m/s to about 1.5 m/s. At higher wind speeds (~ 10 m/s), asymptotic limits of about 5° for σ_θ and about 0.15 for σ_u/u are evident. The following empirical formulas fit these data:

$$\sigma_{\Delta \theta} = (5^\circ)^2 + (60^\circ/u)^2 \quad (A-5)$$

$$(\sigma_{\Delta u}/u)^2 = (0.15)^2 + (0.6/u)^2 \quad (A-6)$$

where u is in m/s and σ_θ is in degrees.

Theoretical Analyses of Spatial Structure

Panofsky and Dutton (1984, Chapter 9) discuss the technical issues related to the differences in wind velocities measured at two points. They look at the problem from the point of view of the spectrum of sizes of turbulent eddies. They make a distinction between vertical separations, Δz , lateral (cross-wind) separations, Δy , and longitudinal (along-wind) separations, Δx , between the locations of the measurements. Because turbulent eddies tend to maintain their identities as they travel with the wind, at a given separation the along-wind correlations in wind velocities between the measurement stations should be larger than the vertical or cross-wind correlations.

These authors also point out that most of the correlation between wind velocities at two points is due to larger turbulent eddies, with dimensions approximately equal to or larger than the separation between the points. By the same argument, the wind fluctuations in small eddies at one point are uncorrelated with the wind fluctuations in the same size of eddies at a distant point.

Because of the fact that the larger eddies move with the wind flow and slowly change with time, the maximum correlation between two time series of wind velocities at two points separated by an along-wind distance, Δx , may occur at a time lag of about $\Delta x/\bar{u}$, where \bar{u} is the mean wind speed. This is the approximate time required for an air parcel to travel from the first point to the second point.

The issues raised in the previous three paragraphs have led Panofsky and Dutton (1984) and others to the hypothesis that the spatial correlations are functions of the eddy size, the wind speed, and the separation between the wind observation points. They use a mathematical expression known as the coherence, which "is a measure of the square of the correlation between the Fourier component of two time series with their phases adjusted to obtain maximum correlation." The coherence is a function of eddy frequency, n , and is given by:

$$\text{coh}(n) = \frac{[\text{Co}^2(n) + Q^2(n)]}{S_1(n) S_2(n)} \quad (\text{A-7})$$

where $S_1(n)$ and $S_2(n)$ are estimates of the spectral density of the two time series at points 1 and 2, $\text{Co}(n)$ is the cospectrum, and $Q(n)$ the quadrature spectrum. The frequency, n , can have units of cycles per second or radians per second. The cospectrum refers to the correlation due to in-phase fluctuations and the quadrature spectrum refers to the correlation due to fluctuations that are 90° out of phase. The coherence ranges from zero, for no correlation, to one for perfect correlation. In order to calculate $\text{coh}(n)$ for two long time series, specialized computer software for carrying out time series analysis is needed.

Pielke and Panofsky (1970) generalized an empirical expression for the coherence, $\text{coh}(n)$, based on a suggestion by Davenport (1961):

$$\text{coh}(n) = \exp(-a_i n \Delta x_i / u) \quad (\text{A-8})$$

where the subscript i refers to the direction component and the dimensionless "constant", a_i , is called the "decay parameter." Observations show that " a_i " is typically in the range from 1 to 10. The dimensionless variable, $n \Delta x_i / u$, is often referred to as the reduced frequency. It is found that the "constant," a_i , is in fact a function of station separation, Δx . Other investigators have found a_i to be a function of the ambient stability, the turbulence intensity, and the integral time or distance scale of the turbulence. For example, Perry et al (1978) propose the following formula for horizontal station separations, Δx :

$$a = (65\sigma_w / u) + (6.3\sigma_v \Delta x / u L_y) \quad (\text{A-9})$$

where σ_w and σ_v are the standard deviations of turbulent velocity fluctuations in the vertical and cross-wind directions, and L_y is the lateral integral distance scale of the lateral turbulence.

3. Proposed Formula

The relation between wind speed, u , or wind direction, θ , observed at two stations at positions 1 and 2 can be expressed in terms of a variance or a correlation. The relationship between the two quantities can be derived by beginning with the identity:

$$\sigma_{\Delta u}^2 = \overline{(u_2' - u_1')^2} = \overline{u_2'^2} + \overline{u_1'^2} - 2 \overline{u_1' u_2'} \quad (\text{A-10})$$

where the primes refer to fluctuations (i.e., the means have been already subtracted) and the overbar refers to a time average. If the two variances $\overline{u_2'^2}$ and $\overline{u_1'^2}$ are equal, then equation (A-10) can be written in the form:

$$\sigma_{\Delta u}^2 / 2\sigma_u^2 = 1 - R_{12} \quad (A-11)$$

where $\sigma_u^2 = \overline{u'^2}$ and the correlation coefficient $R_{12} = \overline{u'_1 u'_2} / \sigma_u^2$. Thus if the correlation equals 1, 0, or -1, the ratio $\sigma_{\Delta u}^2 / 2\sigma_u^2$ will equal 0, 1, or 2, respectively. For two stations that are separated by such a large distance that the correlation equals zero, then Equation (A-11) states that $\sigma_{\Delta u}^2 = 2\sigma_u^2$.

After investigating the semi-theoretical formulas (A-8) and (A-9), it was decided that there was so much adjustment of "constants" taking place that it was best to begin with a simpler formula based on dimensional analysis. This simpler formula does not explicitly include the frequency, n , but does account for frequency effects through the implicit assumption that wind speed autocorrelograms are exponential (i.e., $R = \exp(-\Delta t/T_I)$), implying that a so-called Markov-energy spectrum is valid) and are completely determined once an integral time scale, T_I , or space scale, Λ_I , is specified. The following dimensionless relationship can then be postulated:

$$\overline{\sigma_{\Delta u}^2 / 2\sigma_u^2} = f(\Delta x, T_I, \Lambda_I, T_a) \quad (A-12)$$

where f is a universal dimensionless function, and variables and parameters are defined in the following way:

$$\overline{\sigma_{\Delta u}^2} = \overline{(u'_2 - u'_1)^2}, \quad \text{where } u'_1 \text{ and } u'_2 \text{ are wind speed fluctuations at positions 1 and 2.}$$

$$\overline{\sigma_u^2} = (\sigma_{u_1}^2 + \sigma_{u_2}^2)/2 \quad \text{is the average turbulent energy at positions 1 and 2.}$$

Δx is the horizontal separation between positions 1 and 2.

T_I is the integral time scale of the time series of wind speed fluctuations measured at position 1 or position 2.

Λ_I is the integral space scale of the correlogram of wind fluctuation differences $(u_i' - u_1')$ measured between positions 1 and i for several positions.

T_a is the averaging time.

The averaging time, T_a , is very important because it is typically of the same order of magnitude as the integral time scale (i.e., within the range from 1 min to 1 hr). As T_a approaches zero, the ratio $\sigma_{\Delta u}^2 / 2\sigma_u^2$ reaches a maximum at any given station separation, since there are poor correlations between wind fluctuations in smaller eddies at two positions.

Exponential shapes are proposed for all correlation functions:

$$R(\Delta x/\Lambda_I) = \exp(-\Delta x/\Lambda_I) \quad (A-13a)$$

$$R(\Delta t/T_I) = \exp(-\Delta t/T_I) \quad (A-13b)$$

The following approximation to Taylor's equation is used to account for the effects of averaging time on variances:

$$\sigma^2(T_a)/\sigma^2(0) = (1 + T_a/2T_I)^{-1} \quad (A-14)$$

For a given separation, Δx , the spatial correlation $R(\Delta x/\Lambda_I)$ is also going to depend on averaging time, T_a , since the effects of the fluctuations due to small eddies will drop to zero at large averaging times. Consequently, $R(\Delta x/\Lambda_I)$ should approach unity as T_a increases, and the second term in the following empirical formula is proposed to account for this effect:

$$\begin{aligned} R(T_a, \Delta x) &= [\overline{u_2' u_1'}/\sigma_{u_1} \sigma_{u_2}] (T_a, \Delta x) \\ &= \exp(-\Delta x/\Lambda_I) + (1 - \exp(-\Delta x/\Lambda_I)) g(T_a \Delta x/\Lambda_I) \end{aligned} \quad (A-15)$$

where the dimensionless function $g(T_a \Delta x/\Lambda_I)$ approaches zero as T_a approaches zero and approaches unity as T_a becomes very large.

4. Field Experiment at Hereford, Colorado

The research programs summarized in Section 2 all took advantage of wind observations made at two or more locations. However, none of these wind observations satisfied all of the following desired characteristics of a study

in which differences in wind observations are being calculated.

- Flat terrain with few obstructions.
- All wind instruments alike, with relatively fast response and adequate calibration procedures.
- Five or more wind stations along a line with spacings ranging from a few hundred meters to 10000 meters.
- Two perpendicular lines of wind stations.
- Several days or more of one-minute averaged wind observations.

A field experiment was designed to satisfy these characteristics, using instruments and technicians from the National Center for Atmospheric Research (NCAR). Thirteen identical wind stations from NCAR's Portable Automated Mesonet (PAM) were set up in flat, open farmland (mostly covered by short, winter-weathered grass) near Hereford, Colorado, and operated for the two week period between 30 March 1990 and 14 April 1990. The instruments were installed, maintained and calibrated by experienced NCAR technicians. The anemometers were located at an elevation of 10 m above the ground. A schematic diagrams of the relative instrument locations is given in Figure A-1. The slope of the terrain is less than about 1% over the entire network. It is seen that logarithmic spacings (312.5m, 625m, 1250m, 2500m, 5000m, 10000m) are used for the instruments along each leg of the "L"-shaped network. The perpendicular axes were used in order to determine if there was a significant difference between the along-wind and cross-wind statistics.

The resulting "Hereford" dataset contained values of N-S and E-W components of the wind velocity at one minute resolution. First, these wind components were converted to wind speed, u , and wind direction, θ , for each minute. Because the threshold of these instruments was about 0.5m/s, periods with reported wind speeds less than 0.5m/s were flagged and not used in the analysis. 5-minute averages of u and θ were made and the resulting time series for each station plotted for the entire 16 day duration of the study (see Figure A-2 for an example of the time series plots for 31 March 1990 Station 6). Visual inspection of the 15 days of time series in the figure revealed that, most of the time, the wind speed and direction are quite variable and unsteady in time. For example, during the afternoon on 1 April and 10 April, the wind speed went through a cycle in which it increased from

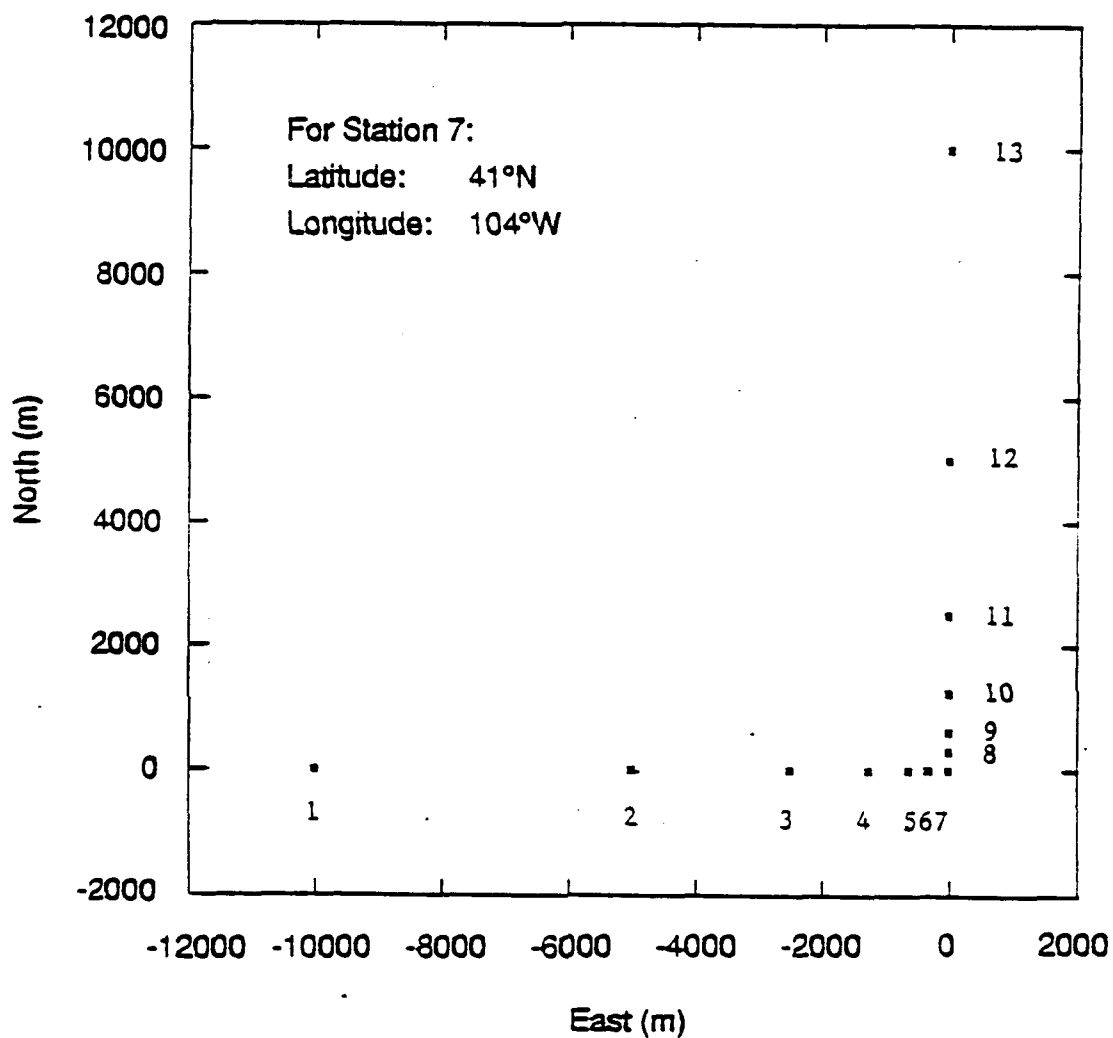


Figure A-1. Schematic diagram of wind station locations at the Hereford site. Terrain sloped slightly downward from west to east with an average slope of 1%. North is towards the top of the figure and there is 10 km spacing between stations 1 and 7 or stations 7 and 13.

nearly zero to about 10 m/s and decreases back down to zero again. This large half-sine-wave would totally dominate any statistical analysis of these wind data.

Because it became clear that any time series analysis of the 16 days would be overly influenced by diurnal changes and synoptic effects, it was decided to confine the analysis to time periods on the order of 6 to 10 hours, when the wind speed and direction appeared to be relatively steady. The eleven steady-state periods that were chosen are listed in Table A-1. Two of these periods are indicated by thick lines in Figure A-2. Median values of wind speed, u , wind direction, θ , standard deviation of wind speed, σ_u , and standard deviation of wind direction, σ_θ , are also listed on the table. These eleven periods are seen to cover a wide range of wind speeds (2.5 to 10.5 m/s), wind directions (170° to 330°) and times of the day.

5. Analysis of Hereford Data

This section presents the results of the analysis of the Hereford data and the next section presents some empirical formulas that fit this dataset. As a first step, variances and time and space correlations were calculated for averaging times of 1, 10, and 60 minutes. A linear trend (estimated from the data from all 13 stations) was removed from the data from each run. Because steady-state periods have been selected and linear trends have been removed, much of the influence of larger mesoscale and regional eddies has been removed there statistics. As will be shown, mesoscale eddies with time scales less than the sampling time are still strongly reflected in the statistics.

5.1 Single Station Variances as a Function of Averaging Time

The variances in the wind speed and wind direction time series were calculated for each of the eleven "steady-state" runs, for each of the thirteen stations, for averaging times of 1, 10, and 60 min. The data are presented in a Table A-2, in the form of ratios of the variance for 10 or 60 minute time periods to the variance for the one minute time period. The medians over the thirteen stations are listed. The overall medians at the

Table A-1

Steady-State Periods from the Hereford Dataset Selected for Analysis.

Meteorological Parameters Represent Medians over 13 Stations

Date/Run	Time	Wind Speed $u(\text{m/s})$	Wind Direction $\theta(^{\circ})$	$\sigma_u(\text{m/s})$	$\sigma_{\theta}(^{\circ})$
0330	00-10	2.5	130	0.7	17
0330	14-24	3.0	215	0.8	17
0331	00-08	3.5	200	0.45	10
0331	16-24	7.5	325	1.2	13
0404	06-12	5.5	90	1.2	13
0404	12-20	7.5	135	1.2	10
0406	18-24	4.0	215	0.9	14
0409	14-24	10.5	10	1.3	8
0411	06-16	3.0	170	0.9	13
0412	00-08	5.5	140	1.1	11
0413	14-20	7.5	330	1.1	10

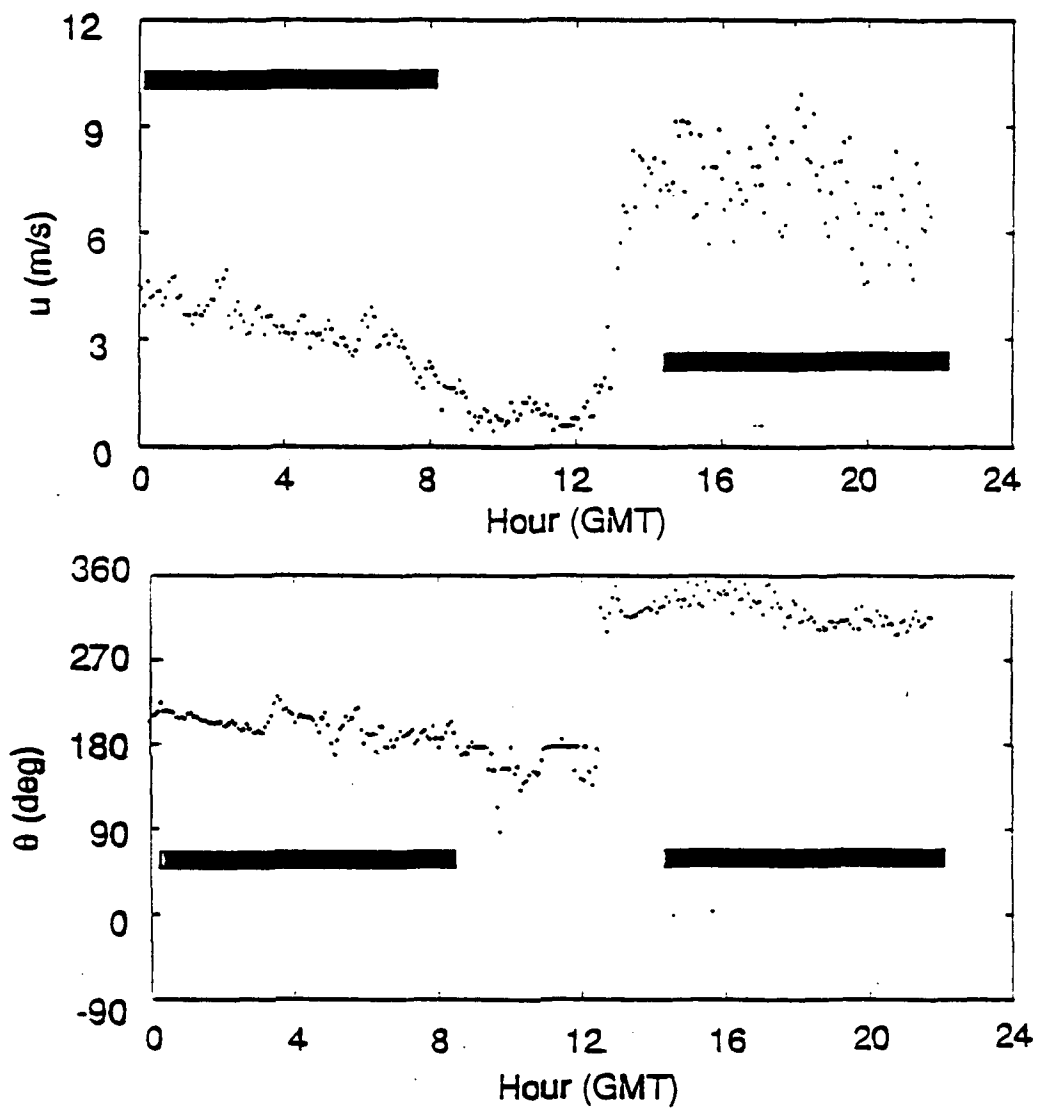


Figure A-2. Time series of five-minute averaged wind speed (u) and wind direction (θ) for Station 3 for 31 March 1990 at the Hereford site. Thick lines indicate steady-state periods selected for analysis.

bottom of the table suggest that there is little difference between the statistics for wind speed and wind direction, with medians of the variance ratios of about 0.68 for $\sigma^2(10 \text{ min})/\sigma^2(1 \text{ min})$ and about 0.39 for $\sigma^2(60 \text{ min})/\sigma^2(1 \text{ min})$. The run-to-run variability in the median variance ratios is about ± 0.20 , with no dependence on wind speed, wind direction, σ_u , σ_θ , or time of day. For a given day, the station-to-station variability in the variance ratios is typically about ± 0.05 to 0.10.

Table A-2 suggests that observed median values of $\sigma^2(10 \text{ min})/\sigma^2(1 \text{ min})$ and $\sigma^2(60 \text{ min})/\sigma^2(1 \text{ min})$ are 0.68 and 0.37, respectively. Solving Equation (14) for the integral time scale T_I , we obtain $T_I \approx 9 \text{ min}$ for $T_a = 10 \text{ min}$ and $T_I \approx 15 \text{ min}$ for $T_a = 60 \text{ min}$. This trend is duplicated in all types of calculations in this analysis, i.e., the derived time and distance integral scales increase as the averaging time, T_a , or station separation, Δx , increase. Persistent mesoscale eddies are associated with turbulence at time scales of several hours and distance scales of several tens of kilometers. Superimposed on these "baseline mesoscale eddies" are the smaller turbulent eddies normally thought to be associated with the atmospheric boundary layer. Consequently it is assumed that the turbulent velocity field is described by two times scales, one (T_{I1}) associated with boundary layer turbulence, and another (T_{I2}) associated with mesoscale eddies. These two time scales are assumed to contribute equally to $\sigma^2(T_a)$, leading to the following modification to Equation (A-14):

$$\frac{\sigma^2(T_a)}{\sigma^2(0)} = \frac{0.5}{1 + T_a/2T_{I1}} + \frac{0.5}{1 + T_a/2T_{I2}} \quad (\text{A-16})$$

The Hereford dataset is best-fit by $T_{I1} \approx 300\text{s}$ and $T_{I2} \approx 1800\text{s}$, which yield $\sigma^2(10)/\sigma^2(1) = 0.71$ (slightly above the median observation of 0.68) and $\sigma^2(60)/\sigma^2(1) = 0.35$ (slightly below the median observation of 0.37).

5.2 Statistics for Pairs of Observing Stations

The spatial statistics to be presented are all keyed to wind station (7) at the corner of the "L" of the network shown in Figure A-1. The results in this section are given for the spatial correlation coefficient,

Table A-2

Ratios of Variances $\sigma^2(T_a)/\sigma^2(1 \text{ min})$ for Averaging Times, T_a , of 10 and 60 min., for Wind Speed and Wind Direction at the Hereford Site. Results are Given for Each of Eleven Runs. The Median of the Ratios for the Thirteen Stations is Given. The Scatter of the Ratios for the Thirteen Stations about any Median has a Standard Deviation of about 0.05 to 0.10. Medians over all Dates are Given at the Bottom.

Run Date/Time	$\sigma_u^2(T_a)/\sigma_u^2(1 \text{ min})$		$\sigma_\theta^2(T_a)/\sigma_\theta^2(1 \text{ min})$	
	Wind Speed		Wind Direction	
	10 Minute	60 Minute	10 Minute	60 Minute
0330/00-10	.88	.61	.93	.58
0330/14-24	.71	.58	.69	.50
0331/00-08	.74	.39	.77	.36
0331/16-24	.41	.21	.64	.25
0404/06-12	.55	.19	.81	.50
0404/12-20	.51	.37	.42	.17
0406/18-24	.31	.13	.40	.10
0409/14-24	.68	.58	.63	.34
0411/06-16	.81	.51	.76	.38
0412/00-08	.80	.56	.92	.52
0413/14-20	.38	.15	.50	.20
Overall Median	0.68	0.39	0.69	0.36

$R(\Delta x, T_a) = \frac{\overline{u_i' u_7'}}{\sigma_{u_i'} \sigma_{u_7'}}$, which are functions of the separation, Δx , of stations i and 7, the averaging time, T_a and the integral scale of the turbulence. Averaging times of 1, 10 and 60 min are used. Results are presented separately for the E-W and N-S legs of the "L". Rather than showing the correlation for all eleven time periods or runs, we present the median of the 11 periods. These correlations, are plotted in Figure A-3. There does not appear to be a strong dependence on E-W or N-S leg, or on whether wind speed or wind direction is being plotted.

As expected, the calculated correlations are lowest for the shorter averaging times and the largest station separations, due to the fact that the dominant turbulent eddies are characterized by space scales of a few hundred meters and time scales on the order of a few minutes.

At the 10 km separation distance, the correlations average about 0.5. Because of the relation between spatial correlation, R_{12} , spatial variance, $\sigma_{\Delta u}^2$, and variance, σ_u^2 , indicated by Equation (A-11), it follows that, at 10 km separation, $\sigma_{\Delta u}^2 = \sigma_u^2$. Knowing that $\sigma_u^2(T_a = 1 \text{ min}) \approx 1.2 \text{ m}^2/\text{s}^2$, and using the median values of $\sigma_u^2(T_a)/\sigma_u^2(1 \text{ min})$ in Table A-2, it can be concluded that $\sigma_{\Delta u}^2 \sim 1.1 \text{ m}^2/\text{s}^2$ for $T_a = 1 \text{ min}$, $\sigma_{\Delta u}^2 \sim 0.8 \text{ m}^2/\text{s}^2$ for $T_a = 10 \text{ min}$, and $\sigma_{\Delta u}^2 \sim 0.4 \text{ m}^2/\text{s}^2$ for $T_a = 60 \text{ min}$ at the 10 km separation distance. This value of $\sigma_{\Delta u} \sim 0.7 \text{ m/s}$ for one-hour averages is close to that found with the St. Louis RAPS data, as discussed in Section 2.

At small averaging times, T_a , Equation (A-15) suggests that the correlation coefficient for wind speed fluctuations at two points separated by a distance, Δx , should be an exponential function of Δx . Therefore, if $\ln R$ is plotted against Δx , a straight line should be seen. Observations of R from this wind network are plotted in Figure A-4, for the six Δx values (312.5, 625, 1250, 2500, 5000, and 10000 m) and three averaging times (1, 10, and 60 min) of interest. Because the correlations in Figure A-3 did not indicate much dependence on E-W or N-S direction, and were similar for wind speed and wind direction, all runs, legs, and variables are combined in this table and figure.

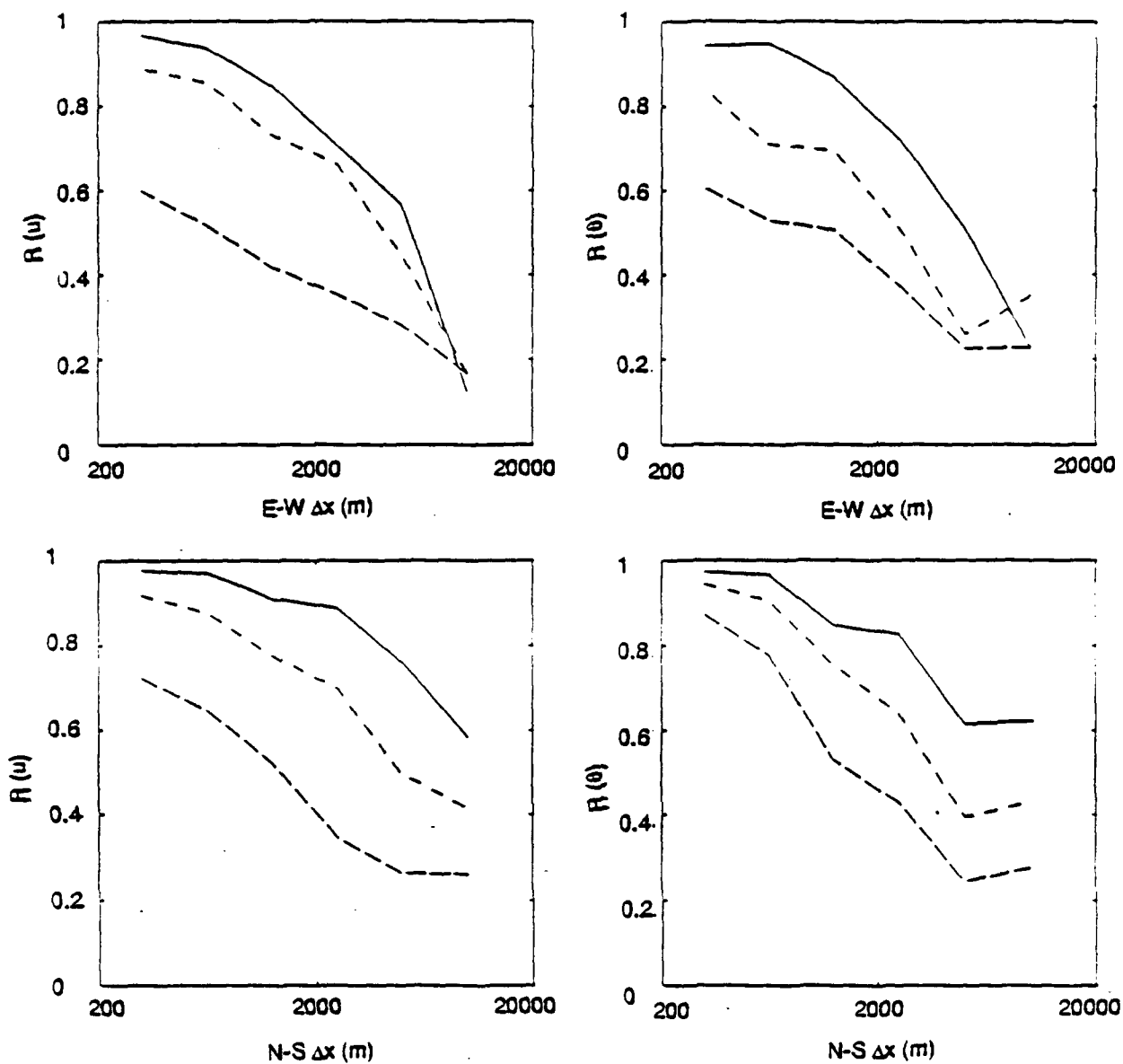


Figure A-3. Spatial correlation coefficient, R , as a function of station separation for E-W and N-S legs of Hereford monitoring network. Wind speed (u) correlations are on the left, and wind direction (θ) correlations are on the right. Medians over all eleven runs are shown for averaging times of 1 min. (Long Dashes), 10 min. (Short Dashes), and 60 Min. (Solid Line). The standard deviation of the scatter of the 11 points about each line is about 0.2.

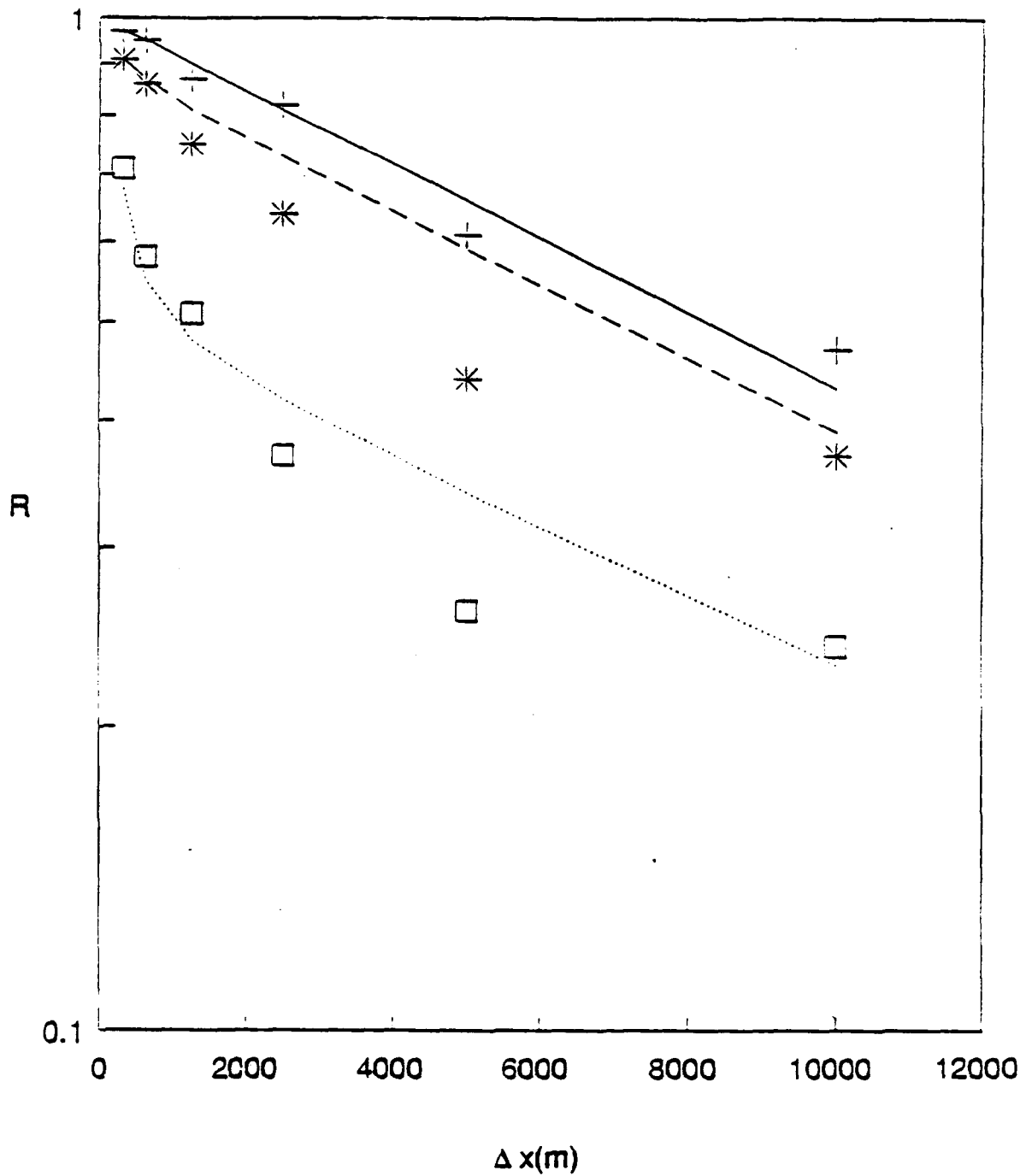


Figure A-4. Spatial correlation coefficients, R , for various spatial separations, Δx , and averaging times, T_a (\square 1 min; * 10 min; + 60 min), from Hereford site. Plotted are the medians over eleven runs. E-W and N-S legs, and wind speed and wind direction observations. Typical scatter of all the data about each line is about 0.2 at a correlation of 0.5. Empirical curves from Equation (A-17) are drawn (dotted, $T_a = 1$ min.; dashed, $T_a = 10$ min.; solid, $T_a = 60$ min.).

The points in the figure follow a straight line only for the largest averaging time (60 min). For the smallest averaging time (1 min), there is a much more rapid drop-off in correlation at small separation distances. This behavior can be explained by the same two-scale phenomenon discussed under Section 5.1 in the analysis of the effects of averaging time; i.e., the results are influenced by a smaller eddy scale, Λ_1 , representative of boundary layer processes, and a larger eddy scale, Λ_2 , representative of mesoscale fluctuations. However, the effects of the smaller scales tend to disappear at large averaging times, T_a , when the condition $T_a > \Lambda_1/u$ is satisfied. Thus, equation (A-15) appears to be satisfied, with the limits:

$$R(\Delta x, T_a \rightarrow 60 \text{ min}) = e^{-\Delta x/\Lambda_2}$$

$$R(\Delta x, T_a \rightarrow 1 \text{ min}) = 0.5e^{-\Delta x/\Lambda_1} + 0.5e^{-\Delta x/\Lambda_2}$$

The following empirical equation fits these data and has the proper asymptotic behavior:

$$R(\Delta x, T_a) = e^{-\Delta x/\Lambda_2} - 0.5 \left(e^{-\Delta x/\Lambda_2} - e^{-\Delta x/\Lambda_1} \right) / \left(1 + (T_a u/a\Lambda_1)^2 \right) \quad (\text{A-17})$$

where $\Lambda_1 = 300 \text{ m}$, $\Lambda_2 = 12000 \text{ m}$, and $a = 5$ when $u \approx 5 \text{ m/s}$. The predicted curves are drawn on Figure A-4. The value of $a = 5$ is consistent with "Pasquill's Beta" = 4, which is the known proportionality factor between Lagrangian and Eulerian scales. Because the actual eddy diameters are equal to about five times the integral scales Λ , the smaller eddy diameters would be about 1500 m and the larger eddy diameters would be about 60 km. Of course the confidence limits on the data (\pm about 0.2) are so broad that a much wider range of scales, Λ_1 and Λ_2 , is possible. Furthermore, these results are limited to this particular site and time of year, and to the ranges of Δx , T_a , and meteorological conditions that we have considered. The sampling time (a maximum of 10 hours) also imposes a maximum limit on integral scales.

6. Recommended Empirical Formula for Variances

Our analysis of the Hereford data has suggested that the variances and correlations for wind speed and wind direction are similar. In addition, we

have found that, despite the theoretical prediction that along-wind correlations will be larger than cross-wind correlations, there is no clear dependency of the correlations on wind direction (or any other meteorological variable). This apparent lack of dependency may be due to the fact that this effect is overwhelmed by the natural variability in the observations.

The similarity relations in Equation (A-8) have been shown to be valid, resulting in Equation (A-16) for the effects of averaging time and Equation (A-17) for the effects of station separation. These equations can be combined into the following general equation:

$$\frac{\sigma_{\Delta u}^2(\Delta x, T_a)}{2\sigma_u^2(T_a = 0)} = \left[\frac{0.5}{1 + T_a/2T_{I1}} + \frac{0.5}{1 + T_a/2T_{I2}} \right] \cdot \left[1 - e^{-\Delta x/\Lambda_2} + 0.5 \frac{(e^{-\Delta x/\Lambda_2} - e^{-\Delta x/\Lambda_1})}{(1 + (T_a w/a\Lambda_1)^2)} \right] \quad (A-18)$$

where $T_{I1} \sim 300$ s $T_{I2} \sim 1800$ s

$\Lambda_1 \sim 300$ m $\Lambda_2 \sim 1200$ m

a (Lagrangian-Eulerian scale) ~ 5

This equation should be tested with independent data from a different site. Slightly different values of the time and distance scales may be appropriate at a different site. For any given time and place, the confidence limits on the results would be expected to be in the same range (about 20% to 30%) has been found here.

7. Test of General Equation with Independent Data

A set of independent wind data from the so-called XM21 field study at Dugway Proving Ground, Utah, were provided by C. Biltoft. Data were available from two towers, separated by 500m, on a relatively flat test range. Instruments were located at heights of 2, 4, 8, 16, and 32m, and measurements were made at a frequency of one per second. Because the towers were constructed of scaffolding, it was necessary to disregard periods when the

wind blew through one of the towers. Two periods of valid data were analyzed--from 1110 to 1651 on 11 April 1989, and from 0937 to 2059 on 2 May 1989. Both periods were marked by wind speeds of about 3.5 m/s and relatively strong turbulence intensities ($\sigma_u/\bar{u} \sim 0.3$ and $\sigma_\theta \sim 30^\circ$).

Because the integral scales of the horizontal components of turbulence are not strongly dependent on height, the results from all five levels are combined in our analysis. This assumption will cause a slight error, since the various ratios $\sigma^2(T_a)/\sigma^2(1\text{sec})$ and correlations are observed to increase by about 10% to 20% between heights of 2m and 32m. In addition, the wind speed and direction results appear similar and are combined in our analysis. The combined data results (two variables, two days, five levels) are presented in Table A-3.

The predictions of $\sigma^2(T_a)/\sigma^2(1\text{sec})$ in the table have been made using Equation (A-16), with the same time scales derived from the NCAR wind network ($T_1 = 300\text{s}$ and $T_2 = 1800\text{s}$). There is a $\pm 10\%$ agreement between the predictions and the observed medians, and the predictions are within the \pm standard deviation error bounds of the observations. It can be concluded that the variances $\sigma^2(T_a)$ show similar behavior at the two sites, and that Equation (A-16) can adequately simulate this behavior.

Equation (A-17) (for spatial correlations) does not transfer as well to the new site. Its predictions are shown under column (2), assuming the parameters ($\Lambda_1 = 300\text{m}$, $\Lambda_2 = 12000\text{m}$, and $a = 5$) derived from the NCAR wind network. Clearly the predictions of $R_{\Delta u}(T_a)$ are too low by about 10 to 30%. If the Λ_1 , Λ_2 , and "a" parameters are "tuned" with these new data, the predictions under column (3) are all within $\pm 4\%$ of the observations. However, the smaller of the length scales, Λ_1 , has to be increased from 300m to 1000m, and the Lagrangian-Eulerian parameter "a" has to be reduced from 5 to 0.2. It appears that the weakest part of Equation (A-17) is the correction term, $(1 + (uT_a/a\Lambda_1)^2)^{-1}$, for averaging time, T_a . This term is intended to cause an increase in the spatial correlation as averaging time increases. However, the functional form for this correction term is not obvious and more thought is clearly needed.

Table A-3

Observations and Model Predictions for Dugway Proving Ground Wind Data,
 with Tower Separation of 500m, for All Levels Combined,
 and Wind Speed and Direction Combined. Medians are Listed for the
 Observed Values. Model Parameters are given in the
 Footnotes.

Averaging Time T_a	$\frac{\sigma^2(T_a)}{\sigma^2(1\text{sec})}$	$\frac{\sigma^2(T_a)}{\sigma^2(1\text{sec})}$	$R_{\Delta u}(T_a)$	
	Observed (1)	Predicted	Observed (2)	Predicted (3)
1 sec			0.78	0.57 0.77
60 sec	0.87	0.95	0.83	0.58 0.86
600 sec	0.68	0.65	0.94	0.83 0.95

- Footnotes: (1) Equation (A-16) is used, with the same values for the parameters as derived from the NCAR data ($T_1 = 300\text{s}$ and $T_2 = 1800\text{s}$)
- (2) Equation (A-17) is used, with the same values for the parameters as derived from the NCAR data ($\Lambda_1 = 300\text{m}$, $\Lambda_2 = 12000\text{m}$, and $a = 5$)
- (3) Equation (A-17) is used, with $\Lambda_1 = 1000\text{m}$, $\Lambda_2 = 12000\text{m}$, and $a = 0.2$.

Acknowledgements:

This research would not have been possible without the assistance of scientists and technicians from the National Center for Atmospheric Research who were responsible for all aspects of the Hereford field study. In particular, the authors thank Dr. Thomas Horst, who managed the study.

The authors appreciate the assistance of Christopher Biltoft, and James Bowers of the U.S. Army Dugway Proving Ground. This research was co-sponsored by the U.S. Army (James Bowers, Project Monitor) and the U.S. Air Force (Captain Michael Moss, Project Monitor.)

References:

- Davenport, A.G., :1961, "The Spectrum of Horizontal Gustiness near the Ground in High Winds," *Quart. J. Roy. Meteorol. Soc.* 87, 194-211.
- Hanna, S.R. :1982, "Applications in Air Pollution Modeling," Ch. 7 in *Atmospheric Turbulence and Air Pollution Modelling*. (Eds: F.T.M. Nieuwstadt and H. van Dop), 275-310.
- Lockhart, T.J. and Irwin J.S., :1980, "Methods for Calculating the Representativeness of Data," Proceedings, *DOE Symposium on Intermediate Range Atmospheric Transport Processes and Technology Assessment*, CONF801064, NTIS, 169-176.
- Panofsky, H.A. and Dutton J.A., :1984, "Atmospheric Turbulence," John Wiley and Sons, New York, Chapter 9.
- Perry, S.G., Norman J.M., Panofsky H.A. and Martsolf J.D., :1978, "Horizontal Coherence Decay near Large Mesoscale Variations in Topography," *J. Atmos. Sci.* 35, 1884-1889.
- Pielke, R.A. and Panofsky H.A., :1970, "Turbulence Characteristics along Several Towers," *Bound. Lay. Meteorol.* 1, 115-130.

Intentionally Blank

APPENDIX B-1

UNCERTAINTY ASSOCIATED WITH EMISSION RATE ESTIMATION

Appendix B-1

Table of Contents

Uncertainty Associated with Emission Rate Estimation

	Page
1. Introduction	B-1
2. Measurement of Smoke Munition Emissions	B-2
2.1 Wind Tunnel Experiments	B-2
2.2 Field Experiments	B-4
3. The Emission Rate Expression	B-6
3.1 Input Parameters	B-6
3.2 Approach to Estimating Uncertainty in the Emission Rate	B-10
3.3 Uncertainty Analysis Results	B-16
4. Conclusions and Recommendations	B-19
References	B-21

Definition of Terms

A, B, C, D	coefficients which are determined by fitting the observed wind tunnel experiments to a curve
COV_{xy}	covariance of xy
CV_x^2	squared coefficient of variation of x, $\frac{\sigma_x^2}{\bar{x}^2}$
CV_y^2	squared coefficient of variation of y, $\frac{\sigma_y^2}{\bar{y}^2}$
h	relative humidity
M_o	initial mass
M_x	mass of zinc or phosphorus aerosolized, as measured in the wind tunnel experiments
MYF	munition yield factor, the ratio $\frac{M_x}{M_o}$
Q_t	mass emission rate
q	$\frac{Q_t}{M_o}$
\bar{x}	mean of x
\bar{y}	mean of y
YF	yield factor, theoretical adjustment to mass of aerosol based on the ability of the active ingredient to absorb water vapor
ΔM	mass lost during burn, initial mass less final mass, as measured by the load cell
σ_{xy}^2	variance of the product xy
σ_x^2	variance of x
σ_y^2	variance of y

Appendix B-1
UNCERTAINTY ASSOCIATED WITH EMISSION RATE ESTIMATION

1. Introduction

To estimate the uncertainty of an entire model it is necessary to evaluate the uncertainty of its components. The input data for atmospheric dispersion models consists of emission rate data and meteorological data. In this discussion we address the issue of uncertainty associated with the estimation of emission rates of aerosols from smoke munitions. Emission rates are generally expressed in terms of weight per unit time; in this case they are expressed as grams of active ingredient, (e.g., phosphorus) per second.

The issue of estimating the emission rate of obscurant munitions is complex, aside from the issue of estimating the associated uncertainty. There are several reasons for this. First, the critical property which provides the obscurant effect is not directly emitted by the munition; it results from an interaction of the active ingredient, e.g., red phosphorus, and moisture in the ambient atmosphere to form a dense smoke cloud. Second, munitions contain other materials which burn simultaneously but do not contribute directly to the obscurant effect; thus measuring total weight loss over burn time only indirectly measures the amount of active ingredient which has been released. Third, to experimentally determine the amount of active ingredient released, the mass of the active ingredient in the entire smoke cloud must be determined and this measurement can only be carried out in a wind tunnel. Thus, data from the wind tunnel experiments are extrapolated to the field setting. These issues affect emission rate estimation as well as contribute to the associated uncertainty.

This discussion covers the following topics: how emissions are measured in both wind tunnel and field experiments, the model used for estimating emission rates, a technique for estimating uncertainty (using existing data as an example), and conclusions and recommendations for the collection of additional data which would enhance the uncertainty analysis. Several reports were reviewed for this analysis, but the information on the method of measuring and modeling emission rates is based on two reports: Basic

Smoke Characterization Test (DPG-FR-77-311) (DPG, 1978) and *Methodology Investigation Final Report Validation of a Transport and Dispersion Model for Smoke* (DPG-FR-702) (Carter et al., 1979). These reports contain data on three different types of smoke obscurant munitions: white phosphorus, red phosphorus, and zinc oxide-hexachloroethane-aluminum. Because only limited amounts of appropriate data are available for the uncertainty analysis, the conclusions drawn from this analysis must be considered tentative.

2. Measurement of Smoke Munition Emissions

2.1 Wind Tunnel Experiments

The most detailed measurement of emission rates of submunitions were conducted in wind tunnel experiments. Although field measurements have been collected, these data are not adequate for developing a model. Thus, the model used to predict emission rates is based on the wind tunnel experiments. The experiments and the data described in this section are summarized from DPG (1978).

The wind tunnel experiments were conducted at the Dugway wind tunnel. In the experiments, single submunitions (e.g., an individual component which contains the smoke producing compound) of zinc and white phosphorus were burned. In actual field use of smoke munitions, multiple submunitions are loaded into a canister and burn simultaneously. For red phosphorus, three submunitions (wedges) were burned simultaneously. The wind tunnel tests were conducted at a wind speed of 2 m/s and the ambient temperature, relative humidity, (%RH), and barometric pressures were recorded. Pre-weighed submunitions were placed on a load cell in the center line of the tunnel and fired remotely. The load cell recorded the elapsed time and weight loss of the submunition as it burned. The end of the tunnel had a barrier that contained a grid of holes through which the air in the tunnel passed. The air passed into sampling lines and through collection devices, impingers. (See Figure B-1.) The impingers were then analyzed for zinc or phosphorus, the appropriate active ingredient. The concentrations in all impingers were summed to determine the total amount of active ingredient which had been aerosolized during the burn. Data collected on each test included: weight loss with burn time, total zinc or phosphorus, tunnel wind speed, temperature, and relative humidity.

CROSS SECTION
Sampling Grid

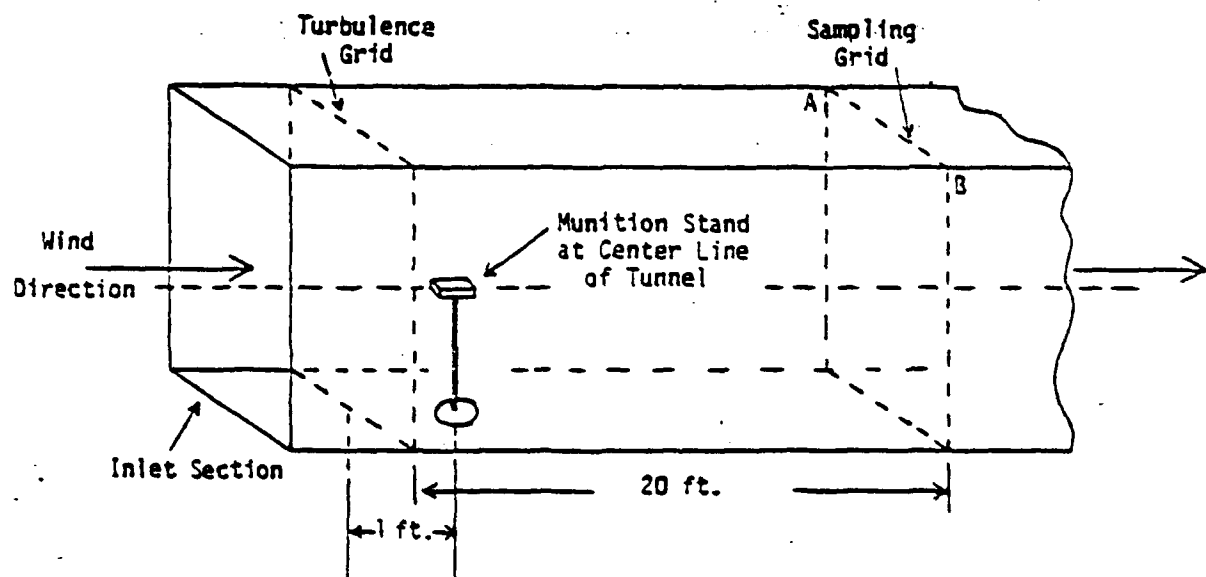
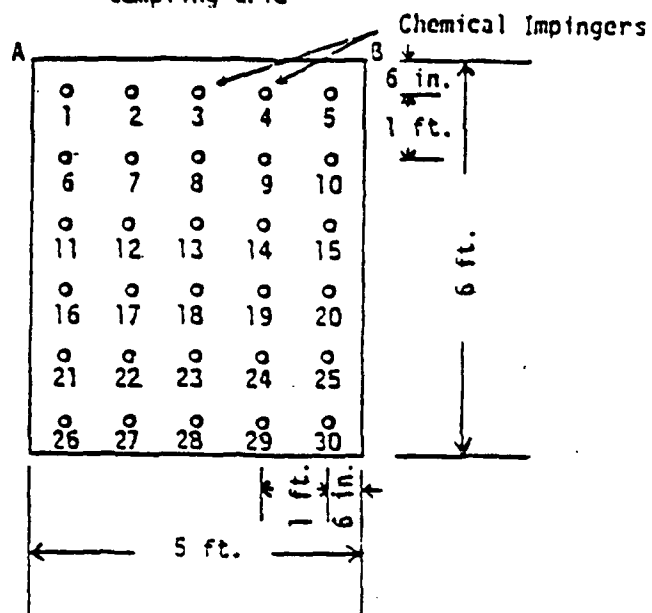


Figure B-1. Diagram of Wind Tunnel.

Source: DPG, 1978

Transmittance, which is routinely measured in the field, cannot be measured in the wind tunnel because the concentrations are too high. The types of submunitions tested (as reported in DPG (1978)) were:

155mm HC M1 Canister (zinc)
155mm HC M2 Canister (zinc)
105mm HC M1 Canister (zinc)
6 inch WP Wick (white phosphorus)
2.75 inch Rocket WP Wick (white phosphorus)
81mm Navy RP Wedge (red phosphorus)
155mm Navy RP Wedge (red phosphorus)
81mm German RP Wedge (red phosphorus).

For each type of submunition, two burns were conducted.

2.2 Field Experiments

The field experiments were conducted at the Horizontal Grid, Dugway Proving Ground, Utah. The experiments described in this section are summarized from DPG (1978). The data were collected by means of photography, aerosol sampling with aerosol photometers, particle size analyzers, and impingers. Samplers were located 1.22 meters above the ground. Motion pictures recorded the size and shape of the smoke cloud; aerosol photometers recorded total particle concentration; particle size analyzers recorded size distributions; and impingers measured zinc or phosphorus concentrations. The mass of zinc or phosphorus from these impingers cannot be summed to calculate total zinc or phosphorus aerosolized as was done in the wind tunnel experiments because the total smoke cloud is not collected by the impingers.

Figure B-2 (DPG, 1978) shows the layout of the instruments for these experiments. The sampling line was always oriented perpendicular ($\pm 45^\circ$) to the prevailing wind direction. The impingers were located halfway between the aerosol photometers. As in the wind tunnel experiments, the munitions were placed in a load cell so that data on weight loss with burn time were recorded. The types of submunitions tested were the same as those used in the wind tunnel experiments. For each type of submunition, two burns were conducted.

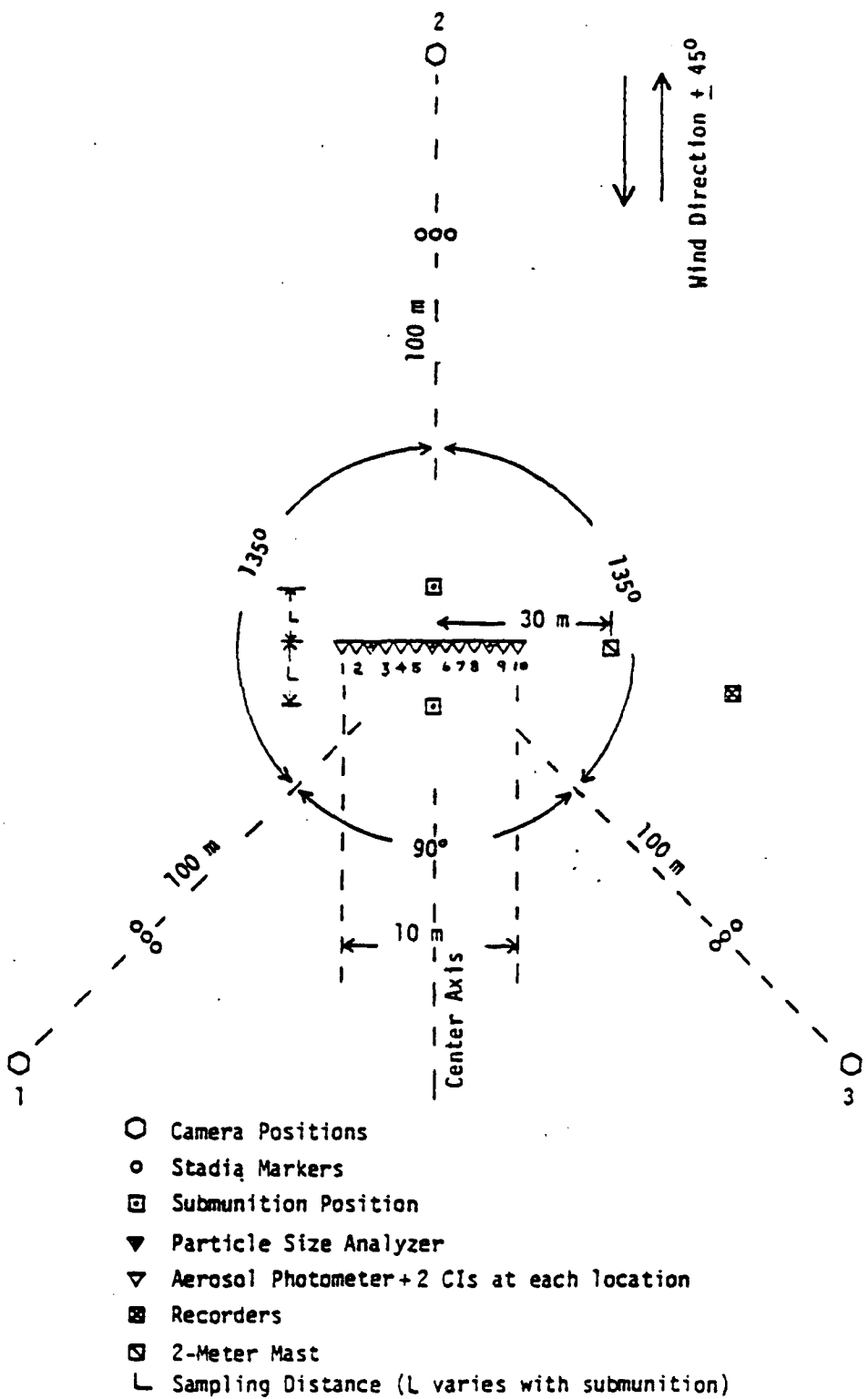


Figure B-2. Grid for munition cloud characterization. Source: DPG, 1978

The meteorological data recorded in these experiments included: wind speed and direction, temperature, and relative humidity.

3. The Emission Rate Expression

The critical parameter to be derived from these experiments is the amount of smoke generated per second of burn time. In its simplest form, this would be calculated by dividing the mass lost by the burn time to derive a value in units of grams per second. However, the amount of smoke generated is more than a function of the mass burned; it is also a function of the interaction of the zinc or phosphorus with water vapor to create the smoke. Zinc and phosphorus are hydroscopic, absorbing upwards of four times their mass in water vapor. Thus, the actual emission rate of interest is total amount of hydrated smoke generated per second. To add one further complexity to the equation, the burn rate of the munitions is not constant with time. There is an initial growth period, followed by a plateau of relatively constant rate of emissions, followed by a rapid decline. In field tests, there are data which indicate munitions can burn unevenly; this is characterized as "flashing" toward the end of the burn time by the observers.

The following discussion covers two topics. The first topic presents the parameters in the emission rate expression and the second discusses the uncertainty associated with those parameters and presents a technique for computing the uncertainty in the overall emission rate value.

3.1 Input Parameters

The emission rate of hydrated smoke is a function of the initial mass of the munition, the fraction of this mass which is the aerosolized zinc or phosphorus, the increase in mass of the aerosol due to hydration, and burn time. The expression which was developed from the wind tunnel experiments to estimate the emission rate is as follows (DPG, 1978):

$$Q_e = M_0 \text{ MYF } YF(A/t_b + 2Bt/t_b^2 + 3Ct^2/t_b^3 + 4Dt^3/t_b^4) \quad (\text{B-1})$$

where: Q_t = mass emission rate
 M_0 = initial mass
MYF = munition yield factor
YF = yield factor
A, B, C, D = coefficients which are determined by fitting the observed data in the wind tunnel experiments to a curve.
They are constrained to sum to unity.

The munition yield factor, MYF, is the ratio of the mass of zinc or phosphorus burned, M_x , to the initial mass of the munition, M_0 . M_x is determined from the wind tunnel experiments and is calculated by summing the mass of zinc or phosphorus collected by all the impingers. These wind tunnel values of M_x are used to predict the emission rate, Q_t , for field experiments, as M_x cannot be measured in the field setting.

The yield factor takes into account the hydroscopic growth of the aerosolized zinc or phosphorus and is a function of ambient relative humidity. For the three different types of smoke munitions, yield factors are based on theoretical calculations or experimental data. The conceptual definition of the yield factor is:

$$YF = \frac{\text{mass of smoke (including aerosol)}}{\text{mass of starting material}}$$

In the case of phosphorus, the final material is primarily hydrated orthophosphoric acid, $(H_3PO_4 + nH_2O)$. According to DPG (1977), it is assumed that the hydration of the droplets of H_3PO_4 proceeds until their aqueous vapor pressure equals the partial pressure of H_2O in the atmosphere. The mass of hydrated H_3PO_4 is then constant (assuming no other environmental changes occur) and the yield factor can be expressed as:

$$YF = \frac{\text{mass } H_3PO_4 + nH_2O}{\text{mass P}}$$

DPG (1977) contains the following example of how a yield factor is calculated. Yield factors for phosphorus can be readily computed from tables correlating aqueous vapor pressures with the composition of various mixtures

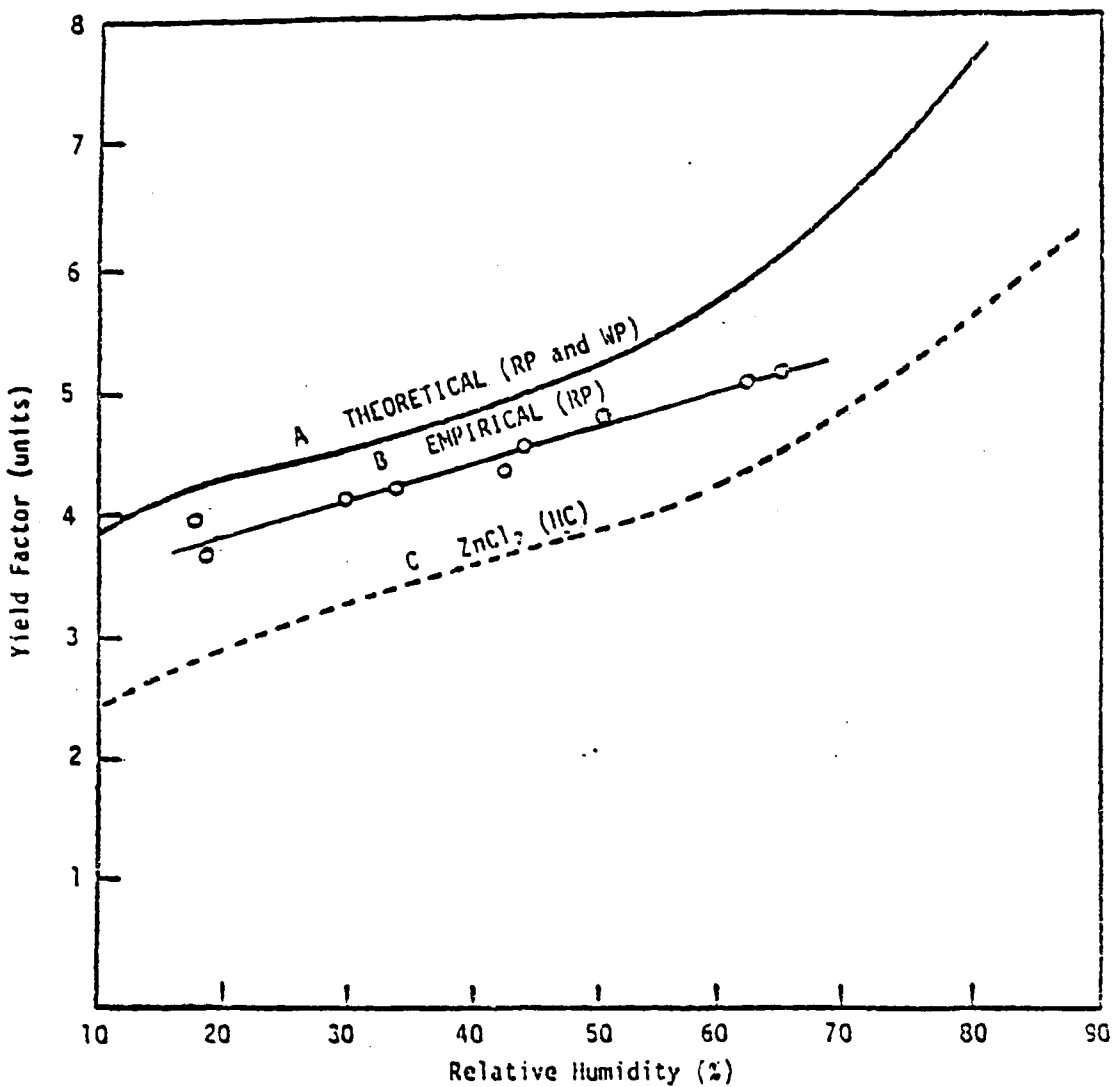
of H_3PO_4 , when the concentration of H_3PO_4 in the solution is expressed as weight %, (i.e., mass (H_3PO_4) \times 100/mass ($H_3PO_4 + nH_2O$)). For a specified aqueous vapor pressure, the ratio of the molecular weight of H_3PO_4 to the atomic weight of P is 3.16:

$$YF = \frac{100 \times 3.16}{H_3PO_4 \text{ (wt \%)} } = \frac{316}{H_3PO_4 \text{ (wt \%)} }$$

Taking, as an example, the burning of 1 gram of P in the air at 25°C and containing moisture at a partial pressure of 22.39 mmHg, the oxidation to phosphoric oxide and hydrolysis of phosphoric oxide will result in $1 \times 98/31$ gram or 3.16 gram H_3PO_4 . H_3PO_4 will then hydrate until the aqueous vapor pressure of the diluted H_3PO_4 ($H_3PO_4 + nH_2O$) equals the ambient vapor pressure. At 22.39 mmHg and 25°C, the equilibrium composition of the mixture is found to be 20.07 weight % H_3PO_4 . The YF is then $316/20.07 = 15.7$, (i.e., under these conditions, the mass of smoke is 15.7 gram for every gram of P burned). An additional correction will be necessary if the munition efficiency is not 100%.

DPG (1978) notes that the theoretical curve for phosphorus assumes that orthophosphoric acid is produced immediately during combustion. If this assumption does not hold, the yield factor may overestimate the effective dosage. DPG (1977) also presents a derivation which proves that YF's are insensitive to temperature up to 100°C.

Figure B-3 (DPG, 1978) presents yield factor curves based on theoretical calculations for P as well as empirical data for red phosphorus and theoretical calculations for zinc oxide-hexachloroethane-aluminum (HC). It can be seen from these figures that the slope of the lines for all three materials, white phosphorus, red phosphorus, and the zinc based munition, is relatively shallow over the range of relative humidity from approximately 20% to 65%. For example, over the range of 20% to 65% RH, the yield factor for red phosphorus increases by a factor of 1.4. However, the theoretical curves rise sharply at humidities greater than 65%. Between humidity levels of 65% to 80% red and white phosphorus increase by a factor of approximately 1.3 and hydrated zinc chloride by a factor of 1.7. For field tests conducted on one day, the relative humidity would not be expected to vary over this wide a range, so that



- Curve A: Yield factors for the conversion of P to hydrated H_3PO_4 (ref. 8).
 Curve B: Yield factors empirically determined for RP.
 Curve C: Yield factors for the conversion of Zn to hydrated $ZnCl_2$ (ref. 5).

Figure B-3. Yield factors as a function of relative humidity for various smoke producing agents. Source: DPG, 1978.

the yield factor between burns should not vary substantially. For example, an increase from 40% to 50% RH only produces a difference in the yield factor of 1.04 for red phosphorus. During the field experiments, which took place on several different days, the relative humidity varied from 40% to 80%, but within a given day the RH only varied by 2%-4%.

3.2 Approach to Estimating Uncertainty in the Emission Rate

A direct method for determining uncertainty values would be to compare modeled emission rates with actual emission rates; however, emission rate measurements from the field experiments are not available. In the absence of actual data, uncertainty values can be modeled based on estimated uncertainty values for the input parameters and on the uncertainty inherent in the emissions rate model. To estimate uncertainty values for the variables, there should be sufficient data available to calculate the probability density functions (i.e., measures of variability) of the input variables. To model the uncertainty in the emission rate model, an assumption must be made regarding the independence or dependence of the variables in the model, as there are different approaches for each case.

The following discussion presents both a qualitative and quantitative assessment of the emission rate uncertainty of the various smoke munitions. The qualitative assessment highlights the sources of uncertainty of the input parameters to the emission rate model and the limitations imposed by the amount of data (for each type of munition) available for the analysis. The quantitative assessment presents a model for estimating the emission rate uncertainty and an example application for several munitions.

Two factors limit the uncertainty analysis of the smoke munitions data. First, too few experiments were conducted for each type of munition to determine robust probability density functions for the various parameters. For both wind tunnel and field experiments only two burns were conducted for each type of submunition, thus means or variances will not be stable or robust. Confidence intervals are large when $n = 2$. Therefore the quantitative uncertainty analysis presented subsequently is neither a precise nor an accurate measure of uncertainty, but the method is valid with sufficient data.

Second, the data from the wind tunnel experiment are suspect. For five of the nine munitions tested in the wind tunnel, the mass of aerosolized active ingredient, M_x , as measured by the bubblers exceeded the mass burned, ΔM , as measured by the load cell on which the munition was placed. This clearly violates the law of conservation of mass. There are two plausible hypotheses for these results. First, the design of the wind tunnel is suspect. It has been observed that there may have been insufficient downwind distance from the load cell to establish laminar flow at the sampling point (Carter, (1991), personal communication). Second, the wind speed was measured at only one location and the assumption of constant velocity may not be correct (Bowers, (1991), personal communication). Either or both of these situations could have led to an overestimation of air velocity at the point of sampling. Although this condition most likely existed for all tests, it was not evident in the data from the three types of zinc oxide-hexachloroethane-aluminum (HC) smoke munitions (155mm M1 and M2 and the 105mm canisters) and one red phosphorus (RP) munition (81mm Navy wedge). (This observation is based on data reported in DPG, 1978.) The reason for the differences between munitions is not readily evident, and it is not possible to ascertain given the age of the data. The error associated with the inaccuracy of the bubbler data will affect all field experiment data because of the fundamental assumption in the emission rate model. Namely, the MYF relationship (the ratio of the mass of active ingredient aerosolized, M_x , to the initial mass of the munition, M_0), as measured in the wind tunnel experiments, is assumed to apply to the field experiments. As the wind tunnel tests overestimated the MYF, the emission rate, Q_t , would also be overestimated.

A simple analysis was performed to (1) determine if there was a consistent bias in the data which could be used to adjust the mass aerosolized, M_x , and the MYF for those munitions where M_x was greater than the mass burned, ΔM , and (2) evaluate the within munition variability for M_x and ΔM . The computation performed was:

$$\text{bias} = 1 - M_x / \Delta M$$

where a negative value indicates the mass of Zn or P aerosolized is greater than the mass burned and a positive value indicates this relationship is reversed.

The data were taken from DPG (1978) and the results are shown in Table B-1. The first five entries in the table are for the munitions where M_x , the mass of Zn or P aerosolized, exceeds ΔM mass burned; the next four entries are for munitions where M_x is less than ΔM . For one munition, the 155mm RP Navy Wedge, in one test result M_x was less than ΔM and for the second test M_x was greater than ΔM . The reason for this anomaly within a munition type is not clearly evident. It can be observed from this table that for munitions where the mass of Zn or P is less than the mass burned, the within munition variability is relatively small, less than 20%. However, for the munitions where the mass of Zn or P is greater than the mass burned, the within variability was much larger, ranging from approximately 45%-88%. Because the within munition variability is so large for those cases when M_x is greater than ΔM , it is not appropriate to adjust M_x or MYF for these munitions.

Three conclusions can be made based on this analysis. First, those munitions for which the mass of Zn or P aerosolized exceeds the mass burned will be dropped from further analysis because the data violate the law of conservation of mass and the large within munition variability precludes adjusting the original data. Second, the results indicate that there may be another source of error affecting the data in addition to the wind tunnel design. One would anticipate that the design error would affect all munitions equally, however, this is clearly not the case. There could appear to be other sources of variation related to the type of munition (e.g., mass aerosolized is less than mass burned is for all of the zinc canister munitions). Or there may have been some other source of experimental error associated with the operation of the wind tunnel or in the analyses of the bubblers. These additional sources of error cannot be evaluated further due to the age of the data. Third, if one assumes that the affect of the wind tunnel design on the munitions is constant across all experiments, then it must be concluded that M_x , the mass of Zn or P aerosolized, is overestimated for all munitions even if M_x is less than ΔM , the mass burned. It follows then that the MYF, which is the ratio of mass aerosolized to mass burned, is overestimated for all munitions.

To estimate the uncertainty in the emission rate model the issue of independence or dependence of the variables must be considered. The

Table B-1
Evaluating Wind Tunnel Bias

		Initial Mass (M _o)	Mass burned (ΔM)	Mass ¹ Aerosolized (M _x)	Bias ²
2.75" WP Wedge	A9	217	125	150	-.20
	A10	203	116	129	-.11
6" WP Wick	A5	102	59	64	-.09
	A6	101	51	77	-.51
3" WP Wick	A7	63	40	45	-.13
	A8	52	36	Void	
155mm RP Navy Wedge	A15	114	78	72	+.08
	A16	117	69	79	-.15
81mm RP German Wedge	A11	30	15	24	-.60
	A14	35	14	15	-.07
155mm HC M1 Canister	A1	3450	2330	425	+.82
	A2	3572	2412	382	+.84
155mm HC M2 Canister	A12	2055	1162	369	+.68
	A13	1987	1182	391	+.67
105mm HC Canister	A3	1178	646	154	+.76
	A4	1177	633	234	+.63
81mm Navy RP Wedge	A17	117	73	64	+.12
	A18	116	68	61	+.10

¹ Zn or P

² Bias = 1 - $\frac{M_x}{\Delta M}$

assumption of independence allows one to use a relatively simple expression to calculate overall model uncertainty as the covariance terms can be neglected. However, if this assumption is incorrect and the variables are dependent, the estimated uncertainty will be unrealistically low.

In the case where the variables can be assumed to be independent, Goodman (1960) presents the expression:

$$\sigma_{xy}^2 = \bar{x}^2 \sigma_y^2 + \bar{y}^2 \sigma_x^2 = (\bar{xy})^2 [CV_x^2 + CV_y^2] \quad (B-2)$$

where σ_{xy}^2 = variance of the product xy

\bar{x} = mean of x

σ_x^2 = variance of $X = \frac{\sum(x - \bar{x})^2}{n - 1}$

\bar{y} = mean of Y

σ_y^2 = variance of Y

CV_x^2 = squared coefficient of variation of x , $\frac{\sigma_x^2}{\bar{x}^2}$

CV_y^2 = squared coefficient of variation of y , $\frac{\sigma_y^2}{\bar{y}^2}$

The variables in the emission rate model (see equation B-1) are not independent, both the munition yield fraction, MYF, and the yield fraction, YF, depend on the type of active ingredient. The variance of the product of two or more variables, which are not independent, is given as (Goodman, 1960):

$$\sigma_{xy}^2 = \bar{x}^2 \sigma_y^2 + \bar{y}^2 \sigma_x^2 + 2\bar{x}\bar{y}(\text{COV}_{xy})$$

where the variables are defined as above and COV_{xy} , the covariance of xy , is expressed as:

$$\text{COV}_{xy} = \sigma_x \sigma_y = \frac{1}{N} \sum_{i=1}^N (x_i - \bar{x})(y_i - \bar{y}) = \frac{1}{N} \sum_{i=1}^N (x_i - \bar{x})(y_i - \bar{y}) - \bar{x}\bar{y} \quad (B-3)$$

To apply Equation (B-2) to the model for Q_t , the emission rate, integrating over the total burn time, it is written as:

$$Q = \int_0^{t_b} dt Q_t = M_0 \cdot MYF \cdot YF \quad (B-4)$$

Let $E = MYF$ and $Y = YF$. Assuming the uncertainty associated with the initial mass, M_0 , is small (i.e., the load cell is accurate), Q_t can be divided by M_0 and expressed as q

$$q = \frac{Q_t}{M_0} = E \cdot Y \quad (B-5)$$

The variance of $q(\sigma_q^2)$ is

$$\sigma_q^2 = \bar{Y} \sigma_E^2 + \bar{E} \sigma_Y^2 + 2\bar{E} \bar{Y} \text{COV}_{EY} \quad (B-6)$$

where COV_{EY} is the covariance of the munition yield fraction, now expressed as E , with the yield factor, now expressed as Y . Since the yield factor is a function of the relative humidity ($Y = Y(h)$ where h is fractional relative humidity), this value can be incorporated into the expression for σ_q^2 as follows:

$$\sigma_q^2 = \bar{Y} \sigma_E^2 + \bar{E} Y' \sigma_h^2 + 2\bar{E} \bar{Y} Y' \text{COV}_{Eh} \quad (B-7)$$

The fractional relative humidity, h , is = 0 at zero humidity and 1 at 100% humidity and Y' is defined as:

$$Y' = \left. \frac{\Delta y}{\Delta h} \right|_{h=\bar{h}} \quad (B-8)$$

As there are only two values for each munition, Y' is simply the slope of the straight line between the two points. The term COV_{Eh} is the covariance of the munition yield fraction (E) with relative humidity (h).

3.3 Results of Uncertainty Analysis

Table B-2 presents a sample set of data taken from DPG (1978) and used to calculate the variance of the quantity Q_t/M_o , expressed as σ_q^2 . The munitions included in this analysis were only those where the mass of Zn or P aerosolized, M_x , was less than mass burned, ΔM , as discussed previously. An example of how the variance of Q_t/M_o (or σ_q^2) is calculated is given below for the zinc munition 155mm HC M1 canister.

Step 1. Calculate the covariance of the munition yield fraction (E) and relative humidity (h) for trials B1R1 and B2R1. The values for E and h are given in Table B-2. Equation B-3 is the definitional formula for covariance; the computation formula is:

$$\text{COV}_{E,h} = \frac{N(\Sigma E \cdot h) - (\Sigma E)(\Sigma h)}{N^2}$$

$$\begin{aligned}\text{COV}_{E,h} &= \frac{2([0.12 \times 0.76] + [0.11 \times 0.72]) - ([0.12 + 0.11][0.76 + 0.72])}{2^2} \\ &= \frac{0.3408 - 0.3404}{4} \\ &= 1 \times 10^{-4}\end{aligned}$$

Step 2. Calculate Y' according to Equation B-8 where y, the yield factors (YF), are 5.2 and 5.0, and h, the fractional relative humidity, is 0.76 and 0.72.

$$\begin{aligned}Y' &= \frac{\Delta y}{\Delta h} \\ &= \frac{5.2 - 5.0}{0.76 - 0.72} \\ &= 5\end{aligned}$$

Table B-2^a

Variance of the Ratio of the Emission Rate to the Initial
 Mass, (Q_t/M_0) for Selected Munitions

Munition	Trial	Munition ^b Yield Fraction	Relative Humidity	Yield ^c Factor	Variance of Q_t/M_0
155mm HC M1 Canister	B1R1	.12	76	5.2	2.15×10^{-3}
	B2R1	.11	72	5.0	
155mm HC M2 Canister	B3R1	.18	75	5.2	5.41×10^{-3}
	B4R1	.20	75	5.2	
105mm HC Canister	B15	.13	73	5.1	4.68×10^{-2}
	B16	.19	73	5.1	
81mm Navy RP Wedge	B11	.55	70	6.6	0.160
	B12	.52	80	7.8	

- a. Data taken from Tables III and IV in DPG (1978) for the field experiments conducted at the horizontal grid.
- b. MYF values are from the wind tunnel data for the particular munitions.
- c. Estimated values from Figure B-3 for ZnCl₂ (Curve C) and for the theoretical curve for white phosphorus and red phosphorus (Curve A).

Step 3. Calculate σ_q^2 according to Equation B-7. The variance of E, the munition yield fraction, is

$$\sigma_E^2 = 2 \times 10^{-4}. \text{ Equation B-7 is as follows:}$$

$$\sigma_q^2 = \bar{Y} \sigma_E^2 + \bar{E} Y' \sigma_h^2 + 2\bar{E} \bar{Y} Y' \text{COV}_{Eh}$$

and by making the following substitutions:

$$\begin{aligned}\sigma_q^2 &= (5.1)^2 (5 \times 10^{-5}) + (0.115)^2 (5)^2 (8 \times 10^{-4}) + 2(0.115)(5.1) \\ &\quad (5)(1 \times 10^{-4}) \\ &= 2.15 \times 10^{-3}\end{aligned}$$

Interpretation of the variance estimates is limited by the potential error in the munition yield fraction (MYF) values and the limited amount of data ($n = 2$) for each type of munition. However, some summary comments can be made about these data and this approach to calculating variance. The variance of the 81mm Navy red phosphorus wedge is larger than the three zinc based munitions (zinc oxide-hexachloroethane-aluminum). The cause of this difference could be due to the type of munition. For example, the red phosphorus MYF is larger than the MYF for zinc munitions. Further, for phosphorus munitions the relative humidity on the two days of red phosphorus tests differed by 10% whereas for two of the zinc munition tests it was constant. If there is no variation in relative humidity the variance of q is the product of the mean of the yield factor and the variance of the MYF (see Equation B-7).

Bevington (1969) defines the standard deviation, σ , as the estimated error or uncertainty of a parameter. When a parameter, e.g., x , is a function of two or more other variables ($x = ab$) the standard deviations of a and b, when combined, give the uncertainty of x . To put the standard deviation values for each munition in perspective, Table B-3 presents the mean emission rates integrated over time, the standard deviation, σ , (as calculated according to Equation B-7), and the standard deviation expressed as a percentage of the mean. This table shows that the emission rates of the two 155mm HC (zinc) canisters (M1 and M2) have the least uncertainty and the 105mm HC (zinc) wedge has the greatest uncertainty. The uncertainty of the 81mm Navy RP wedge is only slightly greater than the 155mm HC canisters.

Table B-3
Comparison of the Mean and Standard Deviation

of the Ratio of the Emission Rate to the Initial Mass

$$\left(\frac{Q_t}{M_0} \right)$$

Munition	Mean $\frac{Q_t}{M_0}$	Standard Deviation of $\frac{Q_t}{M_0}$	Standard Deviation as a % of the mean
155mm HC M1 Canister	0.587	0.046	7.8
155mm HC M2 Canister	0.962	0.074	7.7
105mm HC Canister	0.817	0.216	26.6
81mm Navy RP Wedge	3.844	0.40	10.4

* Q_t is integrated over the burn time, thus the quantity $\frac{Q_t}{M_0}$ is actually

$$\frac{Q_t}{M_b} \cdot t_b$$

An approach to evaluating emission test results from future experiments would be to compute the 95% confidence interval ($95\% \text{ CI} = \bar{x} \pm 1.96\sigma$) of the quantity $\frac{Q_t}{M_o}$ for each munition. If a subsequent experiment produced a $\frac{Q_t}{M_o}$ value outside of the confidence interval, than it could be concluded that the munition was significantly different from the original sample of munitions. Ideally, a larger dataset than that currently available would be necessary to assure that the standard deviations were stable.

An interesting comparison can be made between these results and the findings presented in *Methodology Investigation Final Report, Validation of Transport and Dispersion Model for Smoke* (DPG, 1979). In DPG, (1979), modeled concentrations along the line of sight (CL) were compared to field measurements as well as comparisons between measured and modeled concentration line integrated dosage (CLID). DPG (1979) reports that the CLID were consistently underpredicted for the zinc based munitions (HC) by a factor of 1.4-1.5 and overpredicted by a factor of 2 for the red and white phosphorus munitions. A comparison of these air dispersion modeling results to standard deviations of the source term (presented in Table B-3) shows a similar relationship among munitions. The zinc based munitions exhibited less variability than the red phosphorus munition. One hypothesis which could partially explain the discrepancies in the modeled versus measured comparisons in DPG (1979) is uncertainty in source terms. The red phosphorus has the largest uncertainty (as measured by the standard deviation) and it also shows the greatest difference between measured and modeled values. The large uncertainty in the red phosphorus source term may account for a portion of the uncertainty in the modeled red phosphorus concentrations.

4. Conclusions and Recommendations

The smoke munitions data from DPG (1978) have been reviewed and a method for estimating uncertainty, as expressed as the standard deviation, in the emission rates has been presented. Available data for the present analysis is limited, but the approach to variance estimation is applicable to larger data sets. The quality of the smoke munitions data is suspect due to design problems with the wind tunnel. The number of tests conducted on each munition, $n = 2$, means the variance computations are not stable. The uncertainty

analysis of the source terms indicated that the 105mm HC munition has the largest uncertainty, being slightly more than 3 times the uncertainty of the 155mm HC munitions and 2.6 times the 81mm Navy RP wedge. For the two 155mm HC canisters, the relative humidity was constant for the M2 test runs and varied for the M1 test runs. However, when uncertainty is expressed by the standard deviation as a percent of the mean, the two munitions have almost the same uncertainty.

Two recommendations can be made based on the preceding analysis. First, the munition yield factor should be determined in an accurate and precise manner. This variable is critical, as it is applied to all the field test data. Second, to assess meaningfully the uncertainty in the emission rate values, more than two sets of data must be available for the results to be more stable, and thus reliable.

To use this technique of computing variance to evaluate munition variability, the following plan is suggested. Assuming the wind tunnel design issue has been resolved and accurate MYF's determined, field data from numerous test burns should be collected. This should be done at the horizontal grid, but without simultaneous aerosol and meteorological monitoring. This is because to compute uncertainty for the emission rate value, the only parameters needed are initial weight, M_0 , munition yield fraction, and yield factor (as computed based on relative humidity); thus only M_0 and %RH would need to be recorded. Numerous burns for each type of munition should be conducted, e.g., $N = 30$. Tests should be conducted under as wide a range of humidities as possible. Such a database could then be used to compute robust variance and 95% confidence intervals. Subsequent test results would be compared to this confidence interval to determine if the emission rate is statistically different. Further, with sufficient data to compute stable variances, these values could be incorporated into an expression with meteorological variances to compute overall model uncertainty.

References

- Bevington, P.R., 1969: *Data Reduction and Error Analysis for the Physical Sciences*, McGraw-Hill Book Co., NY.
- Carter, F.L., R.K. Dumbauld and J.E. Rafferty, 1979: Methodology Investigation, Final Report, Validation of Transport and Dispersion Model for Smoke, TECOM Project No. 7-CO-PB8-DP1-004, U.S. Army Dugway Proving Ground, Dugway, UT.
- DPG, 1977: Methodology Investigation for Testing Effectiveness of Smoke/Aerosol Munitions Pilot Study, Final Report, TECOM Project No. CO-RD6-DPI-005, U.S. Army Dugway Proving Ground, Dugway, UT.
- DPG, 1978: Basic Smoke Characterization Test, Final Report, TECOM Project No. 7-CO-RD7-DPI-001, U.S. Army Dugway Proving Ground, Dugway, UT.
- Goodman, L.A., 1960: On the exact variance of products, *J. of the American Statistical Assoc.*, 55, 708-713.

APPENDIX B-2

ANALYSIS OF FOG-OIL SMOKE EMISSIONS

Appendix B-2

Table of Contents

Analysis of Fog-Oil Smoke Emissions

	Page
1. Introduction	B-25
2. Method	B-25
3. Results	B-35
4. Conclusions	B-36

Appendix B-2
Analysis of Fog-Oil Smoke Emissions

1. Introduction

This analysis focuses on the fog-oil smoke generator emission rates as tested at the Dugway Proving Ground in March and April, 1985 (Liljegren et al., 1988). Liljegren et al. (1988) reported the details of how the experiment was conducted. Only the method of computing the emission rate will be addressed here. The objectives of this analysis are threefold: (1) to assess the variability in the emission rate from the fog-oil smoke generator, (2) to compare two methods of computing the emission rate, and (3) to evaluate the influence of averaging time on emission rate variability.

2. Method

The fog-oil smoke emission data were taken from Liljegren et al. (1988). The configuration of the smoke test provided for the "instantaneous" measurement of the emission rate based on the weight loss of the oil drum and the exit velocity of the generator. Due to mechanical difficulties, the weight loss values are actually 1-minute averages, as opposed to "instantaneous" values. Plots of these data (and exit temperature) versus time for seven experiments were reported in Figures 3.2 through 3.8 in Liljegren et al. (1988). (For reference, copies of those figures are included, with the original figure numbers.) These data were digitized and the means, \bar{x} , and standard deviations, σ , were computed for each experiment. These values and the coefficient of variation (σ/\bar{x}) for each test are presented in Table B-1. Some experiments were screened to remove values which were approximately zero at the end of the test. Otherwise, the data reflect the actual emissions for the duration of the experiment.

Liljegren et al. (1988) computed a time integrated emission rate based on the total mass of oil burned divided by the duration of operation of the smoke generator. These values, taken from Table 3.1, are shown in Table B-2.

To evaluate the influence of averaging time on the variability in the emission rate, the emission rates were re-calculated based on averaging times up to 510 seconds. To do this the data were processed through a program which

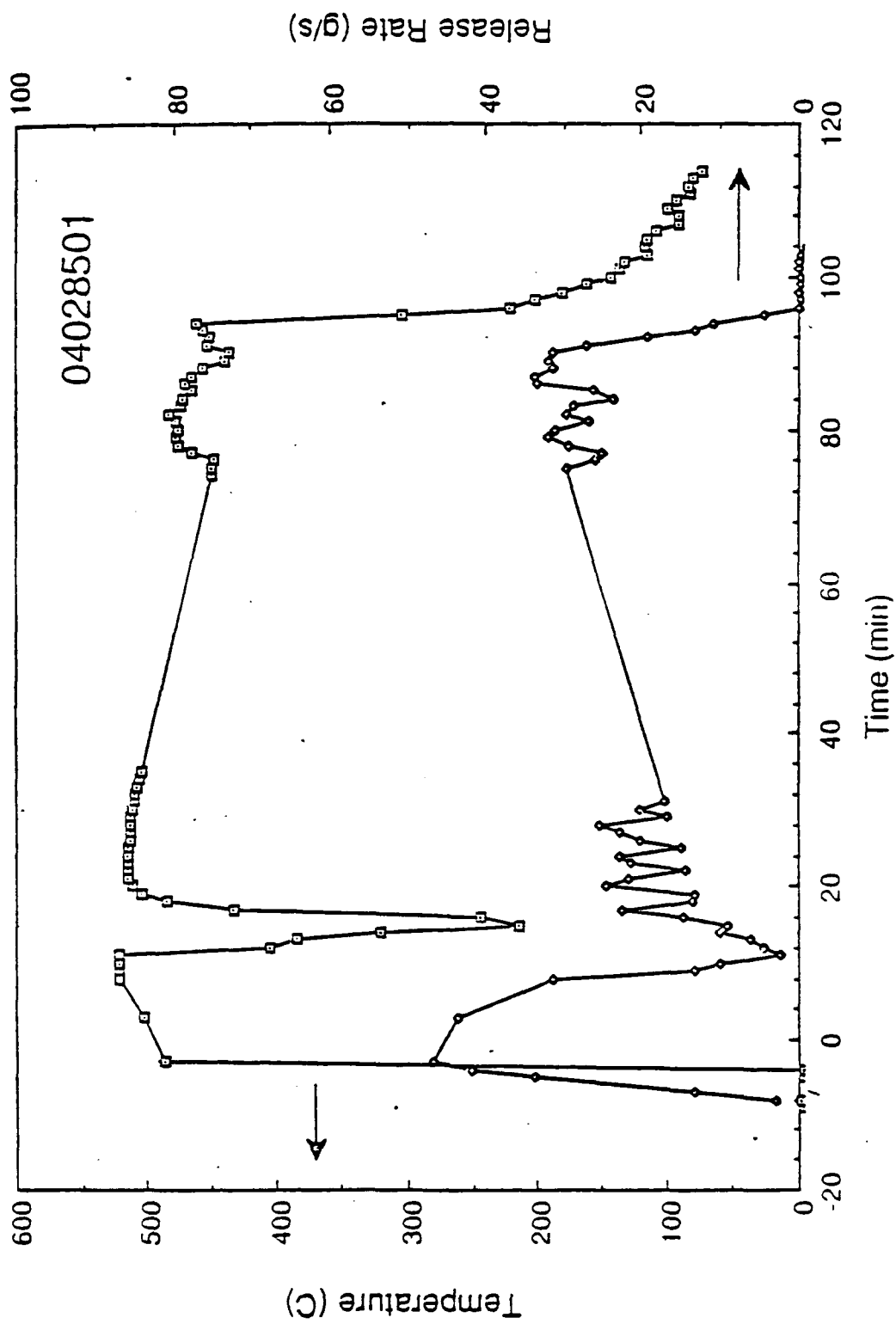
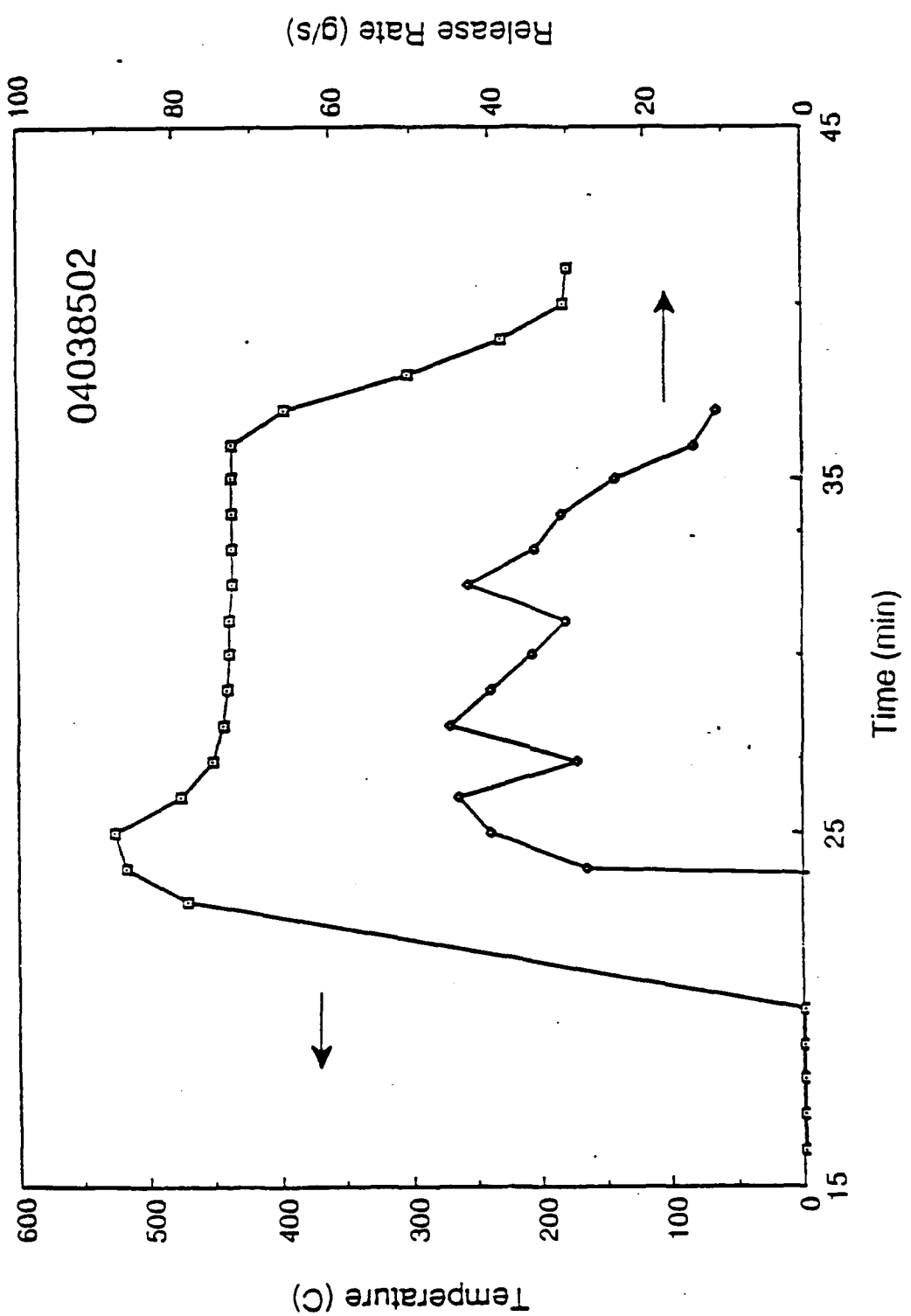


Figure 3.2. Exit Temperature ($^{\circ}$ C) and Release Rate (g/s) as a function of time for test 10003 (2 April 85).
 Missing data due to equipment failure (tape jam) "Taken from L.I.Jegren et al., (1988)".



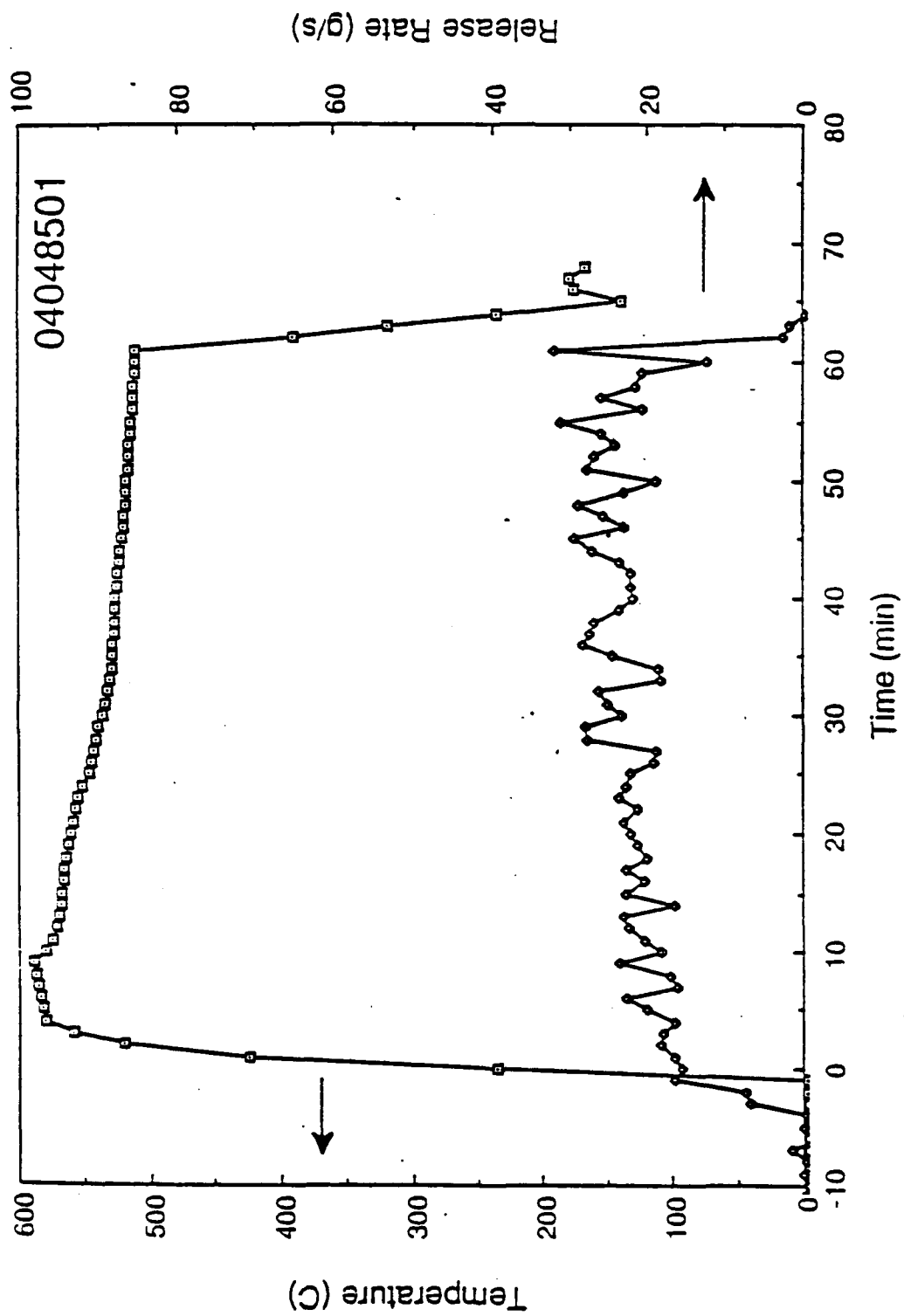


Figure 3.4. Exit Temperature (°C) and Release Rate (g/s) as a function of time for test T0005 (4 April 1985).
 "Taken from Lilljegren et al., (1988)".

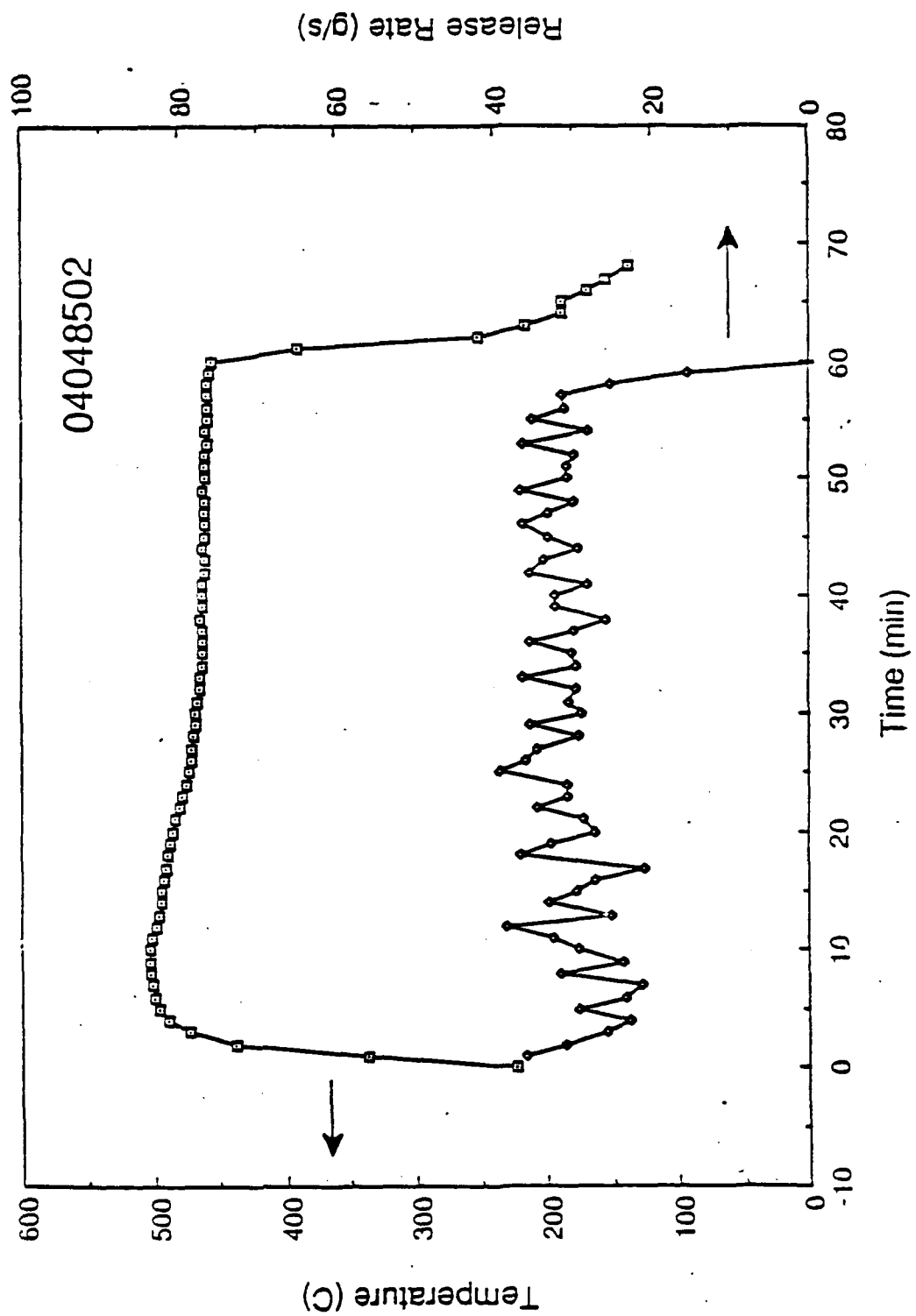


Figure 3.5. Exit Temperature ($^{\circ}\text{C}$) and Release Rate (g/s) as a function of time for test T0006 (4 April 1985).
"Taken from L.I. Legren et al., (1988)".

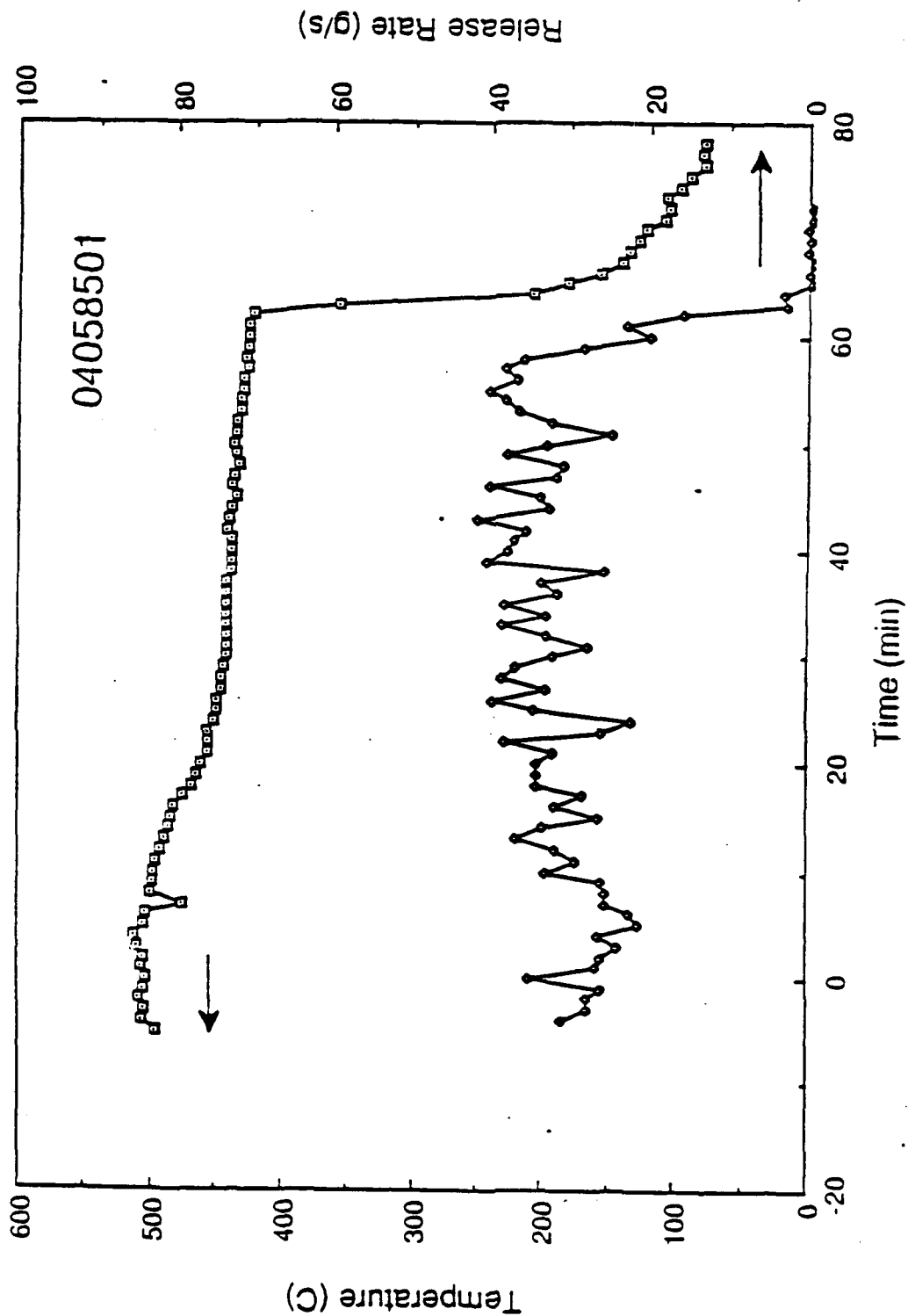
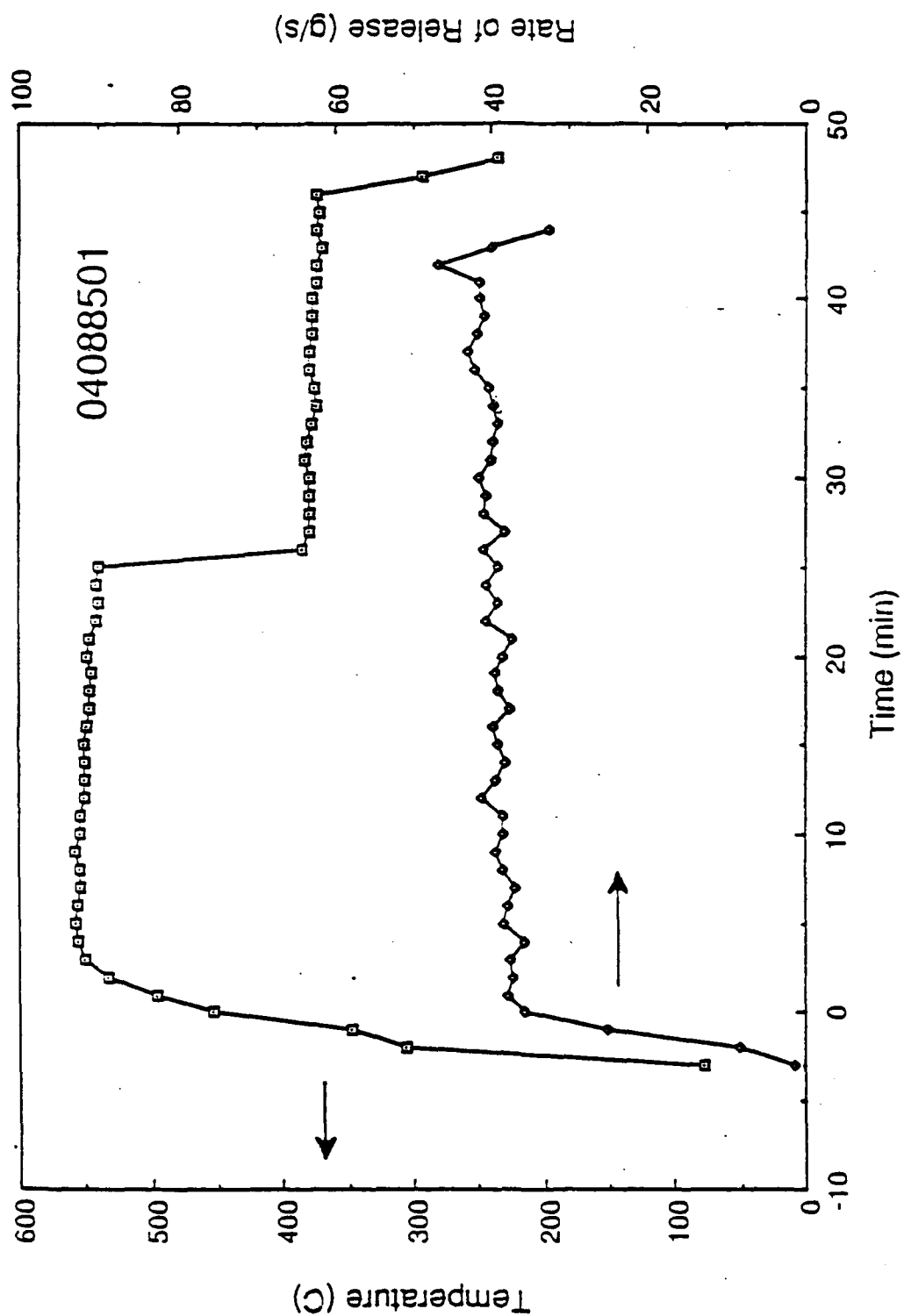


Figure 3.6. Exit Temperature ($^{\circ}$ C) and Release Rate (g/s) as a function of time for test T0007 (5 April 1985).
"Taken from Lijegren et al., (1988)".



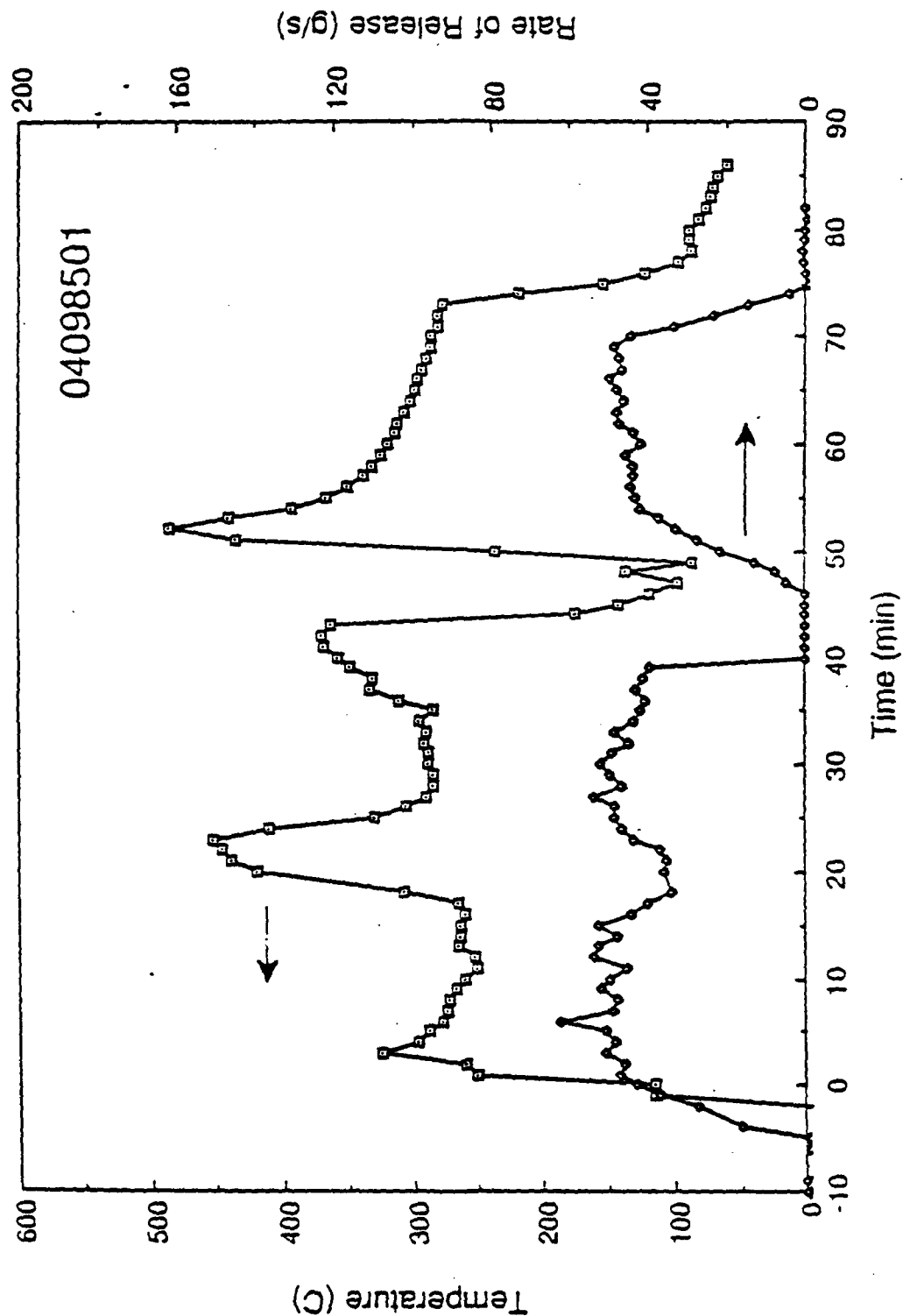


Figure 3.8. Exit Temperature ($^{\circ}\text{C}$) and release Rate (g/s) as a function of time for test 10009 (9 April 1985).
"Taken from L.J. Jegren et al., (1988)".

Table B-1

Variation in Instantaneous (i.e., one-minute averaged)
Fog-Oil Smoke Emission Rates

Figure No.	Test No.	Average Instantaneous Emission Rate (g/s)	Standard Deviation	Coefficient of Variation
3.2	T0003	21.7	10.9	0.5
3.3	T0004	33.8	8.9	0.3
3.4	T0005	21.5	5.9	0.3
3.5	T0006	31.1	4.2	0.1
3.6	T0007	30.9	7.5	0.2
3.7	T0008	37.9	7.5	0.2
3.8	T0009	37.9	16.8	0.4

Table B-2

Comparison of Integrated and Averaged Instantaneous Methods
of Calculating Emission Rates

Figure No.	Test No.	Integrated Emission Rate (g/s)	Average Instantaneous Emission Rate (g/s)	Percent Difference
3.2	T0003	24.3	21.7	-12
3.3	T0004	22.5	33.8	+33
3.4	T0005	22.4	21.5	-4
3.5	T0006	28.7	31.1	+8
3.6	T0007	30.7	30.9	-0.1
3.7	T0008	36.3	37.9	+6
3.8	T0009	43.2	37.9	-12

Taken from Liljegren et al., (1988), Table 3.1

interpolated the emission rate at 30 second intervals from the existing data which are at approximately one minute intervals. From this processed data, means and standard deviations were computed by grouping the data at 30 sec, 60 sec, 90 sec, etc. increments up to 510 seconds (8.5 minutes). To evaluate how the variability changed with averaging time, the following equation was used

$$R' = \left(\frac{\sigma_i \text{ sec}}{\sigma_{30 \text{ sec}}} \right) \quad (\text{B-1})$$

where σ_i is the standard deviation for the i -th averaging time ($i = 60$ sec, 90 sec, 120 sec, 510 sec) and $\sigma_{30 \text{ sec}}$ is the standard deviation from the 30 second averaging time.

3. Results

The first objective of this analysis is to evaluate the variance in the fog-oil generator emissions. Table B-1 shows that the variation in the emission rate, expressed as the standard deviation, can be large. The coefficient of variation (CV) normalizes the standard deviation by the mean. Test T0006 has the smallest CV - 0.1. Tests T0003 and T0009 have the largest CV's, 0.5 and 0.4 respectively. During these tests the smoke generator malfunctioned and the emissions were particularly erratic (see Figures 3.2 and 3.8).

The second objective of this analysis is to compare the methods for calculating the average emission rate. Table B-2 shows a comparison of the two methods of computing the mean emission rate. Liljegren et al. (1988) calculated the time integrated average by dividing the mass of oil burned by the duration of operation of the smoke generator. Our approach averaged the "instantaneous" 1 minute emission rates, as digitized from plots. The percent difference between the two methods ranges from -12% to +33%. The largest difference in the computed emission rates is for experiment T0004. A review of Figure 3.3 and the digitizing indicates that there were no errors in that step and that the mean rate of 33.8 g/sec accurately reflects the data in the plot. It is hypothesized that there may be an error in the field data relating to oil burned or duration of operation of the smoke generator, which may have caused Liljergren et al. to compute a lower emission rate. (In addition, Liljergren et al. note that the data for this experiment were divided into two groups based on a shift in wind direction. It is not clear

how this was done or if this would affect the emission rate calculation. The smallest difference was for T0007, an experiment when the smoke generator functioned in a very consistent mode (see Figure 3.6). There does not appear to be a bias in the Liljegren et al. method, with their approach producing a higher mean rate four times and a lower rate three times. The r^2 for the two methods of computing the emission rate is 0.56. This means the time integrated method of computing emissions can only account for 56% of the variance in the method based on averaging the "instantaneous" values.

The third objective of this analysis is to evaluate how the variability in the emission rate changes with averaging time. The data from five experiments, T0005 (Figure 3.4) through T0009 (Figure 3.8), were analyzed using equation (B-1). Two experiments, T0003 and T0004 (Figures 3.2 and 3.3, respectively), were excluded from this analysis due to insufficient data. Table B-3 presents the squared standard deviation ratios by averaging time for the five experiments as well as the median ratio for each averaging interval. These data are plotted in Figure B-1, with the solid line representing the median value and the minimum and maximums represented by the boxes.

A theoretical curve is also plotted in Figure B-1, representing the equation:

$$\frac{\sigma^2(T_a)}{\sigma^2(30s)} = \frac{1 + 30s/2T_I}{1 + T_a/2T_I} \quad (B-2)$$

where T_I is the integral time scale of the physical process. This equation is based on work by G. I. Taylor in the 1920's and is further discussed in Section VIII of the main text. This theory assumes that the time scales of the fluctuations cover a wide range of values, and the time series data in the figures verify that this is the case. An integral scale, T_I , of 150 seconds provides the best fit to the data in Table B-1.

4. Conclusions

This analysis shows that the variation in the one-minute averaged emission rate from the fog-oil smoke generator can vary from 10% to 50% of the mean rate, based on the coefficient of variation. From the comparison of the two methods of computing the emission rate, it appears that when the smoke

Table B-3

Variations in Emission Rate with Averaging Time

Averaging Times (s)	Squared Standard Deviation Ratios *					Median Ratio
	T0005	T0006	T0007	T0008	T0009	
30.	1.000	1.000	1.000	1.000	1.000	1.000
60.	0.879	0.848	0.934	0.922	0.950	0.9220
90.	0.858	0.746	0.837	0.806	0.932	0.8370
120.	0.738	0.605	0.745	0.774	0.872	0.7450
150.	0.639	0.465	0.695	0.823	0.823	0.6950
180.	0.649	0.473	0.696	0.697	0.818	0.6960
210.	0.609	0.415	0.574	0.716	0.804	0.6090
240.	0.652	0.388	0.537	0.551	0.752	0.5510
270.	0.627	0.460	0.574	0.560	0.747	0.5740
300.	0.554	0.356	0.534	0.524	0.636	0.5340
330.	0.544	0.319	0.506	0.483	0.666	0.5060
360.	0.523	0.267	0.518	0.670	0.742	0.5230
390.	0.529	0.300	0.484	0.426	0.498	0.4840
420.	0.557	0.334	0.537	0.680	0.391	0.5370
450.	0.481	0.303	0.484	0.411	0.384	0.4110
480.	0.510	0.278	0.436	0.469	0.573	0.4690
510.	0.492	0.318	0.444	0.700	0.650	0.4920

$$R' = \left(\frac{\sigma_i \text{ sec}}{\sigma_{30 \text{ sec}}} \right)^2$$

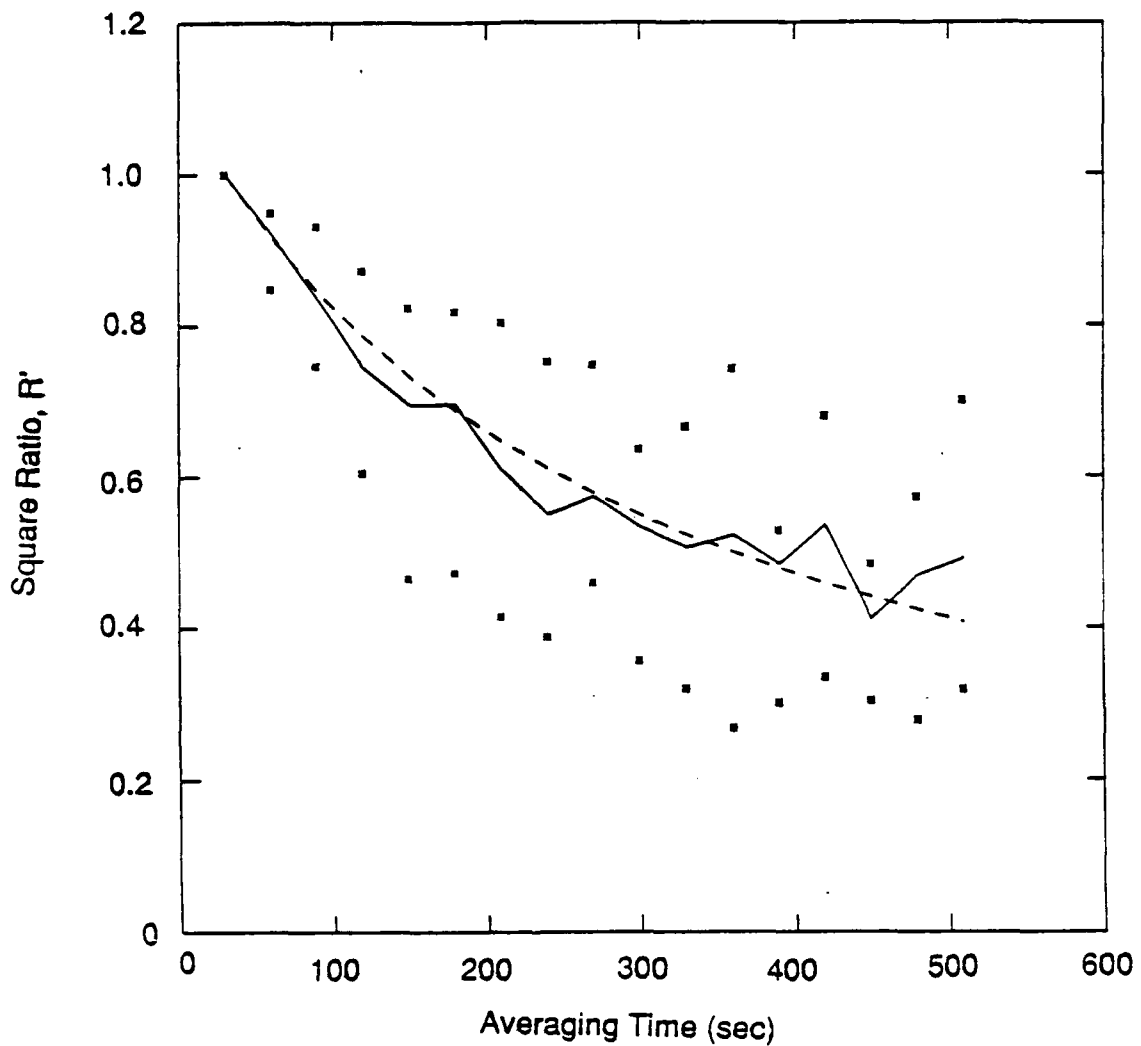


Figure B-1. Variation of emission rate fluctuation variance with averaging time. The solid line represents the median of the five experiments and the stars represent the range at that averaging time. The dashed line represents the theoretical curve given by Equation (B-2).

generator is operating in a consistent manner, both computational methods produce the same result (e.g., T0007, Figure 3.6). However, when the smoke generator malfunctions (e.g., T0003 and T0009, Figures 3.2 and 3.8, respectively), emissions can be highly variable, and the method of Liljegren et al. will over estimate emissions relative to our method of averaging "instantaneous" emissions. An analysis of the emission rate variability with different averaging time showed that a time interval of 150 seconds best represented the experimental data.

5. References

Liljegren, J.C., W.E. Dunn, G.E. DeVaul, A.J. Policastro, Field Study of Fog-Oil Smokes, Supported by U.S. Army Medical Research and Development Command, Fort Detrick, MD, January, 1988.

Intentionally Blank

APPENDIX C

UNCERTAINTIES IN SOURCE EMISSION RATE ESTIMATES
USING DISPERSION MODELS

Reprint from Atmospheric Environment, 24A 2971-2980 (1990)

UNCERTAINTIES IN SOURCE EMISSION RATE ESTIMATES USING DISPERSION MODELS

STEVEN R. HANNA, JOSEPH S. CHANG and DAVID G. STRIMAITIS
Sigma Research Corp., 234 Littleton Rd., Suite 2E, Westford, MA 01886, U.S.A.

(First received 7 April 1990 and in final form 5 June 1990)

Abstract—The source emission rates during the Prairie Grass dispersion experiments were carefully observed and were adjusted by the experimentalists so that they were about twice as high during unstable conditions as during stable conditions. The question was asked whether observed concentrations and meteorological conditions could be used in dispersion models in order to predict source emission rates and verify this factor of two difference. Three types of simple dispersion models were applied to this problem, with the result that for the model based on Monin-Obukhov similarity theory, the uncertainties in predictions of source emission rates for individual runs were at best about $\pm 10\text{--}20\%$ when observed cross-wind integrated concentrations from the 50 m arc were used. Consequently this model could discern the factor of two difference in average source emission rates for the two sets of field trials which consisted of about 10 runs each. However, some models, such as the Gaussian plume model, exhibit uncertainties of about $\pm 70\%$ to a factor of two in predictions for individual runs, and hence could not discern the difference in average source emission rates when concentration observations at downwind distances of 100–300 m are used. It is found that the use of observed cross-wind integrated concentrations produces more accurate conclusions than the use of observed point concentrations, for the uncertainties in predictions of source emission rates are about a factor of two larger when the observed point concentrations are used.

Key word index: Dispersion models, uncertainties in models, source emission estimates.

OBJECTIVE AND METHODS

As source emission rates for air pollutants are seldom well-known, air pollution control decisions must often be made based on observations of air pollution concentrations on monitoring networks. Observed concentrations can be combined with meteorological observations (e.g. wind speed and direction, stability, and mixing depth) and used in so-called hybrid source-receptor models in order to estimate source emission rates (Watson, 1989). These models are based on the concept that atmospheric transport and dispersion models are a mathematical link between observed concentrations and predicted source emission rates.

The specific objective of this research, funded by the U.S. Army, is to develop methods for estimating whether there is a significant difference in the source emission rate of similar types of sources from one experiment to another. For example, a typical source might be a fog oil generator (used for smoke obscuration purposes), and the question may be whether the source characteristics of the fog oil generator have significantly changed between 1980 and 1990. It is assumed that the source emission rate is not directly measured, but that several field trials are carried out at the same site in 1980 and in 1990. In each field trial, cross-wind integrated concentrations are observed at a distance 100 m downwind of the source, and wind velocities, turbulence, and vertical temperature gradients are observed on a tower near the source. The source position and orientation is not varied. Some

data of this type exist, and the procedures will eventually be tested with these data; however, first we have chosen to apply the source emission rate estimation methods to a simpler data set.

The Prairie Grass dispersion experiments produced a high-quality database (Barad, 1958) that has been used extensively in the development and testing of dispersion models. The experiments were simple, with near-ground-level continuous point sources, and extensive concentration and meteorological observations were made over the flat, homogeneous terrain. Source emission rates were also reported, and were deliberately varied so that they were twice as high during the day as during the night. Because of the care with which the Prairie Grass experiments were conducted, this database serves as an excellent test bed for study of the uncertainty in source emission rate estimation procedures. If the procedures cannot discern the known factor of two difference in average source emission rates in this highly controlled set of experiments, it would be of little use at more complicated sites, where the terrain may be more complex and the observations are likely to contain more errors.

Three representative dispersion models are used to relate observed concentrations and meteorological conditions to source emission rates. The three models include a statistical regression model, a Monin-Obukhov similarity model, and a Gaussian plume model. The Student-*t* test is used to determine whether the models can discern a factor of two difference, at the 95% confidence level, between average night and day

source emission rates. Another output of this procedure is an estimate of the typical error or uncertainty the source emission rate estimate.

DESCRIPTION OF PRAIRIE GRASS DATABASE

Barad (1958) discusses the Prairie Grass database in great detail. SO₂ tracer gas was released over periods of about 10 min from a point source located at an elevation of 0.45 m. Ten minute averaged tracer concentrations were obtained from measurements observed at an elevation of 1.5 m along arcs at distances of 50, 100, 200, 400 and 300 m from the source. Supporting meteorological observations were made from a nearby tower, located in a flat area, representative of the site, where the average surface roughness, z_0 , was determined to be 0.6 cm. Data from 44 experiments were used in our analysis, covering a wide range of meteorological conditions. The data are approximately equally divided into unstable and stable periods.

The Prairie Grass data are listed in Table 1, based on information in the report by Barad (1958) and in papers by van Ulden (1978), Nieuwstadt (1980), and Briggs (1982). The 2 m wind speed, u , the 2 m standard deviation of wind direction fluctuations σ_θ , and the 16 m to 1 m temperature difference, DT , were given in Barad's (1958) report, and the friction velocity, u_* , and the Monin-Obukhov length, L , were estimated by van Ulden (1978). The mixing depth and convective scaling velocity, w_* , were calculated for most unstable experiments by Nieuwstadt (1980). The stability class, SC, is estimated using observations of surface roughness, z_0 , Monin-Obukhov length, L , and Golder's (1972) nomogram. Briggs (1982) carefully reviewed all of the data and suggested that certain arcs for some experiments be removed from the data set because of problems with those particular data. At each downwind distance, the table lists observations of C/Q , C'/Q , and σ_θ , where C is the maximum concentration on that arc, C' is the cross-wind integrated concentration and σ_θ is the standard deviation of the lateral concentration distribution. The C' and σ_θ data were given by Nieuwstadt (1980) for most of the unstable periods. The standard deviation of vertical wind direction fluctuations, σ_z , has been estimated using boundary layer similarity theory.

DISPERSION MODELS

Data from the Prairie Grass experiments (Barad, 1958) were used extensively by Pasquill (1961) and others in the development and testing of a Gaussian diffusion model now known as the Pasquill-Gifford-Turner model (Gifford, 1962, 1968, 1976; Turner, 1967), which is the basis for most decisions regarding air pollution control in the U.S. The data were also part of the database used by Nou (1963) in the

development of the empirical OB-DG model, which is the basis of the U.S. Air Force procedures for calculating toxic gas impacts. Because the early data analyses did not make use of Monin-Obukhov similarity modeling or convective scaling concepts, there was a flurry of activity with reanalyses of the Prairie Grass data from this new point of view in the late 1970s (e.g. van Ulden, 1978; Horst, 1979; Nieuwstadt, 1980; Venkatram, 1981; Briggs, 1982). In several of these papers, the new scaling parameters (e.g. the mixing depth, h , the friction velocity, u_* , and the Monin-Obukhov length, L) were derived by reanalyzing the original field data.

The variety of dispersion models in the references listed above can be grouped into three classes.

- Class 1. Empirical or statistical regression models (e.g. Nou, 1963).
- Class 2. Similarity models (e.g. Briggs, 1982).
- Class 3. Gaussian plume models (e.g. Gifford, 1976).

Because Nou's (1963) empirical or statistical regression formula was based on several other databases besides the Prairie Grass database, and he did not suggest a formula for the cross-wind integrated concentration, we decided not to use his formula directly, but instead we applied a multivariate linear regression procedure to the data in Table 1 in order to derive the following best-fit power-law formulas:

$$C/Q = 0.000137x^{-1.81}(DT - 10^\circ F)^{4.72} \quad (1)$$

$$C'/Q = 0.00666x^{-1.03}(DT + 10^\circ F)^{2.84} \quad (2)$$

where C/Q and C'/Q are in units of $s m^{-3}$ and $s m^{-2}$, respectively, x is in units of m and DT is in units of $^\circ F$. This is the same statistical procedure applied by Nou (1963), and the units for all variables are consistent with those that he used. Nou (1963) also used the $10^\circ F$ additive factor, which is necessary to prevent negative values of the temperature term. These formulas explain 91 and 84%, respectively, of the variance in the C/Q and C'/Q observations, where most of the variance is explained by the x term. Note that these formulas are not based at all on physical insights, but are based on least-square fits of linear relationships to the data.

The group of similarity models proposed by van Ulden (1978), Horst (1979), Nieuwstadt (1980), Venkatram (1981) and Briggs (1982) is based on applications of Monin-Obukhov similarity theory and convective scaling similarity theory. According to Monin-Obukhov similarity theory, the following functional relations can be postulated for dispersion from continuous ground-level point sources in the surface boundary layer (Briggs, 1982):

$$Cu_*x^2/Q = f_1(x/L) \quad (3)$$

$$C'u_*x/Q = f_2(x/L) \quad (4)$$

where f_1 and f_2 are non-dimensional universal functions. The friction velocity, u_* , and the Monin-

Table 1. Prairie Grass database for 44 experiments, including observations of wind speed, u , and standard deviation, σ_u , at 2 m, temperature difference $D = T(16\text{ m}) - T(2\text{ m})$, and mixing depth, L . Derived values of friction velocity, w_* , convective scaling velocity, u_* , Monin-Obukhov length, L_* , and stability class, SC , are listed. Observations on five monitoring sites ($x = 50, 100, 200, 400$ and 800 m) of peak normalized concentration, C'/C_0 , and lateral standard deviation, σ_x , are also given. If a blank appears, then that piece of data is unavailable

Obukhov length, L , are the fundamental scaling velocity and scaling length in the surface boundary layer, according to Monin-Obukhov similarity theory. The Prairie Grass data are plotted in Fig. 1 in the dimensionless forms suggested by Equations (2) and (3), illustrating that the data are ordered quite well by these similarity relations.

Because the data in the four parts of Fig. 1 appear to approach a constant as x/L approaches zero, the following functional relation is proposed:

$$f(x/L) = a(1 + bx/L)^c. \quad (5)$$

A least-squares algorithm was applied to each figure, with the following results:

$$f_1(x/L) = 3.37(1 - 0.019x/L)^{-1.36} \quad x/L < 0 \quad (6)$$

$$f_1(x/L) = 3.01(1 - 2.20x/L)^{0.57} \quad x/L > 0 \quad (7)$$

$$f_2(x/L) = 1.06(1 - 0.021x/L)^{-1.74} \quad x/L < 0 \quad (8)$$

$$f_2(x/L) = 1.07(1 + 0.10x/L)^{0.68} \quad x/L > 0. \quad (9)$$

These curves are drawn on the figures and appear to

provide a good fit at all values of x/L . However, they have been derived with no requirements that certain physically-based asymptotic functional relationships be satisfied. For example, Briggs (1982) points out that $f_2(x/L)$ should be proportional to $(-x/L)^{1/2}$ in the limit of free convection ($-x/L \rightarrow \infty$). Consequently, Briggs' (1982) suggests a third term in Equation (5), which he claims to better account for "convective sweep-out" of the plume at large $|x/L|$. The similarity model is represented by Equations (6)-(9) in our analysis rather than the equations proposed in any of the above references because the other equations are based on a slightly different subset of the Prairie Grass database.

The Gaussian plume models comprise the third class of models in our analysis. The Gaussian model is based on the formulas (Gifford, 1976)

$$C/Q = (\pi u \sigma_x \sigma_z)^{-1} \exp(-(z_r - z_s)^2 / 2\sigma_z^2) \quad (10)$$

$$C'/Q = (2/\pi)^{1/2} (u \sigma_z)^{-1} \exp(-(z_r - z_s)^2 / 2\sigma_z^2). \quad (11)$$

The source height, z_s , and receptor height, z_r , equal

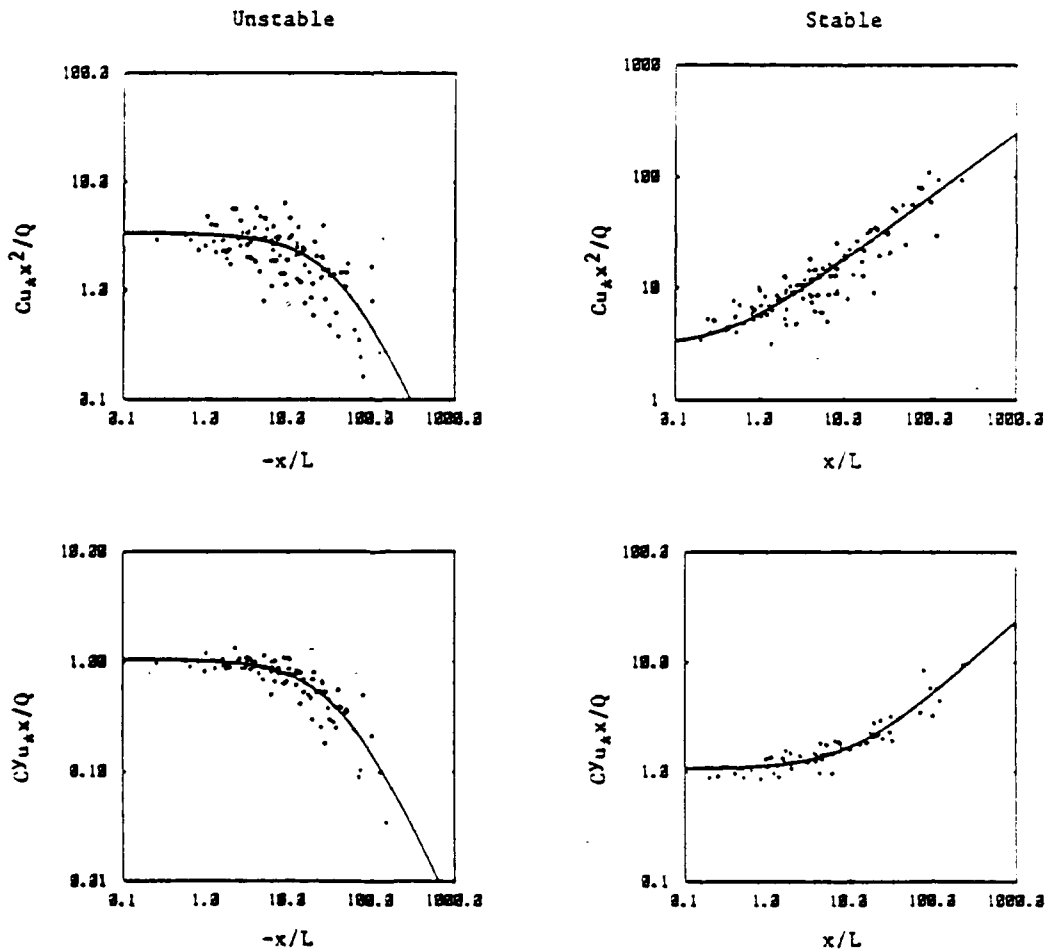


Fig. 1. Prairie Grass data plotted in the dimensionless form suggested by Equations (3) and (4). Best-fit lines of the form $a(1 + bx/L)^c$ are drawn on each figure (see Equations (6)-(9)).

0.45 m and 1.5 m, respectively, in the Prairie Grass experiments. The wind speed, u , is assumed to be that measured at a height of 2 m (see Table 1). The values for lateral and vertical dispersion coefficients, σ_x and σ_z , that are substituted into Equations (10) and (11) are based on suggestions by Briggs (1973), who used the Prairie Grass experiments, along with many other field experiments, in their derivation. These σ_x and σ_z formulas are given in Table 2. The required stability class is found in Table 1 for each Prairie Grass test.

Note that the empirical and similarity classes of dispersion models have been best-fit to the exact same data (Table 1) that will be used for further testing. The Gaussian plume model has not been subjected to these same best-fit procedures, but has been based on data from many experiments. Because of these differences in databases used to derive the models, it is expected that the Gaussian plume model will have the least success in any comparisons with field data from the Prairie Grass database.

The dispersion models in Equations (3) and (4) and (6)–(10) are inverted in order to predict source emission rates:

$$Q_p = C_o / (C/Q)_o \quad (12)$$

$$Q_p = C'_o / (C'/Q)_o, \quad (13)$$

where subscripts o and p represent observed and predicted variables, respectively. Because of the characteristics of the multiple linear regression or least-squares statistical procedures, an equation that produces a best-fit for C/Q or C'/Q may not necessarily produce a best-fit for Q . These statistical procedures attempt to minimize the mean-square error and to force the mean of the observed variable to equal the mean of the predicted variable. We should therefore not be surprised if an equation which produces zero mean bias in C/Q is discovered to produce a mean bias of 20–30% or more in Q .

STATISTICAL PROCEDURES

A primary objective of this research is the development of methods for estimating whether there is a significant difference in the source emission rate of similar types of sources from one experiment to another, as determined by observations of meteorological conditions and of point concentrations or

cross-wind integrated concentrations. Dispersion models, such as the three presented above, can be used to remove the effects on the concentration observations of variations in meteorological parameters and downwind position of the concentration monitor.

A listing of the observed source emissions, Q , during the Prairie Grass experiment is given in Table 1, and the data are plotted in Fig. 2 as a function of the stability parameter $1/L$ (the point for run 46 has been excluded, since it was an evening transition period when Q was still high although $1/L$ had just become positive). During the Prairie Grass experiment the night-time emissions, Q_n , of tracer gas were controlled so that Q averaged 45.2 g s^{-1} with a range from about 38 to 58 g s^{-1} and a standard deviation of 5.91 g s^{-1} , and the daytime emissions were controlled so that Q averaged 98.25 g s^{-1} with a range from about 90 to 105 g s^{-1} and a standard deviation of 4.48 g s^{-1} . The experimentalists deliberately maintained this factor of 2 difference in day-night Q s so that the magnitude of concentrations at the monitors would not vary much from day to night. With 19 stable (night) runs and 20 unstable (day) runs, the Student-t parameter (Panofsky and Brier, 1968, p. 63) can be calculated in order to determine if the daytime \bar{Q}_d is significantly different from the night-time \bar{Q}_n :

$$t = (\bar{Q}_d - \bar{Q}_n) / \left(\frac{\sqrt{N_d \sigma_d^2 + N_n \sigma_n^2} \left(\frac{1}{N_d} - \frac{1}{N_n} \right)}{\sqrt{N_d - N_n - 2} \sqrt{N_d N_n}} \right)^{1/2} \quad (14)$$

where subscripts d and n indicate day and night. If $|t|$ is less than 2.04, then the difference $(\bar{Q}_d - \bar{Q}_n)$ is not significantly different from zero, at the 95% confidence level. In fact, using the observed \bar{Q} and σ_Q

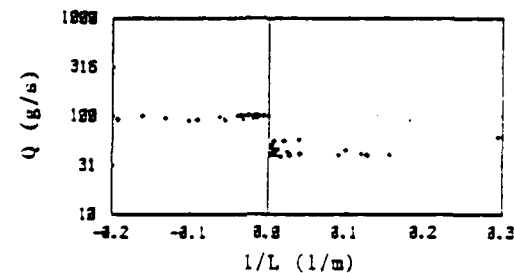


Fig. 2. Observed tracer gas source emission rates, Q , as a function of inverse Monin-Obukhov length, $1/L$, for the Prairie Grass data (run 46 excluded).

Table 2. Formulas recommended by Briggs (1973) for σ_x and σ_z , for rural conditions

Stability class	σ_x (m)	σ_z (m)
A	$0.22 \times (1 - 0.0001x)^{-1/2}$	$0.20x$
B	$0.16 \times (1 - 0.0001x)^{-1/2}$	$0.12x$
C	$0.11 \times (1 - 0.0001x)^{-1/2}$	$0.08 \times (1 - 0.0002x)^{-1/2}$
D	$0.08 \times (1 + 0.0001x)^{-1/2}$	$0.06 \times (1 + 0.0015x)^{-1/2}$
E	$0.06 \times (1 - 0.0001x)^{-1/2}$	$0.03 \times (1 + 0.0003x)^{-1}$
F	$0.04 \times (1 - 0.0001x)^{-1/2}$	$0.016 \times (1 - 0.0003x)^{-1}$

figures quoted above, the calculated Student-*t* parameter is 30.86 for the difference between the mean night-time and daytime emission rates, which implies that the difference is significant at far greater than the 95% confidence level.

Because there is such a clear difference in the observed day and night tracer gas source emission rates, Q_s , at the Prairie Grass site, it is interesting to ask whether the dispersion models would be able to predict this significant difference in the mean emission rates, based on observed concentrations and meteorological variables. The three types of models described earlier were used to prepare predictions of source emission rate, \bar{Q}_s (one set of predictions using C_o , and another set using C'_o). This calculation of \bar{Q}_s was made individually using data from each of five monitoring arcs (50, 100, 200, 400 and 800 m) for C_o , and each of three monitoring arcs (50, 200 and 800 m) for C'_o . For each set of predictions, values of night-time and daytime \bar{Q}_s and $\sigma_{\bar{Q}_s}$ were calculated. Then Equation (14) was used to calculate the Student-*t* parameter. If the resulting *t* value exceeds 2.04, it is concluded that the model successfully simulated the difference in source emission rates. If *t* is less than 2.04, then it is concluded that the model has failed to simulate the difference.

Besides investigating the day-night difference in mean source emission rate predictions, it is also of interest to investigate the ability of the models to predict emission rates for all Prairie Grass runs taken as a group. For this purpose, the following performance measures are calculated (where an overbar represents an average over all the database).

Relative bias: $(\bar{Q}_s - Q_s)/\bar{Q}_s$.

Correlation: $r = \overline{(Q_s - \bar{Q}_s)(Q_s - \bar{Q}_s)} / \sigma_{Q_s} \sigma_{\bar{Q}_s}$.

Fractions of predictions, Q_s , within a factor of two of observations, \bar{Q}_s .

Normalized mean square error: $\overline{(Q_s - \bar{Q}_s)^2} / \bar{Q}_s \bar{Q}_s$.

These performance measures are tabulated for each model and for C_o and C'_o on each monitoring arc. In addition, the individual residuals ($Q_s - \bar{Q}_s$) are plotted as a function of downwind distance for each model.

RESULTS AND CONCLUSIONS

Predictions of average daytime and night-time source emission rates

The procedures for estimating the daytime and night-time average source emission rates reviewed above were applied to the Prairie Grass database, with the results given in Tables 3 and 4, for C_o and C'_o , respectively. By comparing the numbers in the two tables, it is evident that use of the observed cross-wind integrated concentration, C'_o , produced better results than use of the observed point concentration, C_o . The standard deviations, $\sigma_{\bar{Q}_s}$, of the predicted source emission rates are about 50% larger during the night and a factor of 2 or 3 larger during the day, for C_o , than for C'_o . Consequently the calculated Student-*t* parameters are about twice as large for C'_o than for C_o , implying that there is more confidence in the conclusions for C'_o . We expected that there would be a difference, because

Table 3. Predictions of source emission rate, \bar{Q}_s (gs^{-1}), for night-time and daytime Prairie Grass runs, using observed maximum concentrations, C_o , on monitoring arcs at distances of 50, 100, 200, 400 and 800 m. Three different models are used to calculate $\bar{Q}_s = C_o(\bar{C}/Q)_o$. The average, \bar{Q}_s , and standard deviation, $\sigma_{\bar{Q}_s}$, for night-time and daytime conditions is listed. Student-*t* is calculated using Equation (14)

Model	Monitoring distance (m)	Student- <i>t</i>	Night ($N = 19$)		Day ($N = 20$)	
			\bar{Q}_s (gs^{-1})	$\sigma_{\bar{Q}_s}$ (gs^{-1})	\bar{Q}_s (gs^{-1})	$\sigma_{\bar{Q}_s}$ (gs^{-1})
Observed Q		30.86	45.2	5.9	98.2	4.5
Regression	50	7.40	30.1	12.0	144.6	64.7
	100	5.47	43.8	19.4	139.1	71.6
	200	4.27	52.0	23.0	123.3	72.5
	400	2.20	61.2	27.3	93.4	56.2
	800	-1.19	84.2	51.6	64.5	48.9
Similarity	50	5.68	39.9	14.1	70.8	18.5
	100	4.62	49.2	16.2	84.0	37.1
	200	5.51	48.7	16.2	101.1	37.1
	400	5.52	45.8	15.6	105.4	43.2
	800	4.80	46.3	14.6	116.2	60.1
Gaussian	50	2.40	55.2	45.5	115.5	96.9
	100	1.07	76.3	94.9	109.2	92.2
	200	0.05	98.1	150.9	100.2	70.1
	400	-0.88	118.8	196.3	76.8	62.7
	800	-1.67	150.1	264.1	48.0	30.1

Table 4. Predictions of source emission rate, \bar{Q}_s (gs^{-1}), for night-time and daytime Prairie Grass runs, using observed cross-wind integrated concentrations, C_s^* , on monitoring arcs at distances of 50, 200 and 300 m. Three different models are used to calculate $\bar{Q}_s = C_s^*(C_s' Q)_s$. The average, \bar{Q}_s , and standard deviation, σ_{Q_s} , for night-time and daytime conditions listed. Student- t is calculated using Equation (14)

Model	Monitoring distance (m)	Student t	Night ($N = 19$)		Day ($N = 20$)	
			\bar{Q}_s (gs^{-1})	σ_{Q_s} (gs^{-1})	\bar{Q}_s (gs^{-1})	σ_{Q_s} (gs^{-1})
Observed Q		27.27	45.2	5.9	97.8	4.7
Regression	50	17.19	29.7	9.8	140.1	24.8
	200	7.43	46.9	16.9	124.8	40.1
	800	-0.58	69.4	34.3	62.1	36.4
Similarity	50	16.24	39.7	8.3	39.6	9.0
	200	9.54	49.0	9.0	100.1	20.3
	800	4.38	45.2	13.8	99.6	50.2
Gaussian	50	6.18	61.7	30.9	161.0	58.4
	200	2.33	65.5	60.3	116.6	34.9
	800	-0.99	85.5	145.1	46.9	20.3

σ , is another complicating factor included in C_s , that would act to increase the uncertainty, but did not expect that the difference would be this large.

The ability of the models to arrive at the proper answer (i.e. that the daytime \bar{Q} is significantly larger than the night-time \bar{Q} , with at least 95% confidence) can be seen by identifying cases where $t \geq 2.04$ in Tables 3 and 4. It is seen that most models are able to reproduce this conclusion at most arc distances. However, false conclusions ($t < 2.04$) are reached for the following arcs and models.

- C_s : 100 m arc: Gaussian
- 200 m arc: Gaussian
- 400 m arc: Gaussian
- 800 m arc: Regression and Gaussian.
- C_s' : 800 m arc: Regression and Gaussian.

It is seen that the use of C_s and C_s' from the closest arc (50 m) leads to the correct conclusion for all three models, with a value for Student- t ranging from 2.4 to 7.4 for C_s , and 5.2 to 17.2 for C_s' . The regression and similarity models are seen to be better able to simulate the difference in observed Q (i.e. they yield a higher t) than the Gaussian model. However, the number of false conclusions increases as downwind distance increases. At the 800 m arc in both tables, only the similarity model yields the proper conclusion. Figs 3 and 4 contain extreme examples of plots of predicted source emission rates, \bar{Q}_s , as a function of $1/L$, in the same format as the observations in Fig. 2. The similarity model predictions in Fig. 3, using observations of C_s' on the 50 m arc, produce patterns similar to the observed data, but with slightly more scatter. However, the Gaussian plume model predictions in Fig. 4, using observations of C_s on the 800 m arc, obviously miss the overall trend of the observations of Q , as well as containing much more scatter.

The failure of the regression model and the Gaussian model to estimate \bar{Q} using C_s and C_s' observations

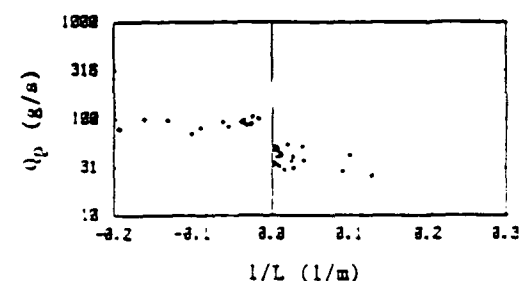


Fig. 3. Tracer gas source emission rates, \bar{Q}_s , predicted by the similarity model as a function of inverse Monin-Obukhov length, $1/L$, for the Prairie Grass data (run 46 excluded). Observed cross-wind integrated concentrations on the 50 m arc are used.

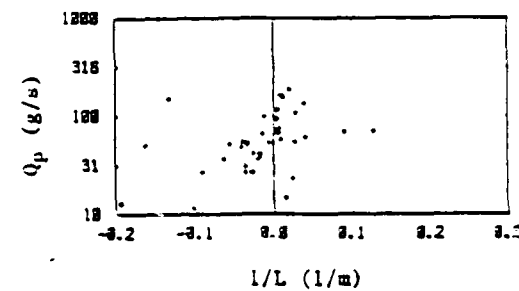


Fig. 4. Gas source emissions rate predicted by the Gaussian plume model, \bar{Q}_s , as a function of inverse Monin-Obukhov length, $1/L$, for the Prairie Grass data (run 46 excluded). Observed concentrations on the 800 m arc are used.

at the longest distances may be seen by investigating the variation of the ratio C_s/C_s' with distance for the three models for stable and unstable conditions (Figs 5 and 6). The C_s/C_s' values for the similarity model have very little trend with distance and are always centered

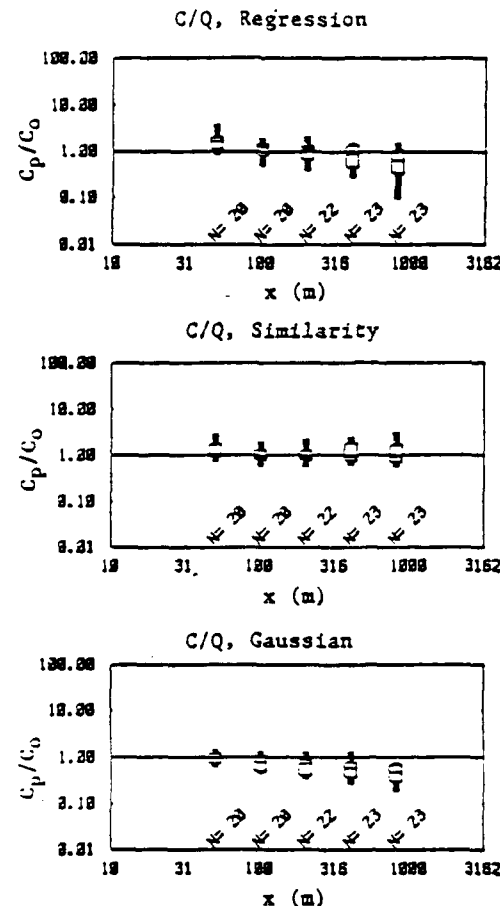


Fig. 5. Ratios of predicted to observed concentrations (C_p/C_o) for the Prairie Grass dataset, as a function of downwind distance, for three models (regression, similarity, and Gaussian) for stable conditions. N is the number of data points at each distance. The midline of each box plot is the median, and the other lines represent \pm one and two standard deviations.

on 1.0. In contrast, at large distances, the regression and Gaussian models tend to underpredict ($C_p/C_o < 1$) during stable conditions (Fig. 3) and overpredict ($C_p/C_o > 1$) during unstable conditions. It is important to note that a model which overpredicts the concentration, C , will underpredict the source emission rate, Q . Consequently, at large distances, the regression and Gaussian models can be expected to overpredict the source emission rate, Q , during stable conditions, and underpredict it during unstable conditions. But since the observed stable \bar{Q} is about 45 g s^{-1} and the unstable \bar{Q} is about 98 g s^{-1} , the \bar{Q} s predicted by these two models will tend to be either nearly the same, or their relative magnitudes may even be switched. This problem is seen to occur for the Gaussian model on the 800 m arc, using the C_o data, where the following discrepancy is found in Table 3 and can be seen in Figs 2 and 4.

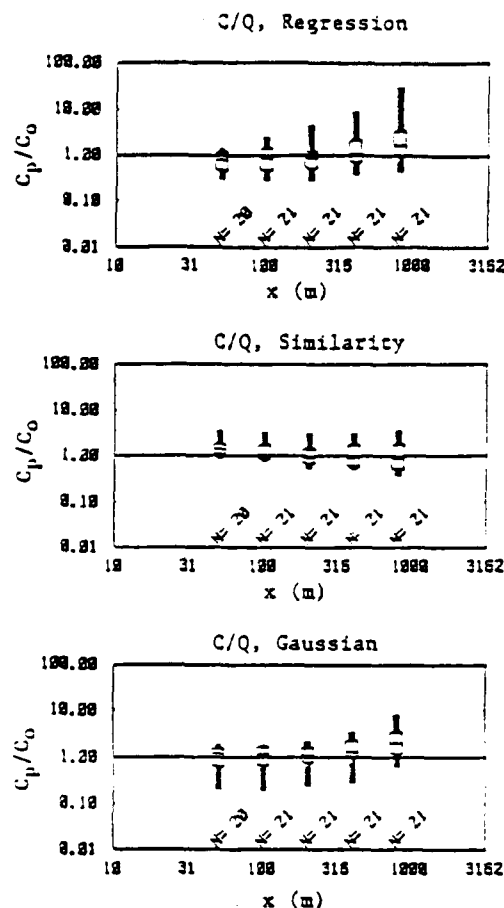


Fig. 6. Ratios of predicted to observed concentrations (C_p/C_o) for the Prairie Grass dataset, as a function of downwind distance, for three models (regression, similarity, and Gaussian) for unstable conditions. N is the number of data points at each distance. The midline of each box plot is the median, and the other lines represent \pm one and two standard deviations.

Thus the Gaussian model leads to the opposite conclusion regarding daytime and night-time \bar{Q} differences if the 300 m C_o data are used. Note that if the experimentalists had controlled the emissions in the opposite way, such that the night-time Q exceeded the daytime Q , then these trends in the errors in the regression and Gaussian models would have led to a correct conclusion regarding the differences in Q .

	Night	Day
Observed \bar{Q}_o	45.2	98.1
Gaussian predicted \bar{Q}_o	150.1	48.0

Consider the best-performing model in Table 6, where C_o^* data from the 50 m arc are used in the similarity model to predict the average source emission rate, \bar{Q} (see Fig. 3). The calculated Student- t value

Table 5. Evaluations of predictions of source emission rate, $\bar{Q}_s(\text{gs}^{-1})$, for all Prairie Grass runs, using observed maximum point concentrations, C_s , on monitoring arcs at distances of 50, 200 and 300 m. Three different models are used to calculate $\bar{Q}_s = C_s/(C'Q)$.

Distance to C_s , observation	Model	$\bar{Q}_s(\text{gs}^{-1})$	$\frac{\bar{Q}_s - \bar{Q}_o}{\bar{Q}_o}$	Correlation r	Fracuon within factor of 2	$\frac{\bar{Q}_s - Q^2}{\bar{Q}_o \bar{Q}_s}$
	Observed	72.4				
50 m	Regression	88.8	0.23	0.77	0.82	0.53
	Similarity	55.7	-0.23	0.74	0.90	0.15
	Gaussian	86.1	0.19	0.36	0.80	0.97
200 m	Regression	91.2	0.26	0.59	0.85	0.51
	Similarity	75.6	0.04	0.71	0.92	0.14
	Gaussian	99.2	0.37	0.02	0.74	2.08
300 m	Regression	74.1	0.02	-0.15	0.54	0.70
	Similarity	32.1	0.13	0.65	0.90	0.34
	Gaussian	97.6	0.35	-0.25	0.49	5.75

Table 6. Evaluation of predictions of source emission rate, $\bar{Q}_s(\text{gs}^{-1})$, for all Prairie Grass runs, using observed cross-wind integrated concentrations, C'_s , on monitoring arcs at distances of 50, 200 and 300 m. Three different models are used to calculate $\bar{Q}_s = C'_s/(C'Q)$.

Distance to C_s , observation	Model	$\bar{Q}_s(\text{gs}^{-1})$	$\frac{\bar{Q}_s - \bar{Q}_o}{\bar{Q}_o}$	Correlation r	Fraction within factor of 2	$\frac{\bar{Q}_s - Q^2}{\bar{Q}_o \bar{Q}_s}$
	Observed	68.4				
50 m	Regression	78.4	0.14	0.94	0.91	0.23
	Similarity	61.7	-0.10	0.98	1.00	0.02
	Gaussian	106.0	0.55	0.74	0.88	0.55
200 m	Regression	81.2	0.19	0.80	0.94	0.21
	Similarity	71.6	0.05	0.89	1.00	0.04
	Gaussian	88.1	0.29	0.46	0.88	0.48
300 m	Regression	66.1	-0.03	-0.07	0.74	0.46
	Similarity	69.2	0.01	0.60	0.88	0.26
	Gaussian	68.4	0.00	-0.15	0.65	1.98

in this case is 16.2. Since $\bar{Q}_o(\text{day}) - \bar{Q}_o(\text{night}) \approx 53 \text{ gs}^{-1}$, it is concluded that a significant difference in \bar{Q} values could be discerned by this model if $\Delta \bar{Q}_o = \bar{Q}_o(\text{day}) - \bar{Q}_o(\text{night})$ drops as low as $53 \times (2.04/16.2) = 6.7 \text{ gs}^{-1}$; that is, if $\Delta \bar{Q}_o$ is about 15% of \bar{Q}_o . Therefore, in these best of research-grade experiments, where there are about 20 daytime and 20 night-time tests, and where a dispersion model is fit to these same data, a day-night difference in \bar{Q} of less than 15% of the mean would not be estimated to be significant by this procedure.

Predictions of source emission rates for all cases

Putting aside the question of differences in daytime and night-time averages in \bar{Q} , it is possible to use the complete database to estimate the overall ability of the models to estimate the 39 individual source emission rates. The relative bias, the correlation, the fraction of predictions within a factor of two of observations, and the normalized mean square error for the three models are listed in Table 5 and 6, for maximum point concentrations and cross-wind integrated concentra-

tions, respectively. These performance measures are calculated using data from the 50 m, 200 m and 300 m arcs.

In most cases, the similarity model shows the most accuracy and the Gaussian model shows the least accuracy. Also, the use of observed cross-wind integrated concentrations, C'_s , leads to better results than the use of observed point maximum concentrations. The deterioration of model performance as distance increases can also be seen. Focusing on Table 6, for cross-wind integrated concentrations, it is seen that the most accurate model, the similarity model, produces a mean relative bias with a magnitude of 0.10 or less on all three distance arcs. The correlation drops from 0.98 to 0.60 as distance increases from 50 to 300 m, and the fraction within a factor of two drops from 1.00 to 0.88 over the same distance. The normalized mean-square-error increases from 0.02 to 0.26 over those distances, implying that the root-mean-square-error (rmse) increases from about 15% to 50% of the mean. In contrast, the Gaussian model yields a

much larger rmse that increases from about 70% to 300% of the mean.

The factor of 5 or 6 difference in rmse between the similarity and Gaussian models implies that the similarity model can discern differences in source emission rates that are a factor of 5 or 6 less than the minimum differences in source emission rates discerned by the Gaussian model. By comparing these numbers between Tables 5 and 6, it is seen that the relative rmse using C_0 observations are about 50% to 100% larger than the relative rmse using C_0^2 observations. Consequently the use of C_0^2 data permits one to discern differences in source emission rate that are 50% to 100% smaller than the minimum differences in source emission rates discerned by C_0 data.

IMPLICATIONS FOR FUTURE RESEARCH

The uncertainties in estimating source emission rates were first investigated using the Prairie Grass database, since the source conditions were simplified (a single continuous non-buoyant point source near the ground), the source emission rate was closely monitored, the site was flat and uniform, comprehensive meteorological data were taken, and observations of ground-level concentrations were taken at many points along monitoring arcs at five downwind distances. This experiment represents the optimum database of its type, and has been used in numerous research programs on atmospheric turbulence and dispersion. For this reason, the uncertainties in any analysis procedure should be minimized at this site. Conversely, if these procedures were to be applied to other experiments at other sites, where conditions are not so steady, smooth, or carefully-observed, the uncertainties would be expected to be larger.

In the future, we will test these procedures using less ideal observations from other field experiments. These will include U.S. Army field tests of fog oil generators, which are used for smoke obscuration purposes. The plumes from fog oil generators are more complicated than those in the Prairie Grass experiments, since the fog oil plumes are characterized by significant momentum and buoyancy fluxes. Furthermore, the supporting meteorological data are not as complete as at Prairie Grass. Future tests will also include experimental data obtained for plumes from tall power plant stacks, where plume rise and mixing depth are complicating factors. From each set of experiments, the relative uncertainty of the procedures for estimating source emission rate will be assessed. It is expected that the uncertainty will increase as source conditions become more complex or as input data are less complete.

This study has demonstrated that models that do well (in a least squares sense) in estimating point concentrations do not necessarily do well when they are 'turned around' to estimate source emission rate. The reason for this difference is the strong variation

with distance of the plume centerline concentration. Consequently it is possible that a model which has zero mean bias in its concentration estimates, will have a 50% mean bias in its source emission rate estimates. For the same reason, if a variable is first made non-dimensional and the model is 'tuned' with the data (e.g. the similarity model described above), the predictions of the non-dimensional variable (e.g. $C_{u,x}r^2/Q$) may have zero bias, while the predictions of the concentration, C , may have significant bias. For optimum results, any tuning or regression analysis should be done with the variable that is of ultimate interest.

Acknowledgements—This research was sponsored by the U.S. Army. The authors appreciate the assistance of Mr James Bowers, Mr Christopher Bilotit and Mr James Raiferty of Dugway Proving Ground.

REFERENCES

- Barad M. L. (ed.) (1958) Project Prairie Grass. A field program in diffusion. *Geophys. Res. Paper No. 59*, Vols. I and II, AFCRL-TR-58-235, Air Force Cambridge Research Center, Bedford, MA.
- Briggs G. A. (1973) Diffusion estimation for small emissions. ATDL Cont. File No. 79, ATDL, Oak Ridge, TN.
- Briggs G. A. (1982) Similarity forms for ground source surface layer diffusion. *Boundary-Layer Met.* 23, 489-502.
- Draxler R. R. (1984) Diffusion and transport experiments. Chapter 9 In *Atmospheric Science and Power Production*. Chapter 9 (edited by D. Randerson), pp. 367-422. DOE/TIC-27601, USDOE.
- Gifford F. A. (1961) Use of routine meteorological observations for estimating atmospheric dispersion. *Nucl. Saf.* 2, 47-57.
- Gifford F. A. (1968) An outline of theories of diffusion in the lower layers of the atmosphere. In *Meteorology and Atomic Energy—1968* (edited by D. H. Slade), pp. 66-116. USAEC Report TID-24190, NTIS, 66-116.
- Gifford F. A. (1976) Turbulent diffusion typing schemes. A review. *Nucl. Saf.* 17, 68-86.
- Golder D. (1972) Relations among stability parameters in the surface layer. *Boundary-Layer Met.* 3, 47-58.
- Horst T. W. (1979) Lagrangian similarity modeling of vertical diffusion from a ground-level source. *J. appl. Met.* 18, 733-740.
- Nieuwstadt F. T. M. (1980) Application of mixed-layer similarity to the observed dispersion from a ground-level source. *J. appl. Met.* 19, 157-162.
- Nou J. V. (1963) The Ocean Breeze and Dry Guich diffusion programs. AFCRL, Hanscom AFB, MA.
- Pasquill F. (1961) The estimation of dispersion of windborne material. *Met. Mag.* 90, 33-49.
- Turner D. B. (1967) Workbook of atmospheric dispersion estimates. Public Health Service, Pub. No. 999-AP-26, Robert A. Taft Sanitary Engineering Center, Cincinnati, OH.
- van Ulden A. P. (1978) Simple estimates for vertical diffusion from sources near the ground. *Atmospheric Environment* 12, 2125-2129.
- Venkatarao A. (1981) A semi-empirical method to compute concentrations associated with surface releases in the stable boundary layer. *Atmospheric Environment* 15.
- Watson J. G. (ed.) (1989) Receptor models in air resources management. *Transactions of an International Specialty Conference*. Air and Waste Management Association, Pittsburgh, PA.

APPENDIX D

DISPLAY OF RELATIONS AMONG DATA USING BOX PLOTS

APPENDIX D

DISPLAY OF RELATIONS AMONG DATA USING BOX PLOTS

One way of displaying large numbers of data is through the use of box plots, where the cumulative distribution function (cdf) of the dependent variables within a group of data is represented by a set of significant percentile values. For example, the 2th, 16th, 50th, 84th, and 98th percentiles are used in our analyses. These five significant points in the cdf are plotted by the SIGPLOT program using a "box" pattern as seen in the examples below. Variations of one type of data with another can be seen by breaking up the first type of data into groups defined by ranges of the second type of data.

The SIGPLOT plotting package (see Appendix E) is used to generate the box plots. The ANADISTR program, described below, is used to generate the special input file required by SIGPLOT from a file containing multiple columns of data, representing concurrent values of variables such as observations of concentrations, wind speed, or stability. In the ANADISTR program, the user defines certain ranges of the primary variables in the input file to be used for grouping the dependent variables and plotting them by means of box plots. The ANADISTR program requires one input file and generates one output file. The output file then serves as the input file to the SIGPLOT plotting package. There are no default names associated with these files, and the user is prompted for the file names during the execution of the program. The ANADISTR program is written in FORTRAN 77.

The input data file of the ANADISTR program could contain multiple columns of dependent variables (such as concurrent values of concentration observation) and other primary variables such as wind speed and stability. The ranges of the primary variables are also defined in the input file, to be used for grouping the data prior to generating the box plots. Table D-1 describes the format of the input file. Figure D-1 shows an example of an input file. Note that the ANADISTR program makes no corrections or substitutions for missing data; it is the responsibility of the user to provide valid data at each position.

The output file of the ANADISTR program contains distributions (the 2th, 16th, 50th, 84th, and 98th percentiles of the cdf) of the first variable as a function of the second variable. The information stored in this output file can then be plotted using the SIGPLOT plotting package (see Figure D-2 for an example).

During the execution of the ANADISTR program, the following questions will be asked:

- Name of the input file:

The user must specify the name of the input data file here. There is no default answer.

- Name of the output file:

The user must specify the name of the output file. There is no default answer.

- An input file typically contains several columns of dependent and independent data. The ANADISTR program handles one such column or the ratio of any two columns of dependent data, specified by the user, at a time. This is accomplished by asking the user to select any two columns between 0 and MM, (see Table D-2). The distribution of the ratio of the numbers in these columns will be analyzed. Note that column "0" is simply all 1's, and is not part of the input data file. Therefore, if the user wants to investigate the distribution of the dependent data in column 2, then two integers, 2 and 0 should be entered. If the user wants to investigate the distribution of the ratio of the dependent data in column 2 to the data in column 1, then 2 and 1 should be entered.
- Implement a lower threshold for the dependent variable? (y/n):

The user has the option of specifying a lower threshold for the one dependent variable or the ratio of the two dependent variables chosen above. This is sometimes necessary if the logarithmic scale is to be used and there are zero or minute values in the data whose distribution is to be analyzed. The default (i.e., hitting the RETURN key) answer is "y".

TABLE D-1. FORMAT OF THE MANDATORY INPUT DATA FILE OF THE ANADISTR PROGRAM.
 THE FOLLOWING KEY LETTERS ARE USED IN THE FORMAT COLUMN - FF: FREE
 FORMAT, C: CHARACTER, I: INTEGER, AND R: REAL.

LINE NO.	FORMAT	DESCRIPTION
1	FF/I	There are four integer constants in this line, representing the total number of observations (NN, < 501), the total number of dependent variable (MM, < 16), the total number of blocks (KK), and the total number of primary variables (NVAR, < 11). Note that KK is not used by ANADISTR since the blocking of data is performed internally according to the defined ranges of the primary variables. The limits on NN, MM, and NVAR are assigned in the program using the PARAMETER statements, and can be easily changed.
2	FF/I	There are KK integer constants in this line, representing the number of pieces in each block. The sum of all these integers should equal NN. Note that the information in this line is currently not used by the ANADISTR program.
3	FF/I	There are MM character constants in this line; each one can be at most eight characters long, containing the name of each of the dependent variables. All character constants must be enclosed in apostrophes.
4	FF/I	There should be KK character constants in this line. Each one can be at most 20 characters long, containing the name of each of the blocks. All character constants must be enclosed in apostrophes. Note that the information in this line is not used by the ANADISTR program.

LINE NO.	FORMAT	DESCRIPTION
Next NN lines:		
FF/R		There are MM+NVAR real numbers in each line, with the first MM numbers representing the dependent variables, and the following NVAR numbers representing of the primary variables.
Next NVAR lines:		
FF/ I,C,R		Each line describes the way each of the NVAR primary variables is to be blocked. The first parameter is an integer (IXR, < 21), representing the number of ranges for the primary variable. The second parameter is a character constant, at most 40 characters long, enclosed in apostrophes, representing the name of the primary variable. The next IXR+1 real numbers, in numerical ascending order, define the boundaries of the ranges. For example, the following line: 4 'u (m/s)' 0. 2. 5. 10. 20. means that wind speeds should be divided into four groups where the distribution of the dependent variables within each group is to be calculated. The first group is for those data when wind speeds are between 0. and 2. m/s, the second group is for wind speeds between 2. and 5. m/s, etc. The limits on IXR are assigned in the program using the PARAMETER statement, and can be easily changed. Note that the sequence of the NVAR lines must be consistent with that of the last NVAR columns described in the previous section. As an example, if the MM+1th column in the previous section contains information for wind speeds, then the first line in this section should also contain grouping information for wind speeds.

79 4 2 4
 39 40
 'DEPVAR-A' 'DEPVAR-B' 'DEPVAR-C' 'DEPVAR-D'
 'SUBSET1' 'SUBSET2'
 616.0 708.7 594.7 516.5 11 3.0 800. 2
 604.1 689.2 585.8 496.7 12 3.4 1000. 2
 868.0 674.8 580.3 516.8 13 3.5 1100. 2
 498.6 668.8 652.1 548.3 14 3.8 1200. 2
 393.1 560.2 704.7 581.9 15 4.7 1300. 2
 409.0 740.9 570.1 621.4 16 5.2 1000. 3
 640.2 249.6 510.1 553.5 17 5.4 1100. 3
 265.3 259.6 463.4 446.0 18 4.9 1100. 4
 192.7 91.6 131.0 485.0 19 4.2 1100. 5
 1149.1 1217.5 1116.1 520.6 10 2.6 1600. 2
 972.8 1275.8 1175.1 536.9 11 3.2 1900. 2
 1137.5 1225.7 1081.7 617.4 12 3.8 1600. 2
 669.5 1052.8 905.1 637.3 13 4.3 1600. 2
 595.5 862.0 862.0 664.1 14 5.0 1500. 2
 741.2 589.5 767.0 665.3 15 5.1 1500. 2
 612.6 602.4 728.2 672.4 16 5.0 1300. 3
 312.0 398.9 637.5 659.5 17 5.2 1500. 3
 400.2 340.2 412.3 586.0 18 5.1 1500. 4
 264.7 612.1 774.2 705.9 16 5.7 1400. 3
 290.0 428.4 757.3 708.8 17 5.1 1800. 3
 459.5 355.0 512.3 602.4 18 5.1 2000. 4
 444.0 216.0 441.4 681.1 19 4.4 2000. 5
 175.1 216.6 456.1 825.4 20 4.6 2000. 5
 102.3 126.1 255.6 522.9 21 4.9 2000. 6
 128.8 16.5 0.5 834.9 22 4.6 0. 6
 200.2 301.9 208.9 728.0 23 5.4 0. 6
 358.3 481.8 354.0 742.4 24 5.4 0. 6
 611.1 1010.2 987.1 679.0 14 4.4 1500. 2
 499.3 752.5 921.6 725.7 15 5.0 1500. 2
 537.8 724.0 826.8 675.9 16 4.7 1500. 3
 220.0 523.3 908.2 640.8 17 3.9 1800. 3
 479.2 357.5 788.6 544.7 18 4.2 2000. 4
 133.2 195.3 383.1 738.5 19 3.1 1800. 5
 98.2 167.3 213.5 1064.9 20 3.2 1500. 6
 92.5 104.6 142.2 741.2 21 3.1 1200. 6
 21.0 127.4 176.3 805.2 22 3.3 1200. 6
 353.0 307.8 167.1 576.9 20 3.8 2000. 5
 358.0 280.9 188.4 225.3 21 2.3 2000. 4
 233.3 355.3 234.9 719.1 22 2.4 2000. 5
 198.3 12.7 184.0 745.2 23 3.6 2000. 6
 507.2 3.3 126.3 564.3 24 3.5 2000. 6
 313.7 0.3 0.3 567.1 1 4.2 3. 6
 163.1 0.3 0.3 703.9 2 3.6 0. 6
 295.6 329.9 454.6 695.3 4 5.2 0. 6
 527.7 308.0 295.9 775.0 5 4.7 0. 6
 454.1 301.0 1.0 995.6 6 2.9 0. 6
 240.3 417.5 361.1 933.8 7 3.4 0. 6
 590.8 579.3 144.2 666.5 8 3.1 1500. 5
 638.3 756.6 608.9 400.1 9 3.4 1500. 4
 949.8 1004.2 805.4 528.9 10 3.4 1500. 3
 886.8 855.6 706.2 517.4 11 3.0 1300. 2
 635.5 761.0 670.9 596.6 12 4.5 1200. 2
 359.3 412.6 232.5 937.6 1 2.3 1200. 6
 484.7 360.7 226.8 979.0 2 2.5 1200. 6
 529.7 332.0 202.5 980.0 3 2.4 1200. 6
 585.8 291.4 186.1 1100.1 4 2.1 1200. 6
 367.7 368.0 260.2 1005.6 5 2.1 1200. 6
 324.7 270.9 72.7 1058.6 6 2.0 1200. 6
 489.0 274.6 208.5 942.2 7 2.6 1200. 6
 570.8 337.1 218.0 646.5 8 2.8 1200. 5
 419.7 254.4 206.1 344.0 9 4.3 1200. 4
 532.8 414.2 197.9 477.3 9 4.8 1800. 3
 425.2 365.7 198.7 469.5 10 7.1 1700. 4
 467.5 411.5 228.5 455.3 11 7.5 2000. 4
 362.2 306.4 147.6 405.2 12 5.1 2000. 4
 429.2 287.4 139.2 450.6 13 5.4 2000. 4
 446.0 338.1 169.5 461.2 14 5.7 2000. 4
 192.9 253.8 145.6 460.7 15 5.8 2400. 4
 630.3 322.5 257.2 460.5 16 7.3 2700. 4
 364.9 326.7 251.1 510.6 17 7.8 3000. 4
 111.4 196.4 248.5 0.0 23 1.9 250. 4
 89.8 146.5 254.9 0.0 24 1.9 250. 4
 82.5 248.0 160.9 0.0 1 2.9 250. 4
 296.5 253.2 193.2 0.0 2 2.8 250. 4
 215.4 299.7 165.0 0.0 3 2.9 250. 4
 454.5 274.2 154.0 0.0 4 3.5 250. 4
 384.7 324.6 163.2 0.0 5 3.5 250. 4
 253.2 488.3 175.6 0.0 6 3.5 250. 4
 289.5 304.1 193.1 0.0 7 3.1 250. 4

6 'hour of day' -0.01, 4., 8., 12., 16., 20., 24.01
 10 'u (m/s)' 0.5, 1.3, 2.5, 3.5, 4.5, 5.5, 6.5, 7.5, 8.5, 9.5, 10.5
 6 'h (m)' -0.01, 200., 600., 1000., 1500., 2000., 3000.i
 3 'pg class' 0.5 3.5 4.5 6.5

Figure D-1. An example of the input data file for the ANADISTR program.

DEMONSTRATION OF THE RESULTS GENERATED BY THE ANADISTR PROGRAM.

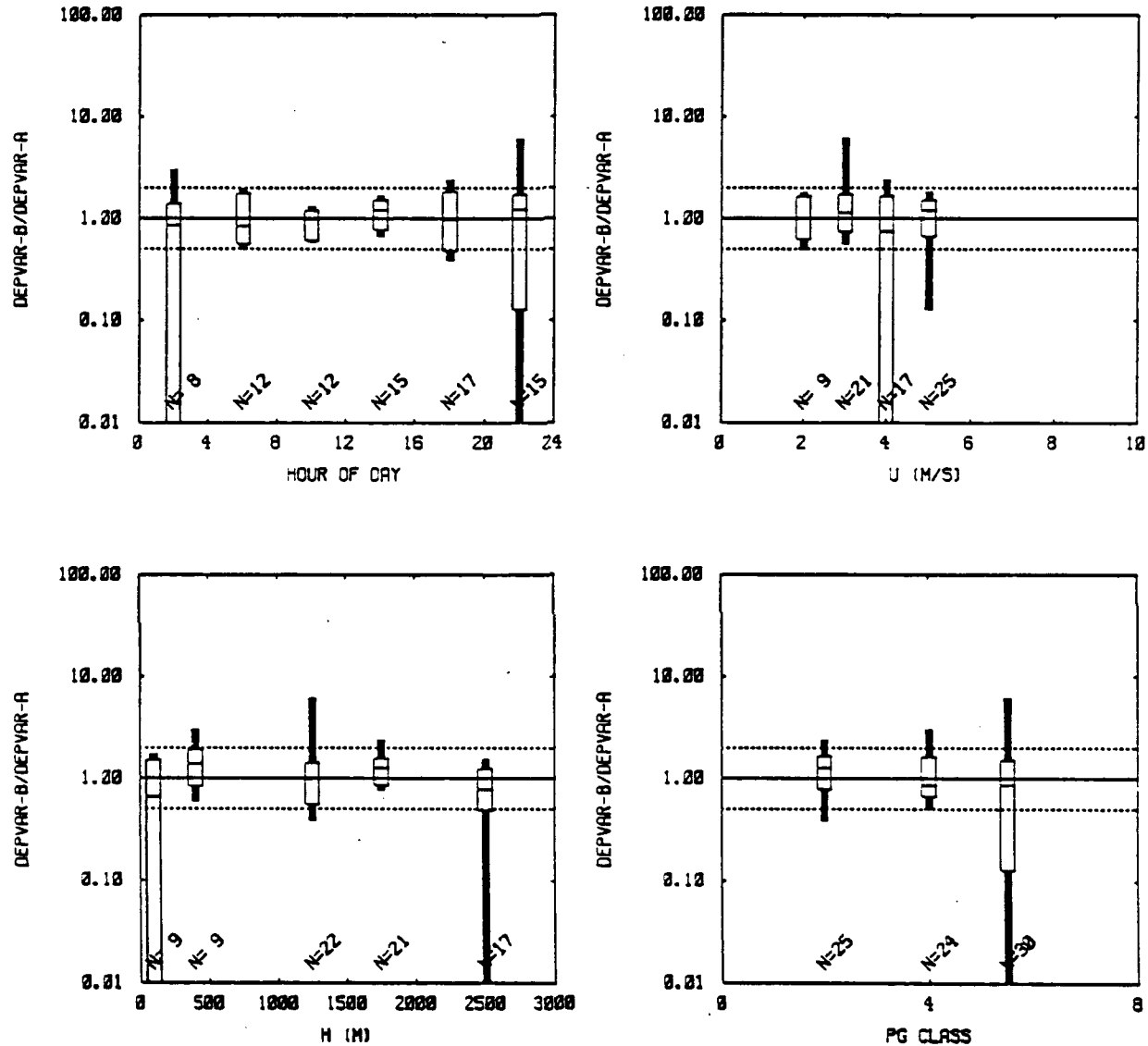


Figure D-2. An example of the results generated by the ANADISTR program and plotted using SIGPLOT. Significant points on each box represent the 2nd, 16th, 50th, 84th, and 98th percentiles. The dashed lines represent the factor of two lines.

The next question will be asked only if the user answers "y" to the above question.

- Enter the lower threshold (e.g. 0.01):

There is no default answer, but 0.01 has proven to be a good choice for the ratio of two dependent variables in our tests.

- Implement an upper threshold for the dependent variable? (y/n):

This is sometimes necessary if the logarithmic scale is to be used and there are very large values in the data whose distribution is to be analyzed. The default (i.e., hitting the RETURN key) answer is "y".

The following question will be asked only if the user answers "y" to the above question.

- Enter the upper threshold of the ratio (e.g. 100.):

There is no default answer, but 100 has proven to be a good choice for the ratio of two dependent variables in our tests.

Intentionally Blank

APPENDIX E

USER'S GUIDE FOR THE SIGPLOT PLOTTING PACKAGE

APPENDIX E

A. USER'S GUIDE FOR THE SIGPLOT PLOTTING PACKAGE

The SIGPLOT plotting package developed at Sigma Research Corporation is a versatile tool for producing different kinds of two-dimensional plots, such as scatter plots, graphs, box plots (sometimes called residual or whisker plots), or error bar plots. The user can specify many parameters including the number of frames per page, the aspect ratio of the frame, and the mapping of the coordinates. The graphics library routines used by SIGPLOT, together with the screen and printer drivers (described later) were originally developed by Dr. Arlindo daSilva of the University of Wisconsin at Milwaukee.

SIGPLOT requires two input files: 1) the template file that contains the control parameters which influence the appearance of the plots, and 2) the input data file that contains the data to be plotted. Tables E-1 and E-2 describe the formats of the template file and the input data file, respectively. Examples of the template file are shown in Figures E-1 and E-2. Examples of the input data file are shown in Figures E-3 and E-4.

SIGPLOT creates a Tektronix picture file that can be viewed directly on any kind of the PC graphics environments (e.g., Hercules, CGA, EGA, and VGA) using the screen driver, TEKPC. Hard copy output can also be generated from the Tektronix picture file with a printer driver. There are three printer drivers, TEKEPS, TEKELQ, and PS, that are currently available. The first two drivers are used to drive an EPSON-compatible dot matrix printer, with TEKEPS for low resolution and TEKELQ for high resolution. The PS program is used to drive a PostScript printer, such as Apple LaserWriter, NEC LC-890, or TI MicroLaser PS35. It is recommended that the user have access to a PostScript printer to obtain the best results in the shortest time.

SIGPLOT requires about 200KB of memory. The other screen and printer drivers require less than 100KB of memory, except for TEKELQ, where 450KB of memory is required due to the high resolution and the use of the bitmap approach in the driver program. The SIGPLOT plotting package and the graphics library routines were written in FORTRAN. The screen and printer drivers were written in C.

TABLE E-1. THE FORMAT OF THE TEMPLATE FILE OF SIGPLOT. THE FOLLOWING KEY LETTERS ARE USED IN THE FORMAT COLUMN - FF: FREE FORMAT, C: CHARACTER, I: INTEGER, AND R: REAL.

The global control parameters are specified in the first section of the template file, lines 1 through 16.

LINE NO.	FORMAT	DESCRIPTION
1-3		Reserved for comments
4	FF/C	Name of the input data file, currently not used
5	FF/C	Name of the output Tektronix picture file, currently not used
6	FF/I	Flag for the frame aspect ratio, 1-5, 1: x:y = 1:1 2: x:y = 1:2 3: x:y = 2:1 4: x:y = 1:3 5: x:y = 3:1
7	FF/I	Number of frames per page, 1-4
8-9	A80	Title for the page (no title will be drawn if "0" appears as the first character of the line)
10	FF/C	Flag (PAXIS) for the axis along which the first column, representing the independent variable, of the data in the input data file (see Table E-2) will be plotted (x or y). PAXIS must = x if IPATTN (described below) = 4, and PAXIS must = y if IPATTN = 6
11	FF/I	Flag for mapping, 1-4, 1: linear in x, linear in y 2: linear in x, logarithmic in y 3: logarithmic in x, linear in y 4: logarithmic in x, logarithmic in y

TABLE E-1. THE FORMAT OF THE TEMPLATE FILE OF SIGPLOT. THE FOLLOWING KEY LETTERS ARE USED IN THE FORMAT COLUMN - FF: FREE FORMAT, C: CHARACTER, I: INTEGER, AND R: REAL. Continued.

LINE NO.	FORMAT	DESCRIPTION
12	FF/I	Flag (IPATN) for plot pattern, 1-6, 1: scatter plot 2: line graph 3: scatter plot except line graph for the last variable 4: box plot 5: error bar plot 6: same as 5 but with extra labelling
13	FF/I	Flag for background, 0 or 2, 0: no background 2: gridded background
14	FF/C	Flag for system time, y or n, if y: system time will be printed out on the upper right corner of each page
15	SA1	Five point patterns for the scatter plot
16	FF/I	Flag (IEXTRA) for the plotting of extra lines. 1: x=0 will be plotted 2: y=0 will be plotted 3: x=0 and y=0 will be plotted 4: x=1 will be plotted 5: y=1 will be plotted 6: x=1 and y=1 will be plotted 7: diagonal line will be plotted 8: y=0.5 and y=2 (factor of two) will be plotted 9: x=-0.667, 0, and 0.667, and $y=4x^2/(4-x^2)$. (see text) will be plotted. else: no extra lines will be plotted. Note that IEXTRA = 9 is effective only if IPATN = 6

TABLE E-1. THE FORMAT OF THE TEMPLATE FILE OF SIGPLOT. THE FOLLOWING KEY LETTERS ARE USED IN THE FORMAT COLUMN - FF: FREE FORMAT, C: CHARACTER, I: INTEGER, AND R: REAL. Continued.

The next section of the template file (lines 17 through 29) contains the parameters that are applicable to a frame. This section can be repeated if there are multiple frames to be plotted in a print job. However, the user can prepare just one such section if the same information is to be used repeatedly by all frames.

LINE NO.	FORMAT	DESCRIPTION
17-19		Reserved for comments
20	FF/R	Constants, a and b, for the linear transformation of the independent variable, where $x_{\text{new}} = a*x_{\text{old}} + b$, a=1 and b=0 means no transformation is needed
21	FF/R	Constants, a and b, for the linear transformation of the first dependent variable, where $y_{1,\text{new}} = a*y_{1,\text{old}} + b$, a=1 and b=0 means no transformation is needed
22	FF/R	Same as above, but for the second dependent variable
23	FF/R	Same as above, but for the third dependent variable
24	FF/R	Same as above, but for the fourth dependent variable

TABLE E-1. THE FORMAT OF THE TEMPLATE FILE OF SIGPLOT. THE FOLLOWING KEY LETTERS ARE USED IN THE FORMAT COLUMN - FF: FREE FORMAT, C: CHARACTER, I: INTEGER, AND R: REAL. Concluded.

LINE NO.	FORMAT	DESCRIPTION
25	FF/R	Same as above, but for the fifth dependent variable. Note that lines 22 through 25 cannot be omitted even if only one group of data were to be plotted
26	FF/R	xmin, xmax, and dx of the x-axis
27	FF/R	ymin, ymax, and dy of the y-axis
28	FF/C	Format specifier for the numerical labels of the x-axis. If ":" appears as the first character of the line, the appropriate format will be determined internally by the program; otherwise, the user should supply a simple FORTRAN I-, F-, or E-format specifier, enclosed in parentheses, e.g., (I5), (F6.3), and (E8.1) are accepted, but (3I5), (I5,f6.3), (1P,E8.1), and (G9.1) are not accepted
29	FF/C	Format specifier for the numerical labels of the y-axis

TABLE E-2. THE FORMAT OF THE INPUT DATA FILE OF SIGPLOT. THE FOLLOWING KEY LETTERS ARE USED IN THE FORMAT COLUMN - FF: FREE FORMAT, C: CHARACTER, I: INTEGER, AND R: REAL.

LINE NO.	FORMAT	DESCRIPTION
1	A40	Title for the frame (no title will be drawn if "0" appears as the first character of the line)
2	A40	Label for the x-axis (no label will be drawn if "0" appears as the first character of the line)
3	A40	Label for the y-axis (no label will be drawn if "0" appears as the first character of the line)
4	FF/I	Two integers specifying the number of points (NPTS) and the number of groups of data (MANY) to be plotted. MANY cannot be > 5 for IPATTN = 1, 2, 3, and 5, and MANY must be = 1 for IPATTN = 4 and 6. NPTS cannot be > 700 for IPATTN = 1, 2, and 3. NPTS cannot be > 50 for IPATTN = 4, 5, and 6 (see text).

Next NPTS lines:

For IPATTN = 1, 2, and 3,

FF/R There are 1+MANY real numbers in each line. The first number represents the independent variable, which can be plotted either along the x- or the y-axis depending the value of PAXIS (see Table E-1). The next MANY numbers represent the dependent variables. For example, if three curves (MANY=3), $f_1(x)$, $f_2(x)$, and $f_3(x)$ were to be plotted, then each line here should contain four real numbers, x_i , $f_{1,i}$, $f_{2,i}$, and $f_{3,i}$, where $i=1, NPTS$. If PAXIS = "x", the x will be plotted along the abscissa, and f_1 , f_2 , and f_3 will be plotted along the ordinate; vice versa PAXIS = "y".

TABLE E-2. THE FORMAT OF THE INPUT DATA FILE OF SIGPLOT. THE FOLLOWING KEY LETTERS ARE USED IN THE FORMAT COLUMN - FF: FREE FORMAT, C: CHARACTER, I: INTEGER, AND R: REAL. Continued.

LINE NO.	FORMAT	DESCRIPTION
For IPATTN = 4,		
	FF/R, I	There are six real numbers and one integer in each line. The first real number represents the independent variable. The next five real numbers represent the values of the dependent variable at the 2th, 16th, 50th, 84th, and 98th percentiles, respectively. Note that the value of the independent variable listed here frequently represents a range of the independent variable; for example, a wind speed of 7 m/s actually represents wind speeds in the range of 6 to 8 m/s. The integer represents the number of data points based on which the distribution of the dependent variable is derived. No box will be plotted if the number of data points is less than five since not enough information is available to define a distribution.
For IPATTN = 5,		
	FF/R	There are 1+3*MANY real numbers in each line. The first number represents the independent variable. The remaining numbers for the dependent variables are in MANY groups of three numbers. The three numbers, which must be in order, represent the distribution of a dependent variable. This distribution can be 1) $\mu-\sigma$, μ , and $\mu+\sigma$, where μ is the mean, and σ is the standard deviation, or 2) lower c.l., nominal value, and upper c.l., where c.l. is the confidence limit.

TABLE E-2. THE FORMAT OF THE INPUT DATA FILE OF SIGPLOT. THE FOLLOWING KEY LETTERS ARE USED IN THE FORMAT COLUMN - FF: FREE FORMAT, C: CHARACTER, I: INTEGER, AND R: REAL. Concluded

LINE NO.	FORMAT	DESCRIPTION
----------	--------	-------------

For IPATTN = 6,

FF/R,C There are four real numbers and one character constant (no more than 17 characters long) in each line. The definition of the first four real numbers is identical to that when IPATTN = 5, except now MANY must = 1. The character constant, enclosed in apostrophes, is used to label each data point.

The above 4+NPTS lines provide enough information to plot a frame. Additional data, similar in structure, can be appended here if the plotting of more than one frames in a print job is desired.

```

!-----  

! Main switches for plotting.  

!-----0-----0-----0-----  

uzrs.1 Name of input data file.  

tek1.pic Name of output tektronix file.  

1 Aspect ratio (integer, 1 - 5).  

1 Number of plots per page (integer, 1 - 4).  

demo of ipattn=2  

0  

x Which axis serves as independent variable (x or y).  

1 Flag indicating log or linear mapping (1 - 4).  

2 Pattern.  

0 Background specification.  

y Print out system time on the upper right hand corner (y or n).  

.toss Patterns of scatter plots (5al)  

0 Extra line,1:x=0,2:y=0,3:x,y=0,4:x=1.5:y=1,6:x,y=1,7:diag,8:y=fac. 2.,9:fb-nmse, else:nothing.  

!-----  

! Parameters for plot 1.  

!-----  

1. 0. ascale, bscale for the independent variable axis.  

1. 0. ascale, bscale for curve 1.  

1. 0. ascale, bscale for curve 2.  

1. 0. ascale, bscale for curve 3.  

1. 0. ascale, bscale for curve 4.  

1. 0. ascale, bscale for curve 5.  

-6.28319 6.28319 3.141595 xmin, xmax, and dx for the x axis.  

-1.2 1.2 0.3 ymin, ymax, and dy for the y axis.  

(f5.2) format for x label  

(f4.1) format for y label

```

Figure E-1. An example of the template file of SIGPLOT. Refer to Figure E-6 for the results.

Figure E-2. An example of the template file of SIGPLOT. Refer to Figure E-9 for the results.

0
 x
 y
 50 5
 -6.03186 0.248690 -0.368124 -0.844328 -0.998027 -0.770514
 -5.78053 0.481754 -0.125333 -0.684547 -0.982287 -0.904827
 -5.52920 0.684547 0.125333 -0.481753 -0.904827 -0.982287
 -5.27788 0.844328 0.368125 -0.248690 -0.770513 -0.998027
 -5.02655 0.951057 0.587786 0.397359E-06 -0.587785 -0.951056
 -4.77522 0.998027 0.770513 0.248690 -0.368125 -0.844328
 -4.52389 0.982287 0.904827 0.481754 -0.125333 -0.684547
 -4.27257 0.904827 0.982287 0.684547 0.125333 -0.481753
 -4.02124 0.770513 0.998027 0.844328 0.368125 -0.248690
 -3.76991 0.587785 0.951056 0.951057 0.587785 0.254308E-06
 -3.51858 0.368125 0.844328 0.998027 0.770513 0.248690
 -3.26726 0.125333 0.684547 0.982287 0.904827 0.481754
 -3.01593 -0.125333 0.481753 0.904827 0.982287 0.684547
 -2.76460 -0.368125 0.248690 0.770513 0.998027 0.844328
 -2.51327 -0.587785 0.397359E-07 0.587785 0.951056 0.951057
 -2.26195 -0.770513 -0.248690 0.368124 0.844328 0.998027
 -2.01062 -0.904827 -0.481754 0.125333 0.684547 0.982287
 -1.75929 -0.982287 -0.684547 -0.125334 0.481753 0.904827
 -1.50796 -0.998027 -0.844328 -0.368124 0.248690 0.770513
 -1.25664 -0.951057 -0.951057 -0.587785 -0.556284E-07 0.587785
 -1.00531 -0.844328 -0.998027 -0.770513 -0.248690 0.368124
 -0.753983 -0.684547 -0.982287 -0.904827 -0.481753 0.125333
 -0.502655 -0.481754 -0.304827 -0.382287 -0.684547 -0.125333
 -0.251328 -0.248690 -0.770513 -0.998027 -0.344328 -0.368125
 0.000000 0.300000 -0.587785 -0.951056 -0.951057 -0.587785
 0.251328 0.248690 -0.368124 -0.844328 -0.998027 -0.770513
 0.502655 0.481753 -0.125333 -0.684547 -0.982287 -0.904827
 0.753982 0.684547 0.125333 -0.481754 -0.904827 -0.982287
 1.00531 0.844328 0.368125 -0.248690 -0.770513 -0.998027
 1.25664 0.951056 0.587785 -0.381470E-06 -0.587786 -0.951057
 1.50796 0.998027 0.770513 0.248690 -0.368125 -0.844328
 1.75929 0.982287 0.904827 0.481754 -0.125333 -0.684547
 2.01062 0.904827 0.982287 0.684547 0.125333 -0.481754
 2.26195 0.770513 0.998027 0.844328 0.368125 -0.248690
 2.51327 0.587785 0.951056 0.951057 0.587785 0.190735E-06
 2.76460 0.368124 0.844328 0.998027 0.770513 0.248690
 3.01593 0.125334 0.684548 0.982287 0.904827 0.481753
 3.26726 -0.125333 0.481754 0.904827 0.982287 0.684547
 3.51858 -0.368124 0.248690 0.770514 0.998027 0.844328
 3.76991 -0.587785 0.341731E-06 0.587785 0.951057 0.951056
 4.02124 -0.770513 -0.248690 0.368125 0.244328 0.998027
 4.27257 -0.904827 -0.481754 0.125333 0.684547 0.982287
 4.52389 -0.982287 -0.684547 -0.125333 0.481754 0.904827
 4.77522 -0.998027 -0.844327 -0.368124 0.248691 0.770514
 5.02655 -0.951057 -0.951056 -0.587785 0.723200E-06 0.587786
 5.27787 -0.844328 -0.998027 -0.770513 -0.248689 0.368125
 5.52920 -0.684548 -0.982287 -0.904827 -0.481753 0.125334
 5.78053 -0.481754 -0.904827 -0.982287 -0.684547 -0.125333
 6.03186 -0.248690 -0.770513 -0.998027 -0.844328 -0.368124
 6.28319 -0.301992E-06 -0.587785 -0.951057 -0.951056 -0.587785

Figure E-3. An example of the input data file of SIGPLOT. Refer to Figure E-6 for the results.

```
all periods
n-s distance (m)
var(dws) / median l-min var(ws) /2
6 3
 312.5 -0.029  0.002  0.034 -0.027  0.043  0.112  0.166  0.275  0.383
 625.0 -0.009  0.005  0.019  0.011  0.048  0.085  0.209  0.361  0.513
1250.0 -0.035  0.012  0.059 -0.007  0.070  0.148  0.330  0.480  0.630
2500.0 -0.155  0.015  0.185 -0.126  0.100  0.325  0.359  0.565  0.771
5000.0 -0.033  0.170  0.373  0.013  0.323  0.633  0.440  0.751  1.062
10000.0 -0.417  0.061  0.539 -0.137  0.369  0.876  0.406  0.873  1.339
```

Figure E-4. An example of the input data file of SIGPLOT. Refer to Figure E-9 for the results.

As one can see from Table E-1, SIGPLOT is capable of creating the following kinds of plots:

- IPATTN = 1: scatter plot (e.g., Fig. E-5)
- IPATTN = 2: line graph (e.g., Fig. E-6)
- IPATTN = 3: scatter plot except line graph for the last variable (e.g., Fig. E-7)
- IPATTN = 4: box plot (e.g., Fig. E-8)
- IPATTN = 5: error bar plot (e.g., Fig. E-9)
- IPATTN = 6: same as IPATTN = 5 but with extra labelling (e.g., Fig. E-10)

The usage of each option is described below.

For IPATTN = 1, groups of data are represented by different dot patterns that are defined in the template file (see Table E-1). At most, five groups of data (MANY = 5) can be plotted, with a maximum of 700 points for each group.

IPATTN = 2 is similar to IPATTN = 1 except that points are now connected. The following line patterns are used to represent different curves: solid, short-dashed, long-dashed, dot-dashed, and dotted. At most, five curves (MANY = 5) can be plotted, with a maximum of 700 points for each group. No user customization of the line patterns is allowed. It is important that the data points in the input file are sorted according to the independent variable.

IPATTN = 3, a combination of IPATTN = 1 and 2, is useful when the user wants to see how well a theoretical curve fits the observed data. Although the order of the data points does not matter for a scatter plot, in this case it is important that the data points in the input file are sorted according to the independent variable. At most, five groups of data (MANY = 5) can be plotted, with a maximum of 700 points for each group.

The IPATTN = 4 option is an alternative to the scatter plot when the number of data points is large. In preparing the input data file for SIGPLOT,

the user first defines certain ranges of the independent variable to be used for grouping the dependent variable. The distribution of the dependent variables within each group is then determined and represented by five significant points in the cumulative distribution function (cdf). These five values could be the 2th, 16th, 50th, 84th, and 98th percentiles of the cdf, or the mean and mean \pm one and two standard deviations. SIGPLOT then uses a box pattern to represent the distribution of the dependent variable within each grouping or range of the independent variable. Only one set of data (i.e., MANY = 1, even though five points are needed to define a box) is accepted for this option, with a maximum of 50 boxes.

IPATTN = 5 is similar to IPATTN = 4 except that three values (vs. five) are needed to define an error bar (vs. a box). These three values can be the mean and mean \pm one standard deviation of a dependent variable, or the nominal value of a dependent variable and its 95% confidence limits. At most, five groups (MANY = 5) of data can be plotted, with a maximum of 50 error bars for each group. The following error bar patterns are used: filled square, empty square, filled triangle, empty triangle, and cross.

IPATTN = 6 is similar to IPATTN = 5 except that the user can label each data point. Because of the additional information to be plotted, only one group of data (MANY = 1) is accepted, with a maximum of 50 error bars. This option is designed primarily to plot the FB (fractional bias), together with its confidence limits, against the NMSE (normalized mean square error), where

$$FB = \frac{(\bar{C}_o - \bar{C}_p)}{0.5(\bar{C}_o + \bar{C}_p)} \quad (E-1)$$

$$NMSE = \frac{\overline{(C_o - C_p)^2}}{\bar{C}_o \bar{C}_p} \quad (E-2)$$

If IEXTRA = 9 (see Table E-1), SIGPLOT will plot the additional $x = -0.667, 0$, and 0.667 lines, representing the factor of two and zero FB lines, together with the $y = 4x^2/(4-x^2)$ line, representing the "minimum" NMSE (due only to the mean bias) as a function of FB.

The information concerning the usage of the driver programs, TEKPC, TEKELQ, TEKEPS, and PS, can be obtained by simply executing the programs without providing any arguments, and will not be repeated here.

Finally, an example is given below of the procedures followed to use the graphics package.

- Step 1: The user prepares the template file (DEMO.INQ) and the input data file (DEMO.DAT) according to the formats described in Tables E-1 and E-2. The user can create his own template file by editing the sample template file. The input data file is usually generated by some other programs.
- Step 2: After the execution of SIGPLOT, a Tektronix picture file (DEMO.PIC) is generated.
- Step 3: The user can view the results on screen by typing:
TEKPC DEMO.PIC
if a Hercules graphics card is installed, or
TEKPC DEMO.PIC 16
if an EGA (with a resolution of 640x350 pixels) graphics card is installed.
- Step 4: A high resolution hard copy output can be generated on an EPSON-compatible dot matrix printer by typing:
TEKELQ DEMO.PIC.
- Step 5: Or if the user has access to a PostScript printer, a PostScript file (DEMO.PS) will be created by typing:
PS DEMO.PIC,
and this file can be printed out by typing:
PRINT DEMO.PS

DEMO OF IPATTN=1

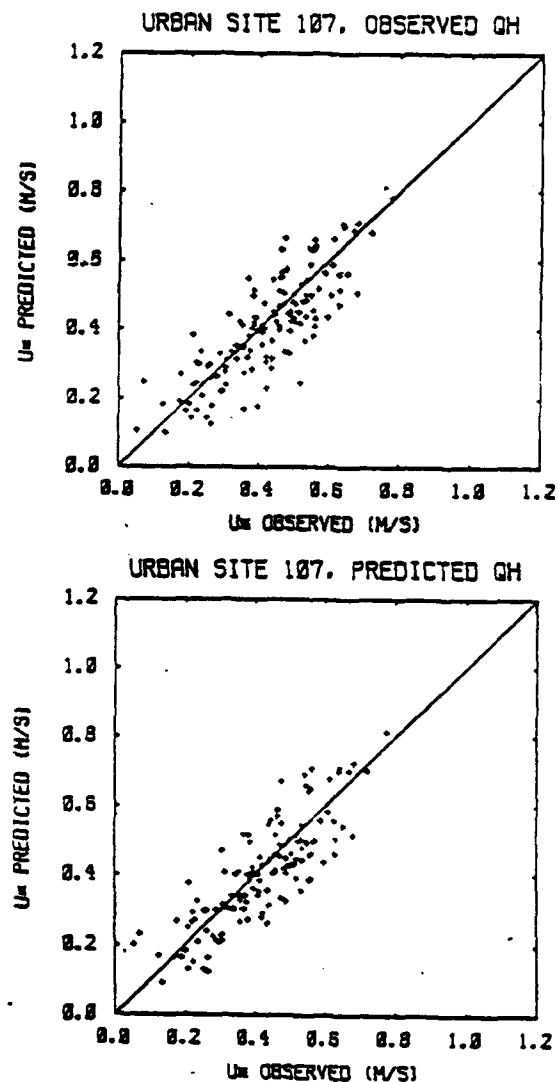


Figure E-5. A sample scatter plot (IPATTN = 1) generated by SIGPLOT.

DEMO OF IPATTN=2

03/25/91

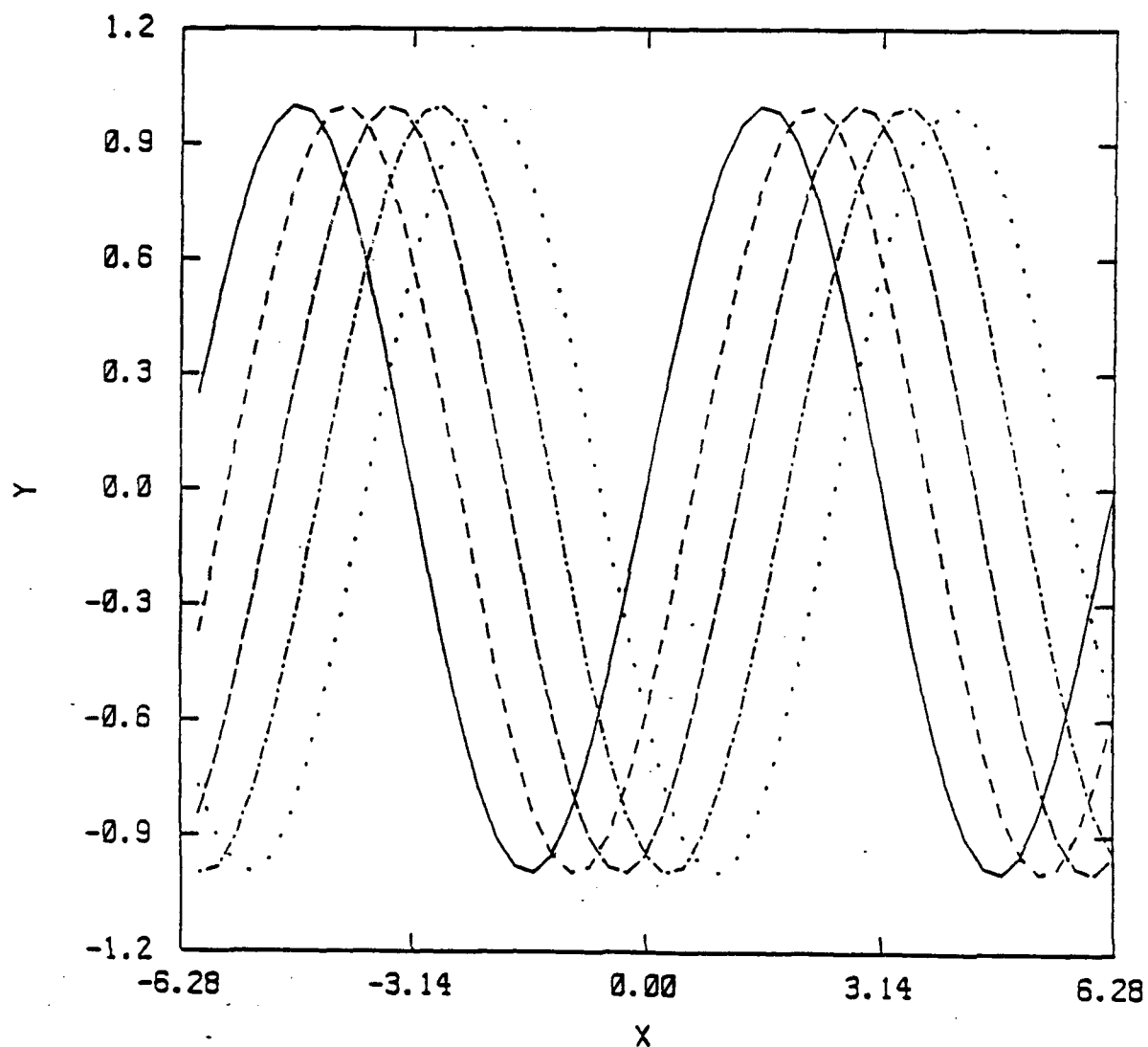


Figure E-6. A sample line graph (IPATTN = 2) generated by SIGPLOT. Refer to Figures E-1 and E-3 for the template and data files used for this figure.

DEMO OF IPATTN=3

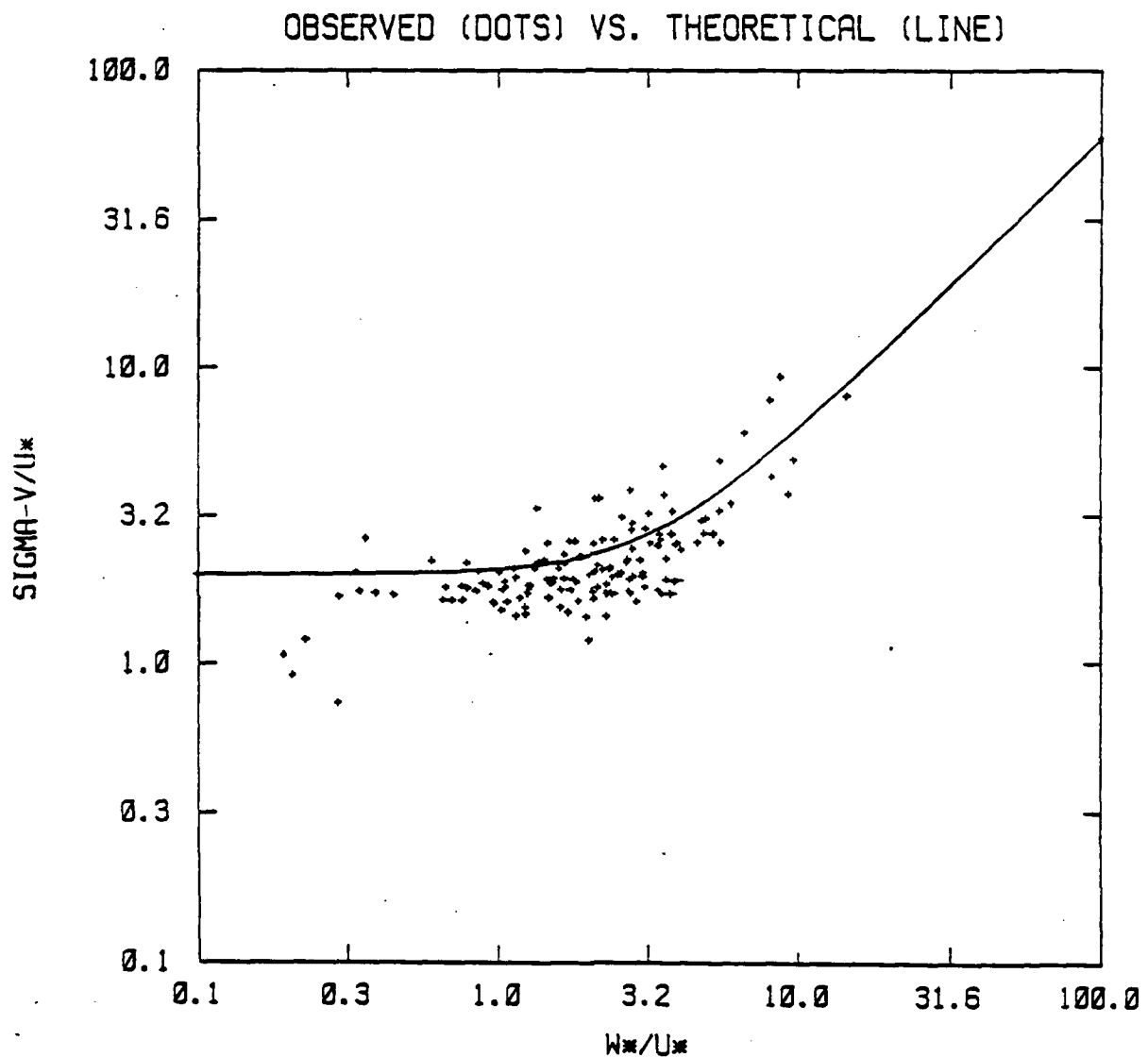


Figure E-7. A sample scatter plot and line graph (IPATTN = 3) generated by SIGPLOT.

DEMO OF IPATTN=4

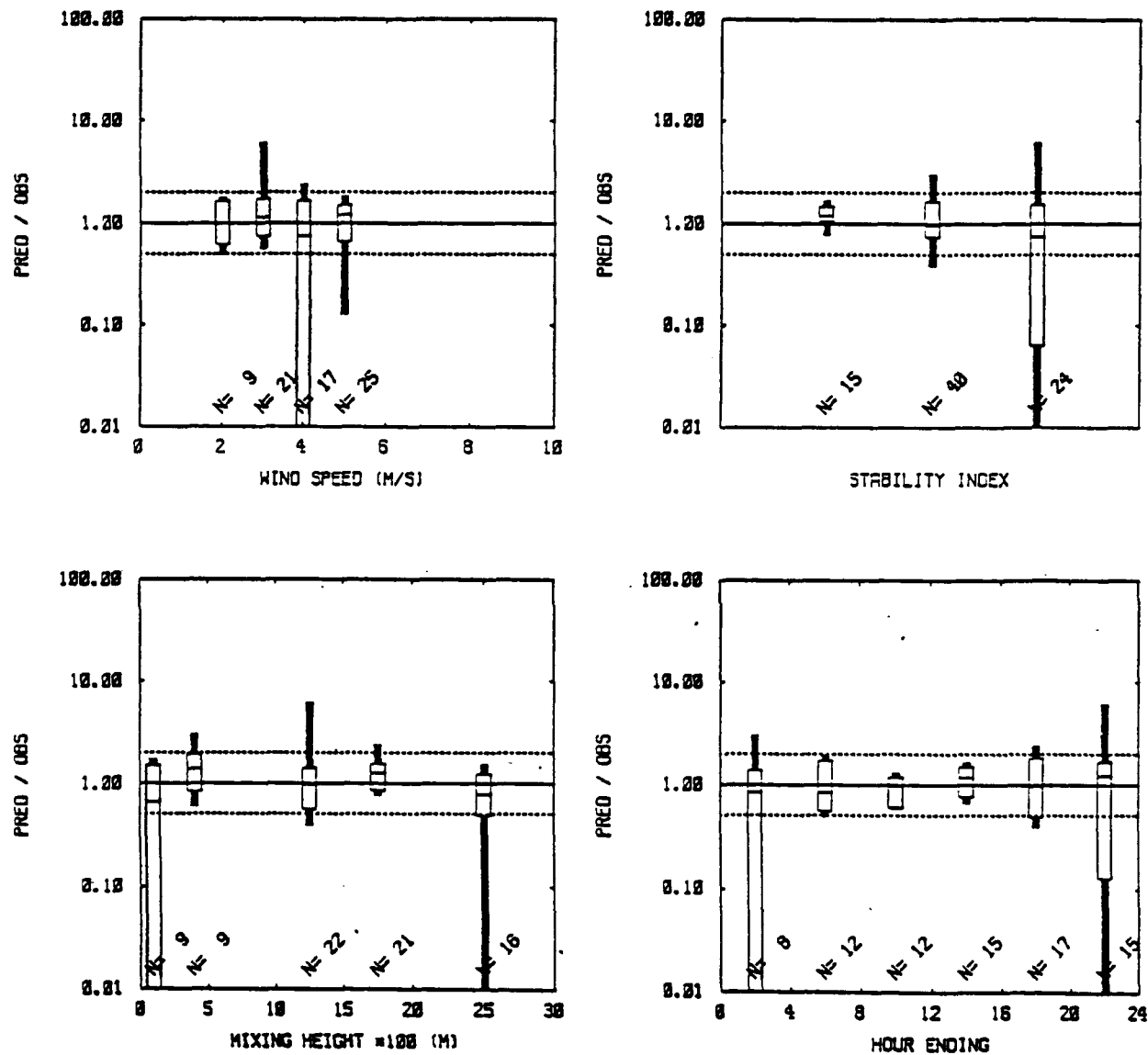


Figure E-8. A sample box plot (IPATTN = 4) generated by SIGPLOT.

DEMO OF IPATTN=5

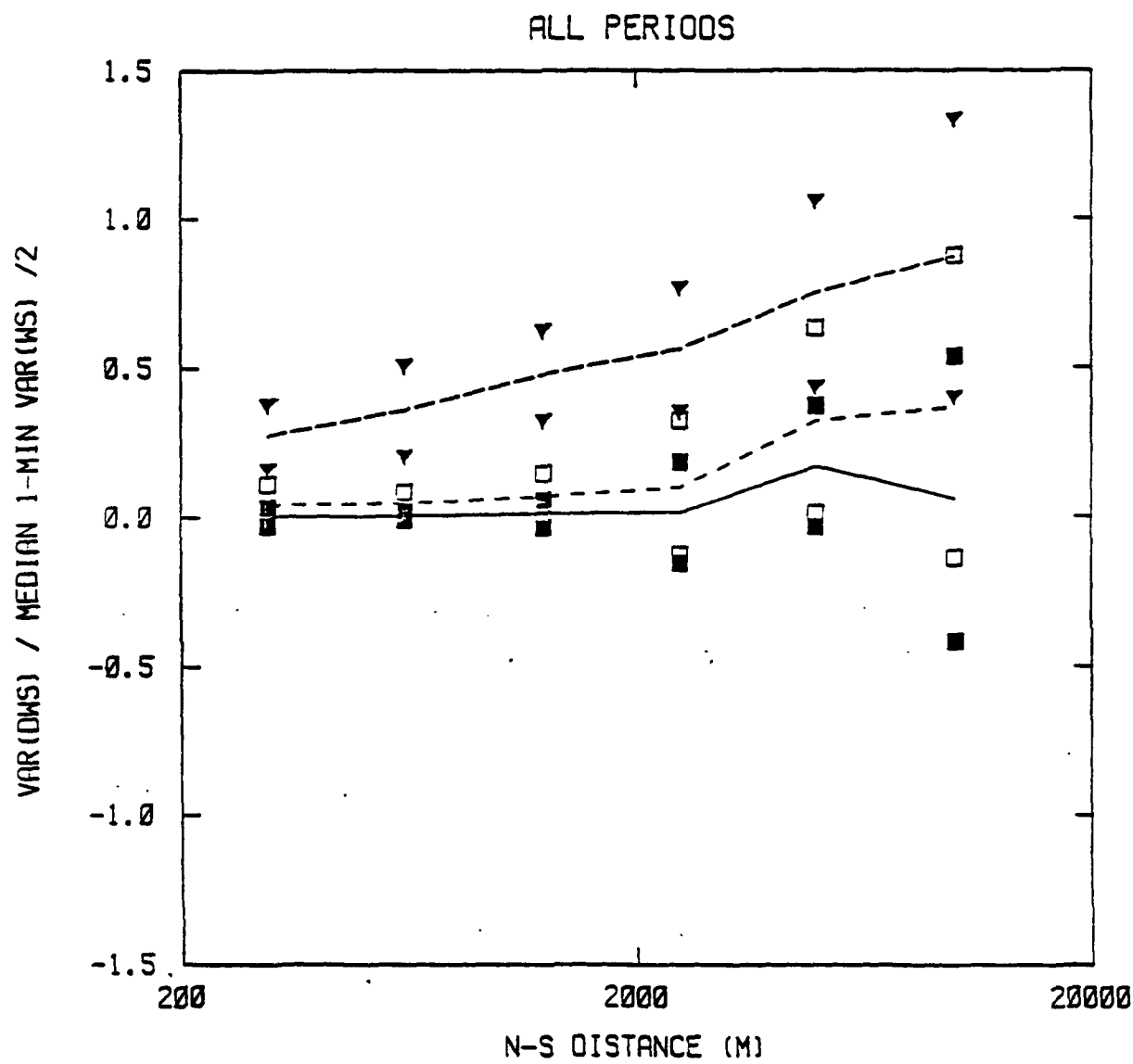


Figure E-9. A sample error bar plot (IPATTN = 5) generated by SIGPLOT. Refer to Figures E-2 and E-4 for the template and data files used for this figure.

DEMO OF IPATTN=6

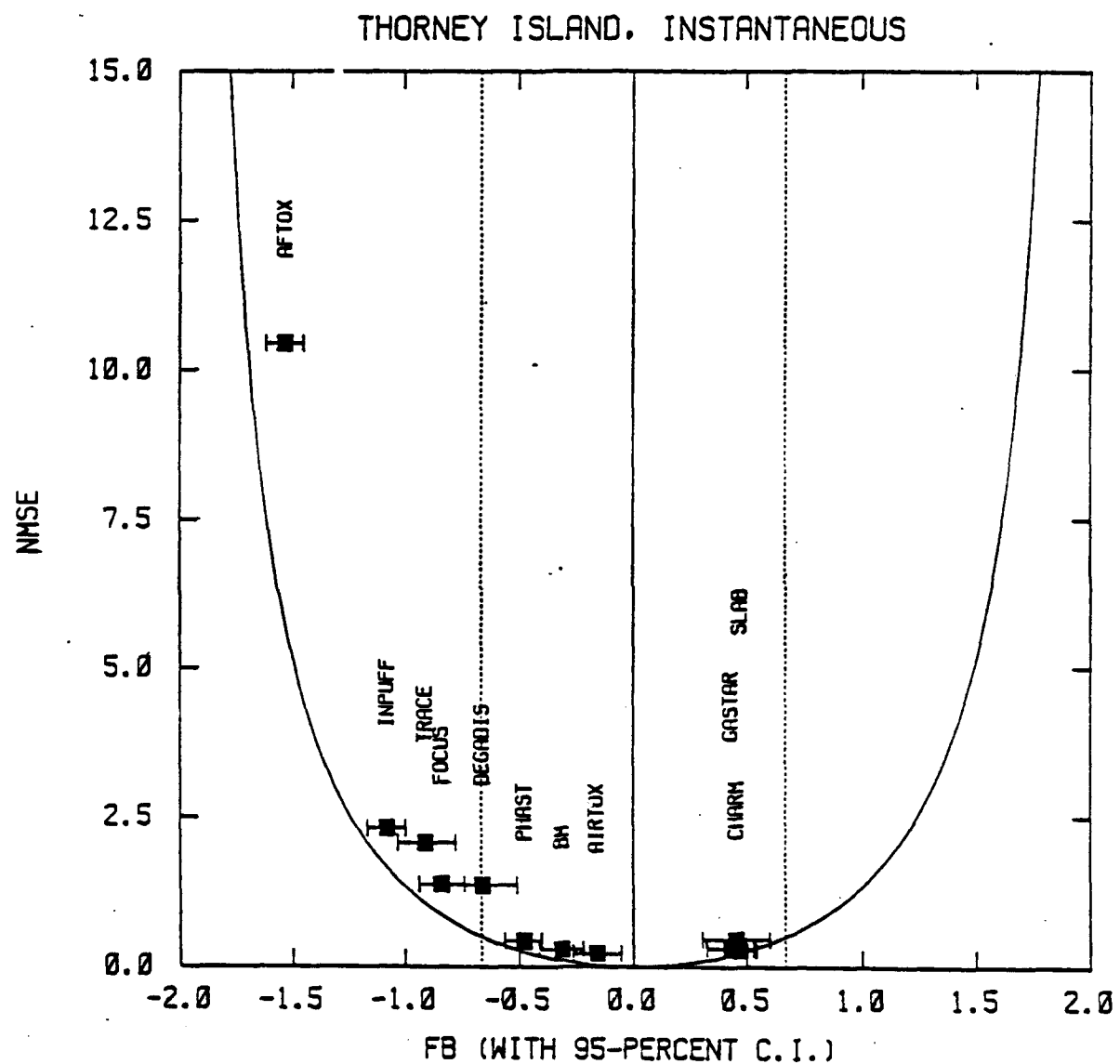


Figure E-10. A sample error bar plot with labelling (IPATTN = 6) generated by SIGPLOT.

Intentionally Blank

APPENDIX F-1

LISTINGS OF THE DUGWAY DATA ARCHIVES - HISTORICAL DATASETS

Dry Gulch, Course B

12 : Number of trials included in DDA

3 : time zone designation

34.50 : latitude (deg)

120.50 : longitude (deg)

dgb1 : dgbb2 : dgbc3 : dgbd4 : dgbe5 : dgbf6 : dgbg7 : dgbi8 : dgbl9 : dgbo10 : dgbu11 : dgbc12 : trial 10

6	6	6	6	6	6	6	6	6	6	6	6
12	16	21	23	26	26	26	28	30	30	30	30
1961	1961	1961	1961	1961	1961	1961	1961	1961	1961	1961	1961
12	9	18	15	18	15	15	15	15	15	15	15
14	55	57	55	30	30	30	4	4	4	4	4
1	1	1	1	1	1	1	1	1	1	1	1
0.0	0.0	0.0	0.0	0.0	0.0	0.0	0.0	0.0	0.0	0.0	0.0
0.0	0.0	0.0	0.0	0.0	0.0	0.0	0.0	0.0	0.0	0.0	0.0
2.50	2.50	2.50	2.50	2.50	2.50	2.50	2.50	2.50	2.50	2.50	2.50
0.656	0.689	0.661	1.278	0.677	0.661	0.677	0.677	0.677	0.677	0.677	0.677
1800.0	1800.0	1800.0	1800.0	1800.0	1800.0	1800.0	1800.0	1800.0	1800.0	1800.0	1800.0
-99.9	-99.9	-99.9	-99.9	-99.9	-99.9	-99.9	-99.9	-99.9	-99.9	-99.9	-99.9
0.000	0.000	0.000	0.000	0.000	0.000	0.000	0.000	0.000	0.000	0.000	0.000
0.000	0.000	0.000	0.000	0.000	0.000	0.000	0.000	0.000	0.000	0.000	0.000
-99.9	-99.9	-99.9	-99.9	-99.9	-99.9	-99.9	-99.9	-99.9	-99.9	-99.9	-99.9
-99.9	-99.9	-99.9	-99.9	-99.9	-99.9	-99.9	-99.9	-99.9	-99.9	-99.9	-99.9
289.15	289.15	289.15	289.15	289.15	289.15	289.15	289.15	289.15	289.15	289.15	289.15
1.80	1.80	1.80	1.80	1.80	1.80	1.80	1.80	1.80	1.80	1.80	1.80
288.95	288.95	288.95	288.95	288.95	288.95	288.95	288.95	288.95	288.95	288.95	288.95
16.50	16.50	16.50	16.50	16.50	16.50	16.50	16.50	16.50	16.50	16.50	16.50
5.00	2.10	0.80	1.00	1.00	1.00	1.00	1.00	1.00	1.00	1.00	1.00
3.70	3.70	3.70	3.70	3.70	3.70	3.70	3.70	3.70	3.70	3.70	3.70
5.00	2.10	0.80	1.00	1.00	1.00	1.00	1.00	1.00	1.00	1.00	1.00
292.0	292.0	292.0	292.0	292.0	292.0	292.0	292.0	292.0	292.0	292.0	292.0
-99.90	-99.90	-99.90	-99.90	-99.90	-99.90	-99.90	-99.90	-99.90	-99.90	-99.90	-99.90
15.40	21.00	18.60	19.30	14.00	21.00	14.00	14.00	14.00	14.00	14.00	14.00
-99.90	-99.90	-99.90	-99.90	-99.90	-99.90	-99.90	-99.90	-99.90	-99.90	-99.90	-99.90
3.70	3.70	3.70	3.70	3.70	3.70	3.70	3.70	3.70	3.70	3.70	3.70
292.0	292.0	292.0	292.0	292.0	292.0	292.0	292.0	292.0	292.0	292.0	292.0
-99.90	-99.90	-99.90	-99.90	-99.90	-99.90	-99.90	-99.90	-99.90	-99.90	-99.90	-99.90
0.2000	0.2000	0.2000	0.2000	0.2000	0.2000	0.2000	0.2000	0.2000	0.2000	0.2000	0.2000
-99.900	-99.900	-99.900	-99.900	-99.900	-99.900	-99.900	-99.900	-99.900	-99.900	-99.900	-99.900
-99.900	-99.900	-99.900	-99.900	-99.900	-99.900	-99.900	-99.900	-99.900	-99.900	-99.900	-99.900
0.30	0.30	0.30	0.30	0.30	0.30	0.30	0.30	0.30	0.30	0.30	0.30
5.00	5.00	5.00	5.00	5.00	5.00	5.00	5.00	5.00	5.00	5.00	5.00
-99.9	-99.9	-99.9	-99.9	-99.9	-99.9	-99.9	-99.9	-99.9	-99.9	-99.9	-99.9
37.5	0.0	0.0	0.0	0.0	0.0	0.0	0.0	0.0	0.0	0.0	0.0
-99.9	-99.9	-99.9	-99.9	-99.9	-99.9	-99.9	-99.9	-99.9	-99.9	-99.9	-99.9
2820.0	2820.0	2820.0	2820.0	2820.0	2820.0	2820.0	2820.0	2820.0	2820.0	2820.0	2820.0
4.57	4.57	4.57	4.57	4.57	4.57	4.57	4.57	4.57	4.57	4.57	4.57
2	2	2	2	2	2	2	2	2	2	2	2
2301.0	2301.0	2301.0	2301.0	2301.0	2301.0	2301.0	2301.0	2301.0	2301.0	2301.0	2301.0
5.800E-04	1.900E-03	2.190E-03	2.210E-03	1.050E-03	7.600E-04	5.400E-04	7.310E-04	5.210E-04	1.190E-03	1.520E-03	1.090E-03
-9.950E-01											
5.665	5.665	5.665	5.665	5.665	5.665	5.665	5.665	5.665	5.665	5.665	5.665
2.900E-04	4.400E-04	4.060E-05	8.700E-04	9.310E-04	9.280E-05	5.650E-04	4.410E-04	4.190E-03	1.600E-03	1.010E-03	1.000E-03
-9.900E-01											
-99.9	-99.9	-99.9	-99.9	-99.9	-99.9	-99.9	-99.9	-99.9	-99.9	-99.9	-99.9
0	0	0	0	0	0	0	0	0	0	0	0
0	0	0	0	0	0	0	0	0	0	0	0

Dry Gulch, Course B
12 : number of trials included in DOA
0 : time zone designation

F-2

Dry Gulch, Course B
1/2 : Number of trials included in DDA

Dry Gulch, Course 8

12 : number of trials included in DDA

0 : time zone designation

34.50 : latitude (deg)

120.50 : longitude (deg)

dgb37 dgb38 dgb39 dgb40

dgb41 dgb42 dgb43 dgb44

dgb45 dgb46 dgb47 dgb48

dgb49 dgb50 dgb51 dgb52

dgb53 dgb54 dgb55 dgb56

dgb57 dgb58 dgb59 dgb60

dgb61 dgb62 dgb63 dgb64

dgb65 dgb66 dgb67 dgb68

dgb69 dgb70 dgb71 dgb72

dgb73 dgb74 dgb75 dgb76

dgb77 dgb78 dgb79 dgb80

dgb81 dgb82 dgb83 dgb84

dgb85 dgb86 dgb87 dgb88

dgb89 dgb90 dgb91 dgb92

dgb93 dgb94 dgb95 dgb96

dgb97 dgb98 dgb99 dgb100

dgb101 dgb102 dgb103 dgb104

dgb105 dgb106 dgb107 dgb108

dgb109 dgb110 dgb111 dgb112

dgb114 dgb115 dgb116 dgb117

dgb119 dgb120 dgb121 dgb122

dgb124 dgb125 dgb126 dgb127

dgb129 dgb130 dgb131 dgb132

dgb135 dgb136 dgb137 dgb138

dgb141 dgb142 dgb143 dgb144

dgb147 dgb148 dgb149 dgb150

dgb153 dgb154 dgb155 dgb156

dgb159 dgb160 dgb161 dgb162

dgb165 dgb166 dgb167 dgb168

dgb171 dgb172 dgb173 dgb174

dgb177 dgb178 dgb179 dgb180

dgb183 dgb184 dgb185 dgb186

dgb189 dgb190 dgb191 dgb192

dgb197 dgb198 dgb199 dgb200

dgb203 dgb204 dgb205 dgb206

dgb211 dgb212 dgb213 dgb214

dgb217 dgb218 dgb219 dgb220

dgb224 dgb225 dgb226 dgb227

dgb230 dgb231 dgb232 dgb233

dgb239 dgb240 dgb241 dgb242

dgb245 dgb246 dgb247 dgb248

dgb253 dgb254 dgb255 dgb256

dgb267 dgb268 dgb269 dgb270

dgb273 dgb274 dgb275 dgb276

dgb279 dgb280 dgb281 dgb282

dgb285 dgb286 dgb287 dgb288

dgb291 dgb292 dgb293 dgb294

dgb297 dgb298 dgb299 dgb300

dgb303 dgb304 dgb305 dgb306

dgb309 dgb310 dgb311 dgb312

dgb315 dgb316 dgb317 dgb318

dgb319 dgb320 dgb321 dgb322

dgb325 dgb326 dgb327 dgb328

dgb329 dgb330 dgb331 dgb332

dgb335 dgb336 dgb337 dgb338

dgb341 dgb342 dgb343 dgb344

dgb347 dgb348 dgb349 dgb350

dgb353 dgb354 dgb355 dgb356

dgb359 dgb360 dgb361 dgb362

dgb365 dgb366 dgb367 dgb368

dgb371 dgb372 dgb373 dgb374

dgb377 dgb378 dgb379 dgb380

dgb381 dgb382 dgb383 dgb384

dgb385 dgb386 dgb387 dgb388

dgb391 dgb392 dgb393 dgb394

dgb397 dgb398 dgb399 dgb400

dgb401 dgb402 dgb403 dgb404

dgb405 dgb406 dgb407 dgb408

dgb409 dgb410 dgb411 dgb412

dgb413 dgb414 dgb415 dgb416

dgb417 dgb418 dgb419 dgb420

dgb421 dgb422 dgb423 dgb424

dgb425 dgb426 dgb427 dgb428

dgb429 dgb430 dgb431 dgb432

dgb435 dgb436 dgb437 dgb438

dgb441 dgb442 dgb443 dgb444

dgb445 dgb446 dgb447 dgb448

dgb449 dgb450 dgb451 dgb452

dgb453 dgb454 dgb455 dgb456

dgb457 dgb458 dgb459 dgb460

dgb461 dgb462 dgb463 dgb464

dgb465 dgb466 dgb467 dgb468

dgb469 dgb470 dgb471 dgb472

dgb473 dgb474 dgb475 dgb476

dgb477 dgb478 dgb479 dgb480

dgb481 dgb482 dgb483 dgb484

dgb485 dgb486 dgb487 dgb488

dgb489 dgb490 dgb491 dgb492

dgb493 dgb494 dgb495 dgb496

dgb497 dgb498 dgb499 dgb500

dgb501 dgb502 dgb503 dgb504

dgb505 dgb506 dgb507 dgb508

dgb509 dgb510 dgb511 dgb512

dgb513 dgb514 dgb515 dgb516

dgb517 dgb518 dgb519 dgb520

dgb521 dgb522 dgb523 dgb524

dgb525 dgb526 dgb527 dgb528

dgb529 dgb530 dgb531 dgb532

dgb533 dgb534 dgb535 dgb536

dgb537 dgb538 dgb539 dgb540

dgb541 dgb542 dgb543 dgb544

dgb545 dgb546 dgb547 dgb548

dgb549 dgb550 dgb551 dgb552

dgb553 dgb554 dgb555 dgb556

dgb557 dgb558 dgb559 dgb560

dgb561 dgb562 dgb563 dgb564

dgb565 dgb566 dgb567 dgb568

dgb569 dgb570 dgb571 dgb572

dgb573 dgb574 dgb575 dgb576

dgb577 dgb578 dgb579 dgb580

dgb581 dgb582 dgb583 dgb584

dgb585 dgb586 dgb587 dgb588

dgb589 dgb590 dgb591 dgb592

dgb593 dgb594 dgb595 dgb596

dgb597 dgb598 dgb599 dgb600

dgb601 dgb602 dgb603 dgb604

dgb605 dgb606 dgb607 dgb608

dgb609 dgb610 dgb611 dgb612

dgb613 dgb614 dgb615 dgb616

dgb617 dgb618 dgb619 dgb620

dgb621 dgb622 dgb623 dgb624

dgb625 dgb626 dgb627 dgb628

dgb629 dgb630 dgb631 dgb632

dgb633 dgb634 dgb635 dgb636

dgb637 dgb638 dgb639 dgb640

dgb641 dgb642 dgb643 dgb644

dgb645 dgb646 dgb647 dgb648

dgb649 dgb650 dgb651 dgb652

dgb653 dgb654 dgb655 dgb656

dgb657 dgb658 dgb659 dgb660

dgb661 dgb662 dgb663 dgb664

dgb665 dgb666 dgb667 dgb668

dgb669 dgb670 dgb671 dgb672

dgb673 dgb674 dgb675 dgb676

dgb677 dgb678 dgb679 dgb680

dgb681 dgb682 dgb683 dgb684

dgb685 dgb686 dgb687 dgb688

dgb689 dgb690 dgb691 dgb692

dgb693 dgb694 dgb695 dgb696

dgb697 dgb698 dgb699 dgb700

dgb701 dgb702 dgb703 dgb704

dgb705 dgb706 dgb707 dgb708

dgb709 dgb710 dgb711 dgb712

dgb713 dgb714 dgb715 dgb716

dgb717 dgb718 dgb719 dgb720

dgb721 dgb722 dgb723 dgb724

dgb725 dgb726 dgb727 dgb728

dgb729 dgb730 dgb731 dgb732

dgb733 dgb734 dgb735 dgb736

dgb737 dgb738 dgb739 dgb740

dgb741 dgb742 dgb743 dgb744

dgb745 dgb746 dgb747 dgb748

dgb749 dgb750 dgb751 dgb752

dgb753 dgb754 dgb755 dgb756

dgb757 dgb758 dgb759 dgb760

dgb761 dgb762 dgb763 dgb764

dgb765 dgb766 dgb767 dgb768

dgb769 dgb770 dgb771 dgb772

dgb773 dgb774 dgb775 dgb776

dgb777 dgb778 dgb779 dgb780

dgb781 dgb782 dgb783 dgb784

dgb785 dgb786 dgb787 dgb788

dgb789 dgb790 dgb791 dgb792

dgb793 dgb794 dgb795 dgb796

dgb797 dgb798 dgb799 dgb800

dgb801 dgb802 dgb803 dgb804

dgb805 dgb806 dgb807 dgb808

dgb809 dgb810 dgb811 dgb812

dgb813 dgb814 dgb815 dgb816

dgb817 dgb818 dgb819 dgb820

dgb821 dgb822 dgb823 dgb824

dgb825 dgb826 dgb827 dgb828

dgb829 dgb830 dgb831 dgb832

dgb833 dgb834 dgb835 dgb836

dgb837 dgb838 dgb839 dgb840

dgb841 dgb842 dgb843 dgb844

dgb845 dgb846 dgb847 dgb848

dgb849 dgb850 dgb851 dgb852

dgb853 dgb854 dgb855 dgb856

dgb857 dgb858 dgb859 dgb860

dgb861 dgb862 dgb863 dgb864

dgb865 dgb866 dgb867 dgb868

dgb869 dgb870 dgb871 dgb872

dgb873 dgb874 dgb875 dgb876

dgb877 dgb878 dgb879 dgb880

dgb881 dgb882 dgb883 dgb884

dgb885 dgb886 dgb887 dgb888

dgb889 dgb890 dgb891 dgb892

dgb895 dgb896 dgb897 dgb898

dgb899 dgb900 dgb901 dgb902

dgb903 dgb904 dgb905 dgb906

dgb907 dgb908 dgb909 dgb910

dgb911 dgb912 dgb913 dgb914

dgb915 dgb916 dgb917 dgb918

dgb919 dgb920 dgb921 dgb922

dgb923 dgb924 dgb925 dgb926

dgb927 dgb928 dgb929 dgb930

dgb931 dgb932 dgb933 dgb934

dgb936 dgb937 dgb938 dgb939

dgb935 dgb936 dgb937 dgb938

dgb940 dgb941 dgb942 dgb943

dgb944 dgb945 dgb946 dgb947

dgb948 dgb949 dgb950 dgb951

dgb952 dgb953 dgb954 dgb955

dgb956 dgb957 dgb958 dgb959

dgb950

Dry Gulch, Course D
12 : number of trials included in DOA

Dry Hatch, Course D

12 : number of trials included in DDA

8 : time zone designation

34.30 : latitude (deg)

120.50 : longitude (deg)

dgd25 dgd26 dgd27 dgd28 dgd29 dgd30 dgd31 dgd32 dgd33 dgd34 dgd35

dgd36 : trial ID

3

3

3

3

3

3

3

3

3

3

3

3

3

3

3

3

3

3

3

3

3

3

3

3

3

3

3

3

3

3

3

3

3

3

3

3

3

3

3

3

3

3

3

3

3

3

3

3

3

3

3

3

3

3

3

3

3

3

3

3

3

3

3

3

3

3

3

3

3

3

3

3

3

3

3

3

3

3

3

3

3

3

3

3

3

3

3

3

3

3

3

3

3

3

3

3

3

3

3

3

3

3

3

3

3

3

3

3

3

3

3

3

3

3

3

3

3

3

3

3

3

3

3

3

3

3

3

3

3

3

3

3

3

3

3

3

3

3

3

3

3

3

3

3

3

3

3

3

3

3

3

3

3

3

3

3

3

3

3

3

3

3

3

3

3

3

3

3

3

3

3

3

3

3

3

3

3

3

3

3

3

3

3

3

3

3

3

3

3

3

3

3

3

3

3

3

3

3

3

3

3

3

3

3

3

3

3

3

3

3

3

3

3

3

3

3

3

3

3

3

3

3

3

3

3

3

3

3

3

3

3

3

3

3

3

3

3

3

3

3

3

3

3

3

3

3

3

3

3

3

3

3

3

3

3

3

3

3

3

3

3

3

3

3

3

3

3

3

3

3

3

3

3

3

3

3

3

3

3

3

3

3

3

3

3

3

3

3

3

3

3

3

3

3

3

3

3

3

3

Dry Gulch, Course D
 3 : number of trials included in DDA
 0 : time zone designation
 34.50 : latitude (deg)
 120.50 : longitude (deg)

dgd49 dgds0 dgds1 : trial 10

6	6	6	6	no. of sources
26	26	28	28	x-coord. of source (m)
1962	1962	1962	1962	y-coord. of source (m)
17	21	17	17	z-coord. of source (m)
45	0	30	30	source elevation (m)
1800.0	1800.0	1800.0	1800.0	elevation rate (g/s)
-99.9	-99.9	-99.9	-99.9	elevation duration (s)
0.000	0.000	0.000	0.000	total mass emitted (kg)
0.000	0.000	0.000	0.000	closed at the source (m)
0.000	0.000	0.000	0.000	closed at the source (m)
-99.9	-99.9	-99.9	-99.9	ambient pressure (atm)
-99.9	-99.9	-99.9	-99.9	relative humidity (%)
205.15	201.15	291.15	291.15	temperature at level 41 (K)
1.80	1.80	1.80	1.80	measuring height for temperature #1 (m)
284.35	283.45	289.95	289.95	temperature at level 42 (K)
16.50	16.50	16.50	16.50	measuring height for temperature #2 (m)
5.60	2.40	3.20	3.20	wind speed (m/s) at a tower
1.70	3.70	3.70	3.70	measuring height for wind data (m)
5.10	2.40	3.20	3.20	domain-averaged wind speed (m/s)
32.0	296.0	317.0	317.0	domain-averaged wind direction (deg)
-99.90	-99.90	-99.90	-99.90	domain-averaged sigma-u (m/s)
14.90	10.20	17.70	17.70	domain-averaged sigma-theta (deg)
-99.90	-99.90	-99.90	-99.90	domain-averaged sigma-phi (deg)
3.10	3.10	3.10	3.10	measuring ht for domain-avg wind speed (m)
2820.0	2820.0	2820.0	2820.0	averaging time for domain-avg data (s)
-99.000	-99.900	-99.900	-99.900	wind speed power law exponent
0.5000	0.5000	0.5000	0.5000	surface roughness (m)
-99.900	-99.900	-99.900	-99.900	friction velocity (m/s)
-99.900	-99.900	-99.900	-99.900	Lavre Monili-Obikhov length (1/m)
0.30	0.30	0.30	0.30	albedo
0.20	0.20	0.20	0.20	biomass availability
5.00	5.00	5.00	5.00	down ratio
-99.9	-99.9	-99.9	-99.9	mixing height (m)
0.0	0.0	0.0	0.0	cloud cover (%)
-99	-99	-99	-99	p-G stability class
2020.0	2020.0	2020.0	2020.0	averaging time for concentration (s)
4.57	4.57	4.57	4.57	suggested receptor height (m)
3	3	3	3	no. of distances downwind
953.0	953.0	953.0	953.0	distances downwind (m)
-9.3902e-02	3.4202e-02	3.5202e-03	3.5202e-03	cross-wind integrated conc. (mg/m^3)
-9.3902e-01	-9.3902e-01	-9.3902e-01	-9.3902e-01	cross-wind integrated conc. (mg/m^3)
1500.0	1500.0	1500.0	1500.0	distances downwind (m)
4.6102e-03	1.0105e-03	3.8508e-04	3.8508e-04	concentration (mg/m^3)
-9.3902e-01	-9.3902e-01	-9.3902e-01	-9.3902e-01	cross-wind integrated conc. (mg/m^3)
-99.90	-99.90	-99.90	-99.90	sigma-y (m)
4715.0	4715.0	4715.0	4715.0	distances downwind (m)
5.2402e-04	1.0102e-03	1.9202e-04	1.9202e-04	concentration (mg/m^3)
-9.3902e-01	-9.3902e-01	-9.3902e-01	-9.3902e-01	cross-wind integrated conc. (mg/m^3)
-99.90	-99.90	-99.90	-99.90	sigma-y (m)
0	0	0	0	no. of lines-of-sight

Ocean Breeze 12 : number of trials included in ODA
5 : time zone designation

Ocean Breeze

12 : number of trials included in DDA

5 : time zone designation

28.40 : latitude (deg)

80.70 : longitude (deg)

ob14 : obs1

ob15 : obs2

ob16 : obs3

ob17 : obs4

ob18 : obs5

ob19 : obs6

ob20 : obs7

ob21 : obs8

ob22 : obs9

ob23 : obs10

ob24 : obs11

ob25 : obs12

ob26 : obs13

ob27 : obs14

ob28 : obs15

ob29 : obs16

ob30 : obs17

ob31 : obs18

ob32 : obs19

ob33 : obs20

ob34 : obs21

ob35 : obs22

ob36 : obs23

ob37 : obs24

ob38 : obs25

ob39 : obs26

ob40 : obs27

ob41 : obs28

ob42 : obs29

ob43 : obs30

ob44 : obs31

ob45 : obs32

ob46 : obs33

ob47 : obs34

ob48 : obs35

ob49 : obs36

ob50 : obs37

ob51 : obs38

ob52 : obs39

ob53 : obs40

ob54 : obs41

ob55 : obs42

ob56 : obs43

ob57 : obs44

ob58 : obs45

ob59 : obs46

ob60 : obs47

ob61 : obs48

ob62 : obs49

ob63 : obs50

ob64 : obs51

ob65 : obs52

ob66 : obs53

ob67 : obs54

ob68 : obs55

ob69 : obs56

ob70 : obs57

ob71 : obs58

ob72 : obs59

ob73 : obs60

ob74 : obs61

ob75 : obs62

ob76 : obs63

ob77 : obs64

ob78 : obs65

ob79 : obs66

ob80 : obs67

ob81 : obs68

ob82 : obs69

ob83 : obs70

ob84 : obs71

ob85 : obs72

ob86 : obs73

ob87 : obs74

ob88 : obs75

ob89 : obs76

ob90 : obs77

ob91 : obs78

ob92 : obs79

ob93 : obs80

ob94 : obs81

ob95 : obs82

ob96 : obs83

ob97 : obs84

ob98 : obs85

ob99 : obs86

ob100 : obs87

ob101 : obs88

ob102 : obs89

ob103 : obs90

ob104 : obs91

ob105 : obs92

ob106 : obs93

ob107 : obs94

ob108 : obs95

ob109 : obs96

ob110 : obs97

ob111 : obs98

ob112 : obs99

ob113 : obs100

ob114 : obs101

ob115 : obs102

ob116 : obs103

ob117 : obs104

ob118 : obs105

ob119 : obs106

ob120 : obs107

ob121 : obs108

ob122 : obs109

ob123 : obs110

ob124 : obs111

ob125 : obs112

ob126 : obs113

ob127 : obs114

ob128 : obs115

ob129 : obs116

ob130 : obs117

ob131 : obs118

ob132 : obs119

ob133 : obs120

ob134 : obs121

ob135 : obs122

ob136 : obs123

ob137 : obs124

ob138 : obs125

ob139 : obs126

ob140 : obs127

ob141 : obs128

ob142 : obs129

ob143 : obs130

ob144 : obs131

ob145 : obs132

ob146 : obs133

ob147 : obs134

ob148 : obs135

ob149 : obs136

ob150 : obs137

ob151 : obs138

ob152 : obs139

ob153 : obs140

ob154 : obs141

ob155 : obs142

ob156 : obs143

ob157 : obs144

ob158 : obs145

ob159 : obs146

ob160 : obs147

ob161 : obs148

ob162 : obs149

ob163 : obs150

ob164 : obs151

ob165 : obs152

ob166 : obs153

ob167 : obs154

ob168 : obs155

ob169 : obs156

ob170 : obs157

ob171 : obs158

ob172 : obs159

ob173 : obs160

ob174 : obs161

ob175 : obs162

ob176 : obs163

ob177 : obs164

ob178 : obs165

ob179 : obs166

ob180 : obs167

ob181 : obs168

ob182 : obs169

ob183 : obs170

ob184 : obs171

ob185 : obs172

ob186 : obs173

ob187 : obs174

ob188 : obs175

ob189 : obs176

ob190 : obs177

ob191 : obs178

ob192 : obs179

ob193 : obs180

ob194 : obs181

ob195 : obs182

ob196 : obs183

ob197 : obs184

ob198 : obs185

ob199 : obs186

ob200 : obs187

ob201 : obs188

ob202 : obs189

ob203 : obs190

ob204 : obs191

ob205 : obs192

ob206 : obs193

ob207 : obs194

ob208 : obs195

ob209 : obs196

ob210 : obs197

ob211 : obs198

ob212 : obs199

ob213 : obs200

ob214 : obs201

ob215 : obs202

ob216 : obs203

ob217 : obs204

ob218 : obs205

ob219 : obs206

ob220 : obs207

ob221 : obs208

ob222 : obs209

ob223 : obs210

ob224 : obs211

ob225 : obs212

ob226 : obs213

ob227 : obs214

ob228 : obs215

ob229 : obs216

ob230 : obs217

ob231 : obs218

ob232 : obs219

ob233 : obs220

ob234 : obs221

ob235 : obs222

ob236 : obs223

ob237 : obs224

ob238 : obs225

ob239 : obs226

ob240 : obs227

ob241 : obs228

ob242 : obs229

ob243 : obs230

ob244 : obs231

ob245 : obs232

ob246 : obs233

ob247 : obs234

ob248 : obs235

ob249 : obs236

ob250 : obs237

ob251 : obs238

ob252 : obs239

ob253 : obs240

ob254 : obs241

ob255 : obs242

ob256 : obs243

ob257 : obs244

ob258 : obs245

ob259 : obs246

ob260 : obs247

ob261 : obs248

ob262 : obs249

ob263 : obs250

ob264 : obs251

ob265 : obs252

ob266 : obs253

ob267 : obs254

ob268 : obs255

ob269 : obs256

ob270 : obs257

ob271 : obs258

ob272 : obs259

ob273 : obs260

ob274 : obs261

ob275 : obs262

ob276 : obs263

ob277 : obs264

ob278 : obs265

ob279 : obs266

ob280 : obs267

ob281 : obs268

ob282 : obs269

ob283 : obs270

ob284 : obs271

ob285 : obs272

ob286 : obs273

ob287 : obs274

ob288 : obs275

ob289 : obs276

ob290 : obs277

ob291 : obs278

ob292 : obs279

ob293 : obs280

ob294 : obs281

ob295 : obs282

ob296 : obs283

ob297 : obs284

ob298 : obs285</div

Ocean Breeze
12 : number of trials included in DUA
5 : time zone designation
28, 40 : latitude (deg)
40, 70 : longitude (deg)

ob29	ob30	ob31	ob32	ob33	ob34	ob35	ob36	ob37	ob38	ob39	ob40 : trial ID
1	1	1	1	1	1	1	1	1	1	1	month
18	19	20	20	22	22	23	23	24	24	25	day
1962	1962	1962	1962	1962	1962	1962	1962	1962	1962	1962	year
17	18	13	15	15	15	14	14	14	14	14	hour
24	30	49	42	59	40	25	40	16	31	7	minute
1	1	1	1	1	1	1	1	1	1	1	no. of sources
0.0	0.0	0.0	0.0	0.0	0.0	0.0	0.0	0.0	0.0	0.0	x-coord. of source (m)
0.0	0.0	0.0	0.0	0.0	0.0	0.0	0.0	0.0	0.0	0.0	y-coord. of source (m)
2.50	2.50	2.50	2.50	2.50	2.50	2.50	2.50	2.50	2.50	2.50	source elevation (m)
1.217	1.133	1.661	1.620	1.636	1.689	0.817	1.028	1.638	1.600	1.214	emission rate (g/s)
1800.0	1800.0	1800.0	1800.0	1800.0	1800.0	1800.0	1800.0	1800.0	1800.0	1800.0	emission duration (s)
-99.9	-99.9	-99.9	-99.9	-99.9	-99.9	-99.9	-99.9	-99.9	-99.9	-99.9	total mass emitted (kg)
0.000	0.000	0.000	0.000	0.000	0.000	0.000	0.000	0.000	0.000	0.000	sign at the source (m)
0.000	0.000	0.000	0.000	0.000	0.000	0.000	0.000	0.000	0.000	0.000	sign at the source (m)
0.000	0.000	0.000	0.000	0.000	0.000	0.000	0.000	0.000	0.000	0.000	sign at the source (m)
-99.9	-99.9	-99.9	-99.9	-99.9	-99.9	-99.9	-99.9	-99.9	-99.9	-99.9	ambient pressure (atm)
-99.9	-99.9	-99.9	-99.9	-99.9	-99.9	-99.9	-99.9	-99.9	-99.9	-99.9	relative humidity (%)
290.65	290.05	291.05	288.95	288.95	291.45	292.75	292.25	299.05	290.65	292.65	temperature at level #1 (K)
1.80	1.80	1.80	1.80	1.80	1.80	1.80	1.80	1.80	1.80	1.80	measuring height for temperature #1 (m)
290.65	290.45	292.50	288.75	288.75	291.95	291.15	290.15	290.15	290.15	292.15	temperature at level #2 (K)
16.50	16.50	16.50	16.50	16.50	16.50	16.50	16.50	16.50	16.50	16.50	measuring height for temperature #2 (m)
2.90	1.80	6.90	7.50	2.10	0.50	3.00	2.00	0.50	3.30	2.60	wind speed (m/s)
3.70	3.70	3.70	3.70	3.70	3.70	3.70	3.70	3.70	3.70	3.70	measuring height for wind data (m)
2.90	1.80	6.90	7.50	2.10	0.50	3.00	2.00	0.50	3.30	2.60	domain-averaged wind speed (m/s)
20.0	16.0	20.0	11.0	10.0	10.0	13.0	12.0	12.0	12.0	14.20	domain-averaged wind direction (deg)
-99.90	-99.90	-99.90	-99.90	-99.90	-99.90	-99.90	-99.90	-99.90	-99.90	-99.90	domain-averaged sigma-u (m/s)
-9.90	-9.70	-7.30	4.50	11.20	12.60	15.90	16.30	16.10	12.70	12.40	domain-averaged sigma-theta (deg)
-9.90	-9.90	-9.90	-9.90	-9.90	-9.90	-9.90	-9.90	-9.90	-9.90	-9.90	domain-averaged sigma-phi (deg)
-3.70	-3.70	-3.70	-3.70	-3.70	-3.70	-3.70	-3.70	-3.70	-3.70	-3.70	measuring ht for domain-avg wind speed (m)
280.0	282.0	282.0	282.0	282.0	280.0	280.0	280.0	282.0	282.0	282.0	averaging ht for domain-avg data (s)
-99.900	-99.900	-99.900	-99.900	-99.900	-99.900	-99.900	-99.900	-99.900	-99.900	-99.900	wind speed power law exponent
0.1000	0.1000	0.1000	0.1000	0.1000	0.1000	0.1000	0.1000	0.1000	0.1000	0.1000	surface roughness (m)
-99.900	-99.900	-99.900	-99.900	-99.900	-99.900	-99.900	-99.900	-99.900	-99.900	-99.900	friction velocity (m/s)
-99.900	-99.900	-99.900	-99.900	-99.900	-99.900	-99.900	-99.900	-99.900	-99.900	-99.900	inverse Monin-Obukhov length (1/m)
0.18	0.18	0.18	0.18	0.18	0.18	0.18	0.18	0.18	0.18	0.18	albedo
0.50	0.50	0.50	0.50	0.50	0.50	0.50	0.50	0.50	0.50	0.50	moisture availability
0.50	0.50	0.50	0.50	0.50	0.50	0.50	0.50	0.50	0.50	0.50	Bowen ratio
-99.9	-99.9	-99.9	-99.9	-99.9	-99.9	-99.9	-99.9	-99.9	-99.9	-99.9	mixing height (m)
87.5	100.0	87.5	87.5	87.5	100.0	97.5	100.0	100.0	100.0	100.0	cloud cover (%)
280.0	282.0	282.0	282.0	282.0	282.0	282.0	282.0	282.0	282.0	282.0	P-G stability class
4.57	4.57	4.57	4.57	4.57	4.57	4.57	4.57	4.57	4.57	4.57	averaging time for concentration (s)
3	3	3	3	3	3	3	3	3	3	3	no. of distances downwind
1200.0	1200.0	1200.0	1200.0	1200.0	1200.0	1200.0	1200.0	1200.0	1200.0	1200.0	cross-wind integrated conc. (mg/m^2)
5.010E-02	2.740E-02	2.500E-02	1.740E-02	6.550E-02	7.580E-02	2.900E-02	4.160E-02	1.310E-02	3.350E-02	3.190E-02	3.190E-02
-9.990E-01	concentration (mg/m^3)										
-9.990E-01	alpha (m)										
2400.0	2400.0	2400.0	2400.0	2400.0	2400.0	2400.0	2400.0	2400.0	2400.0	2400.0	distances downwind (m)
1.060E-12	8.880E-03	5.850E-03	3.130E-03	2.000E-02	1.890E-02	8.030E-03	1.000E-02	4.520E-03	5.310E-03	5.310E-03	concentration (mg/m^3)
-9.990E-01	cross-wind integrated conc. (mg/m^2)										
4.600	4.600	4.600	4.600	4.600	4.600	4.600	4.600	4.600	4.600	4.600	alpha (m)
3.470E-03	2.650E-03	2.000E-03	1.410E-03	1.310E-03	1.310E-03	9.990E-01	-9.990E-01	-9.990E-01	-9.990E-01	-9.990E-01	distances downwind (m)
-9.990E-01	concentration (mg/m^3)										
-9.990E-01	cross-wind integrated conc. (mg/m^2)										
-9.990E-01	alpha (m)										
0	0	0	0	0	0	0	0	0	0	0	no. of lines-of-sight

Ocean Breeze

12 : number of trials included in DDA

5 : time zone designation

26,40 : latitude (deg)

80,70 : longitude (deg)

obj41

obj42

obj43

obj44

obj45

obj46

obj47

obj48

obj49

obj50

obj51

obj52

obj53

obj54

obj55

obj56

obj57

obj58

obj59

obj60

obj61

obj62

obj63

obj64

obj65

obj66

obj67

obj68

obj69

obj70

obj71

obj72

obj73

obj74

obj75

obj76

obj77

obj78

obj79

obj80

obj81

obj82

obj83

obj84

obj85

obj86

obj87

obj88

obj89

obj90

obj91

obj92

obj93

obj94

obj95

obj96

obj97

obj98

obj99

obj100

obj101

obj102

obj103

obj104

obj105

obj106

obj107

obj108

obj109

obj110

obj111

obj112

obj113

obj114

obj115

obj116

obj117

obj118

obj119

obj120

obj121

obj122

obj123

obj124

obj125

obj126

obj127

obj128

obj129

obj130

obj131

obj132

obj133

obj134

obj135

obj136

obj137

obj138

obj139

obj140

obj141

obj142

obj143

obj144

obj145

obj146

obj147

obj148

obj149

obj150

obj151

obj152

obj153

obj154

obj155

obj156

obj157

obj158

obj159

obj160

obj161

obj162

obj163

obj164

obj165

obj166

obj167

obj168

obj169

obj170

obj171

obj172

obj173

obj174

obj175

obj176

obj177

obj178

obj179

obj180

obj181

obj182

obj183

obj184

obj185

obj186

obj187

obj188

obj189

obj190

obj191

obj192

obj193

obj194

obj195

obj196

obj197

obj198

obj199

obj200

obj201

obj202

obj203

obj204

obj205

obj206

obj207

obj208

obj209

obj210

obj211

obj212

obj213

obj214

obj215

obj216

obj217

obj218

obj219

obj220

obj221

obj222

obj223

obj224

obj225

obj226

obj227

obj228

obj229

obj230

obj231

obj232

obj233

obj234

obj235

obj236

obj237

obj238

obj239

obj240

obj241

obj242

obj243

obj244

obj245

obj246

obj247

obj248

obj249

obj250

obj251

obj252

obj253

obj254

obj255

obj256

obj257

obj258

obj259

obj260

obj261

obj262

obj263

obj264

obj265

obj266

obj267

obj268

obj269

obj270

obj271

obj272

obj273

obj274

obj275

obj276

obj277

obj278

obj279

obj280

obj281

obj282

obj283

obj284

obj285

obj286

obj287

obj288

obj289

obj290

obj291

obj292

obj293

obj294

obj295

obj296

obj297

obj299

obj300

obj301

obj302

obj303

obj304

obj305

obj306

obj307

obj308

obj309

obj310

obj311

obj312

obj313

obj314

obj315

obj316

obj317

obj318

obj319

obj320

obj321

obj322

obj323

Ocean breeze
12 : number of trials included in DIA

5 : time zone designation

28.40 : latitude (deg)

80.70 : longitude (deg)

ob53	ob54	ob55	ob56	ob57	ob58	ob59	ob60	ob62	ob63	ob64	ob65	ob66 : trial 10	
3	3	3	3	3	3	3	3	3	3	3	3	3	
10	13	13	13	14	14	14	16	16	17	20	22	: month	
1962	1962	1962	1962	1962	1962	1962	1962	1962	1962	1962	1962	: day	
16	13	15	16	15	15	15	15	17	13	14	15	: year	
39	44	2	33	46	20	53	42	51	40	51	51	: hour	
39	1	1	1	1	1	1	1	1	1	1	1	: minute	
-99.9	0.0	0.0	0.0	0.0	0.0	0.0	0.0	0.0	0.0	0.0	0.0	: no. of sources	
0.0	0.0	0.0	0.0	0.0	0.0	0.0	0.0	0.0	0.0	0.0	0.0	x-coord. of source (m)	
2.50	2.50	2.00	2.50	2.50	2.50	2.50	2.50	2.50	2.50	2.50	2.50	y-coord. of source (m)	
1.689	1.661	1.669	1.664	1.644	1.600	1.644	1.661	1.629	1.661	1.539	1.539	source elevation (m)	
1800.0	1800.0	1800.0	1800.0	1800.0	1800.0	1800.0	1800.0	1800.0	1800.0	1800.0	1800.0	elevation rate (m/s)	
-99.9	-99.9	-99.9	-99.9	-99.9	-99.9	-99.9	-99.9	-99.9	-99.9	-99.9	-99.9	elevation duration (s)	
0.000	0.000	0.000	0.000	0.000	0.000	0.000	0.000	0.000	0.000	0.000	0.000	total mass emitted (kg)	
0.000	0.000	0.000	0.000	0.000	0.000	0.000	0.000	0.000	0.000	0.000	0.000	sign at the source (m)	
0.000	0.000	0.000	0.000	0.000	0.000	0.000	0.000	0.000	0.000	0.000	0.000	sign at the source (m)	
-99.9	-99.9	-99.9	-99.9	-99.9	-99.9	-99.9	-99.9	-99.9	-99.9	-99.9	-99.9	ambient pressure (atm)	
-99.9	-99.9	-99.9	-99.9	-99.9	-99.9	-99.9	-99.9	-99.9	-99.9	-99.9	-99.9	relative humidity (%)	
293.25	294.15	290.35	287.45	284.65	281.85	288.45	285.65	282.85	280.05	277.25	284.45	temperature at level #1 (K)	
1.80	1.80	1.80	1.80	1.80	1.80	1.80	1.80	1.80	1.80	1.80	1.80	measuring height for temperature #1 (m)	
292.05	295.05	289.55	281.05	284.65	287.15	289.05	286.75	285.25	293.05	294.05	294.05	temperature at level #2 (K)	
16.50	16.50	16.50	16.50	16.50	16.50	16.50	16.50	16.50	16.50	16.50	16.50	measuring height for temperature #2 (m)	
2.50	5.50	3.50	1.40	2.90	2.40	4.10	3.20	7.20	8.10	4.30	3.20	wind speed (m/s) at a tower	
3.70	3.70	3.50	3.70	3.70	3.70	3.70	3.70	3.70	3.70	3.70	3.70	measuring height for wind data (m)	
2.50	5.50	3.50	1.40	2.90	2.40	4.10	3.20	7.20	8.10	4.30	3.20	domain-averaged wind speed (m/s)	
21.0	45.0	102.0	19.0	31.0	26.0	22.0	22.0	15.0	23.0	16.2	4.0	domain-averaged wind direction (deg)	
-99.9	-99.9	-99.9	-99.9	-99.9	-99.9	-99.9	-99.9	-99.9	-99.9	-99.9	-99.9	domain-averaged sigma-u (m/s)	
14.80	7.70	12.10	30.40	10.00	10.10	10.10	10.10	10.10	10.10	10.10	10.10	domain-averaged sigma-theta (deg)	
-99.9	-99.9	-99.9	-99.9	-99.9	-99.9	-99.9	-99.9	-99.9	-99.9	-99.9	-99.9	domain-averaged sigma-phi (deg)	
3.70	3.70	3.70	3.70	3.70	3.70	3.70	3.70	3.70	3.70	3.70	3.70	measuring ht for domain-avg wind speed (m)	
2820.0	2820.0	2580.0	2620.0	2800.0	2820.0	2800.0	2820.0	2800.0	2820.0	2820.0	2820.0	averaging time for domain-avg wind speed (s)	
-99.900	-99.900	-99.900	-99.900	-99.900	-99.900	-99.900	-99.900	-99.900	-99.900	-99.900	-99.900	wind speed power law exponent	
0.1000	0.1000	0.1000	0.1000	0.1000	0.1000	0.1000	0.1000	0.1000	0.1000	0.1000	0.1000	surface roughness (m)	
-99.900	-99.900	-99.900	-99.900	-99.900	-99.900	-99.900	-99.900	-99.900	-99.900	-99.900	-99.900	friction velocity (m/s)	
-99.900	-99.900	-99.900	-99.900	-99.900	-99.900	-99.900	-99.900	-99.900	-99.900	-99.900	-99.900	inverse Monin-Obukhov length (1/m)	
F - 15	0.18	0.18	0.18	0.18	0.18	0.18	0.18	0.18	0.18	0.18	0.18	albedo	
0.50	0.50	0.50	0.50	0.50	0.50	0.50	0.50	0.50	0.50	0.50	0.50	Boxen ratio	
0.50	0.50	0.50	0.50	0.50	0.50	0.50	0.50	0.50	0.50	0.50	0.50	moisture availability	
-99.9	-99.9	-99.9	-99.9	-99.9	-99.9	-99.9	-99.9	-99.9	-99.9	-99.9	-99.9	mixing height (m)	
0.0	0.1	0.1	0.1	0.1	0.1	0.1	0.1	0.1	0.1	0.1	0.1	cloud cover (%)	
-99.900	-99.900	-99.900	-99.900	-99.900	-99.900	-99.900	-99.900	-99.900	-99.900	-99.900	-99.900	P-G stability class	
2820.0	2820.0	2580.0	2620.0	2800.0	2820.0	2800.0	2820.0	2800.0	2820.0	2820.0	2820.0	averaging time for concentration (s)	
4.57	4.57	4.57	4.57	4.57	4.57	4.57	4.57	4.57	4.57	4.57	4.57	concentration downwind (mg/m^3)	
3	3	3	3	3	3	3	3	3	3	3	3	no. of distances downwind	
1200.0	1200.0	1200.0	1200.0	1200.0	1200.0	1200.0	1200.0	1200.0	1200.0	1200.0	1200.0	concentration integrated conc. (mg/m^3)	
2.5702.02	4.6708.03	4.3208.02	1.5568.02	3.8008.02	1.9608.02	3.6308.02	5.2008.02	7.4308.02	1.3208.02	2.8408.02	1.200.0	1.200.0	cross-wind integrated conc. (mg/m^3)
-9.3908.01	-9.3908.01	-9.3908.01	-9.3908.01	-9.3908.01	-9.3908.01	-9.3908.01	-9.3908.01	-9.3908.01	-9.3908.01	-9.3908.01	-9.3908.01	concentration (mg/m^3)	
-99.90	-99.90	-99.90	-99.90	-99.90	-99.90	-99.90	-99.90	-99.90	-99.90	-99.90	-99.90	cross-wind integrated conc. (mg/m^3)	
2400.0	2400.0	2400.0	2400.0	2400.0	2400.0	2400.0	2400.0	2400.0	2400.0	2400.0	2400.0	distances downwind (m)	
7.9508.03	5.1308.04	1.2108.03	3.3508.03	4.2308.03	1.0708.02	2.2508.03	1.0002.02	1.1808.03	7.3608.04	5.1208.03	5.1208.03	concentration (mg/m^3)	
-9.3908.01	-9.3908.01	-9.3908.01	-9.3908.01	-9.3908.01	-9.3908.01	-9.3908.01	-9.3908.01	-9.3908.01	-9.3908.01	-9.3908.01	-9.3908.01	cross-wind integrated conc. (mg/m^3)	
4800.0	4800.0	4800.0	4800.0	4800.0	4800.0	4800.0	4800.0	4800.0	4800.0	4800.0	4800.0	distances downwind (m)	
-9.9908.01	5.0208.04	9.4708.04	-9.9908.01	1.1608.03	2.1508.03	7.8008.04	3.1608.03	2.9108.04	1.4908.04	1.2908.03	1.2908.03	concentration (mg/m^3)	
-9.9908.01	-9.9908.01	-9.9908.01	-9.9908.01	-9.9908.01	-9.9908.01	-9.9908.01	-9.9908.01	-9.9908.01	-9.9908.01	-9.9908.01	-9.9908.01	cross-wind integrated conc. (mg/m^3)	
-99.90	-99.90	-99.90	-99.90	-99.90	-99.90	-99.90	-99.90	-99.90	-99.90	-99.90	-99.90	signify (a)	
0	0	0	0	0	0	0	0	0	0	0	0	no. of lines-of-sight	

Octave blocks: Number of octaves included in 800

CLIMATE ZONE DESIGNATION

ab70	latitude (deg) ob67	longitude (deg) ob68	ob69	ob70	ob71	ob72	ob73	ob74
28.40	21.3	3	3	3	3	3	3	3
20.70	24.3	27	27	28	29	29	29	30
24	1962	1962	1962	1962	1962	1962	1962	1962
1962	1962	1962	1962	1962	1962	1962	1962	1962
15	18	18	18	18	18	18	18	18
15	15	15	21	56	20	28	17	38
34	15	1	1	1	1	1	1	48
0.0	0.0	0.0	0.0	0.0	0.0	0.0	0.0	no. of sources
0.0	0.0	0.0	0.0	0.0	0.0	0.0	0.0	x-coord. of source (m)
0.0	0.0	0.0	0.0	0.0	0.0	0.0	0.0	y-coord. of source (m)
2.50	2.50	2.50	2.50	2.50	2.50	2.50	2.50	source elevation (m)
1.661	0.817	1.233	1.256	1.300	1.712	1.639	1.244	emission rate (g/s)
1800.0	1800.0	1800.0	1800.0	1800.0	1800.0	1800.0	1800.0	emission duration (s)
-99.9	-99.9	-99.9	-99.9	-99.9	-99.9	-99.9	-99.9	total mass emitted (kg)
0.000	0.000	0.000	0.000	0.000	0.000	0.000	0.000	signed at the source (m)
0.000	0.000	0.000	0.000	0.000	0.000	0.000	0.000	signy at the source (m)
0.000	0.000	0.000	0.000	0.000	0.000	0.000	0.000	signz at the source (m)
-99.9	-99.9	-99.9	-99.9	-99.9	-99.9	-99.9	-99.9	ambient pressure (atm)
-99.9	-99.9	-99.9	-99.9	-99.9	-99.9	-99.9	-99.9	relative humidity (%)
293.45	293.45	293.45	293.45	293.45	296.05	296.05	298.15	temperature at level 1 (K)
1.80	1.80	1.80	1.80	1.80	1.80	1.80	1.80	measuring height for temperature 1 (m)
299.15	292.95	290.35	290.15	295.75	295.75	298.35	298.35	temperature at level 2 (K)
16.50	16.50	16.50	16.50	16.50	16.50	16.50	16.50	measuring height for temperature 2 (m)
2.70	1.20	4.60	4.10	3.40	4.70	4.50	3.70	wind speed (m/s) at a tower
3.70	3.70	3.70	3.70	3.70	3.70	3.70	3.70	measuring height for wind data (m)
2.70	1.20	4.60	4.10	3.40	4.70	4.50	3.70	domain-averaged wind speed (m/s)
6.60	6.60	13.0	13.0	13.0	15.0	16.0	15.0	domain-averaged wind direction (deg)
-99.90	-99.90	-99.90	-99.90	-99.90	-99.90	-99.90	-99.90	domain-averaged signum-u (m/s)
16.80	16.80	9.60	9.60	6.80	10.40	11.70	10.60	domain-averaged signum-theta (deg)
-99.90	-99.90	-99.90	-99.90	-99.90	-99.90	-99.90	-99.90	domain-averaged signum-ph (deg)
2.80.0	1800.0	2820.0	2820.0	2820.0	2820.0	2820.0	2820.0	measuring ht for domain-avg wind speed (m)
-99.900	-99.900	-99.900	-99.900	-99.900	-99.900	-99.900	-99.900	averaging time for domain-avg data (s)
0.1000	0.1000	0.1000	0.1000	0.1000	0.1000	0.1000	0.1000	wind speed power law exponent
-99.900	-99.900	-99.900	-99.900	-99.900	-99.900	-99.900	-99.900	surface roughness (m)
-99.900	-99.900	-99.900	-99.900	-99.900	-99.900	-99.900	-99.900	friction velocity (m/s)
-99.900	-99.900	-99.900	-99.900	-99.900	-99.900	-99.900	-99.900	invers Monin-Obukhov length (1/m)
0.1000	0.1000	0.1000	0.1000	0.1000	0.1000	0.1000	0.1000	Bowen ratio
0.18	0.18	0.18	0.18	0.18	0.18	0.18	0.18	cloud cover (%)
0.50	0.50	0.50	0.50	0.50	0.50	0.50	0.50	F-G stability class
0.50	0.50	0.50	0.50	0.50	0.50	0.50	0.50	albedo
0.50	0.50	0.50	0.50	0.50	0.50	0.50	0.50	moisture availability
-99.9	-99.9	-99.9	-99.9	-99.9	-99.9	-99.9	-99.9	mixing height (m)
37.5	37.5	0.0	0.0	37.5	0.15	32.5	67.5	no. of distances downwind (m)
-99.9	-99.9	-99.9	-99.9	-99.9	-99.9	-99.9	-99.9	cloud cover (1)
280.0	1800.0	2820.0	2820.0	2820.0	2820.0	2820.0	2820.0	F-G stability class
4.57	4.57	4.57	4.57	4.57	4.57	4.57	4.57	suggested receptor height (m)
3	3	3	3	3	3	3	3	no. of distances downwind (m)
1200.0	1200.0	1200.0	1200.0	1200.0	1200.0	1200.0	1200.0	concentration (mg/m ³)
1.690E-02	1.390E-01	1.390E-02	1.390E-02	1.390E-02	1.390E-02	1.390E-02	1.390E-02	cross-wind integrated conc. (mg/m ²)
-9.990E-01	-9.990E-01	-9.990E-01	-9.990E-01	-9.990E-01	-9.990E-01	-9.990E-01	-9.990E-01	signx (m)
-9.990E-01	-9.990E-01	-9.990E-01	-9.990E-01	-9.990E-01	-9.990E-01	-9.990E-01	-9.990E-01	signy (m)
2.000.0	2.000.0	2.400.0	2.400.0	2.400.0	2.400.0	2.400.0	2.400.0	distances downwind (m)
3.16E-03	3.940E-02	2.600E-03	2.900E-03	1.460E-02	4.910E-03	4.20E-03	5.000E-03	concentration (mg/m ³)
-9.990E-01	-9.990E-01	-9.990E-01	-9.990E-01	-9.990E-01	-9.990E-01	-9.990E-01	-9.990E-01	cross-wind integrated conc. (mg/m ²)
4.800.0	4.800.0	4.800.0	4.800.0	4.800.0	4.800.0	4.800.0	4.800.0	signx (m)
-9.990E-01	-9.990E-01	-9.990E-01	-9.990E-01	-9.990E-01	-9.990E-01	-9.990E-01	-9.990E-01	signy (m)
-9.990E-01	-9.990E-01	-9.990E-01	-9.990E-01	-9.990E-01	-9.990E-01	-9.990E-01	-9.990E-01	no. of lines-of-sight

Green Glow 12 : number of trials included in DDA

Green Glow 12 : number of trials included in DNA

Pratlie Grass

12 : number of tials included in DDA

6 : time designation

42.30 : latitude (deg)

98.30 : longitude (deg)

pg7 pg8 pg9 pg10 pg11 pg12 pg13 pg14 pg15 pg16 pg17 pg18 pg19 pg20

7 7 7 7 7 7 7 7 7 7 7 7 7 7 7

10 11 11 11 11 11 11 11 11 11 11 11 11 11

1956 1956 1956 1956 1956 1956 1956 1956 1956 1956 1956 1956 1956 1956

14 17 16 12 20 8 10 20 10 20 22 23 23 25

15 0 0 0 0 0 0 0 0 0 0 0 0 0 0

1 1 1 1 1 1 1 1 1 1 1 1 1 1

0.0 0.0 0.0 0.0 0.0 0.0 0.0 0.0 0.0 0.0 0.0 0.0 0.0 0.0

0.0 0.0 0.0 0.0 0.0 0.0 0.0 0.0 0.0 0.0 0.0 0.0 0.0 0.0

0.45 0.45 0.45 0.45 0.45 0.45 0.45 0.45 0.45 0.45 0.45 0.45 0.45 0.45

91.100 92.000 92.100 61.100 95.500 93.000 60.000 60.000 56.500 51.600 101.800 101.200 60.000 60.000

600.0 600.0 600.0 600.0 600.0 600.0 600.0 600.0 600.0 600.0 600.0 600.0 600.0 600.0

-99.9 -99.9 -99.9 -99.9 -99.9 -99.9 -99.9 -99.9 -99.9 -99.9 -99.9 -99.9 -99.9 -99.9

0.000 0.000 0.000 0.000 0.000 0.000 0.000 0.000 0.000 0.000 0.000 0.000 0.000 0.000

0.000 0.000 0.000 0.000 0.000 0.000 0.000 0.000 0.000 0.000 0.000 0.000 0.000 0.000

-99.9 -99.9 -99.9 -99.9 -99.9 -99.9 -99.9 -99.9 -99.9 -99.9 -99.9 -99.9 -99.9 -99.9

-99.9 -99.9 -99.9 -99.9 -99.9 -99.9 -99.9 -99.9 -99.9 -99.9 -99.9 -99.9 -99.9 -99.9

305.15 304.15 304.15 293.15 293.15 293.15 292.00 292.00 292.00 292.00 292.00 292.00 292.00 292.00

2.00 2.00 2.00 2.00 2.00 2.00 2.00 2.00 2.00 2.00 2.00 2.00 2.00 2.00

303.55 299.55 302.15 295.05 295.05 295.05 300.15 300.15 300.15 300.15 300.15 300.15 300.15 300.15

16.00 16.00 16.00 16.00 16.00 16.00 16.00 16.00 16.00 16.00 16.00 16.00 16.00 16.00

4.90 6.90 4.60 1.10 3.40 3.40 3.30 3.30 3.30 3.30 3.30 3.30 3.30 3.30

2.00 2.00 2.00 2.00 2.00 2.00 2.00 2.00 2.00 2.00 2.00 2.00 2.00 2.00

6.90 6.90 4.60 1.10 3.40 3.40 3.30 3.30 3.30 3.30 3.30 3.30 3.30 3.30

4.90 4.90 4.90 4.90 4.90 4.90 4.90 4.90 4.90 4.90 4.90 4.90 4.90 4.90

186.0 184.0 184.0 184.0 184.0 184.0 190.0 190.0 190.0 190.0 190.0 190.0 190.0 190.0

-99.90 -99.90 -99.90 -99.90 -99.90 -99.90 -99.90 -99.90 -99.90 -99.90 -99.90 -99.90 -99.90 -99.90

-99.90 -99.90 -99.90 -99.90 -99.90 -99.90 -99.90 -99.90 -99.90 -99.90 -99.90 -99.90 -99.90 -99.90

25.60 -99.90 -99.90 -99.90 -99.90 -99.90 -99.90 -99.90 -99.90 -99.90 -99.90 -99.90 -99.90 -99.90

-99.90 2.00 2.00 2.00 2.00 2.00 2.00 2.00 2.00 2.00 2.00 2.00 2.00 2.00

600.0 600.0 600.0 600.0 600.0 600.0 600.0 600.0 600.0 600.0 600.0 600.0 600.0 600.0

-99.900 -99.900 -99.900 -99.900 -99.900 -99.900 -99.900 -99.900 -99.900 -99.900 -99.900 -99.900 -99.900 -99.900

0.0060 0.0060 0.0060 0.0060 0.0060 0.0060 0.0060 0.0060 0.0060 0.0060 0.0060 0.0060 0.0060 0.0060

0.310 0.310 0.310 0.310 0.310 0.310 0.29491 0.29491 0.29491 0.29491 0.29491 0.29491 0.29491 0.29491

-0.1020 -0.0556 -0.1323 -0.20 0.20 0.20 0.20 0.20 0.20 0.20 0.20 0.20 0.20 0.20

0.50 0.50 0.50 0.50 0.50 0.50 0.50 0.50 0.50 0.50 0.50 0.50 0.50 0.50

2.00 2.00 2.00 2.00 2.00 2.00 2.00 2.00 2.00 2.00 2.00 2.00 2.00 2.00

1539.0 1580.0 1580.0 163.0 163.0 163.0 30.0 30.0 30.0 30.0 30.0 30.0 30.0 30.0

0.0 0.0 0.0 3 3 3 2 2 2 2 2 2 2 2 2

600.0 600.0 600.0 600.0 600.0 600.0 600.0 600.0 600.0 600.0 600.0 600.0 600.0 600.0

1.50 1.50 1.50 1.50 1.50 1.50 1.50 1.50 1.50 1.50 1.50 1.50 1.50 1.50

50.0 50.0 50.0 50.0 50.0 50.0 50.0 50.0 50.0 50.0 50.0 50.0 50.0 50.0

1.704E+02 1.859E+02 1.859E+02 9.990E+01 9.990E+01 9.990E+01 7.093E+01 7.093E+01 7.093E+01 6.102E+02 6.102E+02 6.048E+02 6.048E+02

4.504E+02 4.504E+02 4.504E+02 9.990E+01 9.990E+01 9.990E+01 5.003E+03 5.933E+03 5.933E+03 5.221E+01 5.221E+01 4.500E+03 3.400E+03

1.031E+01 1.031E+01

2.199E+03 2.199E+03 2.199E+03 1.796E+03 1.796E+03 1.796E+03 3.400E+03 3.400E+03 3.400E+03 2.551E+02 2.551E+02 2.494E+02 2.494E+02

1.795E+03 1.795E+03 1.795E+03 1.795E+03 1.795E+03 1.795E+03 1.795E+03 1.795E+03 1.795E+03 1.930E+01 1.930E+01 2.199E+03 2.199E+03

1.600 1.600 1.600 1.600 1.600 1.600 1.600 1.600 1.600 1.600 1.600 1.600 1.600 1.600

200.0 200.0 200.0 200.0 200.0 200.0 200.0 200.0 200.0 200.0 200.0 200.0 200.0 200.0

18.00 18.00 18.00 18.00 18.00 18.00 18.00 18.00 18.00 18.00 18.00 18.00 18.00 18.00

35.00 35.00 35.00 35.00 35.00 35.00 35.00 35.00 35.00 35.00 35.00 35.00 35.00 35.00

400.0 400.0 400.0 400.0 400.0 400.0 400.0 400.0 400.0 400.0 400.0 400.0 400.0 400.0

1.200 1.200 1.200 1.200 1.200 1.200 1.200 1.200 1.200 1.200 1.200 1.200 1.200 1.200

21.00 21.00 21.00 21.00 21.00 21.00 21.00 21.00 21.00 21.00 21.00 21.00 21.00 21.00

1.003E+03 1.003E+03 1.003E+03 1.003E+03 1.003E+03 1.003E+03 1.003E+03 1.003E+03 1.003E+03 1.347E+03 1.347E+03 1.347E+03 1.347E+03

7.101E+02 7.101E+02 7.101E+02 7.101E+02 7.101E+02 7.101E+02 7.101E+02 7.101E+02 7.101E+02 4.799E+02 4.799E+02 4.799E+02 4.799E+02

1.584E+01 1.584E+01 1.584E+01 1.584E+01 1.584E+01 1.584E+01 1.584E+01 1.584E+01 1.584E+01 3.186E+01 3.186E+01 3.186E+01 3.186E+01

1.223E+01 1.223E+01 1.223E+01 1.223E+01 1.223E+01 1.223E+01 1.223E+01 1.223E+01 1.223E+01 1.747E+01 1.747E+01 1.747E+01 1.747E+01

1.102E+02 1.102E+02 1.102E+02 1.102E+02 1.102E+02 1.102E+02 1.102E+02 1.102E+02 1.102E+02 2.487E+00 2.487E+00 2.487E+00 2.487E+00

1.098E+02 1.098E+02 1.098E+02 1.098E+02 1.098E+02 1.098E+02 1.098E+02 1.098E+02 1.098E+02 3.198E+01 3.198E+01 3.198E+01 3.198E+01

1.097E+02 1.097E+02 1.097E+02 1.097E+02 1.097E+02 1.097E+02 1.097E+02 1.097E+02 1.097E+02 4.103E+02 4.103E+02 4.103E+02 4.103E+02

800.0 800.0 800.0 800.0 800.0 800.0 800.0 800.0 800.0 800.0 800.0 800.0 800.0 800.0

1.116E+00 1.116E+00

0 0 0 0 0 0 0 0 0 0 0 0 0 0 0

0 0 0 0 0 0 0 0 0 0 0 0 0 0 0

0 0 0 0 0 0 0 0 0 0 0 0 0 0 0

0 0 0 0 0 0 0 0 0 0 0 0 0 0 0

0 0 0 0 0 0 0 0 0 0 0 0 0 0 0

0 0 0 0 0 0 0 0 0 0 0 0 0 0 0

0 0 0 0 0 0 0 0 0 0 0 0 0 0 0

pg21 : trial 10

pg22 : month

pg23 : day

pg24 : year

pg25 : hour

pg26 : minute

pg27 : no. of sources

pg28 : x-coord. of source (m)

pg29 : y-coord. of source (m)

pg30 : source elevation (m)

pg31 : emission rate (kg/s)

pg32 : total mass emitted (kg)

pg33 : log10 at the source (m)

pg34 : sig10 at the source (m)

pg35 : ambient pressure (atm)

pg36 : relative humidity (%)

pg37 : temperature at level 11 (K)

pg38 : measuring height for temperature 11 (m)

pg39 : temperature at level 12 (K)

pg40 : measuring height for temperature 12 (m)

pg41 : wind speed (m/s)

pg42 : measuring height for wind data (m)

pg43 : domain-averaged wind speed (m/s)

pg44 : domain-averaged sigma-phi (deg)

pg45 : domain-averaged sigma-phi (deg)

pg46 : averaging time for domain-avg wind data (s)

pg47 : wind speed power law exponent

pg48 : surface roughness (m)

pg49 : cloud cover (%)

pg50 : friction velocity (m/s)

pg51 : averaging time for concentration (s)

pg52 : suggested receptor height (m)

pg53 : no. of distances downwind

pg54 : distances downwind (m)

pg55 : concentration (mg/m^3)

pg56 : cross-wind integrated conc. (mg/m^3)

pg57 : concentration (mg/m^3)

pg58 : cross-wind integrated conc. (mg/m^3)

pg59 : concentration (mg/m^3)

pg60 : cross-wind integrated conc. (mg/m^3)

pg61 : concentration (mg/m^3)

pg62 : cross-wind integrated conc. (mg/m^3)

pg63 : concentration (mg/m^3)

pg64 : cross-wind integrated conc. (mg/m^3)

pg65 : concentration (mg/m^3)

pg66 : cross-wind integrated conc. (mg/m^3)

pg67 : concentration (mg/m^3)

pg68 : cross-wind integrated conc. (mg/m^3)

pg69 : concentration (mg/m^3)

pg70 : cross-wind integrated conc. (mg/m^3)

pg71 : concentration (mg/m^3)

pg72 : cross-wind integrated conc. (mg/m^3)

pg73 : concentration (mg/m^3)

pg74 : cross-wind integrated conc. (mg/m^3)

pg75 : concentration (mg/m^3)

pg76 : cross-wind integrated conc. (mg/m^3)

pg77 : concentration (mg/m^3)

pg78 : cross-wind integrated conc. (mg/m^3)

pg79 : concentration (mg/m^3)

pg80 : cross-wind integrated conc. (mg/m^3)

pg81 : concentration (mg/m^3)

pg82 : cross-wind integrated conc. (mg/m^3)

pg83 : concentration (mg/m^3)

pg84 : cross-wind integrated conc. (mg/m^3)

pg85 : concentration (mg/m^3)

pg86 : cross-wind integrated conc. (mg/m^3)

pg87 : concentration (mg/m^3)

pg88 : cross-wind integrated conc

Pratice Grads 12 : number of trials included in DDA

Prakrta Grass 11 : number of trials included in DDA

Prairie Grasses

APPENDIX F-2

LISTINGS OF THE DUGWAY DATA ARCHIVES - SMOKE/OBSCURANT DATASETS

The Inventory Smoke Tests of MC Grenades (INVNC)

6 : number of trials included in DDX

6 : time zone designation

40.20 : latitude (deg)

113.00 : longitude (deg)

T1

T2

T3

T4

T5

T6

T7

T8

T9

trial ID

month

day

hour

minute

second

x-coord. of source (m)

y-coord. of source (m)

no. of sources

source elevation (m)

emission rate (kg/s)

emission duration (s)

total mass emitted (kg)

temperature at level S1 (K)

temperature at level S2 (K)

signo at the source (m)

ambient pressure (atm)

relative humidity (%)

temperature at level S1 (K)

measuring height for temperature S1 (m)

2.00

3.00

4.00

5.00

6.00

7.00

8.00

9.00

10.00

11.00

12.00

13.00

14.00

15.00

16.00

17.00

18.00

19.00

20.00

21.00

22.00

23.00

24.00

25.00

26.00

27.00

28.00

29.00

30.00

31.00

32.00

33.00

34.00

35.00

36.00

37.00

38.00

39.00

40.00

41.00

42.00

43.00

44.00

45.00

46.00

47.00

48.00

49.00

50.00

51.00

52.00

53.00

54.00

55.00

56.00

57.00

58.00

59.00

60.00

61.00

62.00

63.00

64.00

65.00

66.00

67.00

68.00

69.00

70.00

71.00

72.00

73.00

74.00

75.00

76.00

77.00

78.00

79.00

80.00

81.00

82.00

83.00

84.00

85.00

86.00

87.00

88.00

89.00

90.00

91.00

92.00

93.00

94.00

95.00

96.00

97.00

98.00

99.00

100.00

101.00

102.00

103.00

104.00

105.00

106.00

107.00

108.00

109.00

110.00

111.00

112.00

113.00

114.00

115.00

116.00

117.00

118.00

119.00

120.00

121.00

122.00

123.00

124.00

125.00

126.00

127.00

128.00

129.00

130.00

131.00

132.00

133.00

134.00

135.00

136.00

137.00

138.00

139.00

140.00

141.00

142.00

143.00

144.00

145.00

146.00

147.00

148.00

149.00

150.00

151.00

152.00

153.00

154.00

155.00

156.00

157.00

158.00

159.00

160.00

161.00

162.00

163.00

164.00

165.00

166.00

167.00

168.00

169.00

170.00

171.00

172.00

173.00

174.00

175.00

176.00

177.00

178.00

179.00

180.00

181.00

182.00

183.00

184.00

185.00

186.00

187.00

188.00

189.00

190.00

191.00

192.00

193.00

194.00

195.00

196.00

197.00

198.00

199.00

200.00

201.00

202.00

203.00

204.00

205.00

206.00

207.00

208.00

209.00

210.00

211.00

212.00

213.00

214.00

215.00

216.00

217.00

218.00

219.00

220.00

221.00

222.00

223.00

224.00

225.00

226.00

227.00

228.00

229.00

230.00

231.00

232.00

233.00

234.00

235.00

236.00

237.00

238.00

239.00

240.00

241.00

242.00

243.00

244.00

245.00

246.00

247.00

248.00

The Developments Test I of Miles (MC), M603 (MC) and 20225 (MF) Grenades (M16 MC only, OTIC)

15 : number of trials included in RDA
a : time zone designation
48.20 : latitude (deg)
113.66 : longitude (deg)

CIC1	CAC1	GAC1	GIC1	GIC2	GIC3	GIC4	GIC5	GIC6	GIC7	GIC8	GIC9	GIC10	GIC11	GIC12	GIC13	GIC14	GIC15	GIC16	GIC17	GIC18	GIC19	GIC20	GIC21	GIC22	GIC23	GIC24	GIC25	GIC26	GIC27	GIC28	GIC29	GIC30	GIC31	GIC32	GIC33	GIC34	GIC35	GIC36	GIC37	GIC38	GIC39	GIC40	GIC41	GIC42	GIC43	GIC44	GIC45	GIC46	GIC47	GIC48	GIC49	GIC50	GIC51	GIC52	GIC53	GIC54	GIC55	GIC56	GIC57	GIC58	GIC59	GIC60	GIC61	GIC62	GIC63	GIC64	GIC65	GIC66	GIC67	GIC68	GIC69	GIC70	GIC71	GIC72	GIC73	GIC74	GIC75	GIC76	GIC77	GIC78	GIC79	GIC80	GIC81	GIC82	GIC83	GIC84	GIC85	GIC86	GIC87	GIC88	GIC89	GIC90	GIC91	GIC92	GIC93	GIC94	GIC95	GIC96	GIC97	GIC98	GIC99	GIC100	GIC101	GIC102	GIC103	GIC104	GIC105	GIC106	GIC107	GIC108	GIC109	GIC110	GIC111	GIC112	GIC113	GIC114	GIC115	GIC116	GIC117	GIC118	GIC119	GIC120	GIC121	GIC122	GIC123	GIC124	GIC125	GIC126	GIC127	GIC128	GIC129	GIC130	GIC131	GIC132	GIC133	GIC134	GIC135	GIC136	GIC137	GIC138	GIC139	GIC140	GIC141	GIC142	GIC143	GIC144	GIC145	GIC146	GIC147	GIC148	GIC149	GIC150	GIC151	GIC152	GIC153	GIC154	GIC155	GIC156	GIC157	GIC158	GIC159	GIC160	GIC161	GIC162	GIC163	GIC164	GIC165	GIC166	GIC167	GIC168	GIC169	GIC170	GIC171	GIC172	GIC173	GIC174	GIC175	GIC176	GIC177	GIC178	GIC179	GIC180	GIC181	GIC182	GIC183	GIC184	GIC185	GIC186	GIC187	GIC188	GIC189	GIC190	GIC191	GIC192	GIC193	GIC194	GIC195	GIC196	GIC197	GIC198	GIC199	GIC200	GIC201	GIC202	GIC203	GIC204	GIC205	GIC206	GIC207	GIC208	GIC209	GIC210	GIC211	GIC212	GIC213	GIC214	GIC215	GIC216	GIC217	GIC218	GIC219	GIC220	GIC221	GIC222	GIC223	GIC224	GIC225	GIC226	GIC227	GIC228	GIC229	GIC230	GIC231	GIC232	GIC233	GIC234	GIC235	GIC236	GIC237	GIC238	GIC239	GIC240	GIC241	GIC242	GIC243	GIC244	GIC245	GIC246	GIC247	GIC248	GIC249	GIC250	GIC251	GIC252	GIC253	GIC254	GIC255	GIC256	GIC257	GIC258	GIC259	GIC260	GIC261	GIC262	GIC263	GIC264	GIC265	GIC266	GIC267	GIC268	GIC269	GIC270	GIC271	GIC272	GIC273	GIC274	GIC275	GIC276	GIC277	GIC278	GIC279	GIC280	GIC281	GIC282	GIC283	GIC284	GIC285	GIC286	GIC287	GIC288	GIC289	GIC290	GIC291	GIC292	GIC293	GIC294	GIC295	GIC296	GIC297	GIC298	GIC299	GIC299	GIC300	GIC301	GIC302	GIC303	GIC304	GIC305	GIC306	GIC307	GIC308	GIC309	GIC310	GIC311	GIC312	GIC313	GIC314	GIC315	GIC316	GIC317	GIC318	GIC319	GIC320	GIC321	GIC322	GIC323	GIC324	GIC325	GIC326	GIC327	GIC328	GIC329	GIC330	GIC331	GIC332	GIC333	GIC334	GIC335	GIC336	GIC337	GIC338	GIC339	GIC340	GIC341	GIC342	GIC343	GIC344	GIC345	GIC346	GIC347	GIC348	GIC349	GIC350	GIC351	GIC352	GIC353	GIC354	GIC355	GIC356	GIC357	GIC358	GIC359	GIC360	GIC361	GIC362	GIC363	GIC364	GIC365	GIC366	GIC367	GIC368	GIC369	GIC370	GIC371	GIC372	GIC373	GIC374	GIC375	GIC376	GIC377	GIC378	GIC379	GIC380	GIC381	GIC382	GIC383	GIC384	GIC385	GIC386	GIC387	GIC388	GIC389	GIC390	GIC391	GIC392	GIC393	GIC394	GIC395	GIC396	GIC397	GIC398	GIC399	GIC399	GIC400	GIC401	GIC402	GIC403	GIC404	GIC405	GIC406	GIC407	GIC408	GIC409	GIC410	GIC411	GIC412	GIC413	GIC414	GIC415	GIC416	GIC417	GIC418	GIC419	GIC420	GIC421	GIC422	GIC423	GIC424	GIC425	GIC426	GIC427	GIC428	GIC429	GIC430	GIC431	GIC432	GIC433	GIC434	GIC435	GIC436	GIC437	GIC438	GIC439	GIC440	GIC441	GIC442	GIC443	GIC444	GIC445	GIC446	GIC447	GIC448	GIC449	GIC450	GIC451	GIC452	GIC453	GIC454	GIC455	GIC456	GIC457	GIC458	GIC459	GIC460	GIC461	GIC462	GIC463	GIC464	GIC465	GIC466	GIC467	GIC468	GIC469	GIC470	GIC471	GIC472	GIC473	GIC474	GIC475	GIC476	GIC477	GIC478	GIC479	GIC480	GIC481	GIC482	GIC483	GIC484	GIC485	GIC486	GIC487	GIC488	GIC489	GIC490	GIC491	GIC492	GIC493	GIC494	GIC495	GIC496	GIC497	GIC498	GIC499	GIC499	GIC500	GIC501	GIC502	GIC503	GIC504	GIC505	GIC506	GIC507	GIC508	GIC509	GIC510	GIC511	GIC512	GIC513	GIC514	GIC515	GIC516	GIC517	GIC518	GIC519	GIC520	GIC521	GIC522	GIC523	GIC524	GIC525	GIC526	GIC527	GIC528	GIC529	GIC530	GIC531	GIC532	GIC533	GIC534	GIC535	GIC536	GIC537	GIC538	GIC539	GIC539	GIC540	GIC541	GIC542	GIC543	GIC544	GIC545	GIC546	GIC547	GIC548	GIC549	GIC549	GIC550	GIC551	GIC552	GIC553	GIC554	GIC555	GIC556	GIC557	GIC558	GIC559	GIC559	GIC560	GIC561	GIC562	GIC563	GIC564	GIC565	GIC566	GIC567	GIC568	GIC569	GIC569	GIC570	GIC571	GIC572	GIC573	GIC574	GIC575	GIC576	GIC577	GIC578	GIC579	GIC579	GIC580	GIC581	GIC582	GIC583	GIC584	GIC585	GIC586	GIC587	GIC588	GIC589	GIC589	GIC590	GIC591	GIC592	GIC593	GIC594	GIC595	GIC596	GIC597	GIC598	GIC598	GIC599	GIC599	GIC600	GIC601	GIC602	GIC603	GIC604	GIC605	GIC606	GIC607	GIC608	GIC609	GIC610	GIC611	GIC612	GIC613	GIC614	GIC615	GIC616	GIC617	GIC618	GIC619	GIC619	GIC620	GIC621	GIC622	GIC623	GIC624	GIC625	GIC626	GIC627	GIC628	GIC629	GIC629	GIC630	GIC631	GIC632	GIC633	GIC634	GIC635	GIC636	GIC637	GIC638	GIC639	GIC639	GIC640	GIC641	GIC642	GIC643	GIC644	GIC645	GIC646	GIC647	GIC648	GIC649	GIC649	GIC650	GIC651	GIC652	GIC653	GIC654	GIC655	GIC656	GIC657	GIC658	GIC659	GIC659	GIC660	GIC661	GIC662	GIC663	GIC664	GIC665	GIC666	GIC667	GIC668	GIC669	GIC669	GIC670	GIC671	GIC672	GIC673	GIC674	GIC675	GIC676	GIC677	GIC678	GIC678	GIC679	GIC679	GIC680	GIC681	GIC682	GIC683	GIC684	GIC685	GIC686	GIC687	GIC688	GIC689	GIC689	GIC690	GIC691	GIC692	GIC693	GIC694	GIC695	GIC696	GIC697	GIC698	GIC698	GIC699	GIC699	GIC700	GIC701	GIC702	GIC703	GIC704	GIC705	GIC706	GIC707	GIC708	GIC709	GIC709	GIC710	GIC711	GIC712	GIC713	GIC714	GIC715	GIC716	GIC717	GIC718	GIC719	GIC719	GIC720	GIC721	GIC722	GIC723	GIC724	GIC725	GIC726	GIC727	GIC728	GIC729	GIC729	GIC730	GIC731	GIC732	GIC733	GIC734	GIC735	GIC736	GIC737	GIC738	GIC739	GIC739	GIC740	GIC741	GIC742	GIC743	GIC744	GIC745	GIC746	GIC747	GIC748	GIC749	GIC749	GIC750	GIC751	GIC752	GIC753	GIC754	GIC755	GIC756	GIC757	GIC758	GIC759	GIC759	GIC760	GIC761	GIC762	GIC763	GIC764	GIC765	GIC766	GIC767	GIC768	GIC769	GIC769	GIC770	GIC771	GIC772	GIC773	GIC774	GIC775	GIC776	GIC777	GIC778	GIC779	GIC779	GIC780	GIC781	GIC782	GIC783	GIC784	GIC785	GIC786	GIC787	GIC788	GIC789	GIC789	GIC790	GIC791	GIC792	GIC793	GIC794	GIC795	GIC796	GIC797	GIC798	GIC799	GIC799	GIC800	GIC801	GIC802	GIC803	GIC804	GIC805	GIC806	GIC807	GIC808	GIC809	GIC809	GIC810	GIC811	GIC812	GIC813	GIC814	GIC815	GIC816	GIC817	GIC818	GIC819	GIC819	GIC820	GIC821	GIC822	GIC823	GIC824	GIC825	GIC826	GIC827	GIC828	GIC829	GIC829	GIC830	GIC831	GIC832	GIC833	GIC834	GIC835	GIC836	GIC837	GIC838	GIC839	GIC839	GIC840	GIC841	GIC842	GIC843	GIC844	GIC845	GIC846	GIC847	GIC848	GIC849	GIC849	GIC850	GIC851	GIC852	GIC853	GIC854	GIC855	GIC856	GIC857	GIC858	GIC859	GIC859	GIC860	GIC861	GIC862	GIC863	GIC864	GIC865	GIC866	GIC867	GIC868	GIC869	GIC869	GIC870	GIC871	GIC872	GIC873	GIC874	GIC875	GIC876	GIC877	GIC878	GIC879	GIC879	GIC880	GIC881	GIC882	GIC883	GIC884	GIC885	GIC886	GIC887	GIC888	GIC889	GIC889	GIC890	GIC891	GIC892	GIC893	GIC894	GIC895	GIC896	GIC897	GIC898	GIC898	GIC899	GIC899	GIC900	GIC901	GIC902	GIC903	GIC904	GIC905	GIC906	GIC907	GIC908	GIC909	GIC909	GIC910	GIC911	GIC912	GIC913	GIC914	GIC915	GIC916	GIC917	GIC918	GIC919	GIC919	GIC920	GIC921	GIC922	GIC923	GIC924	GIC925	GIC926	GIC927	GIC928	GIC929	GIC929	GIC930	GIC931	GIC932	GIC933	GIC934	GIC935	GIC936	GIC937	GIC938	GIC939	GIC939	GIC940	GIC941	GIC942	GIC943	GIC944	GIC945	GIC946	GIC947	GIC948	GIC949	GIC949	GIC950	GIC951	GIC952	GIC953	GIC954	GIC955	GIC956	GIC957	GIC958	GIC959	GIC959	GIC960	GIC961	GIC962	GIC963	GIC964	GIC965	GIC966	GIC967	GIC968	GIC969	GIC969	GIC970	GIC971	GIC972	GIC973	GIC974	GIC975	GIC976	GIC977	GIC978	GIC979	GIC979	GIC980	GIC981	GIC982	GIC983	GIC984	GIC985	GIC986	GIC987	GIC988	GIC989	GIC989	GIC990	GIC991	GIC992	GIC993	GIC994	GIC995	GIC996	GIC997	GIC998	GIC998	GIC999	GIC999	GIC1000	GIC1001	GIC1002	GIC1003	GIC1004	GIC1005	GIC1006	GIC1007	GIC1008	GIC1009	GIC1009	GIC1010	GIC1011	GIC1012	GIC1013	GIC1014	GIC1015	GIC1016	GIC1017	GIC1018	GIC1019	GIC1019	GIC1020	GIC1021	GIC1022	GIC1023	GIC1024	GIC1025	GIC1026	GIC1027	GIC1028	GIC1029	GIC1029	GIC1030	GIC1031	GIC1032	GIC1033	GIC1034	GIC1035	GIC1036	GIC1037	GIC1038	GIC1039	GIC1039	GIC1040	GIC1041	GIC1042	GIC1043	GIC1044	GIC1045	GIC1046	GIC1047	GIC1048	GIC1049	GIC1049	GIC1050	GIC1051	GIC1052	GIC1053	GIC1054	GIC1055	GIC1056	GIC1057	GIC1058	GIC1059	GIC1059	GIC1060	GIC1061	GIC1062	GIC1063	GIC1064	GIC1065	GIC1066	GIC1067	GIC1068	GIC1069	GIC1069	GIC1070	GIC1071	GIC1072	GIC1073	GIC1074	GIC1075	GIC1076	GIC1077	GIC1078	GIC1079	GIC1079	GIC1080	GIC1081	GIC1082	GIC1083	GIC1084	GIC1085	GIC1086	GIC1087	GIC1088	GIC1089	GIC1089	GIC1090	GIC1091	GIC1092	GIC1093	GIC1094	GIC1095	GIC1096	GIC1097	GIC1098	GIC1098	GIC1099	GIC1099	GIC1100	GIC1101	GIC1102	GIC1103	GIC1104	GIC1105	GIC1106	GIC1107	GIC1108	GIC1109	GIC1109	GIC1110	GIC1111	GIC1112	GIC1113	GIC1114	GIC1115	GIC1116	GIC1117	GIC1118	GIC1119	GIC1119	GIC1120	GIC1121	GIC1122	GIC1123	GIC1124	GIC1125	GIC1126	GIC1127	GIC1128	GIC1129	GIC1129	GIC1130	GIC1131	GIC1132	GIC1133	GIC1134	GIC1135	GIC1136	GIC1137	GIC1138	GIC1139	GIC1140	GIC1141	GIC1142	GIC1143	GIC1144	GIC1145	GIC1146	GIC1147	GIC1148	GIC1149	GIC1150	GIC1151	GIC1152	GIC1153	GIC1154</th

The Development Test I of M116 (MP) and M112 (NP) Grenades (M88) AF only, DTIAR

The Development Team I of NHTIS (INC), NHTIS (NP) and NHTIS (NP) Grottoes (NHTIS NP only, DTINP)

16. Number of details included in NHTIS

4. Line item designation

40-20 : latitude (deg)

113.00 : longitude (deg)

GIAZ

The Development Test 11 of 132mm SHELL GUNNERS (HEM25, 1 projectile, 072041)

17 Number of trials included in DSA

18 Time scale designation

19 20 Latitude (deg)

21 Longitude (deg)

| WPT | WPT1 | WPT2 | WPT3 | WPT4 | WPT5 | WPT6 | WPT7 | WPT8 | WPT9 | WPT10 | WPT11 | WPT12 | WPT13 | WPT14 | WPT15 | WPT16 | WPT17 | WPT18 | WPT19 | WPT20 | WPT21 | WPT22 | WPT23 | WPT24 | WPT25 | WPT26 | WPT27 | WPT28 | WPT29 | WPT30 | WPT31 | WPT32 | WPT33 | WPT34 | WPT35 | WPT36 | WPT37 | WPT38 | WPT39 | WPT40 | WPT41 | WPT42 | WPT43 | WPT44 | WPT45 | WPT46 | WPT47 | WPT48 | WPT49 | WPT50 | WPT51 | WPT52 | WPT53 | WPT54 | WPT55 | WPT56 | WPT57 | WPT58 | WPT59 | WPT60 | WPT61 | WPT62 | WPT63 | WPT64 | WPT65 | WPT66 | WPT67 | WPT68 | WPT69 | WPT70 | WPT71 | WPT72 | WPT73 | WPT74 | WPT75 | WPT76 | WPT77 | WPT78 | WPT79 | WPT80 | WPT81 | WPT82 | WPT83 | WPT84 | WPT85 | WPT86 | WPT87 | WPT88 | WPT89 | WPT90 | WPT91 | WPT92 | WPT93 | WPT94 | WPT95 | WPT96 | WPT97 | WPT98 | WPT99 | WPT100 | WPT101 | WPT102 | WPT103 | WPT104 | WPT105 | WPT106 | WPT107 | WPT108 | WPT109 | WPT110 | WPT111 | WPT112 | WPT113 | WPT114 | WPT115 | WPT116 | WPT117 | WPT118 | WPT119 | WPT120 | WPT121 | WPT122 | WPT123 | WPT124 | WPT125 | WPT126 | WPT127 | WPT128 | WPT129 | WPT130 | WPT131 | WPT132 | WPT133 | WPT134 | WPT135 | WPT136 | WPT137 | WPT138 | WPT139 | WPT140 | WPT141 | WPT142 | WPT143 | WPT144 | WPT145 | WPT146 | WPT147 | WPT148 | WPT149 | WPT150 | WPT151 | WPT152 | WPT153 | WPT154 | WPT155 | WPT156 | WPT157 | WPT158 | WPT159 | WPT160 | WPT161 | WPT162 | WPT163 | WPT164 | WPT165 | WPT166 | WPT167 | WPT168 | WPT169 | WPT170 | WPT171 | WPT172 | WPT173 | WPT174 | WPT175 | WPT176 | WPT177 | WPT178 | WPT179 | WPT180 | WPT181 | WPT182 | WPT183 | WPT184 | WPT185 | WPT186 | WPT187 | WPT188 | WPT189 | WPT190 | WPT191 | WPT192 | WPT193 | WPT194 | WPT195 | WPT196 | WPT197 | WPT198 | WPT199 | WPT200 | WPT201 | WPT202 | WPT203 | WPT204 | WPT205 | WPT206 | WPT207 | WPT208 | WPT209 | WPT210 | WPT211 | WPT212 | WPT213 | WPT214 | WPT215 | WPT216 | WPT217 | WPT218 | WPT219 | WPT220 | WPT221 | WPT222 | WPT223 | WPT224 | WPT225 | WPT226 | WPT227 | WPT228 | WPT229 | WPT230 | WPT231 | WPT232 | WPT233 | WPT234 | WPT235 | WPT236 | WPT237 | WPT238 | WPT239 | WPT240 | WPT241 | WPT242 | WPT243 | WPT244 | WPT245 | WPT246 | WPT247 | WPT248 | WPT249 | WPT250 | WPT251 | WPT252 | WPT253 | WPT254 | WPT255 | WPT256 | WPT257 | WPT258 | WPT259 | WPT260 | WPT261 | WPT262 | WPT263 | WPT264 | WPT265 | WPT266 | WPT267 | WPT268 | WPT269 | WPT270 | WPT271 | WPT272 | WPT273 | WPT274 | WPT275 | WPT276 | WPT277 | WPT278 | WPT279 | WPT280 | WPT281 | WPT282 | WPT283 | WPT284 | WPT285 | WPT286 | WPT287 | WPT288 | WPT289 | WPT290 | WPT291 | WPT292 | WPT293 | WPT294 | WPT295 | WPT296 | WPT297 | WPT298 | WPT299 | WPT300 | WPT301 | WPT302 | WPT303 | WPT304 | WPT305 | WPT306 | WPT307 | WPT308 | WPT309 | WPT310 | WPT311 | WPT312 | WPT313 | WPT314 | WPT315 | WPT316 | WPT317 | WPT318 | WPT319 | WPT320 | WPT321 | WPT322 | WPT323 | WPT324 | WPT325 | WPT326 | WPT327 | WPT328 | WPT329 | WPT330 | WPT331 | WPT332 | WPT333 | WPT334 | WPT335 | WPT336 | WPT337 | WPT338 | WPT339 | WPT340 | WPT341 | WPT342 | WPT343 | WPT344 | WPT345 | WPT346 | WPT347 | WPT348 | WPT349 | WPT350 | WPT351 | WPT352 | WPT353 | WPT354 | WPT355 | WPT356 | WPT357 | WPT358 | WPT359 | WPT360 | WPT361 | WPT362 | WPT363 | WPT364 | WPT365 | WPT366 | WPT367 | WPT368 | WPT369 | WPT370 | WPT371 | WPT372 | WPT373 | WPT374 | WPT375 | WPT376 | WPT377 | WPT378 | WPT379 | WPT380 | WPT381 | WPT382 | WPT383 | WPT384 | WPT385 | WPT386 | WPT387 | WPT388 | WPT389 | WPT390 | WPT391 | WPT392 | WPT393 | WPT394 | WPT395 | WPT396 | WPT397 | WPT398 | WPT399 | WPT400 | WPT401 | WPT402 | WPT403 | WPT404 | WPT405 | WPT406 | WPT407 | WPT408 | WPT409 | WPT410 | WPT411 | WPT412 | WPT413 | WPT414 | WPT415 | WPT416 | WPT417 | WPT418 | WPT419 | WPT420 | WPT421 | WPT422 | WPT423 | WPT424 | WPT425 | WPT426 | WPT427 | WPT428 | WPT429 | WPT430 | WPT431 | WPT432 | WPT433 | WPT434 | WPT435 | WPT436 | WPT437 | WPT438 | WPT439 | WPT440 | WPT441 | WPT442 | WPT443 | WPT444 | WPT445 | WPT446 | WPT447 | WPT448 | WPT449 | WPT450 | WPT451 | WPT452 | WPT453 | WPT454 | WPT455 | WPT456 | WPT457 | WPT458 | WPT459 | WPT460 | WPT461 | WPT462 | WPT463 | WPT464 | WPT465 | WPT466 | WPT467 | WPT468 | WPT469 | WPT470 | WPT471 | WPT472 | WPT473 | WPT474 | WPT475 | WPT476 | WPT477 | WPT478 | WPT479 | WPT480 | WPT481 | WPT482 | WPT483 | WPT484 | WPT485 | WPT486 | WPT487 | WPT488 | WPT489 | WPT490 | WPT491 | WPT492 | WPT493 | WPT494 | WPT495 | WPT496 | WPT497 | WPT498 | WPT499 | WPT500 | WPT501 | WPT502 | WPT503 | WPT504 | WPT505 | WPT506 | WPT507 | WPT508 | WPT509 | WPT510 | WPT511 | WPT512 | WPT513 | WPT514 | WPT515 | WPT516 | WPT517 | WPT518 | WPT519 | WPT520 | WPT521 | WPT522 | WPT523 | WPT524 | WPT525 | WPT526 | WPT527 | WPT528 | WPT529 | WPT530 | WPT531 | WPT532 | WPT533 | WPT534 | WPT535 | WPT536 | WPT537 | WPT538 | WPT539 | WPT540 | WPT541 | WPT542 | WPT543 | WPT544 | WPT545 | WPT546 | WPT547 | WPT548 | WPT549 | WPT550 | WPT551 | WPT552 | WPT553 | WPT554 | WPT555 | WPT556 | WPT557 | WPT558 | WPT559 | WPT560 | WPT561 | WPT562 | WPT563 | WPT564 | WPT565 | WPT566 | WPT567 | WPT568 | WPT569 | WPT570 | WPT571 | WPT572 | WPT573 | WPT574 | WPT575 | WPT576 | WPT577 | WPT578 | WPT579 | WPT580 | WPT581 | WPT582 | WPT583 | WPT584 | WPT585 | WPT586 | WPT587 | WPT588 | WPT589 | WPT590 | WPT591 | WPT592 | WPT593 | WPT594 | WPT595 | WPT596 | WPT597 | WPT598 | WPT599 | WPT600 | WPT601 | WPT602 | WPT603 | WPT604 | WPT605 | WPT606 | WPT607 | WPT608 | WPT609 | WPT610 | WPT611 | WPT612 | WPT613 | WPT614 | WPT615 | WPT616 | WPT617 | WPT618 | WPT619 | WPT620 | WPT621 | WPT622 | WPT623 | WPT624 | WPT625 | WPT626 | WPT627 | WPT628 | WPT629 | WPT630 | WPT631 | WPT632 | WPT633 | WPT634 | WPT635 | WPT636 | WPT637 | WPT638 | WPT639 | WPT640 | WPT641 | WPT642 | WPT643 | WPT644 | WPT645 | WPT646 | WPT647 | WPT648 | WPT649 | WPT650 | WPT651 | WPT652 | WPT653 | WPT654 | WPT655 | WPT656 | WPT657 | WPT658 | WPT659 | WPT660 | WPT661 | WPT662 | WPT663 | WPT664 | WPT665 | WPT666 | WPT667 | WPT668 | WPT669 | WPT670 | WPT671 | WPT672 | WPT673 | WPT674 | WPT675 | WPT676 | WPT677 | WPT678 | WPT679 | WPT680 | WPT681 | WPT682 | WPT683 | WPT684 | WPT685 | WPT686 | WPT687 | WPT688 | WPT689 | WPT690 | WPT691 | WPT692 | WPT693 | WPT694 | WPT695 | WPT696 | WPT697 | WPT698 | WPT699 | WPT700 | WPT701 | WPT702 | WPT703 | WPT704 | WPT705 | WPT706 | WPT707 | WPT708 | WPT709 | WPT710 | WPT711 | WPT712 | WPT713 | WPT714 | WPT715 | WPT716 | WPT717 | WPT718 | WPT719 | WPT720 | WPT721 | WPT722 | WPT723 | WPT724 | WPT725 | WPT726 | WPT727 | WPT728 | WPT729 | WPT730 | WPT731 | WPT732 | WPT733 | WPT734 | WPT735 | WPT736 | WPT737 | WPT738 | WPT739 | WPT740 | WPT741 | WPT742 | WPT743 | WPT744 | WPT745 | WPT746 | WPT747 | WPT748 | WPT749 | WPT750 | WPT751 | WPT752 | WPT753 | WPT754 | WPT755 | WPT756 | WPT757 | WPT758 | WPT759 | WPT760 | WPT761 | WPT762 | WPT763 | WPT764 | WPT765 | WPT766 | WPT767 | WPT768 | WPT769 | WPT770 | WPT771 | WPT772 | WPT773 | WPT774 | WPT775 | WPT776 | WPT777 | WPT778 | WPT779 | WPT780 | WPT781 | WPT782 | WPT783 | WPT784 | WPT785 | WPT786 | WPT787 | WPT788 | WPT789 | WPT790 | WPT791 | WPT792 | WPT793 | WPT794 | WPT795 | WPT796 | WPT797 | WPT798 | WPT799 | WPT800 | WPT801 | WPT802 | WPT803 | WPT804 | WPT805 | WPT806 | WPT807 | WPT808 | WPT809 | WPT810 | WPT811 | WPT812 | WPT813 | WPT814 | WPT815 | WPT816 | WPT817 | WPT818 | WPT819 | WPT820 | WPT821 | WPT822 | WPT823 | WPT824 | WPT825 | WPT826 | WPT827 | WPT828 | WPT829 | WPT830 | WPT831 | WPT832 | WPT833 | WPT834 | WPT835 | WPT836 | WPT837 | WPT838 | WPT839 | WPT840 | WPT841 | WPT842 | WPT843 | WPT844 | WPT845 | WPT846 | WPT847 | WPT848 | WPT849 | WPT850 | WPT851 | WPT852 | WPT853 | WPT854 | WPT855 | WPT856 | WPT857 | WPT858 | WPT859 | WPT860 | WPT861 | WPT862 | WPT863 | WPT864 | WPT865 | WPT866 | WPT867 | WPT868 | WPT869 | WPT870 | WPT871 | WPT872 | WPT873 | WPT874 | WPT875 | WPT876 | WPT877 | WPT878 | WPT879 | WPT880 | WPT881 | WPT882 | WPT883 | WPT884 | WPT885 | WPT886 | WPT887 | WPT888 | WPT889 | WPT890 | WPT891 | WPT892 | WPT893 | WPT894 | WPT895 | WPT896 | WPT897 | WPT898 | WPT899 | WPT900 | WPT901 | WPT902 | WPT903 | WPT904 | WPT905 | WPT906 | WPT907 | WPT908 | WPT909 | WPT910 | WPT911 | WPT912 | WPT913 | WPT914 | WPT915 | WPT916 | WPT917 | WPT918 | WPT919 | WPT920 | WPT921 | WPT922 | WPT923 | WPT924 | WPT925 | WPT926 | WPT927 | WPT928 | WPT929 | WPT930 | WPT931 | WPT932 | WPT933 | WPT934 | WPT935 | WPT936 | WPT937 | WPT938 | WPT939 | WPT940 | WPT941 | WPT942 | WPT943 | WPT944 | WPT945 | WPT946 | WPT947 | WPT948 | WPT949 | WPT950 | WPT951 | WPT952 | WPT953 | WPT954 | WPT955 | WPT956 | WPT957 | WPT958 | WPT959 | WPT960 | WPT961 | WPT962 | WPT963 | WPT964 | WPT965 | WPT966 | WPT967 | WPT968 | WPT969 | WPT970 | WPT971 | WPT972 | WPT973 | WPT974 | WPT975 | WPT976 | WPT977 | WPT978 | WPT979 | WPT980 | WPT981 | WPT982 | WPT983 | WPT984 | WPT985 | WPT986 | WPT987 | WPT988 | WPT989 | WPT990 | WPT991 | WPT992 | WPT993 | WPT994 | WPT995 | WPT996 | WPT997 | WPT998 | WPT999 | WPT1000 | WPT1001 | WPT1002 | WPT1003 | WPT1004 | WPT1005 | WPT1006 | WPT1007 | WPT1008 | WPT1009 | WPT1010 | WPT1011 | WPT1012 | WPT1013 | WPT1014 | WPT1015 | WPT1016 | WPT1017 | WPT1018 | WPT1019 | WPT1020 | WPT1021 | WPT1022 | WPT1023 | WPT1024 | WPT1025 | WPT1026 | WPT1027 | WPT1028 | WPT1029 | WPT1030 | WPT1031 | WPT1032 | WPT1033 | WPT1034 | WPT1035 | WPT1036 | WPT1037 | WPT1038 | WPT1039 | WPT1040 | WPT1041 | WPT1042 | WPT1043 | WPT1044 | WPT1045 | WPT1046 | WPT1047 | WPT1048 | WPT1049 | WPT1050 | WPT1051 | WPT1052 | WPT1053 | WPT1054 | WPT1055 | WPT1056 | WPT1057 | WPT1058 | WPT1059 | WPT1060 | WPT1061 | WPT1062 | WPT1063 | WPT1064 | WPT1065 | WPT1066 | WPT1067 | WPT1068 | WPT1069 | WPT1070 | WPT1071 | WPT1072 | WPT1073 | WPT1074 | WPT1075 | WPT1076 | WPT1077 | WPT1078 | WPT1079 | WPT1080 | WPT1081 | WPT1082 | WPT1083 | WPT1084 | WPT1085 | WPT1086 | WPT1087 | WPT1088 | WPT1089 | WPT1090 | WPT1091 | WPT1092 | WPT1093 | WPT1094 | WPT1095 | WPT1096 | WPT1097 | WPT1098 | WPT1099 |
<th
| --- | --- | --- | --- | --- | --- | --- | --- | --- | --- | --- | --- | --- | --- | --- | --- | --- | --- | --- | --- | --- | --- | --- | --- | --- | --- | --- | --- | --- | --- | --- | --- | --- | --- | --- | --- | --- | --- | --- | --- | --- | --- | --- | --- | --- | --- | --- | --- | --- | --- | --- | --- | --- | --- | --- | --- | --- | --- | --- | --- | --- | --- | --- | --- | --- | --- | --- | --- | --- | --- | --- | --- | --- | --- | --- | --- | --- | --- | --- | --- | --- | --- | --- | --- | --- | --- | --- | --- | --- | --- | --- | --- | --- | --- | --- | --- | --- | --- | --- | --- | --- | --- | --- | --- | --- | --- | --- | --- | --- | --- | --- | --- | --- | --- | --- | --- | --- | --- | --- | --- | --- | --- | --- | --- | --- | --- | --- | --- | --- | --- | --- | --- | --- | --- | --- | --- | --- | --- | --- | --- | --- | --- | --- | --- | --- | --- | --- | --- | --- | --- | --- | --- | --- | --- | --- | --- | --- | --- | --- | --- | --- | --- | --- | --- | --- | --- | --- | --- | --- | --- | --- | --- | --- | --- | --- | --- | --- | --- | --- | --- | --- | --- | --- | --- | --- | --- | --- | --- | --- | --- | --- | --- | --- | --- | --- | --- | --- | --- | --- | --- | --- | --- | --- | --- | --- | --- | --- | --- | --- | --- | --- | --- | --- | --- | --- | --- | --- | --- | --- | --- | --- | --- | --- | --- | --- | --- | --- | --- | --- | --- | --- | --- | --- | --- | --- | --- | --- | --- | --- | --- | --- | --- | --- | --- | --- | --- | --- | --- | --- | --- | --- | --- | --- | --- | --- | --- | --- | --- | --- | --- | --- | --- | --- | --- | --- | --- | --- | --- | --- | --- | --- | --- | --- | --- | --- | --- | --- | --- | --- | --- | --- | --- | --- | --- | --- | --- | --- | --- | --- | --- | --- | --- | --- | --- | --- | --- | --- | --- | --- | --- | --- | --- | --- | --- | --- | --- | --- | --- | --- | --- | --- | --- | --- | --- | --- | --- | --- | --- | --- | --- | --- | --- | --- | --- | --- | --- | --- | --- | --- | --- | --- | --- | --- | --- | --- | --- | --- | --- | --- | --- | --- | --- | --- | --- | --- | --- | --- | --- | --- | --- | --- | --- | --- | --- | --- | --- | --- | --- | --- | --- | --- | --- | --- | --- | --- | --- | --- | --- | --- | --- | --- | --- | --- | --- | --- | --- | --- | --- | --- | --- | --- | --- | --- | --- | --- | --- | --- | --- | --- | --- | --- | --- | --- | --- | --- | --- | --- | --- | --- | --- | --- | --- | --- | --- | --- | --- | --- | --- | --- | --- | --- | --- | --- | --- | --- | --- | --- | --- | --- | --- | --- | --- | --- | --- | --- | --- | --- | --- | --- | --- | --- | --- | --- | --- | --- | --- | --- | --- | --- | --- | --- | --- | --- | --- | --- | --- | --- | --- | --- | --- | --- | --- | --- | --- | --- | --- | --- | --- | --- | --- | --- | --- | --- | --- | --- | --- | --- | --- | --- | --- | --- | --- | --- | --- | --- | --- | --- | --- | --- | --- | --- | --- | --- | --- | --- | --- | --- | --- | --- | --- | --- | --- | --- | --- | --- | --- | --- | --- | --- | --- | --- | --- | --- | --- | --- | --- | --- | --- | --- | --- | --- | --- | --- | --- | --- | --- | --- | --- | --- | --- | --- | --- | --- | --- | --- | --- | --- | --- | --- | --- | --- | --- | --- | --- | --- | --- | --- | --- | --- | --- | --- | --- | --- | --- | --- | --- | --- | --- | --- | --- | --- | --- | --- | --- | --- | --- | --- | --- | --- | --- | --- | --- | --- | --- | --- | --- | --- | --- | --- | --- | --- | --- | --- | --- | --- | --- | --- | --- | --- | --- | --- | --- | --- | --- | --- | --- | --- | --- | --- | --- | --- | --- | --- | --- | --- | --- | --- | --- | --- | --- | --- | --- | --- | --- | --- | --- | --- | --- | --- | --- | --- | --- | --- | --- | --- | --- | --- | --- | --- | --- | --- | --- | --- | --- | --- | --- | --- | --- | --- | --- | --- | --- | --- | --- | --- | --- | --- | --- | --- | --- | --- | --- | --- | --- | --- | --- | --- | --- | --- | --- | --- | --- | --- | --- | --- | --- | --- | --- | --- | --- | --- | --- | --- | --- | --- | --- | --- | --- | --- | --- | --- | --- | --- | --- | --- | --- | --- | --- | --- | --- | --- | --- | --- | --- | --- | --- | --- | --- | --- | --- | --- | --- | --- | --- | --- | --- | --- | --- | --- | --- | --- | --- | --- | --- | --- | --- | --- | --- | --- | --- | --- | --- | --- | --- | --- | --- | --- | --- | --- | --- | --- | --- | --- | --- | --- | --- | --- | --- | --- | --- | --- | --- | --- | --- | --- | --- | --- | --- | --- | --- | --- | --- | --- | --- | --- | --- | --- | --- | --- | --- | --- | --- | --- | --- | --- | --- | --- | --- | --- | --- | --- | --- | --- | --- | --- | --- | --- | --- | --- | --- | --- | --- | --- | --- | --- | --- | --- | --- | --- | --- | --- | --- | --- | --- | --- | --- | --- | --- | --- | --- | --- | --- | --- | --- | --- | --- | --- | --- | --- | --- | --- | --- | --- | --- | --- | --- | --- | --- | --- | --- | --- | --- | --- | --- | --- | --- | --- | --- | --- | --- | --- | --- | --- | --- | --- | --- | --- | --- | --- | --- | --- | --- | --- | --- | --- | --- | --- | --- | --- | --- | --- | --- | --- | --- | --- | --- | --- | --- | --- | --- | --- | --- | --- | --- | --- | --- | --- | --- | --- | --- | --- | --- | --- | --- | --- | --- | --- | --- | --- | --- | --- | --- | --- | --- | --- | --- | --- | --- | --- | --- | --- | --- | --- | --- | --- | --- | --- | --- | --- | --- | --- | --- | --- | --- | --- | --- | --- | --- | --- | --- | --- | --- | --- | --- | --- | --- | --- | --- | --- | --- | --- | --- | --- | --- | --- | --- | --- | --- | --- | --- | --- | --- | --- | --- | --- | --- | --- | --- | --- | --- | --- | --- | --- | --- | --- | --- | --- | --- | --- | --- | --- | --- | --- | --- | --- | --- | --- | --- | --- | --- | --- | --- | --- | --- | --- | --- | --- | --- | --- | --- | --- | --- | --- | --- | --- | --- | --- | --- | --- | --- | --- | --- | --- | --- | --- | --- | --- | --- | --- | --- | --- | --- | --- | --- | --- | --- | --- | --- | --- | --- | --- | --- | --- | --- | --- | --- | --- | --- | --- | --- | --- | --- | --- | --- | --- | --- | --- | --- | --- | --- | --- | --- | --- | --- | --- | --- | --- | --- | --- | --- | --- | --- | --- | --- | --- | --- | --- | --- | --- | --- | --- | --- | --- | --- | --- | --- | --- | --- | --- | --- | --- | --- | --- | --- | --- | --- | --- | --- | --- | --- | --- | --- | --- | --- | --- | --- | --- | --- | --- | --- | --- | --- | --- | --- | --- | --- | --- | --- | --- | --- | --- | --- | --- | --- | --- | --- | --- | --- | --- | --- | --- | --- | --- | --- | --- | --- | --- | --- | --- | --- | --- | --- | --- | --- | --- | --- | --- | --- | --- | --- |

Source Type		Parameter A		Parameter B		Parameter C		Parameter D		Parameter E		Parameter F		Parameter G		Parameter H		Parameter I		Parameter J		Parameter K		Parameter L		Parameter M		Parameter N		Parameter O		Parameter P		Parameter Q		Parameter R		Parameter S		Parameter T		Parameter U		Parameter V		Parameter W		Parameter X		Parameter Y		Parameter Z									
A1		Value 1.0		Value 2.0		Value 3.0		Value 4.0		Value 5.0		Value 6.0		Value 7.0		Value 8.0		Value 9.0		Value 10.0		Value 11.0		Value 12.0		Value 13.0		Value 14.0		Value 15.0		Value 16.0		Value 17.0		Value 18.0		Value 19.0		Value 20.0		Value 21.0		Value 22.0		Value 23.0		Value 24.0		Value 25.0		Value 26.0		Value 27.0		Value 28.0		Value 29.0		Value 30.0	
A2		Value 1.1		Value 2.1		Value 3.1		Value 4.1		Value 5.1		Value 6.1		Value 7.1		Value 8.1		Value 9.1		Value 10.1		Value 11.1		Value 12.1		Value 13.1		Value 14.1		Value 15.1		Value 16.1		Value 17.1		Value 18.1		Value 19.1		Value 20.1		Value 21.1		Value 22.1		Value 23.1		Value 24.1		Value 25.1		Value 26.1		Value 27.1		Value 28.1		Value 29.1		Value 30.1	
A3		Value 1.2		Value 2.2		Value 3.2		Value 4.2		Value 5.2		Value 6.2		Value 7.2		Value 8.2		Value 9.2		Value 10.2		Value 11.2		Value 12.2		Value 13.2		Value 14.2		Value 15.2		Value 16.2		Value 17.2		Value 18.2		Value 19.2		Value 20.2		Value 21.2		Value 22.2		Value 23.2		Value 24.2		Value 25.2		Value 26.2		Value 27.2		Value 28.2		Value 29.2		Value 30.2	
A4		Value 1.3		Value 2.3		Value 3.3		Value 4.3		Value 5.3		Value 6.3		Value 7.3		Value 8.3		Value 9.3		Value 10.3		Value 11.3		Value 12.3		Value 13.3		Value 14.3		Value 15.3		Value 16.3		Value 17.3		Value 18.3		Value 19.3		Value 20.3		Value 21.3		Value 22.3		Value 23.3		Value 24.3		Value 25.3		Value 26.3		Value 27.3		Value 28.3		Value 29.3		Value 30.3	
A5		Value 1.4		Value 2.4		Value 3.4		Value 4.4		Value 5.4		Value 6.4		Value 7.4		Value 8.4		Value 9.4		Value 10.4		Value 11.4		Value 12.4		Value 13.4		Value 14.4		Value 15.4		Value 16.4		Value 17.4		Value 18.4		Value 19.4		Value 20.4		Value 21.4		Value 22.4		Value 23.4		Value 24.4		Value 25.4		Value 26.4		Value 27.4		Value 28.4		Value 29.4		Value 30.4	
A6		Value 1.5		Value 2.5		Value 3.5		Value 4.5		Value 5.5		Value 6.5		Value 7.5		Value 8.5		Value 9.5		Value 10.5		Value 11.5		Value 12.5		Value 13.5		Value 14.5		Value 15.5		Value 16.5		Value 17.5		Value 18.5		Value 19.5		Value 20.5		Value 21.5		Value 22.5		Value 23.5		Value 24.5		Value 25.5		Value 26.5		Value 27.5		Value 28.5		Value 29.5		Value 30.5	
A7		Value 1.6		Value 2.6		Value 3.6		Value 4.6		Value 5.6		Value 6.6		Value 7.6		Value 8.6		Value 9.6		Value 10.6		Value 11.6		Value 12.6		Value 13.6		Value 14.6		Value 15.6		Value 16.6		Value 17.6		Value 18.6		Value 19.6		Value 20.6		Value 21.6		Value 22.6		Value 23.6		Value 24.6		Value 25.6		Value 26.6		Value 27.6		Value 28.6		Value 29.6		Value 30.6	
A8		Value 1.7		Value 2.7		Value 3.7		Value 4.7		Value 5.7		Value 6.7		Value 7.7		Value 8.7		Value 9.7		Value 10.7		Value 11.7		Value 12.7		Value 13.7		Value 14.7		Value 15.7		Value 16.7		Value 17.7		Value 18.7		Value 19.7		Value 20.7		Value 21.7		Value 22.7		Value 23.7		Value 24.7		Value 25.7		Value 26.7		Value 27.7		Value 28.7		Value 29.7		Value 30.7	
A9		Value 1.8		Value 2.8		Value 3.8		Value 4.8		Value 5.8		Value 6.8		Value 7.8		Value 8.8		Value 9.8		Value 10.8		Value 11.8		Value 12.8		Value 13.8		Value 14.8		Value 15.8		Value 16.8		Value 17.8		Value 18.8		Value 19.8		Value 20.8		Value 21.8		Value 22.8		Value 23.8		Value 24.8		Value 25.8		Value 26.8		Value 27.8		Value 28.8		Value 29.8		Value 30.8	
A10		Value 1.9		Value 2.9		Value 3.9		Value 4.9		Value 5.9		Value 6.9		Value 7.9		Value 8.9		Value 9.9		Value 10.9		Value 11.9		Value 12.9		Value 13.9		Value 14.9		Value 15.9		Value 16.9		Value 17.9		Value 18.9		Value 19.9		Value 20.9		Value 21.9		Value 22.9		Value 23.9		Value 24.9		Value 25.9		Value 26.9		Value 27.9		Value 28.9		Value 29.9		Value 30.9	
A11		Value 1.10		Value 2.10		Value 3.10		Value 4.10		Value 5.10		Value 6.10		Value 7.10		Value 8.10		Value 9.10		Value 10.10		Value 11.10		Value 12.10		Value 13.10		Value 14.10		Value 15.10		Value 16.10		Value 17.10		Value 18.10		Value 19.10		Value 20.10		Value 21.10		Value 22.10		Value 23.10		Value 24.10		Value 25.10		Value 26.10		Value 27.10		Value 28.10		Value 29.10		Value 30.10	
A12		Value 1.11		Value 2.11		Value 3.11		Value 4.11		Value 5.11		Value 6.11		Value 7.11		Value 8.11		Value 9.11		Value 10.11		Value 11.11		Value 12.11		Value 13.11		Value 14.11		Value 15.11		Value 16.11		Value 17.11		Value 18.11		Value 19.11		Value 20.11		Value 21.11		Value 22.11		Value 23.11		Value 24.11		Value 25.11		Value 26.11		Value 27.11		Value 28.11		Value 29.11		Value 30.11	
A13		Value 1.12		Value 2.12		Value 3.12		Value 4.12		Value 5.12		Value 6.12		Value 7.12		Value 8.12		Value 9.12		Value 10.12		Value 11.12		Value 12.12		Value 13.12		Value 14.12		Value 15.12</td																															

The Development Test II of 155mm SMOKE GRENADES (XM225, 2 projectiles, DT2W2)

Editorial Note

104

LOS Integrated dosage (mag-s/m^2)									
5.650E+05	7.960E+05	-9.990E+01	5.520E+05	-9.990E+01	-9.990E+01	-9.990E+01	-9.990E+01	-9.990E+01	-9.990E+01
-238.0	-238.0	-238.0	-238.0	-238.0	-238.0	-238.0	-238.0	-238.0	-238.0
-86.2	-86.2	-86.2	-86.2	-86.2	-86.2	-86.2	-86.2	-86.2	-86.2
549.1	549.1	549.1	549.1	549.1	549.1	549.1	549.1	549.1	549.1
350.1	350.1	350.1	350.1	350.1	350.1	350.1	350.1	350.1	350.1
-99.9	-99.9	-99.9	-99.9	-99.9	-99.9	-99.9	-99.9	-99.9	-99.9
4.070E+05	5.640E+05	4.500E+05	2.100E+05	5.100E+05	5.100E+05	4.680E+05	3.580E+05	4.790E+05	4.790E+05
-276.8	-276.8	-276.8	-276.8	-276.8	-276.8	-276.8	-276.8	-276.8	-276.8
-16.2	-16.2	-16.2	-16.2	-16.2	-16.2	-16.2	-16.2	-16.2	-16.2
510.3	510.3	510.3	510.3	510.3	510.3	510.3	510.3	510.3	510.3
420.1	420.1	420.1	420.1	420.1	420.1	420.1	420.1	420.1	420.1
-99.9	-99.9	-99.9	-99.9	-99.9	-99.9	-99.9	-99.9	-99.9	-99.9
2.790E+05	3.880E+05	2.360E+05	1.410E+05	3.110E+05	3.110E+05	3.390E+05	2.420E+05	2.010E+05	2.130E+05
-110.5	-110.5	-110.5	-110.5	-110.5	-110.5	-110.5	-110.5	-110.5	-110.5
281.8	281.8	281.8	281.8	281.8	281.8	281.8	281.8	281.8	281.8
325.9	325.9	325.9	325.9	325.9	325.9	325.9	325.9	325.9	325.9
-505.4	-505.4	-505.4	-505.4	-505.4	-505.4	-505.4	-505.4	-505.4	-505.4
-99.9	-99.9	-99.9	-99.9	-99.9	-99.9	-99.9	-99.9	-99.9	-99.9
-9.990E+01	-9.990E+01	-9.990E+01	-9.990E+01	-9.990E+01	-9.990E+01	-9.990E+01	-9.990E+01	-9.990E+01	-9.990E+01
-40.5	-40.5	-40.5	-40.5	-40.5	-40.5	-40.5	-40.5	-40.5	-40.5
320.6	320.6	320.6	320.6	320.6	320.6	320.6	320.6	320.6	320.6
395.8	395.8	395.8	395.8	395.8	395.8	395.8	395.8	395.8	395.8
-466.6	-466.6	-466.6	-466.6	-466.6	-466.6	-466.6	-466.6	-466.6	-466.6
-99.9	-99.9	-99.9	-99.9	-99.9	-99.9	-99.9	-99.9	-99.9	-99.9
-9.990E+01	7.660E+05	-9.990E+01	2.540E+05	-9.990E+01	-9.990E+01	-9.990E+01	-9.990E+01	-9.990E+01	2.620E+05

The Development Test II of 155mm SMOKE GRENADES (M16A1), 1 projectile, DT2W1
II : number of trials included in DDA

6 : class zone designation

6

-99.9	-99.9	-99.9	-99.9	: relative humidity (%)
300.00	300.00	300.00	300.00	: temperature at level #1 (K)
2.00	2.00	2.00	2.00	: measuring height for temperature #1 (m)
-99.90	-99.90	-99.90	-99.90	: temperature at level #2 (K)
-99.90	-99.90	-99.90	-99.90	: measuring height for temperature #2 (m)
5.40	3.60	5.00	5.00	: wind speed (m/s) at tower
2.00	2.00	2.00	2.00	: measuring height for wind data (m)
5.40	3.60	5.00	5.00	: domain-averaged wind speed (m/s)
160.0	151.0	163.0	194.0	: domain-averaged wind direction (deg)
-99.90	-99.90	-99.90	-99.90	: domain-averaged alfa-u (m/s)
3.10	16.80	10.90	8.00	: domain-averaged alfa-a-hata (deg)
-99.90	-99.90	-99.90	-99.90	: domain-averaged alfa-a-phi (deg)
22.00	22.00	22.00	22.00	: averaging ht for domain-avg wind speed (m)
360.0	359.0	316.0	210.0	: averaging time for domain-avg data (s)
0.016	0.036	0.088	0.090	: wind speed power law exponent
0.0300	0.0300	0.0300	0.0300	: surface roughness (m)
-99.9000	-99.9000	-99.9000	-99.9000	: inverse Moab-Obukhov length (1/m)
0.18	0.18	0.18	0.18	: albedo
0.50	0.50	0.50	0.50	: molal water availability
0.50	0.50	0.50	0.50	: Bowen ratio
-99.9	-99.9	-99.9	-99.9	: missing height (m)
-99.9	-99.9	-99.9	-99.9	: cloud cover (%)
-99.9	-99.9	-99.9	-99.9	: P-G stability class
360.0	390.0	216.0	210.0	: averaging time for concentration (s)
1.50	1.50	1.50	1.50	: suggested receptor height (m)
0.3	0.3	0.3	0.3	: no. of distances downwind
-199.3	-199.3	-199.3	-199.3	: no. of lines-of-sight
-156.2	-156.2	-156.2	-156.2	: x-coord. of 1st end-point for LOS1 (m)
587.9	587.9	587.9	587.9	: y-coord. of 1st end-point for LOS1 (m)
280.1	280.1	280.1	280.1	: x-coord. of 2nd end-point for LOS1 (m)
-99.9	-99.9	-99.9	-99.9	: y-coord. of 2nd end-point for LOS1 (m)
-9.9902e-01	1.0002e-03	-9.9902e-01	-9.9902e-01	: LOS integrated conc. (mg/m ³ e2)
-238.0	-238.0	-238.0	-238.0	: LOS integrated dosage (mg/m ² e2)
-86.2	-86.2	-86.2	-86.2	: x-coord. of 1st end-point for LOS1 (m)
549.1	549.1	549.1	549.1	: y-coord. of 1st end-point for LOS1 (m)
350.1	350.1	350.1	350.1	: x-coord. of 2nd end-point for LOS1 (m)
-91.9	-99.9	-99.9	-99.9	: y-coord. of 2nd end-point for LOS1 (m)
1.1208e-05	7.5008e-05	1.5308e-05	9.3008e-05	: LOS integrated conc. (mg/m ³ e2)
-276.8	-276.8	-276.8	-276.8	: x-coord. of 1st end-point for LOS1 (m)
-16.2	-16.2	-16.2	-16.2	: y-coord. of 1st end-point for LOS1 (m)
510.3	510.3	510.3	510.3	: x-coord. of 2nd end-point for LOS1 (m)
420.1	420.1	420.1	420.1	: y-coord. of 2nd end-point for LOS1 (m)
-91.9	-99.9	-99.9	-99.9	: LOS integrated dosage (mg/m ² e2)
1.6508e-05	3.8008e-04	1.0708e-05	5.2008e-04	: LOS integrated dosage (mg/m ³ e2)

The Development Test 1 of Nine-Space Cartridges (Model 1, A projectile, Ordnance)

13 = number of trials included in DDA

6 = time zone designations

40.30 = latitude (deg)

113.00 = longitude (deg)

102.4 = 102.4

102.5 = 102.5

202.4 = 202.4

202.5 = 202.5

206.4 = 206.4

206.5 = 206.5

306.4 = 306.4

306.5 = 306.5

406.4 = 406.4

406.5 = 406.5

506.4 = 506.4

506.5 = 506.5

606.4 = 606.4

606.5 = 606.5

706.4 = 706.4

706.5 = 706.5

806.4 = 806.4

806.5 = 806.5

906.4 = 906.4

906.5 = 906.5

-1006.4 = -1006.4

-1006.5 = -1006.5

-1106.4 = -1106.4

-1106.5 = -1106.5

-1206.4 = -1206.4

-1206.5 = -1206.5

-1306.4 = -1306.4

-1306.5 = -1306.5

-1406.4 = -1406.4

-1406.5 = -1406.5

-1506.4 = -1506.4

-1506.5 = -1506.5

-1606.4 = -1606.4

-1606.5 = -1606.5

-1706.4 = -1706.4

-1706.5 = -1706.5

-1806.4 = -1806.4

-1806.5 = -1806.5

-1906.4 = -1906.4

-1906.5 = -1906.5

-2006.4 = -2006.4

-2006.5 = -2006.5

-2106.4 = -2106.4

-2106.5 = -2106.5

-2206.4 = -2206.4

-2206.5 = -2206.5

-2306.4 = -2306.4

-2306.5 = -2306.5

-2406.4 = -2406.4

-2406.5 = -2406.5

-2506.4 = -2506.4

-2506.5 = -2506.5

-2606.4 = -2606.4

-2606.5 = -2606.5

-2706.4 = -2706.4

-2706.5 = -2706.5

-2806.4 = -2806.4

-2806.5 = -2806.5

-2906.4 = -2906.4

-2906.5 = -2906.5

-3006.4 = -3006.4

-3006.5 = -3006.5

-3106.4 = -3106.4

-3106.5 = -3106.5

-3206.4 = -3206.4

-3206.5 = -3206.5

-3306.4 = -3306.4

-3306.5 = -3306.5

-3406.4 = -3406.4

-3406.5 = -3406.5

-3506.4 = -3506.4

-3506.5 = -3506.5

-3606.4 = -3606.4

-3606.5 = -3606.5

-3706.4 = -3706.4

-3706.5 = -3706.5

-3806.4 = -3806.4

-3806.5 = -3806.5

-3906.4 = -3906.4

-3906.5 = -3906.5

-4006.4 = -4006.4

-4006.5 = -4006.5

-4106.4 = -4106.4

-4106.5 = -4106.5

-4206.4 = -4206.4

-4206.5 = -4206.5

-4306.4 = -4306.4

-4306.5 = -4306.5

-4406.4 = -4406.4

-4406.5 = -4406.5

-4506.4 = -4506.4

-4506.5 = -4506.5

-4606.4 = -4606.4

-4606.5 = -4606.5

-4706.4 = -4706.4

-4706.5 = -4706.5

-4806.4 = -4806.4

-4806.5 = -4806.5

-4906.4 = -4906.4

-4906.5 = -4906.5

-5006.4 = -5006.4

-5006.5 = -5006.5

-5106.4 = -5106.4

-5106.5 = -5106.5

-5206.4 = -5206.4

-5206.5 = -5206.5

-5306.4 = -5306.4

-5306.5 = -5306.5

-5406.4 = -5406.4

-5406.5 = -5406.5

-5506.4 = -5506.4

-5506.5 = -5506.5

-5606.4 = -5606.4

-5606.5 = -5606.5

-5706.4 = -5706.4

-5706.5 = -5706.5

-5806.4 = -5806.4

-5806.5 = -5806.5

-5906.4 = -5906.4

-5906.5 = -5906.5

-6006.4 = -6006.4

-6006.5 = -6006.5

-6106.4 = -6106.4

-6106.5 = -6106.5

-6206.4 = -6206.4

-6206.5 = -6206.5

-6306.4 = -6306.4

-6306.5 = -6306.5

-6406.4 = -6406.4

-6406.5 = -6406.5

-6506.4 = -6506.4

-6506.5 = -6506.5

-6606.4 = -6606.4

-6606.5 = -6606.5

-6706.4 = -6706.4

-6706.5 = -6706.5

-6806.4 = -6806.4

-6806.5 = -6806.5

-6906.4 = -6906.4

-6906.5 = -6906.5

-7006.4 = -7006.4

-7006.5 = -7006.5

-7106.4 = -7106.4

-7106.5 = -7106.5

-7206.4 = -7206.4

-7206.5 = -7206.5

-7306.4 = -7306.4

-7306.5 = -7306.5

-7406.4 = -7406.4

-7406.5 = -7406.5

-7506.4 = -7506.4

-7506.5 = -7506.5

-7606.4 = -7606.4

-7606.5 = -7606.5

-7706.4 = -7706.4

-7706.5 = -7706.5

-7806.4 = -7806.4

-7806.5 = -7806.5

-7906.4 = -7906.4

-7906.5 = -7906.5

-8006.4 = -8006.4

-8006.5 = -8006.5

-8106.4 = -8106.4

-8106.5 = -8106.5

-8206.4 = -8206.4

-8206.5 = -8206.5

-8306.4 = -8306.4

-8306.5 = -8306.5

-8406.4 = -8406.4

-8406.5 = -8406.5

-8506.4 = -8506.4

-8506.5 = -8506.5

-8606.4 = -8606.4

-8606.5 = -8606.5

-8706.4 = -8706.4

-8706.5 = -8706.5

-8806.4 = -8806.4

-8806.5 = -8806.5

-8906.4 = -8906.4

-8906.5 = -8906.5

-9006.4 = -9006.4

-9006.5 = -9006.5

-9106.4 = -9106.4

-9106.5 = -9106.5

-9206.4 = -9206.4

-9206.5 = -9206.5

-9306.4 = -9306.4

-9306.5 = -9306.5

-9406.4 = -9406.4

-9406.5 = -9406.5

-9506.4 = -9506.4

-9506.5 = -9506.5

-9606.4 = -9606.4

-9606.5 = -9606.5

-9706.4 = -9706.4

-9706.5 = -9706.5

-9806.4 = -9806.4

-9806.5 = -9806.5

-9906.4 = -9906.4

-9906.5 = -9906.5

-10006.4 = -10006.4

-10006.5 = -10006.5

-10106.4 = -10106.4

-10106.5 = -10106.5

-10206.4 = -10206.4

-10206.5 = -10206.5

-10306.4 = -10306.4

-10306.5 = -10306.5

-10406.4 = -10406.4

-10406.5 = -10406.5

-10506.4 = -10506.4

-10506.5 = -10506.5

-10606.4 = -10606.4

-10606.5 = -10606.5

-10706.4 = -10706.4

-10706.5 = -10706.5

-10806.4 = -10806.4

-10806.5 = -10806.5

-10906.4 = -10906.4

-10906.5 = -10906.5

-11006.4 = -11006.4

-11006.5 = -11006.5

-11106.4 = -11106.4

-11106.5 = -11106.5


```

-9.990E+01 -9.990E+01 -9.990E+01 -9.990E+01 -9.990E+01 1.020E+05 9.000E+04 : LOS Integrated dosage (mg-s/m**2)
 21.1    -21.1    -21.1    -21.1    -21.1    -21.7    -21.7 : x-coord. of 1st end-point for LOS1 (m)
 142.3   142.3   142.3   142.3   142.3   142.3   142.3 : y-coord. of 1st end-point for LOS1 (m)
 408.7   408.7   408.7   408.7   408.7   408.7   408.7 : x-coord. of 1st end-point for LOS1 (m)
 -768.2  -768.2  -768.2  -768.2  -768.2  -768.2  -768.2 : y-coord. of 1st end-point for LOS1 (m)
 -99.9   -99.9   -99.9   -99.9   -99.9   -99.9   -99.9 : x-coord. of 2nd end-point for LOS1 (m)
 -99.9   -99.9   -99.9   -99.9   -99.9   -99.9   -99.9 : y-coord. of 2nd end-point for LOS1 (m)
 -9.990E+01 -9.990E+01 -9.990E+01 -9.990E+01 -9.990E+01 -9.990E+01 -9.990E+01 : LOS Integrated dosage (mg-s/m**2)
 -78.6   -78.6   -78.6   -78.6   -78.6   -78.6   -78.6 : x-coord. of 1st end-point for LOS1 (m)
 110.8   110.8   110.8   110.8   110.8   110.8   110.8 : y-coord. of 1st end-point for LOS1 (m)
 395.5   395.5   395.5   395.5   395.5   395.5   395.5 : x-coord. of 1st end-point for LOS1 (m)
 -775.5  -775.5  -775.5  -775.5  -775.5  -775.5  -775.5 : y-coord. of 1st end-point for LOS1 (m)
 -99.9   -99.9   -99.9   -99.9   -99.9   -99.9   -99.9 : x-coord. of 2nd end-point for LOS1 (m)
 -99.9   -99.9   -99.9   -99.9   -99.9   -99.9   -99.9 : y-coord. of 2nd end-point for LOS1 (m)
 -9.990E+01 -9.990E+01 -9.990E+01 -9.990E+01 -9.990E+01 -9.990E+01 -9.990E+01 : LOS Integrated dosage (mg-s/m**2)

```

The Inventory Test 1 of Glare Shade Candidates #232A2, 1 Projectile, 07H1

10 : Number of trials included in GDA

6 : Glare shade designation

40-30 : Latitude (deg)

113.00 : Longitude (deg)

1018 : Date (yy)

1020 : Time (yy)

2020 : Date (yy)

2020 : Time (yy)

3020 : Date (yy)

3020 : Time (yy)

4020 : Date (yy)

4020 : Time (yy)

5020 : Date (yy)

5020 : Time (yy)

6020 : Date (yy)

6020 : Time (yy)

7020 : Date (yy)

7020 : Time (yy)

8020 : Date (yy)

8020 : Time (yy)

9020 : Date (yy)

9020 : Time (yy)

10020 : Date (yy)

10020 : Time (yy)

11020 : Date (yy)

11020 : Time (yy)

12020 : Date (yy)

12020 : Time (yy)

13020 : Date (yy)

13020 : Time (yy)

14020 : Date (yy)

14020 : Time (yy)

15020 : Date (yy)

15020 : Time (yy)

16020 : Date (yy)

16020 : Time (yy)

17020 : Date (yy)

17020 : Time (yy)

18020 : Date (yy)

18020 : Time (yy)

19020 : Date (yy)

19020 : Time (yy)

20020 : Date (yy)

20020 : Time (yy)

21020 : Date (yy)

21020 : Time (yy)

22020 : Date (yy)

22020 : Time (yy)

23020 : Date (yy)

23020 : Time (yy)

24020 : Date (yy)

24020 : Time (yy)

25020 : Date (yy)

25020 : Time (yy)

26020 : Date (yy)

26020 : Time (yy)

27020 : Date (yy)

27020 : Time (yy)

28020 : Date (yy)

28020 : Time (yy)

29020 : Date (yy)

29020 : Time (yy)

30020 : Date (yy)

30020 : Time (yy)

31020 : Date (yy)

31020 : Time (yy)

32020 : Date (yy)

32020 : Time (yy)

33020 : Date (yy)

33020 : Time (yy)

34020 : Date (yy)

34020 : Time (yy)

35020 : Date (yy)

35020 : Time (yy)

36020 : Date (yy)

36020 : Time (yy)

37020 : Date (yy)

37020 : Time (yy)

38020 : Date (yy)

38020 : Time (yy)

39020 : Date (yy)

39020 : Time (yy)

40020 : Date (yy)

40020 : Time (yy)

41020 : Date (yy)

41020 : Time (yy)

42020 : Date (yy)

42020 : Time (yy)

43020 : Date (yy)

43020 : Time (yy)

44020 : Date (yy)

44020 : Time (yy)

45020 : Date (yy)

45020 : Time (yy)

46020 : Date (yy)

46020 : Time (yy)

47020 : Date (yy)

47020 : Time (yy)

48020 : Date (yy)

48020 : Time (yy)

49020 : Date (yy)

49020 : Time (yy)

50020 : Date (yy)

50020 : Time (yy)

51020 : Date (yy)

51020 : Time (yy)

52020 : Date (yy)

52020 : Time (yy)

53020 : Date (yy)

53020 : Time (yy)

54020 : Date (yy)

54020 : Time (yy)

55020 : Date (yy)

55020 : Time (yy)

56020 : Date (yy)

56020 : Time (yy)

57020 : Date (yy)

57020 : Time (yy)

58020 : Date (yy)

58020 : Time (yy)

59020 : Date (yy)

59020 : Time (yy)

60020 : Date (yy)

60020 : Time (yy)

61020 : Date (yy)

61020 : Time (yy)

62020 : Date (yy)

62020 : Time (yy)

63020 : Date (yy)

63020 : Time (yy)

64020 : Date (yy)

64020 : Time (yy)

65020 : Date (yy)

65020 : Time (yy)

66020 : Date (yy)

66020 : Time (yy)

67020 : Date (yy)

67020 : Time (yy)

68020 : Date (yy)

68020 : Time (yy)

69020 : Date (yy)

69020 : Time (yy)

70020 : Date (yy)

70020 : Time (yy)

71020 : Date (yy)

71020 : Time (yy)

72020 : Date (yy)

72020 : Time (yy)

73020 : Date (yy)

73020 : Time (yy)

74020 : Date (yy)

74020 : Time (yy)

75020 : Date (yy)

75020 : Time (yy)

76020 : Date (yy)

76020 : Time (yy)

77020 : Date (yy)

77020 : Time (yy)

78020 : Date (yy)

78020 : Time (yy)

79020 : Date (yy)

79020 : Time (yy)

80020 : Date (yy)

80020 : Time (yy)

81020 : Date (yy)

81020 : Time (yy)

82020 : Date (yy)

82020 : Time (yy)

83020 : Date (yy)

83020 : Time (yy)

84020 : Date (yy)

84020 : Time (yy)

85020 : Date (yy)

85020 : Time (yy)

86020 : Date (yy)

86020 : Time (yy)

87020 : Date (yy)

87020 : Time (yy)

88020 : Date (yy)

88020 : Time (yy)

89020 : Date (yy)

89020 : Time (yy)

90020 : Date (yy)

90020 : Time (yy)

91020 : Date (yy)

91020 : Time (yy)

92020 : Date (yy)

92020 : Time (yy)

93020 : Date (yy)

93020 : Time (yy)

94020 : Date (yy)

94020 : Time (yy)

95020 : Date (yy)

95020 : Time (yy)

96020 : Date (yy)

96020 : Time (yy)

97020 : Date (yy)

97020 : Time (yy)

98020 : Date (yy)

98020 : Time (yy)

99020 : Date (yy)

99020 : Time (yy)

00020 : Date (yy)

00020 : Time (yy)

01020 : Date (yy)

01020 : Time (yy)

02020 : Date (yy)

02020 : Time (yy)

03020 : Date (yy)

03020 : Time (yy)

04020 : Date (yy)

04020 : Time (yy)

05020 : Date (yy)

05020 : Time (yy)

06020 : Date (yy)

06020 : Time (yy)

07020 : Date (yy)

07020 : Time (yy)

08020 : Date (yy)

08020 : Time (yy)

09020 : Date (yy)

09020 : Time (yy)

10020 : Date (yy)

10020 : Time (yy)

11020 : Date (yy)

11020 : Time (yy)

12020 : Date (yy)

12020 : Time (yy)

13020 : Date (yy)

13020 : Time (yy)

14020 : Date (yy)

14020 : Time (yy)

15020 : Date (yy)

15020 : Time (yy)

16020 : Date (yy)

16020 : Time (yy)

17020 : Date (yy)

17020 : Time (yy)

18020 : Date (yy)

18020 : Time (yy)

19020 : Date (yy)

19020 : Time (yy)

20020 : Date (yy)

20020 : Time (yy)

21020 : Date (yy)

21020 : Time (yy)

22020 : Date (yy)

22020 : Time (yy)

23020 : Date (yy)

23020 : Time (yy)

24020 : Date (yy)

24020 : Time (yy)

25020 : Date (yy)

25020 : Time (yy)

Test I of Blau Smoke Cartridges (M375A2, 3 projectiles, DT1M3)

-9.990E+01	3.000E+04	1.530E+05	-9.990E+01	-9.990E+01	-9.990E+01	-9.990E+01	-9.990E+01	1.310E+05	1.660E+05
-21.7	-21.7	-21.7	-21.7	-21.7	-21.7	-21.7	-21.7	-21.7	-21.7
142.3	142.3	142.3	142.3	142.3	142.3	142.3	142.3	142.3	142.3
408.7	408.7	408.7	408.7	408.7	408.7	408.7	408.7	408.7	408.7
-768.2	-768.2	-768.2	-768.2	-768.2	-768.2	-768.2	-768.2	-768.2	-768.2
-99.9	-99.9	-99.9	-99.9	-99.9	-99.9	-99.9	-99.9	-99.9	-99.9
-9.990E+01									
-78.6	-78.6	-78.6	-78.6	-78.6	-78.6	-78.6	-78.6	-78.6	-78.6
110.8	110.8	110.8	110.8	110.8	110.8	110.8	110.8	110.8	110.8
395.5	395.5	395.5	395.5	395.5	395.5	395.5	395.5	395.5	395.5
-775.5	-775.5	-775.5	-775.5	-775.5	-775.5	-775.5	-775.5	-775.5	-775.5
-99.9	-99.9	-99.9	-99.9	-99.9	-99.9	-99.9	-99.9	-99.9	-99.9
-9.990E+01									

The Evaluation of the 1.0 Series Grenades (L81A1)

The Evaluation of the L8 Series Grenades (L81B1)

The Evaluation of the I.D Series, Grenada (L81D1)

5 : number of trials included in DDA

6 : time zone designation

40.20 : latitude (deg)

113.00 : longitude (deg)

B835 B836 B837 B838 B839 B840 trial ID

6	6	6	6	6	6	month
10	10	10	10	10	17	day
01	01	01	01	01	01	year
10	13	14	10	10	12	hour
18	45	42	56	56	29	minute
1	1	1	1	1	1	1 : no. of sources
-62.0	-25.3	-25.3	34.0	34.0	-20.9	x-coord. of source (m)
68.5	88.9	88.9	-84.0	-84.0	91.3	y-coord. of source (m)
0.00	0.00	0.00	0.00	0.00	0.00	source elevation (m)
-99.9	-99.9	-99.9	-99.9	-99.9	-99.9	emission rate (g/s)
115.0	115.0	115.0	115.0	115.0	115.0	emission duration (s)
0.897	0.840	0.840	0.722	0.722	0.853	total mass emitted (kg)
5.413	4.153	4.153	0.446	0.446	3.737	signx at the source (m)
12.343	12.848	12.848	12.971	12.971	12.971	signy at the source (m)
0.120	0.120	0.120	0.120	0.120	0.120	signz at the source (m)
-99.9	-99.9	-99.9	-99.9	-99.9	-99.9	ambient pressure (Pa)
-99.9	-99.9	-99.9	-99.9	-99.9	-99.9	relative humidity (%)
300.00	300.00	300.00	300.00	300.00	300.00	temperature at level A1 (K)
2.00	2.00	2.00	2.00	2.00	2.00	measuring height for temperature A1 (m)
-99.90	-99.90	-99.90	-99.90	-99.90	-99.90	temperature at level B1 (K)
-99.90	-99.90	-99.90	-99.90	-99.90	-99.90	measuring height for temperature B2 (m)
2.10	1.30	4.50	6.80	6.80	6.50	wind speed (m/s) at a tower
2.00	2.00	2.00	2.00	2.00	2.00	measuring height for wind data (m)
2.30	1.30	4.50	6.80	6.80	6.50	domain-averaged wind speed (m/s)
345.0	351.0	351.0	187.0	187.0	25.6	domain-averaged wind direction (deg)
-99.90	-99.90	-99.90	-99.90	-99.90	-99.90	domain-averaged sigma-u (m/s/deg)
13.90	15.70	17.20	13.10	13.10	9.60	domain-averaged sigma-theta (deg)
-99.90	-99.90	-99.90	-99.90	-99.90	-99.90	domain-averaged sigma-phi (deg)
2.00	2.00	2.00	2.00	2.00	2.00	measuring ht for domain-avg wind speed (m)
215.0	240.0	240.0	181.0	181.0	181.0	averaging time for domain-avg data (s)
0.094	0.000	0.000	0.040	0.040	0.042	wind speed power law exponent
0.0300	0.0300	0.0300	0.0300	0.0300	0.0300	surface roughness (m)
-99.900	-99.900	-99.900	-99.900	-99.900	-99.900	friction velocity (m)
-99.9000	-99.9000	-99.9000	-99.9000	-99.9000	-99.9000	inverse Monin-Obukhov length (1/m)
-99.9000	-99.9000	-99.9000	-99.9000	-99.9000	-99.9000	albedo
0.15	0.14	0.14	0.14	0.14	0.14	P-G stability class
0.50	0.50	0.50	0.50	0.50	0.50	averaging time for concentration (s)
0.50	0.50	0.50	0.50	0.50	0.50	suggested receptor height (m)
0.50	0.50	0.50	0.50	0.50	0.50	no. of distances downwind
0	0	0	0	0	0	no. of lines-of-sight
2	2	2	2	2	2	cloud cover (%)
-247.7	-247.7	-247.7	-247.7	-247.7	-247.7	x-coord. of 1st end-point for LOS1 (m)
-68.7	-68.7	-68.7	-68.7	-68.7	-68.7	y-coord. of 1st end-point for LOS1 (m)
169.6	169.6	169.6	169.6	169.6	169.6	z-coord. of 1st end-point for LOS1 (m)
173.7	173.7	173.7	173.7	173.7	173.7	x-coord. of 2nd end-point for LOS1 (m)
-99.9	-99.9	-99.9	-99.9	-99.9	-99.9	y-coord. of 2nd end-point for LOS1 (m)
-99.9	-99.9	-99.9	-99.9	-99.9	-99.9	z-coord. of 2nd end-point for LOS1 (m)
1.210E+04	3.910E+04	3.960E+04	-9.900E+01	1.710E+04	1.05	Integrated dosage (mg/m^2)^2
-189.6	-189.6	-189.6	-189.6	-189.6	-189.6	integrated dosage (mg/m^2)^2
-173.7	-173.7	-173.7	-173.7	-173.7	-173.7	integrated dosage (mg/m^2)^2
247.7	247.7	247.7	247.7	247.7	247.7	integrated dosage (mg/m^2)^2
68.7	68.7	68.7	68.7	68.7	68.7	integrated dosage (mg/m^2)^2
-99.9	-99.9	-99.9	-99.9	-99.9	-99.9	integrated dosage (mg/m^2)^2
-9.990E+01	1.430E+04	-9.990E+01	4.410E+04	-9.990E+01	4.410E+04	integrated dosage (mg/m^2)^2

The Evaluation of the 1.8 Series Grenades (L8112) 6 : number of trials included in DDA

The Evaluation of the LG Series Grenades (LB1, 6 grenades, 1916)

5	number of trials included in DDA	B6b	trial ID
6	time zone designation		
40.20	latitude (deg)		
113.00	longitude (deg)		
B2b	B4b	B5b	
5	4	4	
25	1	1	
82	92	92	
16	17	16	
52	17	16	
52	4	33	
6	-35.7	-35.6	
100.8	100.8	100.8	
0.00	0.00	0.00	
-99.9	-99.9	-99.9	
101.0	101.0	101.0	
0.839	0.992	0.954	
6.98	5.032	1.554	
15.56	16.201	16.893	
0.120	0.120	0.120	
-51.4	-51.4	-51.4	
117.5	117.5	117.5	
0.00	0.00	0.00	
-99.9	-99.9	-99.9	
101.0	101.0	101.0	
0.839	0.992	0.954	
16.917	16.945	16.405	
0.120	0.120	0.120	
-83.1	-83.1	-83.1	
130.3	130.3	130.3	
0.00	0.00	0.00	
-99.9	-99.9	-99.9	
101.0	101.0	101.0	
0.839	0.992	0.954	
1.176	1.176	1.176	
15.119	14.268	12.048	
0.120	0.120	0.120	
-28.0	-28.0	-28.0	
-45.5	-45.5	-45.5	
0.00	0.00	0.00	
-99.9	-99.9	-99.9	
101.0	101.0	101.0	
0.839	0.992	0.954	
15.643	15.643	13.939	
0.120	0.120	0.120	
-26.8	-26.8	-26.8	
79.7	79.7	79.7	
0.00	0.00	0.00	
-99.9	-99.9	-99.9	
101.0	101.0	101.0	
0.839	0.992	0.954	
11.624	10.269	7.237	
12.335	12.503	15.343	
0.120	0.120	0.120	
-25.6	-25.6	-25.6	
56.8	56.8	56.8	
0.00	0.00	0.00	
-99.9	-99.9	-99.9	
101.0	101.0	101.0	
0.839	0.992	0.954	
15.149	14.268	12.048	
0.120	0.120	0.120	
-25.6	-25.6	-25.6	
56.8	56.8	56.8	
0.00	0.00	0.00	
-99.9	-99.9	-99.9	
300.00	300.00	300.00	
102.00	102.00	2.00	
-99.90	-99.90	-99.90	
22.10	10.50	11.40	
5.00	3.00	2.50	
2.60	4.40	4.90	
2.00	2.00	2.00	
2.00	4.40	4.90	
33.10	34.30	35.50	
-99.90	-99.90	-99.90	
22.10	10.50	12.10	
5.00	3.00	3.00	
2.60	2.00	2.00	
300.0	300.0	300.0	
0.0300	0.0300	0.0300	
-99.900	-99.900	-99.900	
-99.9000	-99.9000	-99.9000	

0.16	0.16	0.16	0.16	0.16 : albedo
0.50	0.50	0.50	0.50	0.50 : moisture availability
0.50	0.50	0.50	0.50	0.50 : Bowen ratio
-99.9	-99.9	-99.9	-99.9	-99.9 : mixing height (m)
-99.9	-99.9	-99.9	-99.9	-99.9 : cloud cover (%)
-99.9	-99.9	-99.9	-99.9	-99.9 : P-G stability class
300.0	300.0	300.0	300.0	300.0 : averaging time for concentration (s)
2.00	2.00	2.00	2.00	2.00 : suggested receptor height (m)
0	0	0	0	0 : no. of distances downwind
3	3	3	3	3 : no. of lines-of-sight
-173.8	-173.8	-173.8	-173.8	-173.8 : x-coord. of 1st end-point for LOS1 (m)
-205.7	-205.7	-205.7	-205.7	-205.7 : y-coord. of 1st end-point for LOS1 (m)
-356.0	-356.0	-356.0	-356.0	-356.0 : z-coord. of 1st end-point for LOS1 (m)
76.0	76.0	76.0	76.0	76.0 : x-coord. of 2nd end-point for LOS1 (m)
-197.3	-99.9	-99.9	-99.9	-99.9 : y-coord. of 2nd end-point for LOS1 (m)
-197.3	-197.3	-197.3	-197.3	-197.3 : z-coord. of 2nd end-point for LOS1 (m)
4.200E+04	3.000E+04	4.500E+04	4.800E+04	4.900E+04 : LOS integrated dosage (mg-s/m^2)
-197.3	-161.5	-161.5	-161.5	-161.5 : x-coord. of 1st end-point for LOS1 (m)
-161.5	-132.5	-132.5	-132.5	-132.5 : y-coord. of 1st end-point for LOS1 (m)
-120.2	-120.2	-120.2	-120.2	-120.2 : z-coord. of 1st end-point for LOS1 (m)
-99.9	-99.9	-99.9	-99.9	-99.9 : x-coord. of 2nd end-point for LOS1 (m)
5.000E+04	7.400E+04	5.900E+04	5.900E+04	5.900E+04 : LOS integrated conc. (mg/m^2)
-220.7	-220.7	-220.7	-220.7	-220.7 : LOS integrated dosage (mg-s/m^2)
-117.4	-117.4	-117.4	-117.4	-117.4 : y-coord. of 1st end-point for LOS1 (m)
309.0	309.0	309.0	309.0	309.0 : z-coord. of 1st end-point for LOS1 (m)
164.3	164.3	164.3	164.3	164.3 : x-coord. of 2nd end-point for LOS1 (m)
-99.9	-99.9	-99.9	-99.9	-99.9 : LOS integrated conc. (mg/m^2)
1.240E+05	1.240E+05	1.540E+05	9.800E+04	1.240E+05 : LOS integrated dosage (mg-s/m^2)

The Evaluation of the LB Series Grenades (LB1), 8 grenades, 18158

	6 : number of trials included in DDA	6 : time zone designation	40.20 : latitude (deg)	113.00 : longitude (deg)	B1b : trial ID	B12b : trial ID	B1b : month	B12b : month	B1b : day	B12b : day	B1b : hour	B12b : hour	B1b : minute	B12b : minute	B1b : no. of sources	B12b : no. of sources
6	6	6	6	6	6	6	6	6	7	7	7	7	7	7	6	6
16	92	92	92	92	92	92	92	92	92	92	92	92	92	92	7	7
12	15	15	29	29	41	22	20	20	51	51	51	51	51	51	1	1
7	6	6	6	6	6	6	6	6	6	6	6	6	6	6	6	6
6	62.6	62.6	-35.7	-35.7	62.6	62.6	62.6	62.6	62.6	62.6	62.6	62.6	62.6	62.6	62.6	62.6
5	-71.5	-71.5	100.8	100.8	-71.5	-71.5	-71.5	-71.5	-71.5	-71.5	-71.5	-71.5	-71.5	-71.5	-71.5	-71.5
4	0.00	0.00	0.00	0.00	0.00	0.00	0.00	0.00	0.00	0.00	0.00	0.00	0.00	0.00	0.00	0.00
3	-99.9	-99.9	-99.9	-99.9	-99.9	-99.9	-99.9	-99.9	-99.9	-99.9	-99.9	-99.9	-99.9	-99.9	-99.9	-99.9
2	101.0	101.0	101.0	101.0	101.0	101.0	101.0	101.0	101.0	101.0	101.0	101.0	101.0	101.0	101.0	101.0
1	0.897	0.897	0.897	0.897	0.897	0.897	0.897	0.897	0.897	0.897	0.897	0.897	0.897	0.897	0.897	0.897
0	11.644	11.644	17.259	17.259	2.759	4.031	4.031	4.031	4.031	4.031	4.031	4.031	4.031	4.031	4.031	4.031
12.355	15.200	15.001	16.418	16.418	16.321	16.321	16.321	16.321	16.321	16.321	16.321	16.321	16.321	16.321	16.321	16.321
0.120	0.120	0.120	0.120	0.120	0.120	0.120	0.120	0.120	0.120	0.120	0.120	0.120	0.120	0.120	0.120	0.120
51.4	51.4	51.4	-46.9	-46.9	51.4	51.4	51.4	51.4	51.4	51.4	51.4	51.4	51.4	51.4	51.4	51.4
14.893	12.632	16.577	16.577	16.577	16.577	16.577	16.577	16.577	16.577	16.577	16.577	16.577	16.577	16.577	16.577	16.577
0.120	0.120	0.120	0.120	0.120	0.120	0.120	0.120	0.120	0.120	0.120	0.120	0.120	0.120	0.120	0.120	0.120
37.2	37.2	37.2	-61.1	-61.1	37.2	37.2	37.2	37.2	37.2	37.2	37.2	37.2	37.2	37.2	37.2	37.2
-50.6	-50.6	-50.6	123.6	123.6	-50.6	-50.6	-50.6	-50.6	-50.6	-50.6	-50.6	-50.6	-50.6	-50.6	-50.6	-50.6
0.00	0.00	0.00	0.00	0.00	0.00	0.00	0.00	0.00	0.00	0.00	0.00	0.00	0.00	0.00	0.00	0.00
-99.9	-99.9	-99.9	-99.9	-99.9	-99.9	-99.9	-99.9	-99.9	-99.9	-99.9	-99.9	-99.9	-99.9	-99.9	-99.9	-99.9
101.0	101.0	101.0	101.0	101.0	101.0	101.0	101.0	101.0	101.0	101.0	101.0	101.0	101.0	101.0	101.0	101.0
0.897	0.897	0.897	0.897	0.897	0.897	0.897	0.897	0.897	0.897	0.897	0.897	0.897	0.897	0.897	0.897	0.897
11.002	11.002	11.002	3.601	3.601	8.158	8.158	8.158	8.158	8.158	8.158	8.158	8.158	8.158	8.158	8.158	8.158
14.893	14.022	14.022	0.813	0.813	11.730	11.730	11.730	11.730	11.730	11.730	11.730	11.730	11.730	11.730	11.730	11.730
16.577	9.512	9.512	16.945	16.945	12.255	12.255	12.255	12.255	12.255	12.255	12.255	12.255	12.255	12.255	12.255	12.255
0.120	0.120	0.120	0.120	0.120	0.120	0.120	0.120	0.120	0.120	0.120	0.120	0.120	0.120	0.120	0.120	0.120
20.9	20.9	20.9	-77.4	-77.4	20.9	20.9	20.9	20.9	20.9	20.9	20.9	20.9	20.9	20.9	20.9	20.9
-44.9	-44.9	-44.9	129.4	129.4	-44.9	-44.9	-44.9	-44.9	-44.9	-44.9	-44.9	-44.9	-44.9	-44.9	-44.9	-44.9
0.00	0.00	0.00	0.00	0.00	0.00	0.00	0.00	0.00	0.00	0.00	0.00	0.00	0.00	0.00	0.00	0.00
-99.9	-99.9	-99.9	-99.9	-99.9	-99.9	-99.9	-99.9	-99.9	-99.9	-99.9	-99.9	-99.9	-99.9	-99.9	-99.9	-99.9
101.0	101.0	101.0	101.0	101.0	101.0	101.0	101.0	101.0	101.0	101.0	101.0	101.0	101.0	101.0	101.0	101.0
0.897	0.897	0.897	0.897	0.897	0.897	0.897	0.897	0.897	0.897	0.897	0.897	0.897	0.897	0.897	0.897	0.897
16.051	5.594	5.594	16.157	16.157	6.802	6.802	6.802	6.802	6.802	6.802	6.802	6.802	6.802	6.802	6.802	6.802
0.120	0.120	0.120	0.120	0.120	0.120	0.120	0.120	0.120	0.120	0.120	0.120	0.120	0.120	0.120	0.120	0.120
6.0	6.0	6.0	-30.3	-30.3	6.0	6.0	6.0	6.0	6.0	6.0	6.0	6.0	6.0	6.0	6.0	6.0
-81.4	-81.4	-81.4	90.6	90.6	-81.4	-81.4	-81.4	-81.4	-81.4	-81.4	-81.4	-81.4	-81.4	-81.4	-81.4	-81.4
0.00	0.00	0.00	0.00	0.00	0.00	0.00	0.00	0.00	0.00	0.00	0.00	0.00	0.00	0.00	0.00	0.00
-99.9	-99.9	-99.9	-99.9	-99.9	-99.9	-99.9	-99.9	-99.9	-99.9	-99.9	-99.9	-99.9	-99.9	-99.9	-99.9	-99.9
101.0	101.0	101.0	101.0	101.0	101.0	101.0	101.0	101.0	101.0	101.0	101.0	101.0	101.0	101.0	101.0	101.0
0.897	0.897	0.897	0.897	0.897	0.897	0.897	0.897	0.897	0.897	0.897	0.897	0.897	0.897	0.897	0.897	0.897
13.593	4.033	4.033	10.729	10.729	1.108	1.108	1.108	1.108	1.108	1.108	1.108	1.108	1.108	1.108	1.108	1.108
10.149	16.322	16.322	13.563	13.563	16.928	16.928	16.928	16.928	16.928	16.928	16.928	16.928	16.928	16.928	16.928	16.928
0.120	0.120	0.120	0.120	0.120	0.120	0.120	0.120	0.120	0.120	0.120	0.120	0.120	0.120	0.120	0.120	0.120
72.7	72.7	72.7	-25.6	-25.6	72.7	72.7	72.7	72.7	72.7	72.7	72.7	72.7	72.7	72.7	72.7	72.7
-117.5	-117.5	-117.5	-56.8	-56.8	-117.5	-117.5	-117.5	-117.5	-117.5	-117.5	-117.5	-117.5	-117.5	-117.5	-117.5	-117.5
0.00	0.00	0.00	0.00	0.00	0.00	0.00	0.00	0.00	0.00	0.00	0.00	0.00	0.00	0.00	0.00	0.00
-99.9	-99.9	-99.9	-99.9	-99.9	-99.9	-99.9	-99.9	-99.9	-99.9	-99.9	-99.9	-99.9	-99.9	-99.9	-99.9	-99.9
16.847	0.901	0.901	13.414	13.414	3.311	3.311	3.311	3.311	3.311	3.311	3.311	3.311	3.311	3.311	3.311	3.311
1.993	16.963	16.963	10.355	10.355	16.438	16.438	16.438	16.438	16.438	16.438	16.438	16.438	16.438	16.438	16.438	16.438
0.897	0.897	0.897	0.897	0.897	0.897	0.897	0.897	0.897	0.897	0.897	0.897	0.897	0.897	0.897	0.897	0.897
69.4	4.177	4.177	15.655	15.655	7.504	7.504	7.504	7.504	7.504	7.504	7.504	7.504	7.504	7.504	7.504	7.504
16.435	16.142	16.142	6.539	6.539	15.214	15.214	15.214	15.214	15.214	15.214	15.214	15.214	15.214	15.214	15.214	15.214
0.120	0.120	0.120	0.120	0.120	0.120	0.120	0.120	0.120	0.120	0.120	0.120	0.120	0.120	0.120	0.120	0.120
68.4	68.4	68.4	-29.9	-29.9	68.4	68.4	68.4	68.4	68.4	68.4	68.4	68.4	68.4	68.4	68.4	68.4
-99.9	-99.9	-99.9	-134.1	-134.1	-134.1	-134.1	-134.1	-134.1	-134.1	-134.1	-134.1	-134.1	-134.1	-134.1	-134.1	-134.1
0.00	0.00	0.00	0.00	0.00	0.00	0.00	0.00	0.00	0.00	0.00	0.00	0.00	0.00	0.00	0.00	0.00
-99.9	-99.9	-99.9	-99.9	-99.9	-99.9	-99.9	-99.9	-99.9	-99.9	-99.9	-99.9	-99.9	-99.9	-99.9	-99.9	-99.9
16.788	4.177	4.177	15.655	15.655	7.504	7.504	7.504	7.504	7.504	7.504	7.504	7.504	7.504	7.504	7.504	7.504
0.897	0.897	0.897	0.897	0.897	0.897	0.897	0.897	0.897	0.897	0.897	0.897	0.897	0.897	0.897	0.897	0.897
8.290	8.290	8.290	16.909	16.909	11.196	11.196	11.196	11.196	11.196	11.196	11.196	11.196	11.196	11.196	11.196	11.196
-99.900	14.800	14.800	2.266	2.266	12.753	12.753	12.753	12.753	12.753	12.753	12.753	12.753	12.753	12.753	12.753	12.753
0.120	0.120	0.120	0.120	0.120	0.120	0.120	0.120	0.120	0.120	0.120	0.120	0.120	0.120	0.120	0.120	0.120
-99.9	-99.9	-99.9	-99.9	-99.9	-99.9	-99.9	-99.9	-99.9	-99.9	-99.9	-99.9	-99.9	-99.9	-99.9	-99.9	-99.9

The Evaluation of the 18 Series Grenades (LBAs), 12 Grenades, L01E2)

6 : number of trials included in DDA
6 : time zone designation
40.20 : latitude (deg)
113.00 : longitude (deg)

	B13b	B14b	B15b	B16b	B17b	B18b	trial ID
5	25	26	6	6	6	6	month
25	26	62	62	62	62	6	day
82	82	16	20	21	19	82	year
16	16	13	13	10	16	16	hour
19	19	24	10	32	16	10	minute
19	19	12	11	12	12	12	no. of sources
12	-35.7	62.6	62.6	-35.7	-35.7	-35.7	x-coord. of source (m)
-35.7	62.6	-35.7	-35.5	100.8	100.8	100.8	y-coord. of source (m)
100.8	-73.5	100.8	0.00	0.00	0.00	0.00	source elevation (m)
0.00	0.00	-99.9	-99.9	-99.9	-99.9	-99.9	emission rate (g/s)
-99.9	-99.9	101.0	101.0	101.0	101.0	101.0	emission duration (s)
101.0	101.0	0.859	0.897	0.973	0.440	0.800	total mass emitted (kg)
0.859	0.859	6.425	1.554	7.769	0.015	9.033	sign0 at the source (m)
10.032	15.700	16.893	15.081	16.364	14.316	14.316	sign0 at the source (m)
11.880	0.120	0.120	0.120	0.120	0.120	0.120	sign0 at the source (m)
0.120	0.120	0.455	0.897	0.973	0.840	0.840	sign0 at the source (m)
4.718	0.667	4.318	2.142	5.311	5.311	5.311	sign0 at the source (m)
16.286	16.951	16.405	16.328	15.367	15.367	15.367	sign0 at the source (m)
0.120	0.120	0.120	0.120	0.120	0.120	0.120	sign0 at the source (m)
0.120	0.265	721.8	26.5	721.8	721.8	721.8	sign0 at the source (m)
121.8	121.9	-46.3	127.9	-46.3	127.9	127.9	source elevation (m)
121.9	101.0	101.0	101.0	101.0	101.0	101.0	emission rate (g/s)
101.0	0.00	0.00	0.00	0.00	0.00	0.00	emission duration (s)
0.00	-99.9	-99.9	-99.9	-99.9	-99.9	-99.9	total mass emitted (kg)
-99.9	101.0	101.0	101.0	101.0	101.0	101.0	sign0 at the source (m)
101.0	0.859	0.859	0.897	0.973	0.840	0.840	sign0 at the source (m)
0.859	0.859	5.170	3.743	10.846	2.296	16.209	sign0 at the source (m)
1.108	16.157	13.939	16.346	13.043	16.346	16.346	sign0 at the source (m)
16.328	0.120	0.120	0.120	0.120	0.120	0.120	sign0 at the source (m)
0.120	0.555	-55.5	-42.8	55.5	-42.8	-42.8	source elevation (m)
-42.8	104.4	-64.4	109.4	-64.4	109.4	109.4	emission rate (g/s)
104.4	0.00	0.00	0.00	0.00	0.00	0.00	emission duration (s)
0.00	-99.9	-99.9	-99.9	-99.9	-99.9	-99.9	total mass emitted (kg)
-99.9	101.0	101.0	101.0	101.0	101.0	101.0	sign0 at the source (m)
101.0	0.859	0.859	0.897	0.973	0.840	0.840	sign0 at the source (m)
0.859	0.859	5.170	3.743	10.846	2.296	16.209	sign0 at the source (m)
1.108	16.157	13.939	16.346	13.043	16.346	16.346	sign0 at the source (m)
16.328	0.120	0.120	0.120	0.120	0.120	0.120	sign0 at the source (m)
0.120	0.555	-55.5	-42.8	55.5	-42.8	-42.8	source elevation (m)
-42.8	15.224	16.577	16.906	16.201	16.201	16.201	emission rate (g/s)
15.224	0.120	0.120	0.120	0.120	0.120	0.120	emission duration (s)
0.120	0.555	7.895	11.942	5.559	12.947	5.170	total mass emitted (kg)
4.031	16.418	15.014	12.046	15.645	10.962	16.157	sign0 at the source (m)
16.418	0.120	0.120	0.120	0.120	0.120	0.120	sign0 at the source (m)
0.120	0.555	2.286	7.101	0.813	8.117	13.033	sign0 at the source (m)
1.108	-61.1	37.2	-61.1	37.2	-61.1	-61.1	source elevation (m)
-61.1	123.6	-50.6	123.6	-50.6	123.6	123.6	emission rate (g/s)
123.6	0.00	0.00	0.00	0.00	0.00	0.00	emission duration (s)
0.00	-99.9	-99.9	-99.9	-99.9	-99.9	-99.9	total mass emitted (kg)
-99.9	101.0	101.0	101.0	101.0	101.0	101.0	sign0 at the source (m)
101.0	0.859	0.859	0.897	0.973	0.840	0.840	sign0 at the source (m)
0.859	0.859	5.170	3.743	10.846	2.296	16.209	sign0 at the source (m)
1.108	16.833	16.803	15.406	16.945	14.729	16.551	sign0 at the source (m)
16.833	0.120	0.120	0.120	0.120	0.120	0.120	sign0 at the source (m)
0.120	0.555	9.051	9.792	10.269	3.020	11.107	emission rate (g/s)
9.051	-30.3	-68.6	-68.3	-63.6	-30.3	-30.3	emission duration (s)
-30.3	11.720	14.346	13.853	13.503	12.556	12.556	total mass emitted (kg)
11.720	0.120	0.120	0.120	0.120	0.120	0.120	sign0 at the source (m)
0.120	0.555	-99.9	-99.9	-99.9	-99.9	-99.9	sign0 at the source (m)
-99.9	-25.2	73.1	-28.0	73.1	-23.2	-23.2	source elevation (m)
-25.2	68.3	-106.0	45.5	-106.0	68.3	68.3	emission rate (g/s)
68.3	0.00	0.00	0.00	0.00	0.00	0.00	emission duration (s)
0.00	-99.9	-99.9	-99.9	-99.9	-99.9	-99.9	total mass emitted (kg)
-99.9	101.0	101.0	101.0	101.0	101.0	101.0	sign0 at the source (m)
101.0	0.859	0.859	0.897	0.973	0.840	0.840	sign0 at the source (m)
0.859	0.859	13.411	13.939	14.268	8.347	15.014	sign0 at the source (m)
13.411	15.528	10.385	9.668	9.176	7.898	7.898	sign0 at the source (m)
10.385	6.821	0.120	0.120	0.120	0.120	0.120	sign0 at the source (m)
6.821	0.120	0.120	0.120	0.120	0.120	0.120	sign0 at the source (m)
0.120	-28.0	70.3	-26.8	70.3	-28.0	-28.0	source elevation (m)

208.5	208.5	208.5	208.5	208.5	208.5	208.5
-99.9	-99.9	-99.9	-99.9	-99.9	-99.9	-99.9
-9.990E+01	2.3702E+05	-9.990E+01	2.890E+05	-9.990E+01	-9.990E+01	-9.990E+01
-267.7	-267.7	-267.7	-267.7	-267.7	-267.7	-267.7
-29.1	-29.1	-29.1	-29.1	-29.1	-29.1	-29.1
262.1	262.1	262.1	262.1	262.1	262.1	262.1
252.6	252.6	252.6	252.6	252.6	252.6	252.6
-99.9	-99.9	-99.9	-99.9	-99.9	-99.9	-99.9
-9.990E+01	1.4002E+05	-9.990E+01	1.5302E+05	-9.990E+01	-9.990E+01	-9.990E+01

(mg/m²) (mg/m²) (mg/m²) (mg/m²) (mg/m²) (mg/m²) (mg/m²)

208.5	208.5	208.5	208.5	208.5	208.5	208.5
-99.9	-99.9	-99.9	-99.9	-99.9	-99.9	-99.9
-9.990E+01	2.3702E+05	-9.990E+01	2.890E+05	-9.990E+01	-9.990E+01	-9.990E+01
-267.7	-267.7	-267.7	-267.7	-267.7	-267.7	-267.7
-29.1	-29.1	-29.1	-29.1	-29.1	-29.1	-29.1
262.1	262.1	262.1	262.1	262.1	262.1	262.1
252.6	252.6	252.6	252.6	252.6	252.6	252.6
-99.9	-99.9	-99.9	-99.9	-99.9	-99.9	-99.9
-9.990E+01	1.4002E+05	-9.990E+01	1.5302E+05	-9.990E+01	-9.990E+01	-9.990E+01

(mg/m²) (mg/m²) (mg/m²) (mg/m²) (mg/m²) (mg/m²) (mg/m²)

The Evaluation of the LB Series Grenades (LBG), low condition temp., 5 trials included in DDA

			200.5 : y-coord. of 2nd end-point for LOS1 (m)	
-99.9	-99.9	200.5	209.5	209.5 : y-coord. of 2nd end-point for LOS1 (m)
-99.9	-99.9	208.5	-99.9	-99.9 : LOS integrated conc. (kg/m ²)
-9.99E-01	2.400E-01	2.400E-01	-9.99E-01	2.370E-01 : LOS integrated dosage (kg/m ²)
-261.1	-261.1	-261.1	-261.1	-261.1 : x-coord. of 1st end-point for LOS1 (m)
-29.1	-29.1	-29.1	-29.1	-29.1 : x-coord. of 1st end-point for LOS1 (m)
-262.1	-262.1	-262.1	-262.1	-262.1 : x-coord. of 2nd end-point for LOS1 (m)
-252.6	-252.6	-252.6	-252.6	-252.6 : y-coord. of 2nd end-point for LOS1 (m)
-99.9	-99.9	-99.9	-99.9	-99.9 : LOS integrated conc. (kg/m ²)
-9.99E-01	8.400E-03	8.400E-03	-9.99E-01	1.600E-05 : LOS integrated dosage (kg/m ²)

208.5	208.5	208.5	208.5	208.5	208.5	208.5	208.5	208.5	208.5
-99.9	-99.9	-99.9	-99.9	-99.9	-99.9	-99.9	-99.9	-99.9	-99.9
-9.990E+01	-9.990E+01	-9.990E+01	-9.990E+01	1.550E+05	-9.990E+01	-9.990E+01	2.890E+05	-9.990E+01	2.890E+05
-9.990E+01	-9.990E+01	-9.990E+01	-9.990E+01	1.550E+01	-9.990E+01	-9.990E+01	2.890E+05	-9.990E+01	2.890E+05
-267.7	-267.7	-267.7	-267.7	-267.7	-267.7	-267.7	-267.7	-267.7	-267.7
-29.1	-29.1	-29.1	-29.1	-29.1	-29.1	-29.1	-29.1	-29.1	-29.1
-29.1	-29.1	-29.1	-29.1	-29.1	-29.1	-29.1	-29.1	-29.1	-29.1
262.1	262.1	262.1	262.1	262.1	262.1	262.1	262.1	262.1	262.1
252.6	252.6	252.6	252.6	252.6	252.6	252.6	252.6	252.6	252.6
-99.9	-99.9	-99.9	-99.9	-99.9	-99.9	-99.9	-99.9	-99.9	-99.9
-9.990E+01									
-9.990E+01	-9.990E+01	-9.990E+01	-9.990E+01	1.530E+05	-9.990E+01	1.530E+05	1.530E+05	-9.990E+01	1.530E+05

; Y-coord. of 2nd end-point for LOS1 (m)
; LOS Integrated conc. (mg/m³)
; LOS Integrated dosage (mg-s/m²)
; X-coord. of 1st end-point for LOS1 (m)
; X-coord. of 1st end-point for LOS1 (m)
; Y-coord. of 1st end-point for LOS1 (m)
; Y-coord. of 2nd end-point for LOS1 (m)
; X-coord. of 2nd end-point for LOS1 (m)
; Y-coord. of 2nd end-point for LOS1 (m)
; LOS Integrated conc. (mg/m³)
; LOS Integrated dosage (mg-s/m²)

208.5 : 2nd end-point for LOS1 (m) : y-coord. of 2nd end-point for LOS1 (m)
 -9.990E-01 -9.990E-01 1.180E-05 1.220E-05 -9.990E-01 -9.990E-01 : LOS integrated conc. (mg/m³)
 -267.7 : LOS integrated dosage (mg-s/m²)
 -267.7 : 1st end-point for LOS1 (m) : x-coord. of 1st end-point for LOS1 (m)
 -29.1 : 1st end-point for LOS1 (m) : y-coord. of 1st end-point for LOS1 (m)
 -29.1 : 2nd end-point for LOS1 (m) : x-coord. of 2nd end-point for LOS1 (m)
 -262.1 : 2nd end-point for LOS1 (m) : y-coord. of 2nd end-point for LOS1 (m)
 -252.6 : 252.6 : 252.6 : 252.6 : 252.6 :
 -99.9 : -99.9 : -99.9 : -99.9 : -99.9 :
 -9.990E-01 -9.990E-01 -9.990E-01 5.900E-04 -9.990E-01 -9.990E-01 : LOS integrated conc. (mg/m³)
 -9.990E-01 -9.990E-01 -9.990E-01 : LOS integrated dosage (mg-s/m²)

The Evaluation of the LG Series Grenades (Marked L8A1, 6 grenades, L81K6)

	6 : number of trials included in DnA	6 : time zone designation	40.20 : latitude (deg)	113.00 : longitude (deg)	B19b	B20b	B21b	B22b	B23b	B24b : trial ID
5	5	5	5	5	5	5	5	5	5	5 : month
25	25	25	25	25	1	1	1	1	1	8 : day
62	62	62	62	62	62	62	62	62	62	92 : year
15	15	15	15	15	17	17	18	16	16	20 : hour
28	28	27	27	31	2	2	2	57	57	59 : minute
4	4	4	4	4	6	6	5	5	5	5 : no. of sources
-37.4	-37.4	-37.4	-37.4	-37.4	-37.4	-37.4	-37.4	-37.4	-37.4	-37.4 : x-coord. of source (m)
-99.7	-99.7	-99.7	-99.7	-99.7	-99.7	-99.7	-99.7	-99.7	-99.7	-99.7 : y-coord. of source (m)
0.00	0.00	0.00	0.00	0.00	0.00	0.00	0.00	0.00	0.00	0.00 : source elevation (m)
-99.9	-99.9	-99.9	-99.9	-99.9	-99.9	-99.9	-99.9	-99.9	-99.9	-99.9 : emulsion rate (g/s)
118.0	118.0	118.0	118.0	118.0	118.0	118.0	118.0	118.0	118.0	118.0 : emulsion duration (s)
0.416	0.453	0.453	0.453	0.453	0.453	0.453	0.453	0.453	0.453	0.453 : total mass emitted (kg)
8.424	5.075	5.075	7.176	7.176	0.932	0.932	0.932	0.932	0.932	0.932 : sigx0 at the source (m)
16.162	17.602	17.602	16.724	16.724	16.25	17.414	17.414	17.526	17.526	17.526 : sigy0 at the source (m)
0.120	0.120	0.120	0.120	0.120	0.120	0.120	0.120	0.120	0.120	0.120 : sigz0 at the source (m)
-52.6	-52.6	-52.6	-52.6	-52.6	-52.6	-52.6	-52.6	-52.6	-52.6	-52.6 : x-coord. of source (m)
115.9	115.9	115.9	115.9	115.9	115.9	115.9	115.9	115.9	115.9	115.9 : y-coord. of source (m)
0.00	0.00	0.00	0.00	0.00	0.00	0.00	0.00	0.00	0.00	0.00 : source elevation (m)
-99.9	-99.9	-99.9	-99.9	-99.9	-99.9	-99.9	-99.9	-99.9	-99.9	-99.9 : emulsion rate (g/s)
118.0	118.0	118.0	118.0	118.0	118.0	118.0	118.0	118.0	118.0	118.0 : emulsion duration (s)
0.916	0.659	0.659	0.973	0.973	0.954	0.954	0.859	0.859	0.859	0.859 : total mass emitted (kg)
18.137	16.251	16.251	13.305	13.305	7.33	7.33	0.612	0.612	0.612	0.612 : sigx0 at the source (m)
0.576	1.276	1.276	18.772	18.772	16.033	16.033	18.309	18.309	18.309	18.309 : sigy0 at the source (m)
0.120	0.120	0.120	0.120	0.120	0.120	0.120	0.120	0.120	0.120	0.120 : sigz0 at the source (m)
-83.3	-83.3	-83.3	-83.3	-83.3	-83.3	-83.3	-83.3	-83.3	-83.3	-83.3 : x-coord. of source (m)
128.3	128.3	128.3	128.3	128.3	128.3	128.3	128.3	128.3	128.3	128.3 : y-coord. of source (m)
0.00	0.00	0.00	0.00	0.00	0.00	0.00	0.00	0.00	0.00	0.00 : source elevation (m)
-99.9	-99.9	-99.9	-99.9	-99.9	-99.9	-99.9	-99.9	-99.9	-99.9	-99.9 : emulsion rate (g/s)
118.0	118.0	118.0	118.0	118.0	118.0	118.0	118.0	118.0	118.0	118.0 : emulsion duration (s)
0.916	0.659	0.659	0.973	0.973	0.954	0.954	0.859	0.859	0.859	0.859 : total mass emitted (kg)
16.995	15.202	15.202	16.177	16.177	11.046	11.046	15.550	15.550	15.550	15.550 : sigx0 at the source (m)
0.120	0.120	0.120	0.120	0.120	0.120	0.120	0.120	0.120	0.120	0.120 : sigy0 at the source (m)
-28.7	-28.7	-28.7	-29.9	-29.9	-29.9	-29.9	-29.9	-29.9	-29.9	-29.9 : x-coord. of source (m)
79.2	46.1	46.1	46.1	46.1	46.1	46.1	46.1	46.1	46.1	46.1 : y-coord. of source (m)
0.00	0.00	0.00	0.00	0.00	0.00	0.00	0.00	0.00	0.00	0.00 : source elevation (m)
-99.9	-99.9	-99.9	-99.9	-99.9	-99.9	-99.9	-99.9	-99.9	-99.9	-99.9 : emulsion rate (g/s)
118.0	118.0	118.0	118.0	118.0	118.0	118.0	118.0	118.0	118.0	118.0 : emulsion duration (s)
0.916	0.859	0.859	0.973	0.973	0.954	0.954	0.859	0.859	0.859	0.859 : total mass emitted (kg)
12.612	16.746	16.746	12.617	12.617	13.416	13.416	16.995	16.995	16.995	16.995 : sigx0 at the source (m)
12.238	17.426	17.426	5.023	5.023	12.414	12.414	6.837	6.837	6.837	6.837 : sigy0 at the source (m)
0.110	0.120	0.120	0.120	0.120	0.120	0.120	0.120	0.120	0.120	0.120 : sigz0 at the source (m)
-99.9	-99.9	-99.9	-28.7	-28.7	-28.7	-28.7	-28.7	-28.7	-28.7	-28.7 : x-coord. of source (m)
-99.9	-99.9	-99.9	79.2	79.2	79.2	79.2	79.2	79.2	79.2	79.2 : y-coord. of source (m)
0.00	0.00	0.00	0.00	0.00	0.00	0.00	0.00	0.00	0.00	0.00 : source elevation (m)
-99.9	-99.9	-99.9	-99.9	-99.9	-99.9	-99.9	-99.9	-99.9	-99.9	-99.9 : emulsion rate (g/s)
118.0	118.0	118.0	118.0	118.0	118.0	118.0	118.0	118.0	118.0	118.0 : emulsion duration (s)
0.916	0.859	0.859	0.973	0.973	0.954	0.954	0.859	0.859	0.859	0.859 : total mass emitted (kg)
-99.900	-99.900	-99.900	10.790	12.745	5.382	5.382	11.300	11.300	11.300	11.300 : sigx0 at the source (m)
-99.900	-99.900	-99.900	14.804	13.159	12.551	12.551	14.419	14.419	14.419	14.419 : sigy0 at the source (m)
0.120	0.120	0.120	0.120	0.120	0.120	0.120	0.120	0.120	0.120	0.120 : sigz0 at the source (m)
-99.9	-99.9	-99.9	-27.6	-27.6	-27.6	-27.6	-27.6	-27.6	-27.6	-27.6 : x-coord. of source (m)
-99.9	-99.9	-99.9	57.0	57.0	57.0	57.0	57.0	57.0	57.0	57.0 : y-coord. of source (m)
0.00	0.00	0.00	0.00	0.00	0.00	0.00	0.00	0.00	0.00	0.00 : source elevation (m)
-99.9	-99.9	-99.9	-99.9	-99.9	-99.9	-99.9	-99.9	-99.9	-99.9	-99.9 : emulsion rate (g/s)
118.0	118.0	118.0	118.0	118.0	118.0	118.0	118.0	118.0	118.0	118.0 : emulsion duration (s)
0.916	0.859	0.859	0.973	0.973	0.954	0.954	0.859	0.859	0.859	0.859 : total mass emitted (kg)
-99.900	-99.900	-99.900	15.202	16.477	5.382	5.382	15.550	15.550	15.550	15.550 : sigx0 at the source (m)
-99.900	-99.900	-99.900	10.221	8.006	-99.900	-99.900	9.685	9.685	9.685	9.685 : sigy0 at the source (m)
0.120	0.120	0.120	0.120	0.120	0.120	0.120	0.120	0.120	0.120	0.120 : sigz0 at the source (m)
-99.9	-99.9	-99.9	-99.9	-99.9	-99.9	-99.9	-99.9	-99.9	-99.9	-99.9 : ambient pressure (atm)
-99.9	-99.9	-99.9	-99.9	-99.9	-99.9	-99.9	-99.9	-99.9	-99.9	-99.9 : relative humidity (%)
118.0	118.0	118.0	118.0	118.0	118.0	118.0	118.0	118.0	118.0	118.0 : temperature at level A1 (K)
300.00	300.00	300.00	300.00	300.00	300.00	300.00	300.00	300.00	300.00	300.00 : measuring height for wind data (m)
2.00	2.00	2.00	2.00	2.00	2.00	2.00	2.00	2.00	2.00	2.00 : temperature at level B2 (K)
332.0	344.0	344.0	344.0	344.0	346.0	346.0	342.0	342.0	342.0	342.0 : measuring height for temperature B2 (m)
-99.90	-99.90	-99.90	-99.90	-99.90	-99.90	-99.90	-99.90	-99.90	-99.90	-99.90 : domain-averaged sigma-u (m/s)
16.90	14.40	14.40	14.40	14.40	14.10	14.10	12.40	12.40	12.40	12.40 : domain-averaged sigma-phi (deg)
4.00	5.00	5.00	2.00	2.00	2.00	2.00	2.00	2.00	2.00	2.00 : measuring height for domain-avg wind speed (m/s)
2.00	2.00	2.00	2.00	2.00	2.00	2.00	2.00	2.00	2.00	2.00 : averaging time for domain-avg data (s)
0.088	0.110	0.110	0.093	0.093	0.084	0.084	0.091	0.091	0.091	0.091 : domain-averaged wind speed (m/s)
0.0300	0.0300	0.0300	0.0300	0.0300	0.0300	0.0300	0.0300	0.0300	0.0300	0.0300 : surface roughness (m)
-99.900	-99.900	-99.900	-99.900	-99.900	-99.900	-99.900	-99.900	-99.900	-99.900	-99.900 : friction velocity (m/s)
-99.900	-99.900	-99.900	-99.900	-99.900	-99.900	-99.900	-99.900	-99.900	-99.900	-99.900 : inverse Monin-Obukhov length (1/m)

The Evaluation of the 10 Series Grenades (Reworked LAA), & grenades, L81W67
 \downarrow : number of trials included in DDA

The Evaluation of the L8 Series Grenades (Marked L8A1, 12 grenades, L01R2)

208.5	208.5	208.5	208.5	208.5	208.5	208.5	208.5	208.5	208.5	208.5	208.5	208.5	208.5	208.5	208.5	208.5	208.5	208.5	208.5	
-99.9	-99.9	-99.9	-99.9	-99.9	-99.9	-99.9	-99.9	-99.9	-99.9	-99.9	-99.9	-99.9	-99.9	-99.9	-99.9	-99.9	-99.9	-99.9	-99.9	-99.9
-9.9902e+01	1.5302e+05	-9.9902e+01																		
-9.9902e+01	1.0502e+05	-9.9902e+01																		

208.5	208.5	208.5	208.5	208.5	208.5	208.5	208.5
-99.9	-99.9	-99.9	-99.9	-99.9	-99.9	-99.9	-99.9
-9.990E+01	-9.990E+01	-9.990E+01	-9.990E+01	8.600E+01	8.600E+01	8.600E+01	8.600E+01
-267.7	-267.7	-267.7	-267.7	-267.7	-267.7	-267.7	-267.7
-29.1	-29.1	-29.1	-29.1	-29.1	-29.1	-29.1	-29.1
262.1	262.1	262.1	262.1	262.1	262.1	262.1	262.1
252.6	252.6	252.6	252.6	252.6	252.6	252.6	252.6
-99.9	-99.9	-99.9	-99.9	-99.9	-99.9	-99.9	-99.9
-9.990E+01	-9.990E+01	-9.990E+01	-9.990E+01	4.300E+01	4.300E+01	4.300E+01	4.300E+01

208.5 : Y-coord. of 2nd end-point for LOS1 (m)	208.5 : LOS integrated conc. ($\text{mg}/\text{m}^3/\text{m}^{+2}$)
-99.9 : LOS integrated dosage ($\text{mg}/\text{m}^3/\text{m}^{+2}$)	-267.7 : x-coord. of 1st end-point for LOS1 (m)
-9.990E+01 : LOS integrated dosage ($\text{mg}/\text{m}^3/\text{m}^{+2}$)	-29.1 : y-coord. of 1st end-point for LOS1 (m)
4.300E+01 : LOS integrated dosage ($\text{mg}/\text{m}^3/\text{m}^{+2}$)	262.1 : x-coord. of 2nd end-point for LOS1 (m)
208.5 : Y-coord. of 2nd end-point for LOS1 (m)	252.6 : y-coord. of 2nd end-point for LOS1 (m)
-99.9 : LOS integrated conc. ($\text{mg}/\text{m}^3/\text{m}^{+2}$)	-99.9 : LOS integrated dosage ($\text{mg}/\text{m}^3/\text{m}^{+2}$)
-9.990E+01 : LOS integrated dosage ($\text{mg}/\text{m}^3/\text{m}^{+2}$)	1.030E+01 : LOS integrated dosage ($\text{mg}/\text{m}^3/\text{m}^{+2}$)

The Evaluation of the 16 Series Grenades (Reworked L8A1), medium condition temp., L81RM

208.5 : Y-coord. of 2nd end-point for LOS1 (m)
-99.9 : LOS integrated conc. (mg/m³)
-99.9 : LOS integrated dosage (mg-³/m⁻²)
-9.9902e+01 : LOS integrated dosage (mg-³/m⁻²)
-9.9902e+01 : LOS integrated dosage (mg-³/m⁻²)
1.3802e+05 : LOS integrated dosage (mg-³/m⁻²)
1.2302e+05 : LOS integrated dosage (mg-³/m⁻²)
-9.9902e+01 : LOS integrated dosage (mg-³/m⁻²)
-9.9902e+01 : LOS integrated dosage (mg-³/m⁻²)

The Evaluation of the L8 Series Grenades (Reworked L8A), high condition t_{exp}, 161RH

(6 : number of trials included in DDA

(6 : time zone designation

40.20 : latitude (deg)

113.00 : longitude (deg)

B23a : trial ID

B30a : trial ID

B35a : trial ID

B36a : trial ID

B37a : trial ID

B38a : trial ID

B39a : trial ID

B40a : trial ID

B41a : trial ID

B42a : trial ID

B43a : trial ID

B44a : trial ID

B45a : trial ID

B46a : trial ID

B47a : trial ID

B48a : trial ID

B49a : trial ID

B50a : trial ID

B51a : trial ID

B52a : trial ID

B53a : trial ID

B54a : trial ID

B55a : trial ID

B56a : trial ID

B57a : trial ID

B58a : trial ID

B59a : trial ID

B60a : trial ID

B61a : trial ID

B62a : trial ID

B63a : trial ID

B64a : trial ID

B65a : trial ID

B66a : trial ID

B67a : trial ID

B68a : trial ID

B69a : trial ID

B70a : trial ID

B71a : trial ID

B72a : trial ID

B73a : trial ID

B74a : trial ID

B75a : trial ID

B76a : trial ID

B77a : trial ID

B78a : trial ID

B79a : trial ID

B80a : trial ID

B81a : trial ID

B82a : trial ID

B83a : trial ID

B84a : trial ID

B85a : trial ID

B86a : trial ID

B87a : trial ID

B88a : trial ID

B89a : trial ID

B90a : trial ID

B91a : trial ID

B92a : trial ID

B93a : trial ID

B94a : trial ID

B95a : trial ID

B96a : trial ID

B97a : trial ID

B98a : trial ID

B99a : trial ID

B100a : trial ID

B101a : trial ID

B102a : trial ID

B103a : trial ID

B104a : trial ID

B105a : trial ID

B106a : trial ID

B107a : trial ID

B108a : trial ID

B109a : trial ID

B110a : trial ID

B111a : trial ID

B112a : trial ID

B113a : trial ID

B114a : trial ID

B115a : trial ID

B116a : trial ID

B117a : trial ID

B118a : trial ID

B119a : trial ID

B120a : trial ID

B121a : trial ID

B122a : trial ID

B123a : trial ID

B124a : trial ID

B125a : trial ID

B126a : trial ID

B127a : trial ID

B128a : trial ID

B129a : trial ID

B130a : trial ID

B131a : trial ID

B132a : trial ID

B133a : trial ID

B134a : trial ID

B135a : trial ID

B136a : trial ID

B137a : trial ID

B138a : trial ID

B139a : trial ID

B140a : trial ID

B141a : trial ID

B142a : trial ID

B143a : trial ID

B144a : trial ID

B145a : trial ID

B146a : trial ID

B147a : trial ID

B148a : trial ID

B149a : trial ID

B150a : trial ID

B151a : trial ID

B152a : trial ID

B153a : trial ID

B154a : trial ID

B155a : trial ID

B156a : trial ID

B157a : trial ID

B158a : trial ID

B159a : trial ID

B160a : trial ID

B161a : trial ID

B162a : trial ID

B163a : trial ID

B164a : trial ID

B165a : trial ID

B166a : trial ID

B167a : trial ID

B168a : trial ID

B169a : trial ID

B170a : trial ID

B171a : trial ID

B172a : trial ID

B173a : trial ID

B174a : trial ID

B175a : trial ID

B176a : trial ID

B177a : trial ID

B178a : trial ID

B179a : trial ID

B180a : trial ID

B181a : trial ID

B182a : trial ID

B183a : trial ID

B184a : trial ID

B185a : trial ID

B186a : trial ID

B187a : trial ID

B188a : trial ID

B189a : trial ID

B190a : trial ID

B191a : trial ID

B192a : trial ID

B193a : trial ID

B194a : trial ID

B195a : trial ID

B196a : trial ID

B197a : trial ID

B198a : trial ID

B199a : trial ID

B200a : trial ID

B201a : trial ID

B202a : trial ID

B203a : trial ID

B204a : trial ID

B205a : trial ID

B206a : trial ID

B207a : trial ID

B208a : trial ID

B209a : trial ID

B210a : trial ID

B211a : trial ID

B212a : trial ID

B213a : trial ID

B214a : trial ID

B215a : trial ID

B216a : trial ID

B217a : trial ID

B218a : trial ID

B219a : trial ID

B220a : trial ID

B221a : trial ID

B222a : trial ID

B223a : trial ID

B224a : trial ID

B225a : trial ID

B226a : trial ID

B227a : trial ID

B228a : trial ID

B229a : trial ID

B230a : trial ID

B231a : trial ID

B232a : trial ID

B233a : trial ID

B234a : trial ID

B235a : trial ID

B236a : trial ID

B237a : trial ID

B238a : trial ID

B239a : trial ID

B240a : trial ID

B241a : trial ID

B242a : trial ID

B243a : trial ID

B244a : trial ID

B245a : trial ID

B246a : trial ID

B247a : trial ID

B248a : trial ID

B249a : trial ID

B250a : trial ID

B251a : trial ID

B252a : trial ID

B253a : trial ID

B254a : trial ID

B255a : trial ID

B256a : trial ID

B257a : trial ID

B258a : trial ID

B259a : trial ID

B260a : trial ID

B261a : trial ID

B262a : trial ID

B263a : trial ID

B264a : trial ID

B265a : trial ID

B266a : trial ID

B267a : trial ID

B268a : trial ID

B269a : trial ID

B270a : trial ID

B271a : trial ID

B272a : trial ID

B273a : trial ID

B274a : trial ID

B275a : trial ID

B276a : trial ID

B277a : trial ID

B278a : trial ID

B279a : trial ID

B280a : trial ID

B281a : trial ID

B282a : trial ID

B283a : trial ID

B284a : trial ID

B285a : trial ID

B286a : trial ID

B287a : trial ID

B288a : trial ID

B289a : trial ID

B290a : trial ID

B291a : trial ID

B292a : trial ID

B293a : trial ID

208.5 : 208.5 : 208.5 : 208.5 : 208.5 : y-coord. of 2nd end-point for LOS1 (m)
 -99.9 : -99.9 : -99.9 : -99.9 : -99.9 : LOS integrated conc. (mg/m³)
 -9.990E+01 : -9.990E+01 : 1.010E+05 : -9.990E+01 : -9.990E+01 : -9.990E+01 : LOS integrated dosage (mg-s/m²)
 -261.7 : -261.7 : -261.7 : -261.7 : -261.7 : 105 integrated conc. (mg/m³)
 -261.7 : -261.7 : -261.7 : -261.7 : -261.7 : LOS integrated dosage (mg-s/m²)
 -261.7 : -261.7 : -261.7 : -261.7 : -261.7 : y-coord. of 1st end-point for LOS1 (m)
 -261.7 : -261.7 : -261.7 : -261.7 : -261.7 : LOS integrated conc. (mg/m³)
 -261.7 : -261.7 : -261.7 : -261.7 : -261.7 : LOS integrated dosage (mg-s/m²)
 261.1 : 261.1 : 261.1 : 261.1 : 261.1 : 105 integrated conc. (mg/m³)
 261.1 : 261.1 : 261.1 : 261.1 : 261.1 : LOS integrated dosage (mg-s/m²)
 252.6 : 252.6 : 252.6 : 252.6 : 252.6 : y-coord. of 2nd end-point for LOS1 (m)
 252.6 : 252.6 : 252.6 : 252.6 : 252.6 : LOS integrated conc. (mg/m³)
 252.6 : 252.6 : 252.6 : 252.6 : 252.6 : LOS integrated dosage (mg-s/m²)
 -99.9 : -99.9 : -99.9 : -99.9 : -99.9 : 105 integrated conc. (mg/m³)
 -99.9 : -99.9 : -99.9 : -99.9 : -99.9 : LOS integrated dosage (mg-s/m²)
 -9.990E+01 : -9.990E+01 : 3.400E+04 : -9.990E+01 : -9.990E+01 : -9.990E+01 : 105 integrated dosage (mg-s/m²)

0.18	0.18	0.18	0.18	0.18	0.18	0.18	0.18
0.50	0.50	0.50	0.50	0.50	0.50	0.50	0.50
0.50	0.50	0.50	0.50	0.50	0.50	0.50	0.50
-99.9	-99.9	-99.9	-99.9	-99.9	-99.9	-99.9	-99.9
-99.9	-99.9	-99.9	-99.9	-99.9	-99.9	-99.9	-99.9
-99.9	-99.9	-99.9	-99.9	-99.9	-99.9	-99.9	-99.9
300.0	300.0	300.0	300.0	300.0	300.0	300.0	300.0
2.00	2.00	2.00	2.00	2.00	2.00	2.00	2.00
0	0	0	0	0	0	0	0
3	3	3	3	3	3	3	3
-171.8	-171.8	-171.8	-171.8	-171.8	-171.8	-171.8	-171.8
-205.7	-205.7	-205.7	-205.7	-205.7	-205.7	-205.7	-205.7
356.0	356.0	356.0	356.0	356.0	356.0	356.0	356.0
76.0	76.0	76.0	76.0	76.0	76.0	76.0	76.0
-99.9	-99.9	-99.9	-99.9	-99.9	-99.9	-99.9	-99.9
4.400E-04	2.700E-04	4.500E-04	3.600E-04	5.400E-04	5.400E-04	5.400E-04	9.990E-05
-197.3	-197.3	-197.3	-197.3	-197.3	-197.3	-197.3	-197.3
-161.5	-161.5	-161.5	-161.5	-161.5	-161.5	-161.5	-161.5
332.5	332.5	332.5	332.5	332.5	332.5	332.5	332.5
120.2	120.2	120.2	120.2	120.2	120.2	120.2	120.2
-99.9	-99.9	-99.9	-99.9	-99.9	-99.9	-99.9	-99.9
7.700E-04	5.200E-04	6.600E-04	3.800E-04	6.700E-04	6.700E-04	6.700E-04	9.990E-05
-220.7	-220.7	-220.7	-220.7	-220.7	-220.7	-220.7	-220.7
-117.4	-117.4	-117.4	-117.4	-117.4	-117.4	-117.4	-117.4
309.0	309.0	309.0	309.0	309.0	309.0	309.0	309.0
164.3	164.3	164.3	164.3	164.3	164.3	164.3	164.3
-99.9	-99.9	-99.9	-99.9	-99.9	-99.9	-99.9	-99.9
1.770E-05	1.220E-05	1.380E-05	1.200E-05	1.340E-05	1.340E-05	1.340E-05	1.750E-05

The Evaluation of the 18 Series Grenades (LBAA), & Grenades, L838)

4 : number of trials included in DDA

4 : time zone designation

40.20 : latitude (deg)

113.00 : longitude (deg)

B44b : trial ID

B45b : trial ID

B46b : trial ID

B47b : trial ID

B48b : trial ID

B49b : trial ID

B50b : trial ID

B51b : trial ID

B52b : trial ID

B53b : trial ID

B54b : trial ID

B55b : trial ID

B56b : trial ID

B57b : trial ID

B58b : trial ID

B59b : trial ID

B60b : trial ID

B61b : trial ID

B62b : trial ID

B63b : trial ID

B64b : trial ID

B65b : trial ID

B66b : trial ID

B67b : trial ID

B68b : trial ID

B69b : trial ID

B70b : trial ID

B71b : trial ID

B72b : trial ID

B73b : trial ID

B74b : trial ID

B75b : trial ID

B76b : trial ID

B77b : trial ID

B78b : trial ID

B79b : trial ID

B80b : trial ID

B81b : trial ID

B82b : trial ID

B83b : trial ID

B84b : trial ID

B85b : trial ID

B86b : trial ID

B87b : trial ID

B88b : trial ID

B89b : trial ID

B90b : trial ID

B91b : trial ID

B92b : trial ID

B93b : trial ID

B94b : trial ID

B95b : trial ID

B96b : trial ID

B97b : trial ID

B98b : trial ID

B99b : trial ID

B100b : trial ID

B101b : trial ID

B102b : trial ID

B103b : trial ID

B104b : trial ID

B105b : trial ID

B106b : trial ID

B107b : trial ID

B108b : trial ID

B109b : trial ID

B110b : trial ID

B111b : trial ID

B112b : trial ID

B113b : trial ID

B114b : trial ID

B115b : trial ID

B116b : trial ID

B117b : trial ID

B118b : trial ID

B119b : trial ID

B120b : trial ID

B121b : trial ID

B122b : trial ID

B123b : trial ID

B124b : trial ID

B125b : trial ID

B126b : trial ID

B127b : trial ID

B128b : trial ID

B129b : trial ID

B130b : trial ID

B131b : trial ID

B132b : trial ID

B133b : trial ID

B134b : trial ID

B135b : trial ID

B136b : trial ID

B137b : trial ID

B138b : trial ID

B139b : trial ID

B140b : trial ID

B141b : trial ID

B142b : trial ID

B143b : trial ID

B144b : trial ID

B145b : trial ID

B146b : trial ID

B147b : trial ID

B148b : trial ID

B149b : trial ID

B150b : trial ID

B151b : trial ID

B152b : trial ID

B153b : trial ID

B154b : trial ID

B155b : trial ID

B156b : trial ID

B157b : trial ID

B158b : trial ID

B159b : trial ID

B160b : trial ID

B161b : trial ID

B162b : trial ID

B163b : trial ID

B164b : trial ID

B165b : trial ID

B166b : trial ID

B167b : trial ID

B168b : trial ID

B169b : trial ID

B170b : trial ID

B171b : trial ID

B172b : trial ID

B173b : trial ID

B174b : trial ID

B175b : trial ID

B176b : trial ID

B177b : trial ID

B178b : trial ID

B179b : trial ID

B180b : trial ID

B181b : trial ID

B182b : trial ID

B183b : trial ID

B184b : trial ID

B185b : trial ID

B186b : trial ID

B187b : trial ID

B188b : trial ID

B189b : trial ID

B190b : trial ID

B191b : trial ID

B192b : trial ID

B193b : trial ID

B194b : trial ID

B195b : trial ID

B196b : trial ID

B197b : trial ID

B198b : trial ID

B199b : trial ID

B200b : trial ID

B201b : trial ID

B202b : trial ID

B203b : trial ID

B204b : trial ID

B205b : trial ID

B206b : trial ID

B207b : trial ID

B208b : trial ID

B209b : trial ID

B210b : trial ID

B211b : trial ID

B212b : trial ID

B213b : trial ID

B214b : trial ID

B215b : trial ID

B216b : trial ID

B217b : trial ID

B218b : trial ID

B219b : trial ID

B220b : trial ID

B221b : trial ID

B222b : trial ID

B223b : trial ID

B224b : trial ID

B225b : trial ID

B226b : trial ID

B227b : trial ID

B228b : trial ID

B229b : trial ID

B230b : trial ID

B231b : trial ID

B232b : trial ID

B233b : trial ID

B234b : trial ID

B235b : trial ID

B236b : trial ID

B237b : trial ID

B238b : trial ID

B239b : trial ID

B240b : trial ID

B241b : trial ID

B242b : trial ID

B243b : trial ID

B244b : trial ID

B245b : trial ID

B246b : trial ID

B247b : trial ID

B248b : trial ID

B249b : trial ID

B250b : trial ID

B251b : trial ID

B252b : trial ID

B253b : trial ID

B254b : trial ID

B255b : trial ID

B256b : trial ID

B257b : trial ID

B258b : trial ID

B259b : trial ID

B260b : trial ID

B261b : trial ID

B262b : trial ID

B263b : trial ID

B264b : trial ID

B265b : trial ID

B266b : trial ID

B267b : trial ID

B268b : trial ID

B269b : trial ID

B270b : trial ID

B271b : trial ID

B272b : trial ID

B273b : trial ID

B274b : trial ID

B275b : trial ID

B276b : trial ID

B277b : trial ID

B278b : trial ID

B279b : trial ID

B280b : trial ID

B281b : trial ID

B282b : trial ID

B283b : trial ID

B284b : trial ID

B285b : trial ID

B286b : trial ID

B287b : trial ID

B288b : trial ID

B289b : trial ID

B290b : trial ID

B291b : trial ID

B292b : trial ID

B293b : trial ID

B294b : trial ID

B295b : trial ID

B296b : trial ID

B297b : trial ID

B298b : trial ID

B299b : trial ID

B300b : trial ID

B301b : trial ID

B302b : trial ID

B303b : trial ID

B304b : trial ID

B305b : trial ID

The Evaluation of the L8 Series Grenades (L8A), 12 grenades, L8321

The Evaluation of the LG Series Grenades (L8A3), low condition (exp., L03J)

200.5 : 200.5 : 200.5 : 200.5 : 200.5 : y-coord. of 2nd end-point for LOS1 (m)
 -9.990E+01 -9.990E+01 -9.990E+01 -9.990E+01 -9.990E+01 Los integrated dosage (mg/m²)
 -267.7 : -267.7 : -267.7 : -267.7 : -267.7 Los integrated conc. (mg/m²)
 -29.1 : -29.1 : -29.1 : -29.1 : -29.1
 262.1 : 262.1 : 262.1 : 262.1 : 262.1
 252.6 : 252.6 : 252.6 : 252.6 : 252.6
 -99.9 : -99.9 : -99.9 : -99.9 : -99.9
 -9.990E+01 -9.990E+01 -9.990E+01 -9.990E+01 -9.990E+01 Los integrated dosage (mg/m²)

The Evaluation of the LG Series Grenades (18A), medium condition temp., 103M
6 i Number of trials included in QDA

208.5	208.5	208.5	208.5	208.5	208.5	208.5	208.5	208.5
-99.9	-99.9	-99.9	-99.9	-99.9	-99.9	-99.9	-99.9	-99.9
-9.990E+01								
-267.7	-267.7	-267.7	-267.7	-267.7	-267.7	-267.7	-267.7	-267.7
-29.1	-29.1	-29.1	-29.1	-29.1	-29.1	-29.1	-29.1	-29.1
262.1	262.1	262.1	262.1	262.1	262.1	262.1	262.1	262.1
252.6	252.6	252.6	252.6	252.6	252.6	252.6	252.6	252.6
-99.9	-99.9	-99.9	-99.9	-99.9	-99.9	-99.9	-99.9	-99.9
-9.990E+01								
7.400E-04								

y-coord. of 2nd end-point for LOS1 (m) : -99.9 : LOS integrated conc. (mg/m³)
 LOS integrated dosage (mg/m³m⁻²) : 1.940E+01
 x-coord. of 1st end-point for LOS1 (m) : -267.7 : -267.7 : -267.7 : -267.7 : -267.7 : -267.7 : -267.7 : -267.7 : -267.7
 y-coord. of 1st end-point for LOS1 (m) : -29.1 : -29.1 : -29.1 : -29.1 : -29.1 : -29.1 : -29.1 : -29.1 : -29.1
 x-coord. of 2nd end-point for LOS1 (m) : 262.1 : 262.1 : 262.1 : 262.1 : 262.1 : 262.1 : 262.1 : 262.1 : 262.1
 y-coord. of 2nd end-point for LOS1 (m) : 252.6 : 252.6 : 252.6 : 252.6 : 252.6 : 252.6 : 252.6 : 252.6 : 252.6
 LOS integrated conc. (mg/m³) : -99.9 : -99.9 : -99.9 : -99.9 : -99.9 : -99.9 : -99.9 : -99.9 : -99.9
 LOS integrated dosage (mg/m³m⁻²) : 9.400E+01 : 9.400E+01

The State of Maine Law Enforcement (H.B. 1455, 1995)

The terms of reference include Put 2/Leisurecare (or its local unit), [REDACTED]

State of Foreign Trade Post-Liberalization

State of forests under forest protection (British Isles, 1978)

86122	Total 10
86123	86124
86125	86126
86053	86054
86055	86056
86057	86058
86059	86060
86061	86062
86063	86064
86065	86066
86067	86068
86069	86070
86071	86072
86073	86074
86075	86076
86077	86078
86079	86080
86081	86082
86083	86084
86085	86086
86087	86088
86089	86090
86091	86092
86093	86094
86095	86096
86097	86098
86099	86100
86101	86102
86103	86104
86105	86106
86107	86108
86109	86110
86111	86112
86113	86114
86115	86116
86117	86118
86119	86120
0	1
1	1
2	1
3	1
4	1
5	1
6	1
7	1
8	1
9	1
10	1
11	1
12	1
13	1
14	1
15	1
16	1
17	1
18	1
19	1
20	1
21	1
22	1
23	1
24	1
25	1
26	1
27	1
28	1
29	1
30	1
31	1
32	1
33	1
34	1
35	1
36	1
37	1
38	1
39	1
40	1
41	1
42	1
43	1
44	1
45	1
46	1
47	1
48	1
49	1
50	1
51	1
52	1
53	1
54	1
55	1
56	1
57	1
58	1
59	1
60	1
61	1
62	1
63	1
64	1
65	1
66	1
67	1
68	1
69	1
70	1
71	1
72	1
73	1
74	1
75	1
76	1
77	1
78	1
79	1
80	1
81	1
82	1
83	1
84	1
85	1
86	1
87	1
88	1
89	1
90	1
91	1
92	1
93	1
94	1
95	1
96	1
97	1
98	1
99	1
100	1
101	1
102	1
103	1
104	1
105	1
106	1
107	1
108	1
109	1
110	1
111	1
112	1
113	1
114	1
115	1
116	1
117	1
118	1
119	1
120	1
121	1
122	1
123	1
124	1
125	1
126	1
127	1
128	1
129	1
130	1
131	1
132	1
133	1
134	1
135	1
136	1
137	1
138	1
139	1
140	1
141	1
142	1
143	1
144	1
145	1
146	1
147	1
148	1
149	1
150	1
151	1
152	1
153	1
154	1
155	1
156	1
157	1
158	1
159	1
160	1
161	1
162	1
163	1
164	1
165	1
166	1
167	1
168	1
169	1
170	1
171	1
172	1
173	1
174	1
175	1
176	1
177	1
178	1
179	1
180	1
181	1
182	1
183	1
184	1
185	1
186	1
187	1
188	1
189	1
190	1
191	1
192	1
193	1
194	1
195	1
196	1
197	1
198	1
199	1
200	1
201	1
202	1
203	1
204	1
205	1
206	1
207	1
208	1
209	1
210	1
211	1
212	1
213	1
214	1
215	1
216	1
217	1
218	1
219	1
220	1
221	1
222	1
223	1
224	1
225	1
226	1
227	1
228	1
229	1
230	1
231	1
232	1
233	1
234	1
235	1
236	1
237	1
238	1
239	1
240	1
241	1
242	1
243	1
244	1
245	1
246	1
247	1
248	1
249	1
250	1
251	1
252	1
253	1
254	1
255	1
256	1
257	1
258	1
259	1
260	1
261	1
262	1
263	1
264	1
265	1
266	1
267	1
268	1
269	1
270	1
271	1
272	1
273	1
274	1
275	1
276	1
277	1
278	1
279	1
280	1
281	1
282	1
283	1
284	1
285	1
286	1
287	1
288	1
289	1
290	1
291	1
292	1
293	1
294	1
295	1
296	1
297	1
298	1
299	1
300	1
301	1
302	1
303	1
304	1
305	1
306	1
307	1
308	1
309	1
310	1
311	1
312	1
313	1
314	1
315	1
316	1
317	1
318	1
319	1
320	1
321	1
322	1
323	1
324	1
325	1
326	1
327	1
328	1
329	1
330	1
331	1
332	1
333	1
334	1
335	1
336	1
337	1
338	1
339	1
340	1
341	1
342	1
343	1
344	1
345	1
346	1
347	1
348	1
349	1
350	1
351	1
352	1
353	1
354	1
355	1
356	1
357	1
358	1
359	1
360	1
361	1
362	1
363	1
364	1
365	1
366	1
367	1
368	1
369	1
370	1
371	1
372	1
373	1
374	1
375	1
376	1
377	1
378	1
379	1
380	1
381	1
382	1
383	1
384	1
385	1
386	1
387	1
388	1
389	1
390	1
391	1
392	1
393	1
394	1
395	1
396	1
397	1
398	1
399	1
400	1
401	1
402	1
403	1
404	1
405	1
406	1
407	1
408	1
409	1
410	1
411	1
412	1
413	1
414	1
415	1
416	1
417	1
418	1
419	1
420	1
421	1
422	1
423	1
424	1
425	1
426	1
427	1
428	1
429	1
430	1
431	1
432	1
433	1
434	1
435	1
436	1
437	1
438	1
439	1
440	1
441	1
442	1
443	1
444	1
445	1
446	1
447	1
448	1
449	1
450	1
451	1
452	1
453	1
454	1
455	1
456	1
457	1
458	1
459	1
460	1
461	1
462	1
463	1
464	1
465	1
466	1
467	1
468	1
469	1
470	1
471	1
472	1
473	1
474	1
475	1
476	1
477	1
478	1
479	1
480	1
481	1
482	1
483	1
484	1
485	1
486	1
487	1
488	1
489	1
490	1
491	1
492	1
493	1
494	1
495	1
496	1
497	1
498	1
499	1
500	1
501	1
502	1
503	1
504	1
505	1
506	1
507	1
508	1
509	1
510	1
511	1
512	1
513	1
514	1
515	1
516	1
517	1
518	1
519	1
520	1
521	1
522	1
523	1
524	1
525	1
526	1
527	1
528	1
529	1
530	1
531	1
532	1
533	1
534	1
535	1
536	1
537	1
538	1
539	1
540	1
541	1
542	1
543	1
544	1
545	1
546	1
547	1
548	1
549	1
550	1
551	1
552	1
553	1
554	1
555	1
556	1
557	1
558	1
559	1
560	1
561	1
562	1
563	1
564	1
565	1
566	1
567	1
568	1
569	1
570	1
571	1
572	1
573	1
574	1
575	1
576	1
577	1
578	1
579	1
580	1
581	1
582	1
583	1
584	1
585	1
586	1
587	1
588	1
589	1
590	1
591	1
592	1
593	1
594	1
595	1
596	1
597	1
598	1
599	1
600	1
601	1
602	1
603	1
604	1
605	1
606	1
607	1
608	1
609	1
610	1
611	1
612	1
613	1
614	1
615	1
616	1
617	1
618	1
619	1
620	1
621	1
622	1
623	1
624	1
625	1
626	1
627	1
628	1
629	1
630	1

The Tests of Foreign Smoke Pots/Generators (Japanese 3-00, INT'JA)

The Test of Significance for a Causal Loss

The Test of Significance for a Causal Loss

Development Test 1 of the Man-Portable Smoke Generators (MPSG, fog oil only, POMF)

Number of trials included in DDA

6 : time zone designation

40.20 : latitude (deg)

111.00 : longitude (deg)

F002 F006

F004

0.30

-0.30

-0.30

-0.30

-0.30

-0.30

-0.30

-0.30

-0.30

-0.30

-0.30

-0.30

-0.30

-0.30

-0.30

-0.30

-0.30

-0.30

-0.30

-0.30

-0.30

-0.30

-0.30

-0.30

-0.30

-0.30

-0.30

-0.30

-0.30

-0.30

-0.30

-0.30

-0.30

-0.30

-0.30

-0.30

-0.30

-0.30

-0.30

-0.30

-0.30

-0.30

-0.30

-0.30

-0.30

-0.30

-0.30

-0.30

-0.30

-0.30

-0.30

-0.30

-0.30

-0.30

-0.30

-0.30

-0.30

-0.30

-0.30

-0.30

-0.30

-0.30

-0.30

-0.30

-0.30

-0.30

-0.30

-0.30

-0.30

-0.30

-0.30

-0.30

-0.30

-0.30

-0.30

-0.30

-0.30

-0.30

-0.30

-0.30

-0.30

-0.30

-0.30

-0.30

-0.30

-0.30

-0.30

-0.30

-0.30

-0.30

-0.30

-0.30

-0.30

-0.30

-0.30

-0.30

-0.30

-0.30

-0.30

-0.30

-0.30

-0.30

-0.30

-0.30

-0.30

-0.30

-0.30

-0.30

-0.30

-0.30

-0.30

-0.30

-0.30

-0.30

-0.30

-0.30

-0.30

-0.30

-0.30

-0.30

-0.30

-0.30

-0.30

-0.30

-0.30

-0.30

-0.30

-0.30

-0.30

-0.30

-0.30

-0.30

-0.30

-0.30

-0.30

-0.30

-0.30

-0.30

-0.30

-0.30

-0.30

-0.30

-0.30

-0.30

-0.30

-0.30

-0.30

-0.30

-0.30

-0.30

-0.30

-0.30

-0.30

-0.30

-0.30

-0.30

-0.30

-0.30

-0.30

-0.30

-0.30

-0.30

-0.30

-0.30

-0.30

-0.30

-0.30

-0.30

-0.30

-0.30

-0.30

-0.30

-0.30

-0.30

-0.30

-0.30

-0.30

-0.30

-0.30

-0.30

-0.30

-0.30

-0.30

-0.30

-0.30

-0.30

-0.30

-0.30

-0.30

-0.30

-0.30

-0.30

-0.30

-0.30

-0.30

-0.30

-0.30

-0.30

-0.30

-0.30

-0.30

-0.30

-0.30

-0.30

-0.30

-0.30

-0.30

-0.30

-0.30

-0.30

-0.30

-0.30

-0.30

-0.30

-0.30

-0.30

-0.30

-0.30

-0.30

-0.30

-0.30

-0.30

-0.30

-0.30

-0.30

-0.30

-0.30

-0.30

-0.30

-0.30

-0.30

-0.30

-0.30

-0.30

-0.30

-0.30

-0.30

-0.30

-0.30

-0.30

-0.30

-0.30

-0.30

-0.30

-0.30

-0.30

-0.30

-0.30

-0.30

-0.30

-0.30

<p

Development Test 1 of the Man-Portable Smoke Generators (XMG9, diesel only and diesel + IR, POND)

6 : number of trials included in DDA

6 : time zone designation

40.20 : latitude (deg)

113.00 : longitude (deg)

1020 : DDD1

06352 : DDD10

5 : 5

20 : 20

01 : 01

17 : 19

46 : 37

1 : 1

-190.0 : -280.1

-362.6 : -412.5

0.38 : 0.38

-99.3 : -99.3

240.0 : 240.0

10.658 : 10.658

0.230 : 0.230

0.230 : 0.230

-99.3 : -99.3

-99.3 : -99.3

300.00 : 300.00

300.00 : 300.00

-99.30 : -99.30

-99.30 : -99.30

5.20 : 3.00

2.00 : 2.00

5.20 : 3.00

158.0 : 161.0

-99.90 : -99.90

-99.90 : -99.90

-92.90 : -92.90

-92.90 : -92.90

-92.90 : -92.90

-92.90 : -92.90

-92.90 : -92.90

-92.90 : -92.90

-92.90 : -92.90

-92.90 : -92.90

-92.90 : -92.90

-92.90 : -92.90

-92.90 : -92.90

-92.90 : -92.90

-92.90 : -92.90

-92.90 : -92.90

-92.90 : -92.90

-92.90 : -92.90

-92.90 : -92.90

-92.90 : -92.90

-92.90 : -92.90

-92.90 : -92.90

-92.90 : -92.90

-92.90 : -92.90

-92.90 : -92.90

-92.90 : -92.90

-92.90 : -92.90

-92.90 : -92.90

-92.90 : -92.90

-92.90 : -92.90

-92.90 : -92.90

-92.90 : -92.90

-92.90 : -92.90

-92.90 : -92.90

-92.90 : -92.90

-92.90 : -92.90

-92.90 : -92.90

-92.90 : -92.90

-92.90 : -92.90

-92.90 : -92.90

-92.90 : -92.90

-92.90 : -92.90

-92.90 : -92.90

-92.90 : -92.90

-92.90 : -92.90

-92.90 : -92.90

-92.90 : -92.90

-92.90 : -92.90

-92.90 : -92.90

-92.90 : -92.90

-92.90 : -92.90

-92.90 : -92.90

-92.90 : -92.90

0.18 : 0.18

0.50 : 0.50

0.50 : 0.50

0.50 : 0.50

0.071 : 0.071

0.0300 : 0.0300

-99.9000 : -99.9000

-99.9000 : -99.9000

-99.9000 : -99.9000

-99.9000 : -99.9000

-99.9000 : -99.9000

-99.9000 : -99.9000

-99.9000 : -99.9000

-99.9000 : -99.9000

-99.9000 : -99.9000

-99.9000 : -99.9000

-99.9000 : -99.9000

-99.9000 : -99.9000

-99.9000 : -99.9000

-99.9000 : -99.9000

-99.9000 : -99.9000

-99.9000 : -99.9000

-99.9000 : -99.9000

-99.9000 : -99.9000

-99.9000 : -99.9000

-99.9000 : -99.9000

-99.9000 : -99.9000

-99.9000 : -99.9000

-99.9000 : -99.9000

-99.9000 : -99.9000

-99.9000 : -99.9000

-99.9000 : -99.9000

-99.9000 : -99.9000

-99.9000 : -99.9000

-99.9000 : -99.9000

-99.9000 : -99.9000

-99.9000 : -99.9000

-99.9000 : -99.9000

-99.9000 : -99.9000

-99.9000 : -99.9000

-99.9000 : -99.9000

-99.9000 : -99.9000

-99.9000 : -99.9000

-99.9000 : -99.9000

-99.9000 : -99.9000

-99.9000 : -99.9000

-99.9000 : -99.9000

-99.9000 : -99.9000

-99.9000 : -99.9000

-99.9000 : -99.9000

-99.9000 : -99.9000

-99.9000 : -99.9000

-99.9000 : -99.9000

-99.9000 : -99.9000

-99.9000 : -99.9000

-99.9000 : -99.9000

-99.9000 : -99.9000

-99.9000 : -99.9000

-99.9000 : -99.9000

-99.9000 : -99.9000

-99.9000 : -99.9000

-99.9000 : -99.9000

-99.9000 : -99.9000

-99.9000 : -99.9000

-99.9000 : -99.9000

-99.9000 : -99.9000

-99.9000 : -99.9000

-99.9000 : -99.9000

-99.9000 : -99.9000

-99.9000 : -99.9000

-99.9000 : -99.9000

-99.9000 : -99.9000

-99.9000 : -99.9000

-99.9000 : -99.9000

-99.9000 : -99.9000

-99.9000 : -99.9000

-99.9000 : -99.9000

-99.9000 : -99.9000

-99.9000 : -99.9000

0.18 : 0.18

0.50 : 0.50

0.50 : 0.50

0.50 : 0.50

0.071 : 0.071

0.0300 : 0.0300

-99.9000 : -99.9000

-99.9000 : -99.9000

-99.9000 : -99.9000

-99.9000 : -99.9000

-99.9000 : -99.9000

-99.9000 : -99.9000

-99.9000 : -99.9000

-99.9000 : -99.9000

-99.9000 : -99.9000

-99.9000 : -99.9000

-99.9000 : -99.9000

-99.9000 : -99.9000

-99.9000 : -99.9000

-99.9000 : -99.9000

-99.9000 : -99.9000

-99.9000 : -99.9000

-99.9000 : -99.9000

-99.9000 : -99.9000

-99.9000 : -99.9000

-99.9000 : -99.9000

-99.9000 : -99.9000

-99.9000 : -99.9000

-99.9000 : -99.9000

-99.9000 : -99.9000

-99.9000 : -99.9000

-99.9000 : -99.9000

-99.9000 : -99.9000

-99.9000 : -99.9000

-99.9000 : -99.9000

-99.9000 : -99.9000

-99.9000 : -99.9000

-99.9000 : -99.9000

-99.9000 : -99.9000

-99.9000 : -99.9000

-99.9000 : -99.9000

-99.9000 : -99.9000

-99.9000 : -99.9000

-99.9000 : -99.9000

-99.9000 : -99.9000

-99.9000 : -99.9000

-99.9000 : -99.9000

-99.9000 : -99.9000

-99.9000 : -99.9000

-99.9000 : -99.9000

-99.9000 : -99.9000

-99.9000 : -99.9000

-99.9000 : -99.9000

-99.9000 : -99.9000

-99.9000 : -99.9000

-99.9000 : -99.9000

-99.9000 : -99.9000

-99.9000 : -99.9000

-99.9000 : -99.9000

-99.9000 : -99.9000

-99.9000 : -99.9000

-99.9000 : -99.9000

-99.9000 : -99.9000

-99.9000 : -99.9000

-99.9000 : -99.9000

-99.9000 : -99.9000

-99.9000 : -99.9000

-99.9000 : -99.9000

-99.9000 : -99.9000

-99.9000 : -99.9000

-99.9000 : -99.9000

The Man-Portable Smoke Generator (XMS-1) is only and is part of the **disclaim, FOXI**

	EA25	DE35b	trial ID				
	EA22	EA23	EA24	EA25	DE35b	DE36b	trial ID
40.20 : latitude (deg)	113.00 : longitude (deg)						
113.00 : no. of sources							
5	5	5	5	5	6	6	month
27	27	28	28	28	3	3	day
61	61	61	61	61	61	61	hour
10	10	10	10	10	17	18	minute
50	48	46	34	28	42	35	
-138.1	-294.4	-294.4	-294.4	-204.7	-246.5	-246.5	x-coord. of source (m)
-101.7	-77.4	-77.4	-77.4	-22.7	-52.0	-52.0	y-coord. of source (m)
0.38	0.38	0.38	0.38	0.38	0.39	0.39	z-source elevation (m)
-99.9	-99.9	-99.9	-99.9	-99.9	-99.9	-99.9	emission rate (g/s)
43.633	2.600	3.415	1.510	20.0	240.0	13.0.15	total mass emitted (kg)
0.230	0.230	0.230	0.230	0.230	0.230	0.230	sign0 at the source (m)
0.230	0.230	0.230	0.230	0.230	0.230	0.230	sign0 at the source (m)
0.230	0.230	0.230	0.230	0.230	0.230	0.230	sign0 at the source (m)
-99.9	-99.9	-99.9	-99.9	-99.9	-99.9	-99.9	ambient pressure (atm)
-99.9	-99.9	-99.9	-99.9	-99.9	-99.9	-99.9	relative humidity (%)
300.00	300.00	300.00	300.00	300.00	300.00	300.00	temperature at level 11 (K)
300.00	300.00	300.00	300.00	300.00	300.00	300.00	measuring height for temperature 11 (m)
300.00	300.00	300.00	300.00	300.00	300.00	300.00	temperature at level 12 (K)
300.00	300.00	300.00	300.00	300.00	300.00	300.00	measuring height for temperature 12 (m)
300.00	300.00	300.00	300.00	300.00	300.00	300.00	wind speed (m/s) at a lower
2.00	2.00	2.00	2.00	2.00	2.00	2.00	measuring height for wind data (m)
2.00	2.00	2.00	2.00	2.00	2.00	2.00	domain-averaged wind speed (m/s)
2.00	2.00	2.00	2.00	2.00	2.00	2.00	domain-averaged wind direction (deg)
336.0	371.0	308.0	271.0	357.0	6.0	6.0	domain-averaged signal (m/s)
-99.90	-99.90	-99.90	-99.90	-99.90	-99.90	-99.90	domain-averaged signal-theta (deg)
18.10	16.30	19.40	11.40	13.00	13.00	13.00	domain-averaged signal-phi (deg)
-99.90	-99.90	-99.90	-99.90	-99.90	-99.90	-99.90	measuring ht for domain-avg wind speed (m)
2.00	2.00	2.00	2.00	2.00	2.00	2.00	averaging time for domain-avg data (s)
390.0	390.0	420.0	360.0	420.0	390.0	390.0	wind speed power law exponent
0.74	0.68	0.63	0.64	0.64	0.62	0.62	surface roughness (m)
0.0300	0.0300	0.0300	0.0300	0.0300	0.0300	0.0300	friction velocity (m/s)
39.900	39.900	39.900	39.900	39.900	39.900	39.900	Inverse Monin-Obukhov length (1/m)
-99.900	-99.900	-99.900	-99.900	-99.900	-99.900	-99.900	albedo
0.50	0.50	0.50	0.50	0.50	0.50	0.50	no. of lines-of-sight
0.50	0.50	0.50	0.50	0.50	0.50	0.50	mixing height (m)
0.50	0.50	0.50	0.50	0.50	0.50	0.50	Bouy ratio
-99.9	-99.9	-99.9	-99.9	-99.9	-99.9	-99.9	cloud cover (%)
-99.9	-99.9	-99.9	-99.9	-99.9	-99.9	-99.9	F-G stability class
240.0	240.0	240.0	240.0	240.0	240.0	240.0	averaging time for concentration (s)
2.44	2.44	2.44	2.44	2.44	2.44	2.44	augmented receptor height (m)
0	0	0	0	0	0	0	no. of distances downwind
3	3	3	3	3	3	3	moisture availability
-517.5	-517.5	-517.5	-517.5	-517.5	-517.5	-517.5	x-coord. of 1st end-point for LOS1 (m)
-304.0	-304.0	-304.0	-304.0	-304.0	-304.0	-304.0	y-coord. of 1st end-point for LOS1 (m)
-80.2	-80.2	-80.2	-80.2	-80.2	-80.2	-80.2	z-coord. of 1st end-point for LOS1 (m)
-61.6	-61.6	-61.6	-61.6	-61.6	-61.6	-61.6	x-coord. of 2nd end-point for LOS1 (m)
-114.1	-114.1	-114.1	-114.1	-114.1	-114.1	-114.1	y-coord. of 2nd end-point for LOS1 (m)
-5.0	-5.0	-5.0	-5.0	-5.0	-5.0	-5.0	LOS integrated dosage (mg/m^2)
5.400E-05	1.040E-05	3.200E-04	2.320E-05	2.600E-05	2.600E-05	2.600E-05	LOS integrated dosage (mg/m^2)
5.500E-04	5.500E-04	1.900E-04	1.900E-04	1.900E-04	1.900E-04	1.900E-04	LOS integrated dosage (mg/m^2)
3.000E-04	3.000E-04	4.500E-04	4.500E-04	4.500E-04	4.500E-04	4.500E-04	LOS integrated dosage (mg/m^2)
-459.3	-459.3	-459.3	-459.3	-459.3	-459.3	-459.3	LOS integrated dosage (mg/m^2)
-409.0	-409.0	-409.0	-409.0	-409.0	-409.0	-409.0	LOS integrated dosage (mg/m^2)
-22.0	-22.0	-22.0	-22.0	-22.0	-22.0	-22.0	LOS integrated dosage (mg/m^2)
-166.6	-166.6	-166.6	-166.6	-166.6	-166.6	-166.6	LOS integrated dosage (mg/m^2)
-166.6	-166.6	-166.6	-166.6	-166.6	-166.6	-166.6	LOS integrated dosage (mg/m^2)
-99.9	-99.9	-99.9	-99.9	-99.9	-99.9	-99.9	LOS integrated dosage (mg/m^2)
1.100E-04	1.100E-04	1.100E-04	1.100E-04	1.100E-04	1.100E-04	1.100E-04	LOS integrated dosage (mg/m^2)

Development Test 1 of the Man-Portable Smoke Generators (MK4), foggy part of fogola IR, FOXFC

10 : number of cities included in DDA

11 : time zone designation

12 : latitude (deg)

13 : longitude (deg)

14 : FZ264

15 : FZ27a

16 : FZ28a

17 : FZ29a

18 : FZ30a

19 : FZ31a

20 : FZ32a

21 : FZ33a

22 : FZ34a

23 : FZ35a

24 : FZ36a

25 : FZ37a

26 : FZ38a

27 : FZ39a

28 : FZ40a

29 : FZ41a

30 : FZ42a

31 : FZ43a

32 : FZ44a

33 : FZ45a

34 : FZ46a

35 : FZ47a

36 : FZ48a

37 : FZ49a

38 : FZ50a

39 : FZ51a

40 : FZ52a

41 : FZ53a

42 : FZ54a

43 : FZ55a

44 : FZ56a

45 : FZ57a

46 : FZ58a

47 : FZ59a

48 : FZ60a

49 : FZ61a

50 : FZ62a

51 : FZ63a

52 : FZ64a

53 : FZ65a

54 : FZ66a

55 : FZ67a

56 : FZ68a

57 : FZ69a

58 : FZ70a

59 : FZ71a

60 : FZ72a

61 : FZ73a

62 : FZ74a

63 : FZ75a

64 : FZ76a

65 : FZ77a

66 : FZ78a

67 : FZ79a

68 : FZ80a

69 : FZ81a

70 : FZ82a

71 : FZ83a

72 : FZ84a

73 : FZ85a

74 : FZ86a

75 : FZ87a

76 : FZ88a

77 : FZ89a

78 : FZ90a

79 : FZ91a

80 : FZ92a

81 : FZ93a

82 : FZ94a

83 : FZ95a

84 : FZ96a

85 : FZ97a

86 : FZ98a

87 : FZ99a

88 : FZ100a

89 : FZ101a

90 : FZ102a

91 : FZ103a

92 : FZ104a

93 : FZ105a

94 : FZ106a

95 : FZ107a

96 : FZ108a

97 : FZ109a

98 : FZ110a

99 : FZ111a

100 : FZ112a

101 : FZ113a

102 : FZ114a

103 : FZ115a

104 : FZ116a

105 : FZ118a

106 : FZ119a

107 : FZ120a

108 : FZ121a

109 : FZ122a

110 : FZ123a

111 : FZ124a

112 : FZ125a

113 : FZ126a

114 : FZ127a

115 : FZ128a

116 : FZ129a

117 : FZ130a

118 : FZ131a

119 : FZ132a

120 : FZ133a

121 : FZ134a

122 : FZ135a

123 : FZ136a

124 : FZ137a

125 : FZ138a

126 : FZ139a

127 : FZ140a

128 : FZ141a

129 : FZ142a

130 : FZ143a

131 : FZ144a

132 : FZ145a

133 : FZ146a

134 : FZ147a

135 : FZ148a

136 : FZ149a

137 : FZ150a

138 : FZ151a

139 : FZ152a

140 : FZ153a

141 : FZ154a

142 : FZ155a

143 : FZ156a

144 : FZ157a

145 : FZ158a

146 : FZ159a

147 : FZ160a

148 : FZ161a

149 : FZ162a

150 : FZ163a

151 : FZ164a

152 : FZ165a

153 : FZ166a

154 : FZ167a

155 : FZ168a

156 : FZ169a

157 : FZ170a

158 : FZ171a

159 : FZ172a

160 : FZ173a

161 : FZ174a

162 : FZ175a

163 : FZ176a

164 : FZ177a

165 : FZ178a

166 : FZ179a

167 : FZ180a

168 : FZ181a

169 : FZ182a

170 : FZ183a

171 : FZ184a

172 : FZ185a

173 : FZ186a

174 : FZ187a

175 : FZ188a

176 : FZ189a

177 : FZ190a

178 : FZ191a

179 : FZ192a

180 : FZ193a

181 : FZ194a

182 : FZ195a

183 : FZ196a

184 : FZ197a

185 : FZ198a

186 : FZ199a

187 : FZ200a

188 : FZ201a

189 : FZ202a

190 : FZ203a

191 : FZ204a

192 : FZ205a

193 : FZ206a

194 : FZ207a

195 : FZ208a

196 : FZ209a

197 : FZ210a

198 : FZ211a

199 : FZ212a

200 : FZ213a

201 : FZ214a

202 : FZ215a

203 : FZ216a

204 : FZ217a

205 : FZ218a

206 : FZ219a

207 : FZ220a

208 : FZ221a

209 : FZ222a

210 : FZ223a

211 : FZ224a

212 : FZ225a

213 : FZ226a

214 : FZ227a

215 : FZ228a

216 : FZ229a

217 : FZ230a

218 : FZ231a

219 : FZ232a

220 : FZ233a

221 : FZ234a

222 : FZ235a

223 : FZ236a

224 : FZ237a

225 : FZ238a

226 : FZ239a

227 : FZ240a

228 : FZ241a

229 : FZ242a

230 : FZ243a

231 : FZ244a

232 : FZ245a

233 : FZ246a

234 : FZ247a

235 : FZ248a

236 : FZ249a

237 : FZ250a

238 : FZ251a

239 : FZ252a

240 : FZ253a

241 : FZ254a

242 : FZ255a

243 : FZ256a

244 : FZ257a

245 : FZ258a

246 : FZ259a

247 : FZ261a

248 : FZ262a

249 : FZ263a

250 : FZ264a

251 : FZ265a

252 : FZ266a

253 : FZ267a

254 : FZ268a

255 : FZ269a

256 : FZ270a

257 : FZ271a

258 : FZ272a

259 : FZ273a

260 : FZ274a

Development Test I of the Hanford-possible Smoke Generators (PAK 49, IR part of fog oil + IR, POXIC)

number of trials = 100

卷之三

Altitude-87 : number of trials included in ODA

044 : trial 1D									
act	42	43	44	45	46	47	48	49	50
11	11	4	4	4	4	4	4	4	4
0.0	0.0	0.0	0.0	0.0	0.0	0.0	0.0	0.0	0.0
0.0	0.0	0.0	0.0	0.0	0.0	0.0	0.0	0.0	0.0
1.00	1.00	1.00	1.00	1.00	1.00	1.00	1.00	1.00	1.00
34.600	26.100	1650.0	1650.0	115.8	44.0	0.000	0.000	0.000	0.000
3354.0	3354.0	3354.0	3354.0	0.000	0.000	0.000	0.000	0.000	0.000
-99.3	-99.3	-99.3	-99.3	-99.3	-99.3	-99.3	-99.3	-99.3	-99.3
41.0	296.35	293.15	292.00	292.00	296.14	193.25	300.34	280.26	280.26
219.0	249.0	249.0	1.52	1.52	16.50	11.00	18.60	35.40	35.40
0.2000	0.2000	0.2000	-0.0159	-0.0159	8.00	8.20	8.20	14.90	14.90
1.00	1.00	1.00	0.20	0.20	10.00	10.00	10.00	10.00	10.00
22.00	648.0	648.0	1.00	1.00	10.00	10.00	10.00	10.00	10.00
-99.9	-99.9	-99.9	0.2000	0.2000	0.2000	0.2000	0.2000	0.2000	0.2000
3354.0	1650.0	1.91E-03							
3.018E-06	1.161E-06	4.638E-06	1.601E-02						
1.144E-03	1.144E-03	1.144E-03	-44.3	-44.3	76.9	76.9	76.9	76.9	76.9
175.0	175.0	175.0	-6.8	-6.8	1.76E-02	1.76E-02	1.76E-02	1.76E-02	1.76E-02
0.410E-02	4.705E-02	4.705E-02	1.68E-03	1.68E-03	4.066E-06	4.066E-06	6.740E-06	6.740E-06	6.740E-06
2.021E-02	7.764E-02	7.764E-02	1.215E-07						
330.1	334.9	334.9	191.4	191.4	141.3	141.3	141.3	141.3	141.3
141.5	141.5	141.5	175.0	175.0	175.0	175.0	175.0	175.0	175.0
191.4	191.4	191.4	-44.3	-44.3	-44.3	-44.3	-44.3	-44.3	-44.3
16.1	16.1	16.1	99.9	99.9	99.9	99.9	99.9	99.9	99.9
2.138E-02	1.150E-02	4.318E-02							
1.169E-02	1.169E-02	1.169E-02	1.219E-05	1.219E-05	1.481E-05	1.481E-05	1.481E-05	1.481E-05	1.481E-05
71.7	71.7	71.7	122.1	122.1	122.1	122.1	122.1	122.1	122.1
548.3	548.3	548.3	496.2	496.2	496.2	496.2	496.2	496.2	496.2
521.3	521.3	521.3	573.7	573.7	573.7	573.7	573.7	573.7	573.7
3.619E-01	3.025E-01	8.229E-01	8.229E-01	8.229E-01	9.440E-01	9.440E-01	9.440E-01	9.440E-01	9.440E-01
1.214E-01	6.311E-02	2.380E-01	2.380E-01	2.380E-01	4.311E-01	4.311E-01	4.311E-01	4.311E-01	4.311E-01
331.6	332.6	383.0	383.0	383.0	383.0	383.0	383.0	383.0	383.0
625.4	625.4	573.3	573.3	573.3	573.3	573.3	573.3	573.3	573.3
555.5	555.5	605.9	605.9	605.9	605.9	605.9	605.9	605.9	605.9
40.2	40.2	351.1	351.1	351.1	351.1	351.1	351.1	351.1	351.1
2.034E-02	2.891E-01	1.132E-01	1.132E-01	1.132E-01	1.680E-01	1.680E-01	1.680E-01	1.680E-01	1.680E-01
6.821E-04	4.771E-04	7.681E-04	7.681E-04	7.681E-04	1.132E-04	1.132E-04	1.132E-04	1.132E-04	1.132E-04

Witterbury-87 : number of trials included in DDA

46.8		ac9	trial ID
05.90	: longitude (deg)	47.7	
45.5	: lat (deg)	47.7	
11	: 11	11	11
11	: 12	12	11 month
9	: 10	10	11 day
87	: 87	87	13 day
15	: 11	16	87 year
45	: 27	37	10 hour
1	: 1	1	21 minute
0.0	: 0.0	0.0	1 no. of sources
0.0	: 0.0	0.0	0.0 x-coord. of source (m)
0.0	: 0.0	0.0	0.0 y-coord. of source (m)
0.40	: 1.50	1.50	1.50 source elevation (m)
149.00	: 101.00	77.300	79.100 emission rate (g/s)
1500.0	: 2120.0	2318.0	2742.0 total mass emitted (kg)
222.1	: 229.3	215.5	219.5 ambient pressure (atm)
0.000	: 0.000	0.000	45.0 relative humidity (%)
0.000	: 0.000	0.000	286.95 temperature at level 11 (K)
-99.9	: -99.9	-99.9	286.05 measuring height for temperature 01 (in)
69.0	: 61.0	49.0	275.31 temperature at level 02 (K)
279.05	: 216.35	216.15	286.19 measuring height for temperature 02 (in)
2.00	: 2.00	2.00	10.00 measuring height for temperature 42 (m)
218.37	: 215.10	215.45	10.00 wind speed (m/s) at a tower
10.30	: 10.00	10.00	4.30 measuring height for wind data (m)
4.40	: 7.10	5.20	10.00 domain-averaged wind speed (m/s)
10.00	: 10.00	10.00	4.90 domain-averaged wind direction (deg)
4.40	: 7.10	5.20	224.0 domain-averaged sigma-zeta (m/s)
1.10	: 2.20	2.40	1.32 domain-averaged sigma-zeta (deg)
1.03	: 1.74	1.28	15.30 domain-averaged sigma-psi (deg)
11.00	: 13.20	14.40	9.80 inverse Monin-Obukhov length (1/m)
0.00	: 9.30	8.30	10.00 measuring hr for domain-avg wind speed (m)
10.00	: 10.00	10.00	3942.0 averaging time for domain-avg data (s)
2100.0	: 2350.0	4018.0	0.121 wind speed law exponent
0.130	: 0.132	0.132	0.200 surface roughness (m)
0.2000	: 0.2000	0.2000	0.400 friction velocity (m/s)
0.510	: 0.720	0.570	-0.0169 -0.0169
-0.0217	: -0.0091	-0.0147	-0.0159 -0.0159
-0.020	: 0.20	-0.20	0.20 0.20
1.00	: 1.00	1.00	1.00 1.00
2.00	: 2.00	2.00	2.00 2.00
649.0	: 466.0	434.0	0.16.0 Bowen ratio
-99.9	: -99.9	-99.9	-99.9 mixing height (m)
4	: 4	4	-99.9 cloud cover (%)
1500.0	: 2190.0	2838.0	3 PGRability class
1.00	: 1.00	1.00	1.00 averaging time for concentration (s)
0	: 0	0	1.00 suggested receptor height (m)
4	: 4	4	0 no. of distances downwind
-289.0	: -282.0	-382.0	4 no. of lines-of-sight
389.9	: -389.9	-389.9	9.4 x-coord. of 1st end-point for LOS1 (m)
-190.4	: -190.4	-190.4	59.8 y-coord. of 1st end-point for LOS1 (m)
489.3	: -482.3	-482.3	101.0 x-coord. of 2nd end-point for LOS1 (m)
1.952E+01	: 7.57E+01	3.336E+01	-32.6 y-coord. of 2nd end-point for LOS1 (m)
2.778E+04	: 1.638E+05	5.468E+04	3.365E+03 LOS1 integrated conc. (kg/m^3)
-311.6	: -311.6	-311.6	8.661E+06 LOS1 integrated dosage (kg-s/m^2)
-282.1	: -282.1	-282.1	-20.4 x-coord. of 1st end-point for LOS1 (m)
-92.9	: -59.2	92.9	167.6 y-coord. of 1st end-point for LOS1 (m)
-519.8	: -519.8	-519.8	199.1 x-coord. of 2nd end-point for LOS1 (m)
9.119E+01	: 9.60E+01	3.81E+01	-70.1 y-coord. of 2nd end-point for LOS1 (m)
1.216E+05	: 2.10E+05	1.00E+05	1.249E+03 LOS1 integrated conc. (kg/m^3)
-270.0	: -270.0	-270.0	3.215E+06 LOS1 integrated dosage (kg-s/m^2)
-122.6	: -122.6	-122.6	21.4 x-coord. of 1st end-point for LOS1 (m)
66.8	: -66.8	66.8	327.1 y-coord. of 1st end-point for LOS1 (m)
-459.4	: -459.4	-459.4	358.2 x-coord. of 2nd end-point for LOS1 (m)
5.648E+03	: 8.23E+02	6.32E+02	1.274E+02 LOS1 integrated conc. (kg/m^3)
8.472E+06	: 1.739E+06	1.736E+06	1.707E+05 LOS1 integrated dosage (kg-s/m^2)
-9.119E+01	: 5.60E+01	2.66E+01	1.443E+05 LOS1 integrated conc. (kg/m^3)
1.168E+05	: 1.262E+05	2.145E+05	3.955E+05 1.3022E+06 LOS1 integrated dosage (kg-s/m^2)
-3195.6	: -195.6	-195.6	95.8 x-coord. of 1st end-point for LOS1 (m)
72.8	: 72.8	72.8	52.5 y-coord. of 1st end-point for LOS1 (m)
256.0	: 256.0	256.0	547.4 x-coord. of 2nd end-point for LOS1 (m)
5.375E+04	: 3.27E+02	4.32E+02	4.998E+01 1.274E+02 LOS1 integrated conc. (kg/m^3)
8.472E+06	: 1.739E+06	1.736E+06	1.707E+05 LOS1 integrated dosage (kg-s/m^2)
-9.90E+01	: -9.90E+01	-9.90E+01	-9.90E+01 -9.90E+01 LOS1 integrated conc. (kg-s/m^2)
-9.90E+01	: -9.90E+01	-9.90E+01	-9.90E+01 -9.90E+01 LOS1 integrated dosage (kg-s/m^2)